Electromagnetic Characterization of a PCB Salinity Sensor

by

Frank Thompson Werner

A thesis submitted to the Graduate Faculty of
Auburn University
in partial fulfillment of the
requirements for the Degree of
Master of Science

Auburn, Alabama
August 6, 2016

Keywords: Salinity, Electrical Conductivity, Genetic Algorithm

Approved by

Robert N. Dean, Chair, Professor of Electrical Engineering
Stuart Wentworth, Associate Professor of Electrical Engineering
Mark Adams, Assistant Professor of Electrical Engineering

Abstract

Saltwater intrusion occurs when seawater contaminates sources of freshwater and is a major concern for coastal communities. Presented is a sensor developed for easily measuring saltwater intrusion. The sensor is comprised of two planar electrodes integrated onto a printed circuit board (PCB). PCB technology enables this sensor to be manufactured at high volumes for a modest cost. In this work, the PCB sensor was tested in water samples originating from several locations to prove that it functioned correctly. The sensor's performance was then simulated for multiple electrode geometries to determine the influence different electrode dimensions have on its measurements. The measurement and simulation results were then used by a genetic algorithm to derive an equation describing the behavior of the sensor.

Table of Contents

Abstract ii
List of Figures vi
List of Tables xi
Chapter 1: Introduction 1
Chapter 2: Background 4
2.1 Saltwater Intrusion 4
2.2 Measuring Salinity 8
2.2.1 The Practical Salinity Scale (PSS-78) 8
2.2.2 The Thermodynamic Equation of Seawater (TEOS-10) 10
2.3 Types of Salinity Meters 12
2.3.1 Hydrometers 12
2.3.2 Refractometers 14
2.3.3 Conductivity sensors 18
Chapter 3: The Two-Electrode Contact PCB Conductivity Sensor 21
3.1 Basic Setup for Measuring Resistance 26
3.2 The Cell Constant 30
Chapter 4: Modeling and Simulation 32
4.1 Overview of Electromagnetic Simulators and Numerical Methods 32
4.1.1 Finite Difference Method 34
4.1.2 Finite Element Method 35
4.1.3 Method of Moments 36
4.1.4 Finite Difference Time Domain 38
4.2 Electromagnetic Simulators Used 39
4.3 Simulation Setup 40
4.3.1 The Setup for the EMPro Simulations 42

4.3.2 The Setup for the Q3D Extractor Simulations 47
4.4 Properties not accounted for 53
4.4.1 Temperature 53
4.4.2 Pressure 55
4.4.3 Electrode Polarization 55
Chapter 5: Testing Process 59
5.1 Original Testing Method 60
5.2 Using the Commercial Sensors 64
5.3 Improved Testing Process 66
5.4 Final Testing Method 72
Chapter 6: Testing results 77
6.1 First Round of Testing 77
6.1.1 Pure Water Measurements 78
6.1.2 Commercial Sensor Measurements 79
6.1.3 Original Concentration Test Results 82
6.2 Second Round of Testing 85
6.2.1 Pure Water Measurements 86
6.2.2 Commercial Sensors New Measurements 88
6.2.3 Second Concentration Test Results 91
6.3 Final Round of Testing 96
6.3.1 Calculating the Cell Constant 96
6.3.2 Final Concentration Test Results 103
Chapter 7: Simulations 108
7.1 Electrical Conductivity 108
7.2 Electrode Dimensions 110
7.2.1 Electrode Separation Distance 111
7.2.2 Electrode Length 114
7.2.3 Electrode Width 115
7.2.4 Later Simulations 116
7.3 Size of the Water Sample 119
7.4 Shape of the Water 121

7.5 Simulation Frequency 123
7.6 Simulator Comparisons 124
7.6.1 Conductivity Comparison 125
7.6.2 Electrode Separation Distance Comparison 125
7.6.3 Electrode Length Comparison 127
7.6.4 Electrode Width Comparison 128
Chapter 8: Deriving an Equation 130
8.1 Overview of Genetic Algorithms 130
8.2 The Genetic Algorithm Developed 133
8.3 The Original Equation 139
8.4 Final Equation 146
8.5 Comparison between Predicted and Measured Resistance 156
Chapter 9: Conclusions 165
9.1 Overview of Results 165
9.2 Future Work 166
Bibliography 170
Appendix A: Referenced Tables 175
Appendix B: The Genetic Algorithm MATLAB Script 212
Appendix C: MATLAB Script for Calculating the Cell Constant of a PCB Sensor 218

List of Figures

2.1 Cape Cod National Seashore [2] 5

2.2 Example of the groundwater flow pattern and the transition zone in an aquifer [2] 7

2.3 List of coefficient values used in PSS-78 [11] 10

2.4 The Instant Ocean SeaTest Hydrometer 12

2.5 Comparison of a hydrometer's measurements at 5°C and 35°C [17] 14

2.6 The MA887-BOX Digital Refractometer 15

2.7 Example of how the angle of incidence affects the angle of refraction [19] 16

2.8 The MA887 refractometer's method for measuring the index of refraction of a sample of water [19] 17

2.9 Basic setup of an inductive conductivity sensor [24] 19

2.10 Two and four-electrode contact conductivity sensors [6] 20

3.1 The original PCB salinity sensor 21

3.2 Solder mask instructions for the original PCB sensor 22

3.3 The new PCB sensor design 23

3.4 The gold-plated new PCB sensors 24

3.5 Example of the PCB sensor in use 25

3.6 A panel of PCB sensors 26

3.7 Basic setup for measuring resistance (where the blue rectangle is the object under test and the white bars are the conductors) 27

3.8 Electric field distribution for simple setup 30
3.9 Electric field distribution of the planar PCB salinity sensor 31
4.1 Example of the sensor modeled in EMPro's design environment 33
4.2 An example of the rectangular mesh generated using the FDM [34] 34
4.3 Example of a mesh generated using the FEM [35] 35
4.4 Example of a mesh generated by the MoM [35] 37
4.5 Example of a mesh generated by FDTD [35] 39
4.6 Modeling the PCB sensor's electrodes in EMPro 41
4.7 Simulation setup in EMPro 42
4.8 Example of the EMPro simulations with the default settings 43
4.9 The modified EMPro stop criteria 44
4.10 The modified EMPro initial mesh settings 45
4.11 EMPro's matrix solver settings 45
4.12 Example of the mesh generated by EMPro when simulating the sensor 46
4.13 Zoomed in view of the mesh around the electrodes 46
4.14 Simulation setup in Q3D Extractor 48
4.15 Constraint for the electrodes' mesh elements 49
4.16 Example of the mesh generated for the electrodes 49
4.17 Close up view of the electrode's mesh 50
4.18 Isometric view of the box’s mesh (A) and a view of the mesh near the electrodes (B) ... 50
4.19 The mesh statistics for simulating the sensor 51
4.20 Setup for the simulation in Q3D Extractor 52
4.21 Example of simulation convergence 52

4.22 Comparison between the effect the predicted and measured temperature has on conductivity [25] 54

4.23 Representation of the electrical double layer on the submerged electrode. [42] 56

4.24 Randle's equivalent circuit model [6] [43] 58

5.1 The GW Instek LCR-841 meter 61

5.2 Submerging the PCB sensor in water 62

5.3 The GW Instek LCR-841 meter’s settings during original testing 63

5.4 The 4366 Traceable Conductivity/TDS Pen 65

5.5 Measured resistance as measurement frequency is swept 67

5.6 The settings for measuring resistance recommended by the LCR meter's manual [44] ... 68

5.7 Setup for determining the LCR meter's settings 69

5.8 The GW Instek LCR-841 meter’s new settings 69

5.9 Side view of the concentration testing setup 71

5.10 Top view of the concentration test setup 71

5.11 Stand for holding the PCB sensors during testing 73

5.12 The 4192A LF Impedance Analyzer 76

5.13 Resistance as measurement frequency of the impedance analyzer is swept 76

6.1 Change in measured resistance as seawater was added to water from Turkey Creek 84

6.2 Change in measured resistance as seawater was added to water from Lake Jackson 85

6.3 Results of the second Turkey Creek concentration tests using the original sensors 93

6.4 Results of the second Turkey Creek concentration tests using the new sensors 94

6.5 Results of the second Lake Jackson concentration tests using the original sensors 94

6.6 Results of the second Lake Jackson concentration tests using the new sensors 95

6.7 Results of the first rain concentration tests using the original sensors 95

6.8 Results of the first rain concentration tests using the new sensors 96

6.9 Final Turkey Creek concentration test results using the original sensors..... 104

6.10 Final Turkey Creek concentration test results using the new sensors 104

6.11 Final Lake Jackson concentration test results using the original sensors 105

6.12 Final Lake Jackson concentration test results using the new sensors..... 105

6.13 Final rain water concentration test results using the original sensors..... 106

6.14 Final rain water concentration test results using the new sensors 106

6.15 Comparison between sensor 2's measurements for all three concentration tests..... 107

6.16 Comparison between sensor 4D's measurements for all three concentration tests 107

7.1 Measured conductance vs. the water's conductivity simulated in EMPro and Q3D 109

7.2 Simulated resistance vs. electrode separation distances for four electrode geometries.. 112

7.3 Simulated conductance vs. electrode length for six electrode geometries..... 114

7.4 Simulated measured conductance vs. electrode width for six electrode geometries 115

7.5 Q3D results for all widths when the distance was swept and the length was 1 mm..... 117

7.6 Q3D results for 10 distances when the length was swept and the width was 2 mm..... 118

7.7 Q3D results for 10 distances when the width was swept and the length was 10 mm..... 119

7.8 Simulation setup with water surrounding the sensor 122

7.9 Comparison between EMPro and Q3D results as separation distance was swept..... 126

7.10 Comparison between EMPro and Q3D results as electrode width was swept 128

7.11 Comparison between EMPro and Q3D results as electrode width was swept 129

7.12 Comparison between EMPro and Q3D results as electrode width was swept over a small range 129

8.1 Example of crossover between Parent 1 and Parent 2 133

8.2 The r^2 values for the original solution..... 141

8.3 The r^2 values for the original equation using the second set of data 142

8.4 Comparing the simulated and resistances predicted by the original equation as the separation distance was swept 143

8.5 Comparing the simulated conductance and the conductance predicted by the original equation as the electrode length was swept 144

8.6 Comparing the simulated conductance and the conductance predicted by the original equation as the electrode width was swept 145

8.7 Scatter plot of the simulated verses predicted resistances 149

8.8 Comparison between the simulated and predicted resistance as separation distance was swept, length was 10 mm, and width was 1 mm to 10 mm 150

8.9 Comparison between the simulated and predicted plot with the worst r^2 (distance was swept, length was 1 mm, and width was 10 mm) 151

8.10 Comparison between the simulated and predicted plot with the best r^2 (distance was swept, length was 8 mm, and width was 7 mm) 152

8.11 Comparison between the simulated and predicted resistance as the length was swept, the separation distance was 1 mm to 10 mm, and the width was 2 mm 153

8.12 Comparison between the simulated and predicted conductances as width was swept, the separation distance was 1 mm to 10 mm, and the length was 10 mm 155

8.13 Example of poor agreement between the simulated and predicted conductances when the electrode width was swept, the separation distance was 10 µm, and the length was 8 mm 155

8.14 Comparison between the average measured, simulated, and predicted resistances for the Turkey Creek concentration tests using the original sensors 158

8.15 Comparison between the average measured, simulated, and predicted resistances for the Turkey Creek concentration tests using the new sensors 158

8.16 Cross-section of the PCB sensor with the solder mask ring 161

List of Tables

2.1 Average concentrations of major dissolved constituents of seawater [2] 6

5.1 Equipment used for testing 61

6.1 Results of testing the pure water samples using the original testing process 78

6.2 Salinity measurements obtained using the reflectometer 80

6.3 Salinity measurements obtained using the hydrometer 81

6.4 Salinity measurement obtained using the conductivity pen 82

6.5 Results of testing the new pure water samples using the modified testing process with the original boards 87

6.6 Results of testing the new pure water samples using the modified testing process with the new boards 88

6.7 Salinity measurements of the new water obtained using the reflectometer 89

6.8 Salinity measurements of the new seawater obtained using the hydrometer 90

6.9 Salinity measurement obtained using the conductivity pen 90

6.10 Measured conductivities and average resistances for the Turkey Creek concentration tests 98

6.11 Measured conductivities and average resistance for the Lake Jackson concentration tests 99

6.12 Measured conductivities and average resistance for the rain concentration tests 99

6.13 Cell constants calculated for the original and new PCB sensors 101

7.1 Resistance for difference conductivities as electrode separation distance is swept..... 110

7.2 Measured resistance for different electrode geometries as the block dimensions are swept 121

7.3 Simulation results of surrounding the sensor in water verses the original setup 123

7.4 Effect of increasing the simulation frequency on resistance in Q3D..... 124

8.1 The r^2 values resulting from comparing the original equation to the new data. 146

8.2 The r^2 values resulting from comparing the final equation to the new data 148

8.3 Comparison between measured and predicted cell constants 157

A.1 Resistance as the measurement frequency of the LCR meter is swept while in seawater..... 175

A.2 Testing the accuracy of the LCR meter when in parallel mode with a 1.66 pF capacitor 175

A.3 Testing the accuracy of the LCR meter when in series mode with a 1.66 pF capacitor 176

A.4 Testing the accuracy of the LCR meter when in parallel mode with a 22.29 pF capacitor 176

A.5 Testing the accuracy of the LCR meter when in series mode with a 22.29 pF capacitor 176

A.6 Turkey Creek concentration test results using the original testing setup..... 177

A.7 Lake Jackson concentration test results using the original testing setup 178

A.8 Turkey Creek concentration test results using the modified testing setup and the original sensors 179

A.9 Turkey Creek concentration test results using the modified testing setup and the new sensors..... 180

A.10 Turkey Creek concentration test results using the modified testing setup and the new gold plated sensors..... 181

A.11 Lake Jackson concentration test results using the modified testing setup and the original sensors 182

A.12 Lake Jackson concentration test results using the modified testing setup and the new sensors 183

A.13 Lake Jackson concentration test results using the modified testing setup and the gold plated sensors 184

A.14 Rain water concentration test results using the modified testing setup and the original sensors 185

A.15 Rain water concentration test results using the modified testing setup and the new sensors 186

A.16 Rain water concentration test results using the modified testing setup and the gold plated sensors 187

A.17 Results as the measurement frequency of the impedance analyzer is swept while in seawater 188

A.18 Conductivities calculated for the final Turkey Creek concentration test 188

A.19 Conductivities calculated for the final Lake Jackson concentration test 189

A.20 Conductivities calculated for the final rain water concentration test 191

A.21 Final Turkey Creek concentration test results using the original sensors 192

A.22 Final Turkey Creek concentration test results using the new non-plated sensors 194

A.23 Final Turkey Creek concentration tests using the new gold-plated sensors 195

A.24 Final Lake Jackson concentration test results using the original sensors 197

A.25 Final Lake Jackson concentration test results using the new non-plated sensors 198

A.26 Final Lake Jackson concentration test results using the new gold-plated sensors 200

A.27 Final rain water concentration tests using the original sensors 201

A.28 Final rain water concentration tests using the new non-plated sensors 203

A.29 Final rain water concentration results using the new gold-plated sensors 204

A.30 Comparison of the results of sweeping the conductivity of the test material in EMPro and Q3D 206

A.31 EMPro results of sweeping electrode separation distance for multiple geometries 207

A.32 EMPro results of sweeping electrode length for multiple separation distances 208

A.33 EMPro results of sweeping electrode width for multiple separation distances 209

A.34 Comparison between sweeping the electrode separation distance in EMPro and Q3D . 210

A.35 Comparison between sweeping the electrode length in EMPro and Q3D..... 210

A.36 Comparison between sweeping the electrode width in EMPro and Q3D..... 211

Chapter 1

Introduction

Freshwater aquifers serve as the main source of potable water for coastal communities [1]. Without them, these communities would be forced to rely on costly alternatives such as having the water shipped in. Because of their close proximity to the ocean, saltwater intrusion is a major concern for these communities. Saltwater intrusion is the contamination of sources of freshwater, such as aquifers, by saline water [1], [2]. It can be caused by human activities, such as the overuse of water, or by natural phenomena, such as storm surges [2]. No matter the cause, saltwater can have a large negative impact on coastal communities and the surrounding environment. It can render water unfit for human consumption, destroy freshwater ecosystems, and kill crops [2].

Because of the damage saltwater intrusion can cause, simple methods are needed for detecting and measuring it. Currently, a number of devices are available for measuring the salinity of water. One of the simplest and most wildly used methods is to determine the salinity from the electrical conductivity of the water sample [3], [4]. Salt ions dissolved in water act as charge carriers, causing the conductivity of the water to increase with salinity [5], [6]. Oceanographers have used electrical conductivity as the basis for determining salinity for the past 38 years [3].

A sensor developed for easily measuring saltwater intrusion is presented. The sensor is comprised of two planar electrodes integrated onto a printed circuit board (PCB). PCB

technology enables this sensor to be manufactured at high volumes for a modest cost. Furthermore, it takes little more than a day to manufacture these sensors. As a result, manufacturing the PCB sensors is much cheaper and quicker than similar devices based on traditional sensing technologies such as MEMS [5]. The use of a PCB also makes it simple to integrate electrical components or other sensors onto the device.

Instead of measuring conductivity directly, the PCB sensor measures the resistance between its electrodes when placed in the water sample. With knowledge of the sensor's cell constant and the measured resistance, the conductivity (and the salinity) can be determined. However, before the conductivity can be calculated, the cell constant of the sensor must be determined. The cell constant is independent of the conductivity of the water and is a result of the physical geometry of the sensor. While the physical structure of the PCB sensor makes it simple to manufacture and use, it also makes it difficult to calculate the cell constant. In practice, calculating the cell constant can be avoided by calibrating the sensors in a water sample with a known salt content. The salinities of other samples can then be inferred by comparing their measured resistances to the known point. However, this comparison would need to be done for every sensor with different electrode dimensions. By having a way of accurately determining the cell constant of the PCB sensor, the salinity can be determined from the measurements of a sensor with any electrode dimensions.

In this work, several PCB sensors with different electrode dimensions were tested in a variety of situations. First, the sensors were tested in water samples originating from a variety of locations, including seawater, freshwater from a lake and creek, and rainwater. Then, to observe the influence of salinity on the sensors' measurements, they were tested in water samples whose salt concentration were varied. To determine the influence the electrode's dimensions had on the

measurements, the sensor was simulated using two electromagnetic simulators for a variety of electrode dimensions.

The first goal of this work was to demonstrate that the PCB sensor can accurately measure the salinity of water as well as or better than commercial salinity sensors. The second goal was to use the testing and simulation results to develop an equation that can accurately determine the cell constant of the PCB sensor for any reasonable electrode dimensions. With this equation, the salinity of any water sample measured by the PCB sensor with any electrode dimensions could be determined. To accomplish the second goal, a genetic algorithm was used to generate an equation whose behavior best matched the results of the testing and simulation results.

Chapter 2

Background

The PCB sensor was developed as a simple and accurate way of detecting saltwater intrusion in sources of freshwater. In this chapter, an overview of both the causes and the effects of saltwater intrusion are provided. Next, the current standards used to quantify salinity are outlined. Finally, some of the more common methods for measuring salinity are described.

2.1 Saltwater Intrusion

Currently, nearly half of the world's population lives within 200 km of a coastline, and these communities are some of the fastest growing [1]. Despite being so close to major bodies of water (like in Figure 2.1), having sources of potable water is a major concern. Since seawater is too salty to drink or to be used in agriculture, coastal residents have turned to alternate sources of freshwater, such as freshwater aquifers. Aquifers are underground geologic formations saturated with water. They are comprised of areas of permeable materials (such as sand, sandstone, gravel, or limestone), which allow water to flow through easily. The water is usually confined to the aquifer by less permeable surrounding materials (such as slit and clay) [2]. Close to 50% of the U.S. population receives its water from aquifers [7].

Figure 2.1: Cape Cod National Seashore [2]

For many coastal communities, these aquifers are their only sources of freshwater. In 1995, 30 billion gallons of freshwater were used by the public, industry, and agriculture along the east coast of the United States every day. Of that 30 billion, 7.7 billion gallons came from groundwater [2]. Since then, water usage has increased due to an increase in population, industry, and tourism to and in these regions. Groundwater from these aquifers is also important to the environment along the coast. They are the source for freshwater streams, rivers, ponds, and wetlands.

Because of the reliance on freshwater aquifers and their proximity to the ocean, saltwater intrusion is a major concern for coastal communities. As the name suggests, saltwater intrusion is the contamination of sources of freshwater by saline water, and it can have negative effects on both humans and the environment [2], [7]. The most immediate concern for humans is that it renders water supplies non-potable, requiring costly alternatives such as transporting water from inland sources. Saltwater intrusion can also destroy freshwater ecosystems that rely on the water from aquifers. Saltwater will kill freshwater fish and plants, and the effects will move up the food chain. Like freshwater ecosystems, crops are also sensitive to saltwater [2]. Many far-

ranging water supplies are being contaminated by saltwater in the U.S., including those in Cape May County, New Jersey; southeastern Florida; and multiple counties in California [8].

The United States Geological Survey (USGS) defines saltwater as having a total dissolved-solids (TDS) concentration of greater than 1000 mg/L [2]. Usually a concentration of 2000 to 3000 mg/L is too salty for human consumption. For comparison, seawater has a concentration of 35,000 mg/L [2]. While a number of elements can be found in the seawater (some of which are listed in Table 2.1), the largest quantities and major concerns are the chloride and sodium ions. The EPA recommends that drinking water not have concentrations of sodium or sulfate greater than 250mg/L [2]. Since the concentrations of both are so high in seawater (19,000 mg/L for chloride and 10,500 mg/L of sodium), even a small amount of seawater will render a water supply unsuitable for public use.

Table 2.1: Average concentrations of major dissolved constituents of seawater [2]

Constituent	**Concentration (mg/L)**
Chloride	19,000
Sodium	10,500
Sulfate	2,700
Magnesium	1,350
Calcium	410
Potassium	390
Bicarbonate	142
Bromide	67
Strontium	8
Silica	6.4
Boron	4.5
Fluoride	1.3

Saltwater intrusion has several causes. The main cause is from overuse of freshwater aquifers by humans. Withdrawing too much water from an aquifer will disrupt the balance between freshwater and saltwater at transition zones. As shown on Figure 2.2, transition zones are areas along the coast where freshwater sources empty into the ocean and mix with the

saltwater [9]. When the freshwater is depleted, the outflow of freshwater decreases, causing these transition zones to move inland and the saltwater to contaminate the source. In short, as the amount of freshwater in the aquifers decreases, the pressure of the saltwater will push it into the aquifer where it will contaminate the aquifer, due to the higher density of the saltwater [1], [2]. A second manmade source of saltwater intrusion is pollution. Sewage, industrial waste, oil and gas production, and return flows from irrigation are all examples. Even the solvents used in road de-icing can be a cause [2].

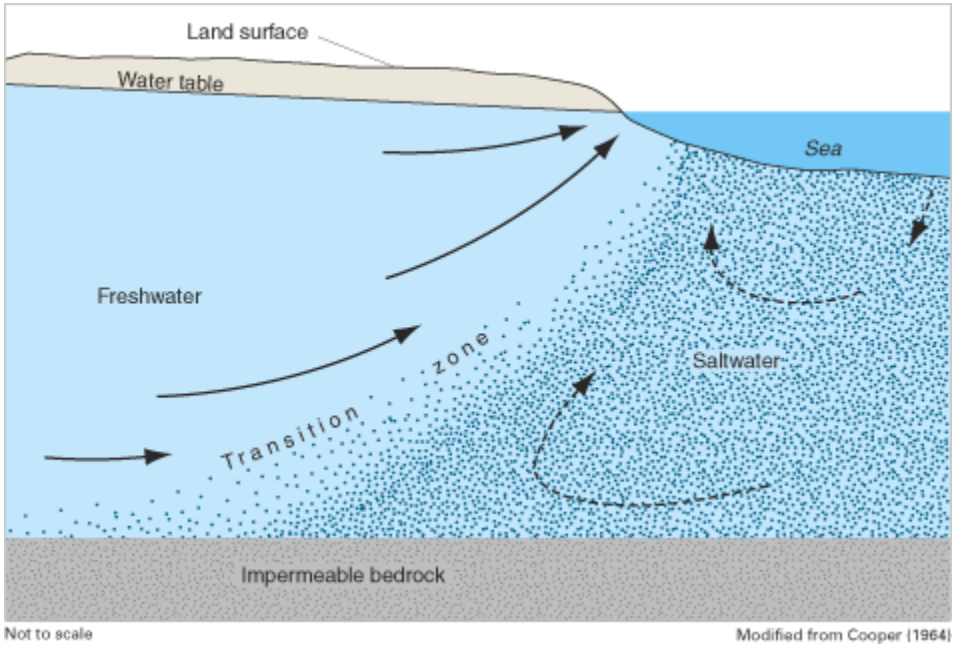

Figure 2.2: Example of the groundwater flow pattern and the transition zone in an aquifer [2]

Precipitation is a natural source of saltwater intrusion. Because of the salts present in the seawater, the atmosphere over the ocean is comprised of a large concentration of salt ions. While this concentration is much lower than the concentration in the seawater, it is still much greater than in the atmosphere inland. Precipitation along the coast will contain some of these salt ions. The rain water can then carry these salt ions into the freshwater sources in the area. Other natural sources of saltwater intrusion include the tides, storm surges, and sea-spray accumulation. Also,

previously trapped saltwater from previously isolated parts of an aquifer can seep in and contaminate the freshwater inside [2].

The extent of the saltwater intrusion depends on several factors. Some of these factors are the rate of water withdrawal compared to how quickly it is replenished, the distances of stresses (such as wells and drainage canals) from the source of the saltwater, and the physical structure and hydraulic properties of the aquifer [2]. The location of the well and the properties of the aquifer determine how soon a well could be affected by saltwater intrusion.

2.2 Measuring Salinity

Currently there are two commonly followed standards for classifying salinity. They are the Practical Salinity Scale (PSS-78) and the Thermodynamic Equation for Seawater (TEOS-2010). While the PSS-78 was replace with the TEOS-2010 in 2010, it is still heavy used.

2.2.1 The Practical Salinity Scale (PSS-78)

The Practical Salinity Scale (PSS-78) was adopted by the Joint Panel of Oceanographic Tables and Standards (JPOTS) in 1981 to define a consistent set of standards for determining various physical properties of water, such as the measured conductivity, temperature, and pressure [3]. Before the PSS-78, the Knudsen salinity scale expressed salinity in terms of chlorine, Cl [10]. This practice worked well until the development of high-precision conductivity sensors [10]. Since conductivity is affected by the presence of other ions besides chlorine, salinity measurements based on chlorine concentration and conductivity contradicted each other. PPS-78 was developed as a compromise in order to remove the ambiguity.

PSS-78 determines the salinity of a water sample based on its conductivity ratio. The conductivity ratio is the ratio between the measured conductivity and the conductivity of a potassium chloride (KCl) solution at 15°C and a pressure of one standard atmospheric pressure

(also referred to K_{15}). This KCl solution is a 1 kg solution containing 32.4356 grams of KCl [3]. By basing salinity on conductivity, all water samples with the same conductivity have the same salinity no matter their composition. Using PSS-78, salinity is represented as a unit-less quantity; however, to avoid confusion it is also referred to as Practical Salinity Units (PSU). Seawater typically has a conductivity of 35 PSU [10] [11].

In 1983, Fofonoff and Millard developed an algorithm to convert (among other things) conductivity to PSU and PSU to conductivity while compensating for temperature and pressure [3]. The algorithm is accurate from relatively low to high salinities (2 PSU to 42 PSU). A simplified form of the equation PSS-78 uses to determine salinity is shown below [10], [3], [11], [12].

$$S = a_0 + a_1 R_T^{1/2} + a_2 R_T + a_3 R_T^{3/2} + a_4 R_T^2 + a_5 R_T^{5/2} + \Delta S \qquad (2.1)$$

where

$$\Delta S = \frac{(T-15)}{1+k(T-15)}\left(b_0 + b_1 R_T^{1/2} + b_2 R_T + b_3 R_T^{3/2} + b_4 R_T^2 + b_5 R_T^{5/2}\right) \qquad (2.2)$$

In the equations, S is the practical salinity, R_T is the conductivity ratio, and T is the measurement temperature. The a, b, and k are all coefficients whose values are shown in Figure 2.3. When using these equations, the temperatures need to be modified. Because of the age of PSS-78, it assumes that all temperature measurements are taken using the International Practical Temperature Scale of 1968 (IPTS-68) [11]. However, the IPTS-68 has since been replaced with the IPTS-90. Temperatures measured using the IPTS-90 can be converted to temperatures in IPTS-68 by multiplying by 1.00024 [11]. Not compensating for the temperature difference leads to a very small error. Forfonoff and Millard also defined a second set of equations for compensating the conductivity ratio for high pressures; however, since all measurements in this work are done at a standard atmospheric pressure, these equations are not relevant.

$a_0 = 0.008$	$b_0 = 0.0005$
$a_1 = -0.1692$	$b_1 = -0.0056$
$a_2 = 25.3851$	$b_2 = -0.0066$
$a_3 = 14.0941$	$b_3 = -0.0375$
$a_4 = -7.0261$	$b_4 = 0.0636$
$a_5 = 2.7081$	$b_5 = -0.0144$
$k = 0.0162$	$-2°C < T < 35°C$

Figure 2.3: List of coefficient values used in PSS-78 [11]

While the PSS-78 was replaced in 2009, it is still used frequently in commercial applications today. In this work, a MATLAB script included in the Gibbs-SeaWater Oceanographic Toolbox is used to convert back and forth from PSU and conductivity [4]. The GSW was provided by the International Association for the Physical Sciences of the Oceans (IAPSO), the Intergovernmental Oceanographic Commission of UNESCO (IOC-UNESCO), and the Special Committee on Oceanic Research (SCOR). The goal of the toolbox is to provide a series of subroutines for evaluating the thermodynamic properties of pure water [13].

2.2.2 The Thermodynamic Equation of Seawater (TEOS-10)

In 2009, PSS-78 was replaced by the Intergovernmental Oceanographic Commission with the Thermodynamic Equation of Seawater (TEOS-10) [13]. The new standard uses a Gibbs function for determining the thermodynamic properties of seawater, including density, sound speed, heat capacity, enthalpy, and entropy. Salinities calculated using the TEOS-10 standard are referred to as Absolute Salinities and are reported in units of g/kg, g/L, or parts-per-thousand (ppt). Absolute Salinity is the mass fraction of inorganic materials dissolved in Standard Seawater (SSW) with the same density as the sample of water being tested [13], [14], [15]. SSW is seawater with a certain composition that is used as a reference for TEOS-10 [15]. In a

laboratory setting, seawater samples are converted into SSW by adding pure water or by removing pure water through evaporation [15]. By definition, the Absolute Salinity can be calculated by summing of the inorganic materials in the solution. A simplified representation of this process is

$$S_A = \sum_{i=1}^{N} c_i M_i \tag{2.3}$$

where N is the number of constituents, c_i is the concentration (in mol/kg) and M_i is the molar mass (in g/mol) [14] [15]. In practice, determining Absolute Salinity using this process is difficult since other properties such as temperature need to be accounted for [14]. Instead, for seawater in the Neptunian range (temperatures between -2°C to 35°C and Absolute Salinities between 2 and 42 ppt) the salinity can be calculated using

$$S_R = u_{PS} \times S_P(R, t_{68}, p) \tag{2.4}$$

where S_R is the Relative Salinity, u_{ps} is a correction factor, and S_P is the Practical Salinity calculated using PSS-78 at the measurement temperature (using IPTS-68) and pressure [14]. The correction factor is equal to 35.16504/35 g/kg, and it puts the measured salinity in terms of the reference SSW. The Relative Salinity is the mass fraction of solute dissolved in SSW with the same conductivity as the sample being measured [15]. It is considered the best available approximation of the mass fraction of the solution [15]. For seawater with the same composition as SSW, the Relative and Absolute Salinities are equal [14], [15]. For seawaters, the salinities can be different since the different constituents can have varying effects on the conductivity and density. In this work, all measurements done using TEOS-10 were first converted to the PSS-78 standard using (2.4), and then the PSS-78 algorithm was used to calculate the conductivity.

2.3 Types of Salinity Meters

Currently a number of techniques are available for measuring the salt content of water. The most common include the use of a hydrometer, a refractometer, or a conductivity sensor. In the following sections, how each type is used to measure salinity is discussed.

2.3.1 Hydrometers

Hydrometers (like the one shown in Figure 2.4) measure the specific gravity of a liquid. A hydrometer is comprised of a clear plastic or glass container with a pointer. To measure the specific gravity, the liquid is poured into the hydrometer. Depending on the density of the liquid, the pointer will either rise or sink [16]. The denser the liquid, the higher the pointer will rise due to its buoyancy. Most hydrometers have a scale printed on them so that the specific gravity of the liquid can be determined easily from the pointer's position. The salinity in water can then be determined from the specific gravity.

Figure 2.4: The Instant Ocean SeaTest Hydrometer

Specific gravity is a dimensionless unit, defined as the ratio of the density of a substance versus the density of pure water [12]. Specific gravity can be calculated as

$$Specific\ Gravity = \frac{\rho_s T_s}{\rho_0 T_0} \tag{2.5}$$

where ρ_s is the density of the sample, T_s is the temperature of the sample is degrees Celsius, ρ_0 is the density of pure water, and T_0 is the temperature the pure water in degrees Celsius when it has a density of ρ_s [17]. Pure water has a density of one gram per centimeter, resulting in a specific gravity of 1.000. For contrast, seawater has a specific gravity of 1.025. The specific gravity of a sample of water can be used to determine the salinity because adding salt increases the density of the solution.

While they are conceptually fairly simple, hydrometers have some drawbacks. Since they are measuring density, they can be very sensitive to temperature. Because the scale on the hydrometer is calibrated at a specific temperature, any slight difference in temperature will affect the hydrometer's accuracy. To demonstrate the effect temperature has on a hydrometer, Figure 2.5 shows a plot of the specific gravity versus the salinity of a water sample measured at 5°C (in blue) compared to plot of the specific gravity versus the salinity of a water sample measured at 35°C (in black) [17]. The specific gravity measurements have been multiplied by 1000. The figure demonstrates that for the same specific gravity, the salinity of the water at 5ºC would be around 8 to 10 PSU smaller than the sample at 35 ºC [17]. Very expensive glass hydrometers are able to compensate for temperature differences, but they are delicate and difficult to use [18].

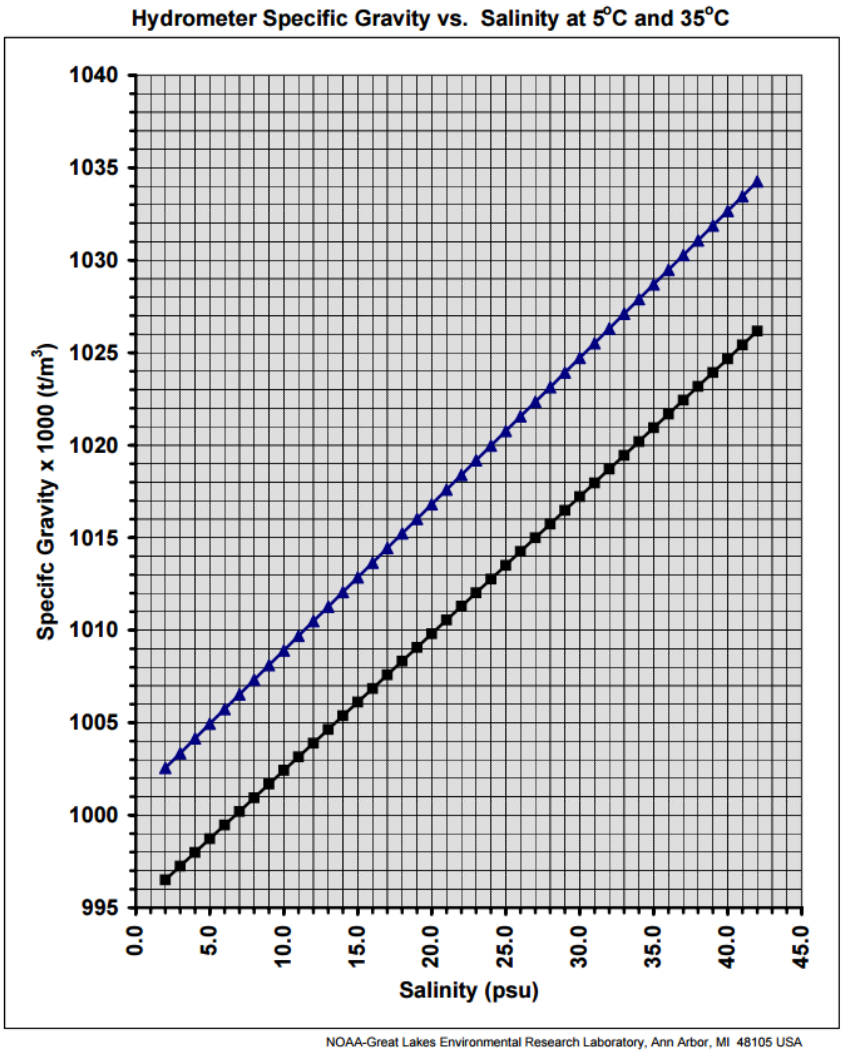

Figure 2.5: Comparison of a hydrometer's measurements at 5°C and 35°C [17]

2.3.2 Refractometers

A refractometer, like the MA887 shown in Figure 2.6, can be used to measure the properties of a material by directly measuring its index of refraction [19]. A material's index of refraction is related to the optical characteristics of the medium, the number of dissolved particles in the medium, the wavelength of the light, and the temperature [19], [20]. Because the index of refraction of water is a function of the number of dissolved particles, a refractometer can be used to determine the salinity of water.

Figure 2.6: The MA887-BOX Digital Refractometer

The index of refraction is a comparison between of the speed of light in a vacuum with the speed of light in the medium. Equation (2.6) can be used to calculate the index of refraction, where n is the index of refraction, v is the speed of light in the medium, and c is the speed of light in a vacuum [21].

$$n = \frac{c}{v} \tag{2.6}$$

When light encounters an interface between two mediums, some of the light will be reflected back into the original medium, and some will be transmitted into the new medium. How much of the light that is reflected and transmitted depends on the angle that the incident light strikes the interface and the index of refraction of the two mediums. When the light strikes the interface at an angle, the transmitted light will bend (or refract). If the original medium has a higher index of refraction than the new medium, the angle of the transmitted wave will be much greater than the angle of the incident wave.

Figure 2.7 shows the impact increasing the incident angle has on the angle of the refracted light. In Case A, the angle of incidence is very small, while the angle of refraction is larger. In Case B, the angle of incidence is large enough that the refracted light is parallel to the interface. The incident angle in this case is referred to as the critical angle. When the angle of incidence becomes greater than the critical angle, as in Case C, none of the light is transmitted into the second medium. Instead, all of the light is reflected back into the original medium.

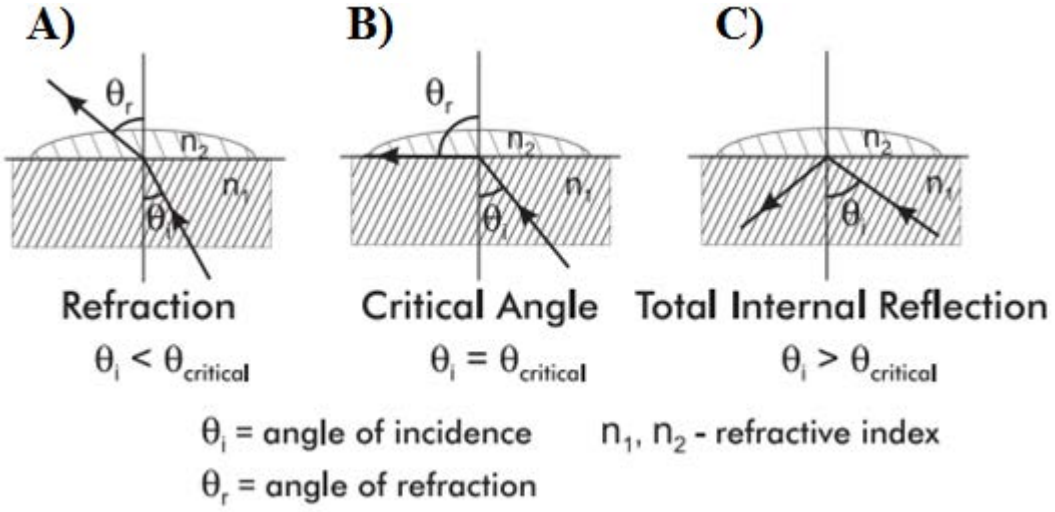

Figure 2.7: Example of how the angle of incidence affects the angle of refraction [19]

Snell's Law of Refraction demonstrates how to calculate the angle of refraction:

$$\frac{n_1}{n_2} = \frac{\sin(\theta_r)}{\sin(\theta_i)} \tag{2.7}$$

In the equation, n_1 is the index of refraction of the original medium, n_2 is the index of refraction of the second medium, θ_i is the angle of incidence, and θ_r is the angle of refraction [21]. When the angle of incidence is equal to the critical angle, Snell's Law can be solved for the critical angle, giving:

$$(\theta_i)_{critical} = \sin^{-1}(\frac{n_2}{n_1}) \tag{2.8}$$

Figure 2.8 shows how the reflectometer measures the index of refraction of a sample of water. First, the water is placed in the sample well. Directly underneath the water is a prism. An LED shines light through the prism, causing the light to disperse. The dispersed light will then strike the interface between the prism and the water sample at multiple angles. Depending on the angle it strikes the interface and the properties of the water, some of the light will be transmitted into the liquid, and some will be reflected back into the prism. All of the light that strikes the interface at an angle greater than or equal to the critical angle will be reflected back into the prism. The reflected light will then exit the prism and strike the light sensor. The light sensor can then find the critical angle by measuring where the intensity of the light decreases over the sensor's area. Since the prism's index of refraction is already known, Snell's Law can be used to calculate the water's index of refraction. The refractometer can then determine the salinity of the liquid based on a lookup table.

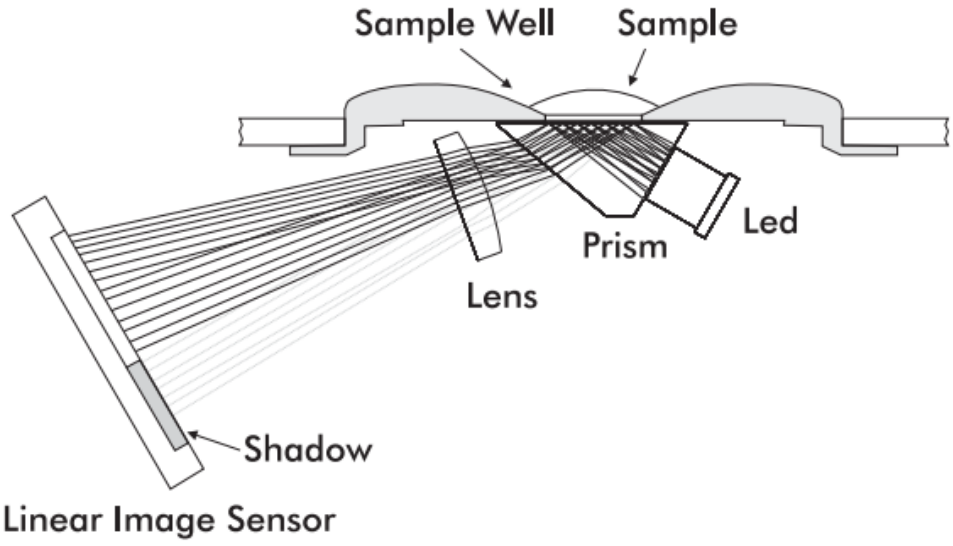

Figure 2.8: The MA887 refractometer's method for measuring the index of refraction of a sample of water [19]

2.3.3 Conductivity sensors

The salinity of water is commonly determined by measuring its electrical conductivity. To determine the conductivity, the sensor measures the water's resistance. Since the resistance is inversely proportional to the conductivity, knowing the resistance of the water makes it possible to find to its conductivity. Since the conductivity of water is directly related to its salinity, conductivity is a good indicator of salinity [1], [6]. The conductivity of water with very dilute concentrations (much lower than seawater) is the sum of concentrations of each ion in the solution [6], [22]. The conductivity can then be calculated as

$$\sigma = \sum_n \lambda_n C_n \tag{2.9}$$

where σ is the electrical conductivity of the water, λ_n is the ionic conductivity of the n-th ion type, and C_n is the molar concentration of the n-th ion type. At high concentrations, this equation will no longer hold because ions will interact with each other, and molar conductivity is no longer proportional to the concentration [6].

Two types of conductivity sensors are inductive sensors and contact sensors [22], [23]. Inductive sensors (also called toroidal sensors) are usually comprised of a pair of coaxial toroidal transformers that are sealed in a nonconductive housing [22]. One transformer induces a current in the water. The current is then measured by the second transformer. The magnitude of the current is proportional to the conductivity of the water [22]. An example of this setup is shown in Figure 2.9. The transformers allow the sensor to avoid having to make physical contact with water, greatly improving its long-term stability. The lack of physical contact with water ensures that inductive sensors do not suffer from electrode polarization (discussed in detail below) or become contaminated or damaged due to prolonged exposure to water (referred to as fouling) [6], [22], [23]. Despite this advantage, inductive sensors have the disadvantage of not being

accurate for measuring low conductivities. Therefore, they are not ideal for measuring anything that does not have a high salt content. Also, their accuracy is affected by proximity effects and changes in the permeability of the transformers' cores due to changes in temperature and pressure on the transformer [23].

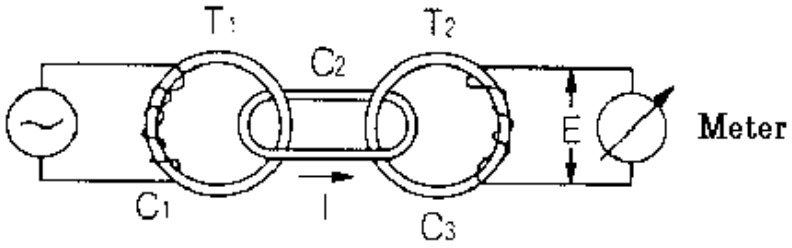

Figure 2.9: Basic setup of an inductive conductivity sensor [24]

Contact conductivity sensors are usually much simpler and more sensitive than inductive sensors. Instead of relying on a transformer to take measurements, contact sensors use electrodes. As the name implies, contact sensors make direct contact with the material they are measuring. Contact sensors measure the conductivity of a material by directly measuring the resistance of the material when placed between the sensor's electrodes and then deriving the conductivity based on knowledge of the physical geometry of the sensor and its surroundings. Because they have to make direct contact with the water, contact sensors are sensitive to electrode polarization and fouling. The effects of both problems can be reduced with a proper design.

Most contact conductivity sensors are comprised of either two or four electrodes. Two-electrode sensors are the simplest and most common but are more sensitive to electrode polarization and fouling [6]. To take measurements, the two electrodes are used for both excitation current injection and voltage sensing (Figure 2.10a). Four-electrode sensors are designed to be much less sensitive to electrode polarization and fouling but are more complicated to use. To make measurements, two of the sensor's electrodes are used for current injection,

while the other two are used for voltage sensing (Figure 2.10b). Using either configuration, the sensor will directly measure the resistance of the medium. The conductivity can then be determined from the measured resistance by taking into account the physical geometry of the measurement setup. The physical geometry is referred to as the cell constant [25]. By design, it is a known quantity and constant for all conductivities. Cell constants are discussed in more detail in Section 3.2.

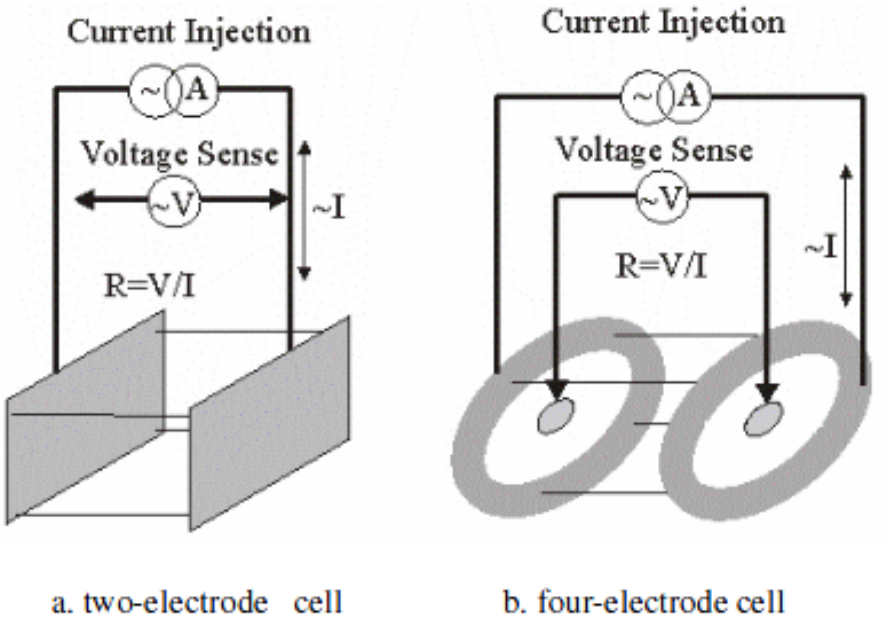

Figure 2.10: Two and four-electrode contact conductivity sensors [6]

Chapter 3

The Two-Electrode Contact PCB Conductivity Sensor

To help coastal communities measure the amount of saltwater intrusion in their water supplies, the planar PCB salinity sensor shown in Figure 3.1 was developed [5]. The design of the sensor is fairly simple and is one of its advantages. It is comprised of two planar, rectangular electrodes on a printed circuit board (or PCB). It is a two-electrode contact conductivity sensor similar to those described in the previous section.

Figure 3.1: The original PCB salinity sensor

The sensor's electrodes are 420 mil long and 120 mil wide. The edges of the electrodes are covered by a non-conducting solder mask. A 400 mil by 100 mil solder mask window was left open over the electrodes (in metric this is 10.16 mm by 2.54 mm). The solder mask instructions for the sensor are shown in Figure 3.2. For the rest of this work, the size of the

electrodes is referred to as being 10 mm by 2.5 mm for simplicity. The sensors' electrodes are separated by 2.54 mm. Two copper traces connect the sensing electrodes to header pins on the other end of the board. The header pins connect the electronics used to measure the resistance. For testing, a table top ohmmeter, such as the Gwinstek LCR-821, was used. In practice, the sensing electronics would be integrated onto the PCB.

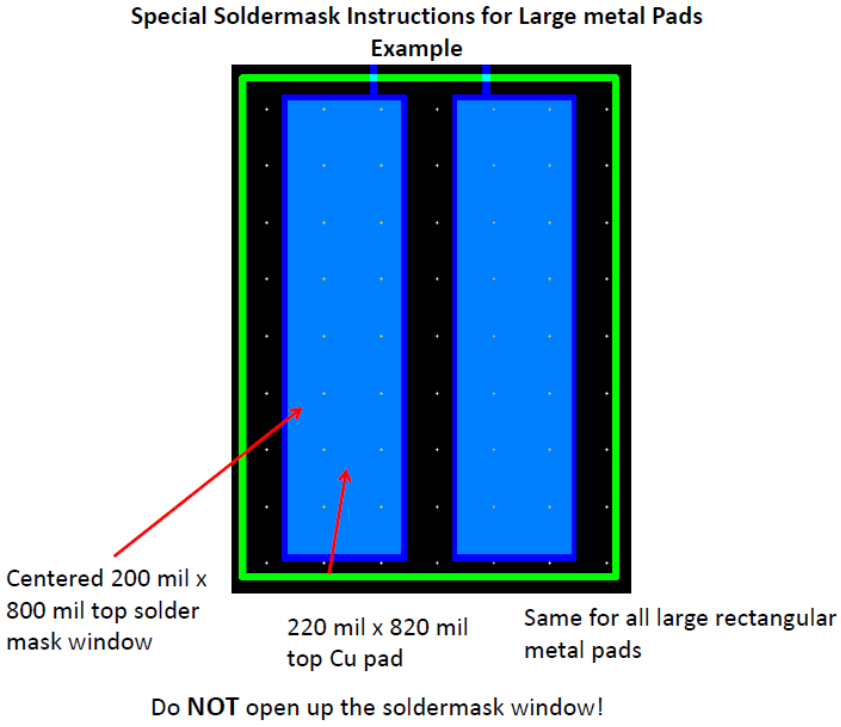

Figure 3.2: Solder mask instructions for the original PCB sensor

The sensor's PCB is a single layer board. It is 97.45mm long, 15.4mm wide, and 1.64mm thick. Besides the copper traces and electrodes, the PCB is comprised of an FR-4 substrate. The front and back of surfaces of the PCB are covered in a solder mask, except on the bare electrodes. The sensor's electrodes are comprised of a copper foil and plated with a tin surface finish to prevent oxidation. The manufacturing process was a low-cost commercial, 2-layer printed circuit board process.

Midway through this work a new set of PCB sensors was designed and constructed. These sensors were nearly the same as the originals, except that the size of their electrodes was 20.32 mm by 5.08 mm, making their area four times larger than the originals'. An example of the new design is shown in Figure 3.3. The reason for this increase in size was to decrease the impact electrode polarization had on the sensor's measurements. As mentioned in Section 4.4.3, the impact of electrode polarization decreases as the size of the electrodes increases [6], [25]. For testing, three of the new PCB sensors were gold-plated (shown in Figure 3.4). The gold plating should protect the electrode from the elements better than the tin plating on the original sensors. The goal was to see if the performance of the gold-plated sensors improved enough to justify the increase in cost. Testing did not show much difference in the performance in the plated and non-plated sensors, other than the gold-plated sensors measured a slightly higher resistance than the non-gold plated. Because there was not much difference, it was concluded that the gold-plating was not worth the increased cost.

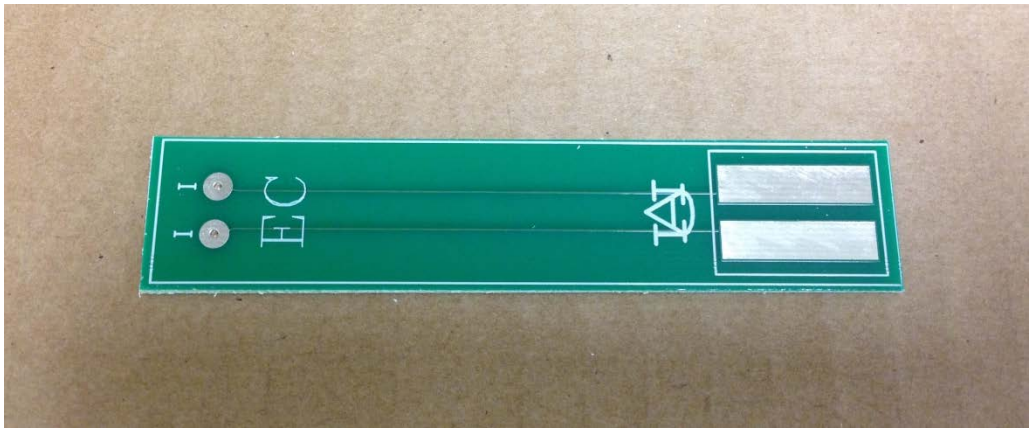

Figure 3.3: The new PCB sensor design

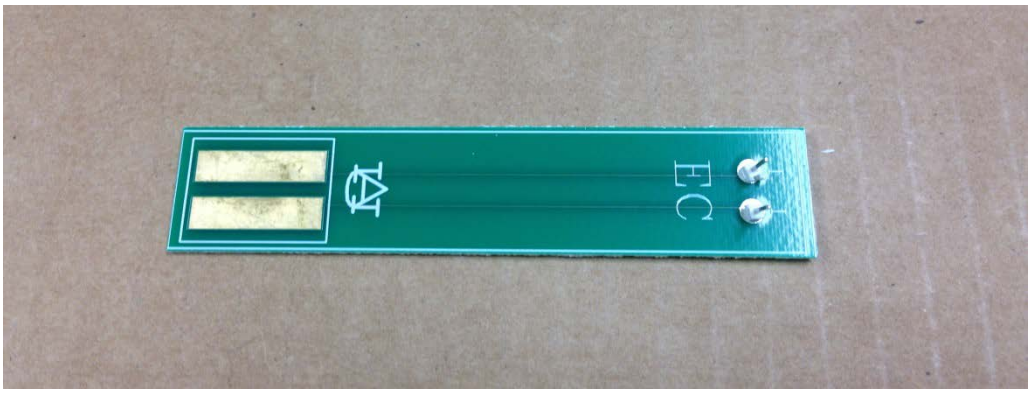

Figure 3.4: The gold-plated new PCB sensors

As mentioned in the previously, two-electrode contact conductivity sensors determine the salinity of water by measuring the electrical conductivity and determine conductivity by measuring the resistance between the two electrodes. Since resistance is inversely proportional to the conductivity, knowing the resistance of the material between the electrodes (the water) makes it possible to find to its conductivity using the electrode geometry. Once the conductivity is known, the salinity of the water can be determined using the PSS-78 algorithm. However, unless the exact salinity is desired, determining the conductivity and salinity is not required. The main goal for the PCB sensors is to detect saltwater intrusion and not measure the salinity. Therefore, the PCB sensors can instead be calibrated by measuring the resistance of water with a known salinity. Then the salinity of any sample of water can be determined by comparing its measured resistance to the resistance measured for the reference sample of water.

In practice, the user would place the half of the sensor with the electrodes into the water, while leaving the headers above the water (shown in Figure 3.5). While the sensor is in the water, a meter is used to find the resistance between the sensor's electrodes. During testing, a tabletop meter was used to take the resistance measurements. In practice, the measurement

electronics would be integrated onto the sensor's PCB. Once the measurements are complete, the sensor is removed from the sample and cleaned using tap water.

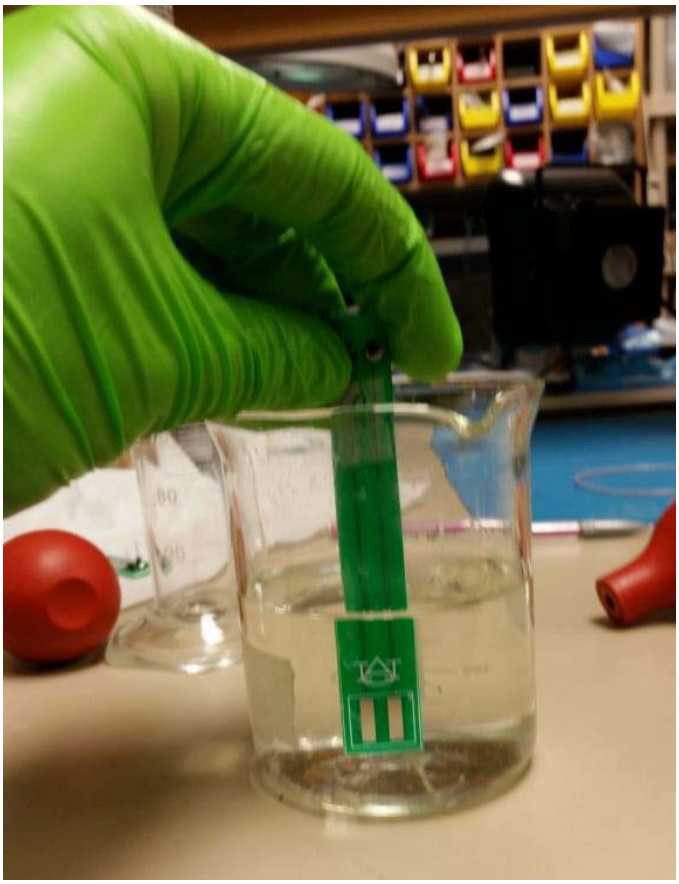

Figure 3.5: Example of the PCB sensor in use

Having the sensor on a PCB gives it a number of advantages. PCB technology makes it simple to fabricate a large number of sensors at once on a single panel (shown in Figure 3.6). Batch PCB fabrication is also much cheaper than producing each sensor individually. The inherent cost of PCB technology is much lower than other manufacturing techniques such as MEMS [5], [26], [27]. Another advantage is that since the sensor is already on a PCB, it is simple to integrate sensing electronics onto the same board [28], [29].

Figure 3.6: A panel of PCB sensors

While having the sensor on a PCB simplifies the design and production of the sensor, it comes with the tradeoff of making it harder to model the sensor's electrical behavior. To show the difficulty of this problem, the operation of a two-electrode contact conductivity sensor needs to be fully explained. As mentioned above, contact conductivity sensors measure the conductivity of a material by directly measuring the resistance of the material. However, resistance is a function of not only the conductivity of the material but also of the electrode geometry and the physical area being probed. Therefore, to find the conductivity from the resistance, the effects of the physical dimensions need to be determined [6].

3.1 Basic Setup for Measuring Resistance

The basic setup for experimentally measuring the resistance of a material is to take a cubic or cylindrical slab of the material to be tested and place it between two parallel electrodes (Figure 3.7). The top and bottom parts of the slab have the same surface area and shape as the electrodes. A voltage difference (V_0) is applied to the electrodes, and the current is measured.

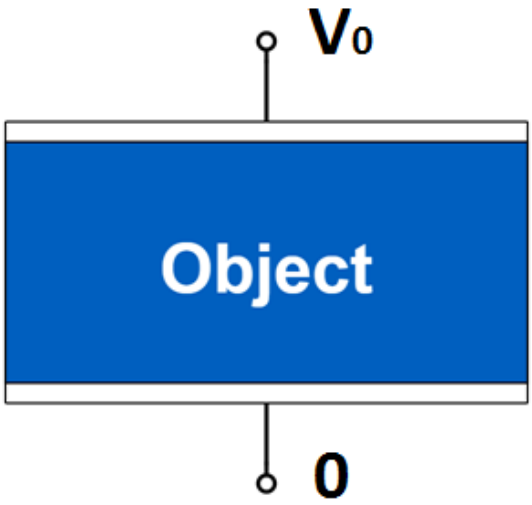

Figure 3.7: Basic setup for measuring resistance (where the blue rectangle is the object under test and the white bars are the conductors)

If the material is a conductor, it is straight forward to derive the solution for calculating the resistance [21], [30], [31]. To begin, Poisson's equation can be used to derive an expression for potential within the material. Poisson's Equation can be written as

$$\nabla^2 V = -\frac{\rho}{\varepsilon} \tag{3.1}$$

where V is the potential, ρ is the charge density in the area of interest, and ε is the dielectric permittivity of the material (which for a perfect conductor is 8.854×10^{-12} F/m). Since the charge density is zero, the Poisson's equation becomes Laplace's equation.

$$\nabla^2 V = 0 \tag{3.2}$$

For simplicity, V is assumed to be changing only over the x direction. From the Laplace's equation the potential can be found.

$$\frac{d^2 V}{dx^2} = 0 \tag{3.3}$$

$$V(x) = C_1 x + C_2 \tag{3.4}$$

In the equation, C_1 and C_2 are constants and can be calculated from the boundary conditions. For this situation, assume that the bottom electrode is at x = 0, with a potential of 0 V, and the top electrode is at x = d, with a potential of V_0. The constants can be calculated to be

$$V(0) = C_1 * 0 + C_2 = 0 \tag{3.5}$$

$$C_2 = 0 \tag{3.6}$$

$$V(d) = C_1 * d = V_0 \tag{3.7}$$

$$C_1 = \frac{V_0}{d} \tag{3.8}$$

Inserting the values in for the constants gives

$$V(x) = \frac{V_0}{d} x \tag{3.9}$$

From the potential, the electric field can be determined as

$$\boldsymbol{E} = -\nabla V = -\frac{dV}{dx} = -\frac{V_0}{d}\boldsymbol{a}_x \tag{3.10}$$

From the electric field, the current density and the current can be determined.

$$\boldsymbol{J} = \sigma \boldsymbol{E} = -\sigma \frac{V_0}{D}\boldsymbol{a}_x \tag{3.11}$$

$$I = \int \boldsymbol{J} \cdot d\boldsymbol{S} = \int -\sigma \frac{V_0}{d}\boldsymbol{a}_x \cdot -\boldsymbol{a}_x dS = \frac{\sigma A V_0}{d} \tag{3.12}$$

The resistance can then be determined from the potential and the current using Ohm's Law.

$$R = \frac{d}{\sigma * A} \tag{3.13}$$

In (3.13), d is the distance between the electrodes, A is the area between the electrodes, and σ is the conductivity of the material.

It is straight-forward to calculate the resistance of this setup because the electric field is uniform and confined to the volume of the conductor. Since the object is a conductor and the surrounding area is free space, the current density, $\boldsymbol{J}$, perpendicular to the sides of the object not touching the electrodes is zero or

$$\boldsymbol{J} \cdot \hat{\boldsymbol{n}} = 0 \tag{3.14}$$

The electric field is equal to the current density multiplied by the conductivity of the medium, meaning the electric field perpendicular to the object's sides (in this case the electric field in the y and z-directions) is also zero [30].

$$\boldsymbol{E} \cdot \hat{\boldsymbol{n}} = 0 \tag{3.15}$$

With no electric field perpendicular to the sides of the object, all of the electric field must instead be perpendicular to the electrodes (in the x-direction). Because the electric field is not changing in the transverse and normal directions, it must be uniform throughout the object.

Figure 3.7 shows a cross-section of the electric field distribution of this setup. The blue bars are the electrodes. The volume between the bars represents the magnitude of the electric field. As shown, the electric field is uniform throughout the object, as evidenced by the same color throughout.

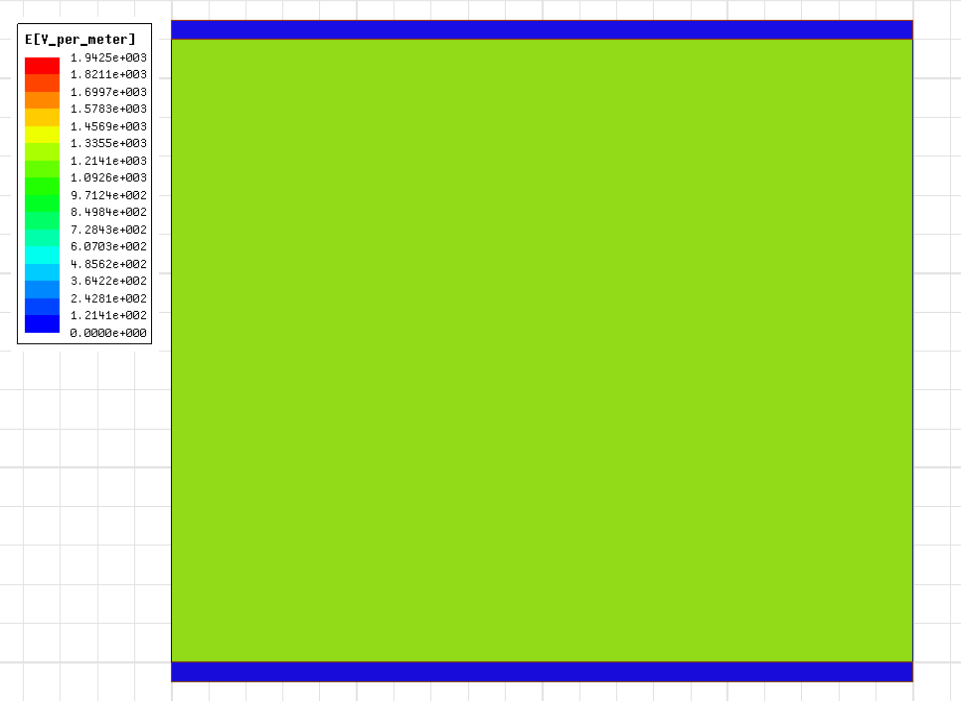

Figure 3.8: Electric field distribution for simple setup

3.2 The Cell Constant

The conductivity can be found be solving (3.16) for the conductivity. This gives

$$\sigma = \frac{d}{R * A} \tag{3.16}$$

A more generalized version of the equation is

$$\sigma = \frac{\kappa}{R} \tag{3.17}$$

where κ is the cell constant (measured in units of m^{-1}) of the region. The cell constant is related to the geometry of the region being measured (or really the distribution of the electric field caused by the positioning and shape of the electrodes and the geometry of the region) [6], [25] [32]. In the simple setup, the electric field is uniform; however, if the setup is changed slightly (such as the position of the electrodes or shape of the object), the electric field will become non-

uniform. Without a uniform electric field, calculating the cell constant becomes difficult. Many contact sensors are designed in such a way as to make finding the cell constant simple.

Unlike in the original setup, the electrodes on the sensor are in the same plane instead of being parallel to each other. The test material is no longer confined to a small volume between the electrodes; instead it can extend a large distance away from the electrodes. The sensor's setup allows the electric field from the electrodes to spread out in all directions, causing it to no longer be uniform. This non-uniform electric field makes it difficult to mathematically derive an equation describing the measured resistance [30].

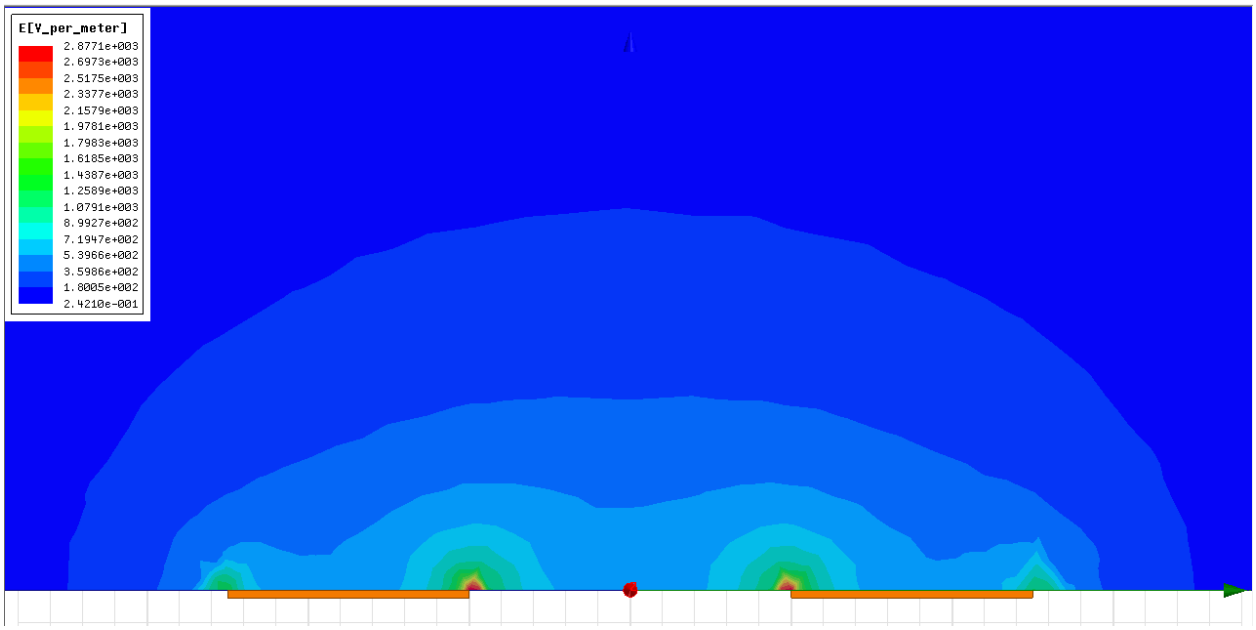

Figure 3.9: Electric field distribution of the planar PCB salinity sensor

Chapter 4

Modeling and Simulation

4.1 Overview of Electromagnetic Simulators and Numerical Methods

To gain an understanding of its behavior, the sensor was simulated using two separate electromagnetic simulators. Textbook electromagnetic problems can be usually be solved with a thorough understanding of calculus and Maxwell's equations. In reality, such problems become so complicated that it is, at best, impractical to solve them by hand. Instead, EM simulators have been developed to solve complex electromagnetic problems using a computer. The same process can also be used to simulate other phenomena such as thermodynamics.

While multiple simulators are currently on the market, most follow the same basic process. First, the model of the object to be simulated is created in the simulator's design environment using its CAD (computer-aided design) tools (example shown in Figure 4.1). In this step, the object's physical structure is built, and its materials are assigned. Second, the parameters of the EM simulation are set. In this step, the space around the object, the simulation domain, is defined. Usually, it is uniform and has the electromagnetic properties of free space (relative permittivity of 1, relative permeability of 1 and electrical conductivity of 0 S/m). The simulation domain is not infinite; instead its extent is defined by the user. Boundary conditions describing the properties outside the domain are applied at the edges. For example, the simulation could assume the electric and magnetic fields are zero at the boundary.

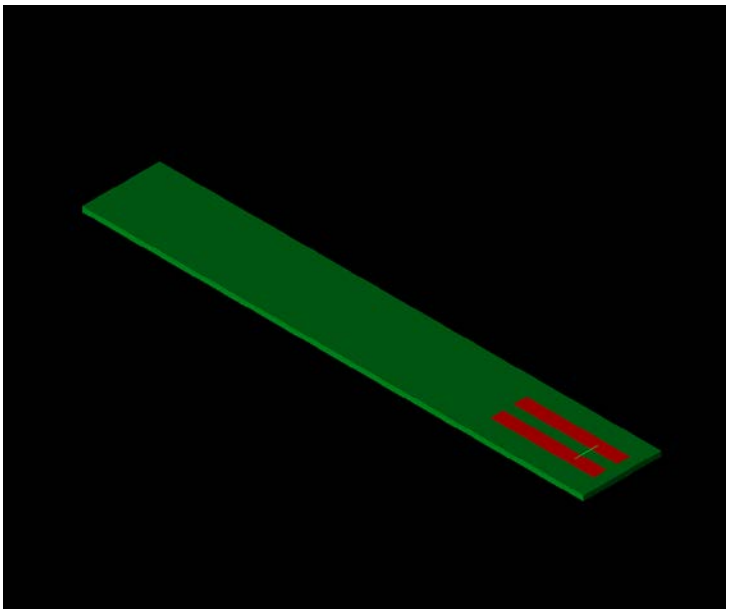

Figure 4.1: Example of the sensor modeled in EMPro's design environment

Third, the EM simulation is performed. Major differences between EM simulators become evident in this step. The primary difference is the numerical methods used to solve Maxwell's equations. Usually, the simulator will divide the simulation domain into cells and then will approximate the electromagnetic fields of each cell. The ways the domain is divided and the fields are solved depend on the techniques used. Once a solution is found, the simulator will repeat the process with smaller cells. It will then compare the percent difference between the two solutions. If the solutions are within a certain percentage of each other, the simulator will move on to the fourth step. Otherwise it will repeat the process.

Fourth, the properties of interest (such as the S-parameter, Far Field Radiation Pattern, and power loss) are calculated. The finite difference method (FDM), finite element method (FEM), method of moments (MoM), and the finite-difference time-domain (FDTD) method are the most common techniques.

4.1.1 Finite Difference Method

Of the numerical techniques mentioned, the finite difference method is the simplest and the easiest to implement. The FDM is a 3D field solver and is, therefore, used to find a field quantity based of the properties of the simulated object, and the boundary conditions are applied to the simulation domain [33].

The simulation domain is broken up into discrete nodes, which together are called a mesh (shown in Figure 4.2). The number of nodes depends on the size of the object being simulated and the desired accuracy. Usually greater accuracy requires a greater number of nodes. The larger the number of nodes, the longer the time required to complete the simulation. The nodes generated with the FDM are regularly spaced across the simulation domain, generating a rectangular mesh. This regularity makes the FDM the easiest method to implement, but it has two drawbacks. First, this method can generate more nodes than are required in uniform areas, increasing simulation time. Second, since the mesh cells generated by this technique are rectangular in shape, the mesh cannot conform to curved shapes, such as cylindrical or spherical boundaries [33].

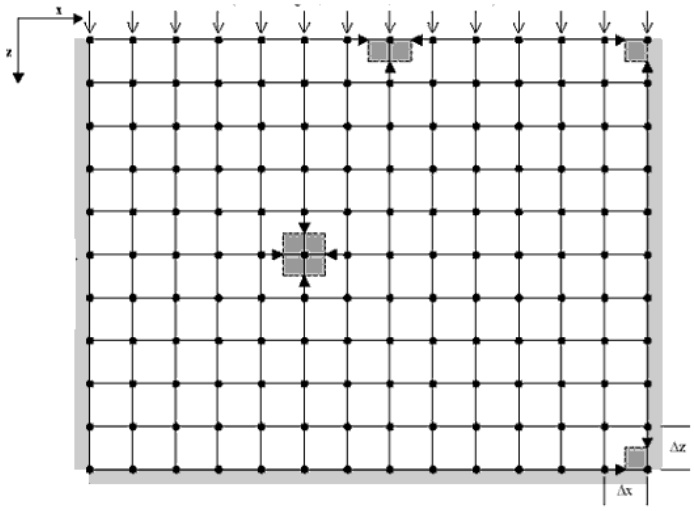

Figure 4.2: An example of the rectangular mesh generated using the FDM [34]

Once the mesh is generated, the differential forms of the appropriate Maxwell's equations for the given problem are converted to finite-difference approximations over the mesh [33]. Next, the correct boundary conditions are applied to the simulation. Then the finite-difference equations are solved over the entire simulation space.

4.1.2 Finite Element Method

The finite element method is similar to the finite difference method. The FEM is a 3D field solver that can be used to analyze irregularly shaped geometries [35]. It solves geometrically complicated EM problems by breaking the domain into a collection of smaller cells and approximating the fields in each cell. Like the FDM, the FEM will first break down the simulation space into nodes. Unlike in the FDM, the nodes are not regularly distributed. Instead, the location of the nodes is based on the energy distribution [33]. The mesh will usually be comprised of tetrahedral mesh cells, with a much denser mesh around the object being simulated [35]. An example of a mesh generated using the FEM is shown in Figure 4.3. Note that the density of the mesh increases the closer it is to the electrode.

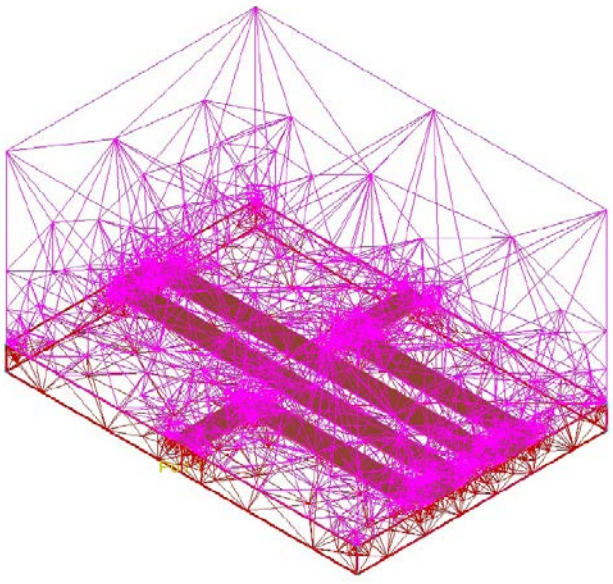

Figure 4.3: Example of a mesh generated using the FEM [35]

The rest of the process is nearly the same as the FDM. After the mesh is generated, the fields are approximated over each mesh cell as the sum of an expansion function with unknown coefficients, generating a sparse matrix. The matrix can be solved to find the unknown coefficients [35]. The biggest advantage of the FEM is that it can easily handle complicated geometries and inhomogeneous domains. Compared to the other methods described, the FEM is considered the most flexible computational technique since it can be used to simulate most arbitrary 3D geometries. The drawback is that for geometrically complex or large structures, the generated mesh can be very complex and comprised of many nodes. Very large meshes will increase the time required for the computer to solve, making the FEM less efficient than other numerical techniques that specialize in specific situations [35].

4.1.3 Method of Moments

The method of moments is another commonly used numerical technique used in computational EM. The MoM is referred to as a 3D planar solver because it is best used for solving structures that are uniform in one direction or a layered stack up of planar objects [35]. Like most other numerical techniques used in computational EM, a MoM simulator will first generate a mesh. Unlike the other techniques, the mesh will cover only the metal interconnects in the structure. An example of a mesh generated using the MoM is shown in Figure 4.4.

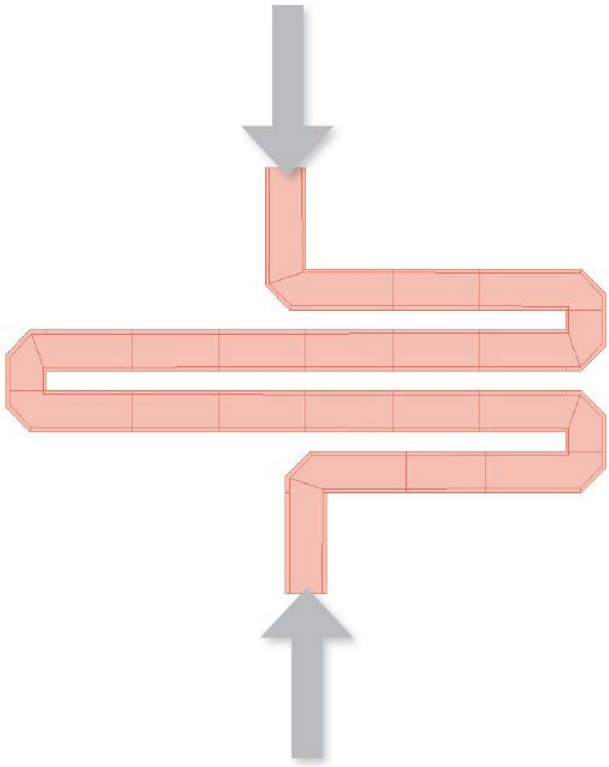

Figure 4.4: Example of a mesh generated by the MoM [35]

In the MoM, the main unknown is the current distribution. An efficient mesh generated with the MoM should be conformal over the metal interconnects and is comprised of rectangular or triangular shaped cells [35]. Generating a mesh only over the metal interconnects reduces the number of mesh cells, decreasing the amount of time needed to generate a solution. The MoM works well in situations where the object is either planar, comprised of a layered stack up (such as a multilayer PCB) or uniform in one dimension [35]. In situations where the simulator is able to generate conformal mesh, the MoM is much more efficient than other techniques like the FEM. Conversely, in situations with an irregular geometry, the MoM is much less efficient than the FEM. Once the mesh is generated, the current density of each cell will be solved by evaluating Green's Function and the coupling integrals [36].

4.1.4 Finite Difference Time Domain

Another commonly used technique is the finite-difference time-domain method. FDTD is another 3D field solver that can be used to analyze arbitrarily shaped structures. Unlike the other methods described, the FDTD uses a finite difference discretization of Maxwell's curl equations in time and space in its analysis [33]. The equations are

$$\nabla \times \boldsymbol{E} = -\mu \frac{\partial \boldsymbol{H}}{\partial t} \tag{4.1}$$

$$\nabla \times \boldsymbol{H} = \varepsilon \frac{\partial \boldsymbol{E}}{\partial t} \tag{4.2}$$

where E is the electric field, H is the magnetic field intensity, μ is the magnetic permeability, and ε is the dielectric permittivity.

Like the other techniques, FDTD starts by breaking the object and the simulation domain around it into nodes. In FDTD, the nodes are usually organized into hexahedral mesh cells called "Yee cells" (shown in Figure 4.5) [33]. Once the mesh is generated, the solver uses a time-stepping algorithm to simulate each mesh cell as an electromagnetic wave propagates through the domain [35]. One benefit of FDTD is that it requires much less memory than the FEM when the problem is very large because it does not need to solve a matrix. It is also easy to run a FDTD in parallel, speeding up the simulation. The main disadvantage of FDTD is that, unlike the FEM and MoM, it can only simulate one port at a time. When a design has multiple ports, each port would need to be simulated separately, increasing the simulation time [35].

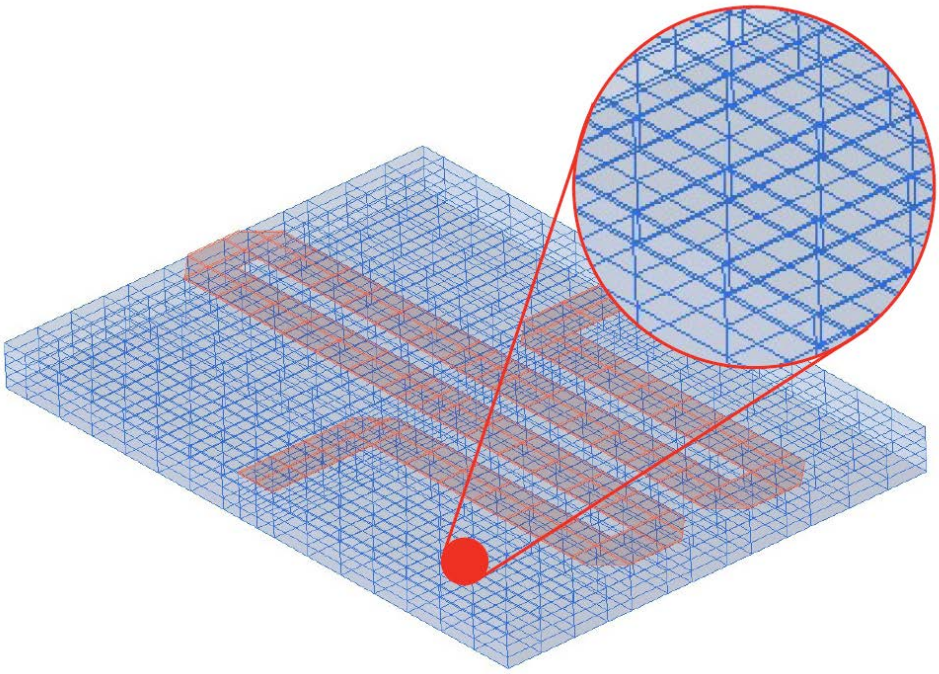

Figure 4.5: Example of a mesh generated by FDTD [35]

4.2 Electromagnetic Simulators Used

In this project, two EM simulators were used for simulating the behavior of the sensor. The first was EMPro from Keysight Technologies. EMPro was designed for analyzing the 3D EM effects for mainly high frequency situations [37]. Examples of its use include simulations of RF IC packages, bondwires, antennas, embedded passives, and PCB interconnects [37]. While EMPro was designed mainly for high frequency situations, it is also able to simulate the behavior of the sensor without much difficulty. EMPro can analyze situations in either the frequency domain using Finite Element Method (FEM) or the time domain using Finite Difference Time Domain (FDTD). When this project was begun, Auburn University had a license for the FEM solver only. Therefore, all simulations were done using it.

While EMPro was able to simulate the PCB sensor under a number of situations, it was not able to easily run series of simulations where the physical properties of the sensor were swept

over a range of values. For those situations, Q3D Extractor from ANSYS was used. Q3D is a 2D and 3D EM simulation tool designed for quasistatic situations [38]. In quasistatic situations, the wavelength of the frequency of interest is much greater than the physical dimensions of the area of interest [39]. Since the wavelength is so large, the electric and magnetic fields do not change much over the area, making it possible to treat the fields as static. Treating the problem as static decouples the electric and magnetic fields, allowing the use of the simplified forms of Maxwell's equations [40]. The simplified forms of Maxwell's equations are

$$\nabla \cdot \boldsymbol{E} = \frac{\rho}{\varepsilon} \tag{4.3}$$

$$\nabla \cdot \boldsymbol{B} = 0 \tag{4.4}$$

$$\nabla \times \boldsymbol{E} = 0 \tag{4.5}$$

$$\nabla \times \boldsymbol{B} = \mu \boldsymbol{J} \tag{4.6}$$

The frequency used in the simulations was 10 Hz, which has a wavelength of 30,000 km. Since this wavelength is much greater than the dimensions of the sensor, a quasistatic approach can be used to simulate the sensor's behavior. Examples of Q3D's uses include modeling cables, PCBs, and touchscreen devices. Q3D uses method of moments (MoM) to solve 3D problems and FEM for 2D problems [38].

4.3 Simulation Setup

As mentioned above, the sensor was modeled in both EMPro and Q3D. To match the original design of the sensor, by default, the electrodes were 10 mm long, 2.5 mm wide and separated 2 mm in both simulators (shown in Figure 4.6). The separation distance was set to be 2 mm because it was originally assumed that the separation distance was 2 mm. It was later discovered that the separation distance was actually 2.54 mm. As a result, much of the early

work done comparing the two simulators used 2 mm, while the later work that compared the results of simulation to actual measurement data used the actual sensor dimensions.

In the simulations, the sizes of all three dimensions were varied to observe the effects on the measured resistance. Other simulations were run to determine the effects the volume and physical distribution of the water had on the measurement. The effect of the electrical conductivity was simulated as well. The goal of the simulations was to determine how the conductivity of the water and the electrodes' separation distance, length, and width affected the measured resistance. From the data gathered, an equation for calculating the resistance was generated. This equation can be used for determining the conductivity of a sample of water based on the measured resistance (discussed in detail in Chapter 8).

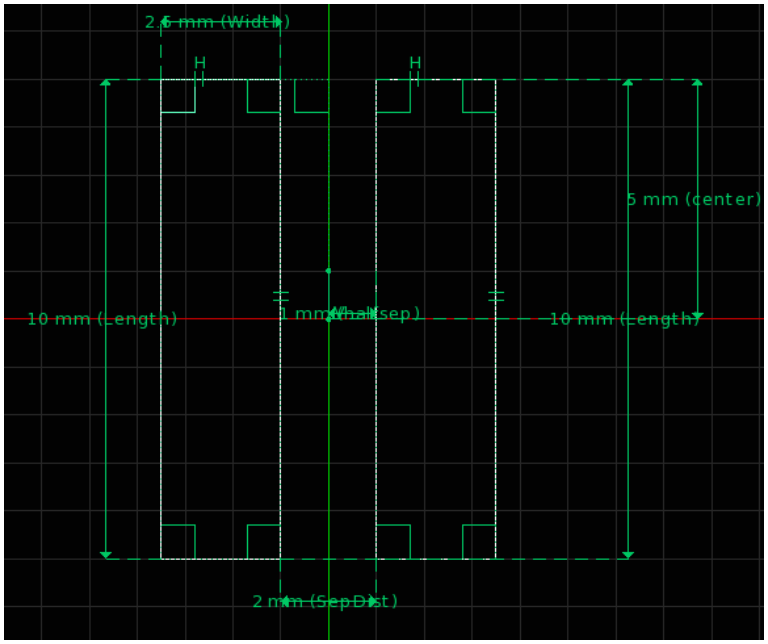

Figure 4.6: Modeling the PCB sensor's electrodes in EMPro

For most of the simulations, the sensor's PCB was not included. The conductivity of PCB's material, FR-4, is so low that Q3D's library listed it as being 0 S/m. Early simulations

indicated that the PCB had little effect on the simulation results. Removing the PCB made the setting up the simulations faster since the simulator did not have to generate a mesh over it.

4.3.1 The Setup for the EMPro Simulations

The setup used for most of the simulations done in EMPro is shown in Figure 4.7. The blue box represents the material being tested. The sensor's electrodes are centered at the bottom of the box. In all of the simulations in EMPro, the box was a 10 m x 10 m x 10 m cube. The dimensions were set so large to ensure that the box appeared nearly infinite to the sensor, no matter the sensor's dimensions. For most tests, the box was comprised of seawater, which had relative permittivity of 81, relative permeability of 0.999991, bulk conductivity of 4 S/m, and dielectric loss tangent of 0. The only exception was in the conductivity tests, where it was swept from 0.001 to 10 S/m.

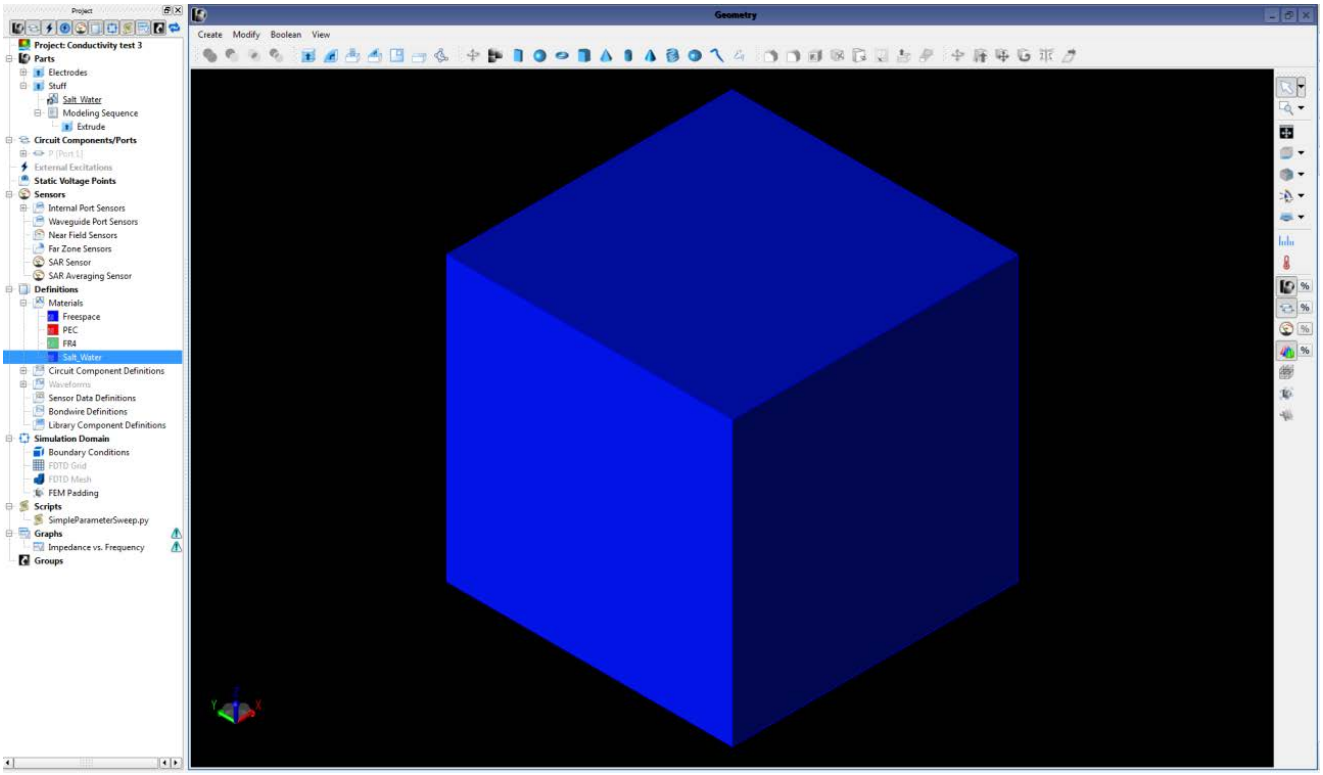

Figure 4.7: Simulation setup in EMPro

Early simulations showed that the under the default settings, the simulation results were not always accurate. This inaccuracy was especially noticeable when sweeping the electrode's separation distance and width. The results varied wildly over the sweep range. Figure 4.8 shows an example of this behavior. The figure was supposed to be a plot of the conductance over width for different electrode separation distances and lengths; however, the plots fluctuate as the width increase. This fluctuation is a result of simulation errors and not the behavior of the sensor.

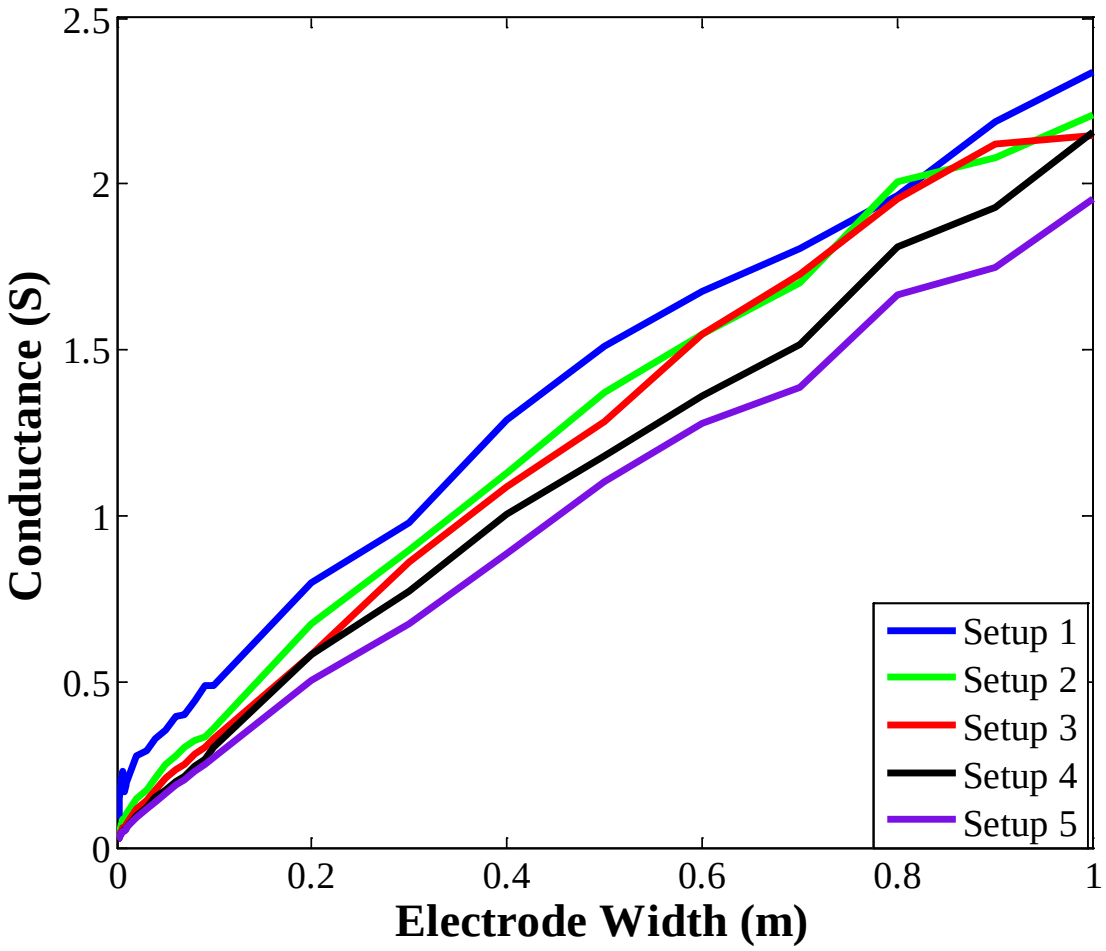

Figure 4.8: Example of the EMPro simulations with the default settings

To improve the accuracy of the simulations, EMPro's simulation setup was modified. Figure 4.9 shows the modified simulation stop criteria. The delta error was set to 0.001, and the

maximum number of passes was set to 18. The delta error is the maximum allowed percent difference between two consecutive simulation results required for the solution to be considered acceptable.

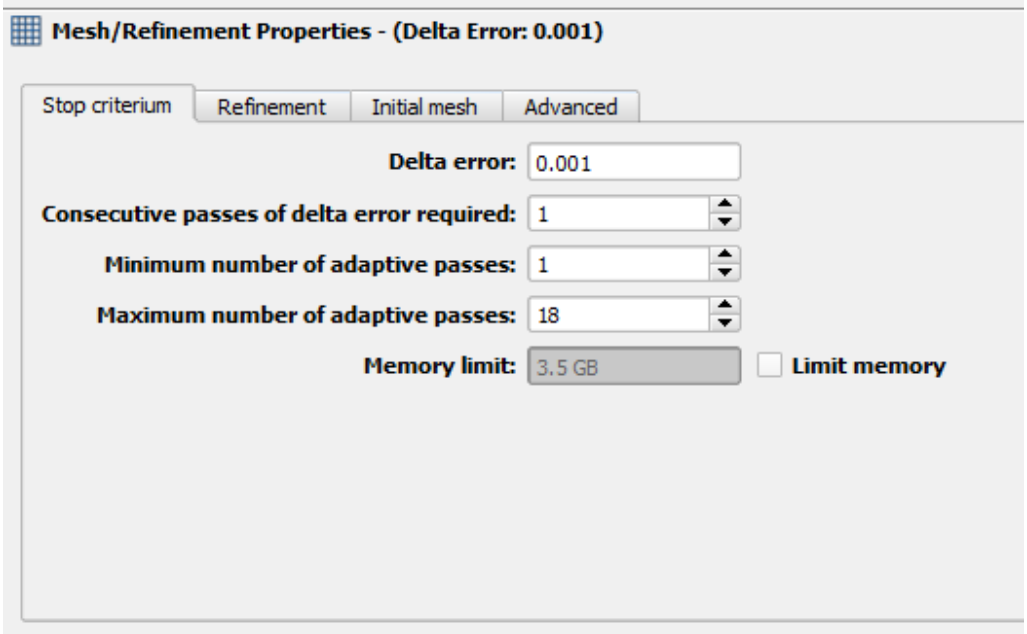

Figure 4.9: The modified EMPro stop criteria

Figure 4.10, shows the initial mesh settings properties. The initial target mesh size was set to 1 meter. Therefore, the mesh elements generated for the initial mesh could not be greater than 1 meter. By default, the initial mesh size was set to be one-third the wavelength of the maximum simulation frequency. For the simulations done on the sensor, the frequency was usually set to be 10 Hz, leading an initial mesh size of 10,000 km. Figure 4.10 also shows that the conductor edge and vertex mesh lengths were set to be equal to the variable Edge. Edge is defined as 0.05 multiplied by the width of the electrode. Both settings greatly decreased the size of the mesh elements around the electrodes, improving the simulation's accuracy.

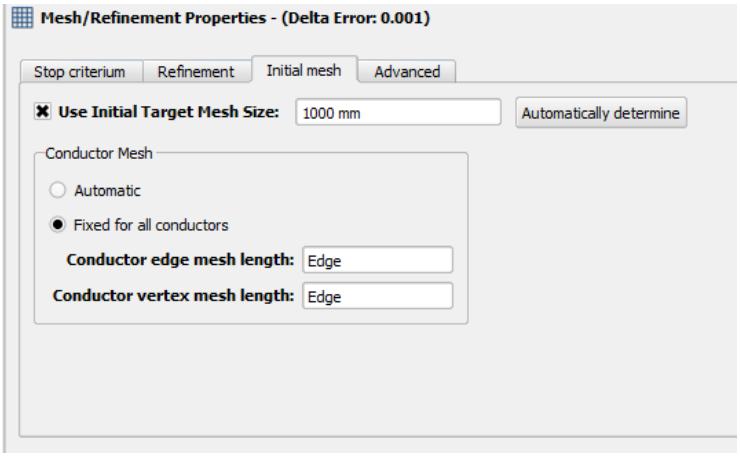

Figure 4.10: The modified EMPro initial mesh settings

Next, the simulator's matrix solver was changed from being iterative to direct, as shown in Figure 4.11. According to EMPro's manual, the direct matrix solver requires more time and memory than the iterative; however, it also does not suffer from potential convergence problems and is guaranteed to generate a solution as long as enough memory is available.

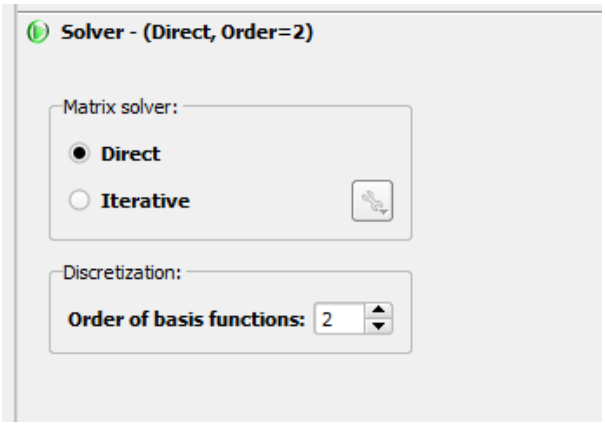

Figure 4.11: EMPro's matrix solver settings

An example of the mesh generated for simulating the sensor is shown Figure 4.12. It is difficult to see, but the mesh becomes denser the closer it is to the electrodes. A picture of the mesh around the electrodes is shown in Figure 4.13.

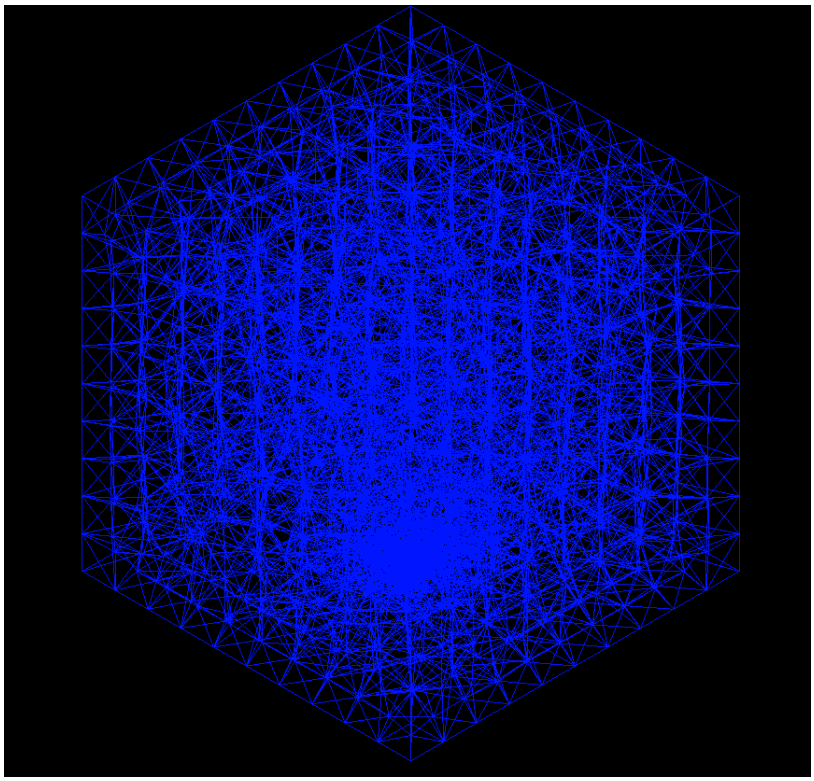

Figure 4.12: Example of the mesh generated by EMPro when simulating the sensor

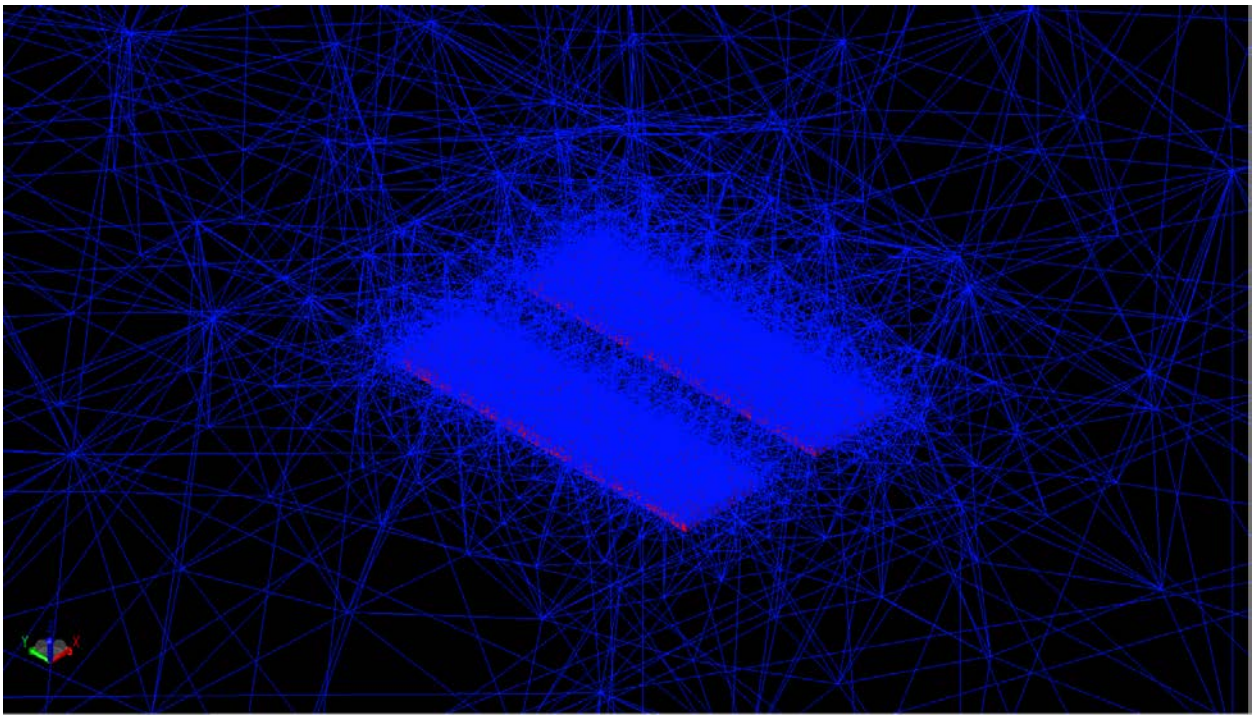

Figure 4.13: Zoomed in view of the mesh around the electrodes

While the modified simulation settings resulted in an increased simulation time, they also greatly improved the accuracy. Unfortunately, other issues with using EMPro occurred. Occasionally, EMPro was unable to generate a mesh for a certain electrode setup. The only way to fix this issue was to modify the geometry. Usually this modification involved increasing or decreasing one of the dimensions by a micron. Another issue was that EMPro could not easily run sweeps over multiple variables, making it difficult to run all of the simulations needed. These two issues led to the switch to Q3D Extractor for simulating the sensor.

4.3.2 The Setup for the Q3D Extractor Simulations

The setup used for most of the simulations done in Q3D Extractor is shown in Figure 4.14. The transparent blue box represents the material being tested. The small orange bars at the bottom of the box represent the two electrodes. In most cases, the box was a 20 cm x 20 cm x 20 cm cube. For most testing, the cube remained the same size; the only exception was for determining the effect the size and shape of the material had on the measurement results. The dimensions of the cube were chosen to be 20 cm by default because the size of a simulated object was limited by Q3D and 20 cm was at least five times greater than any of the dimensions of the electrodes. Later testing showed that the size of the box had little effect on the simulation results (discussed in more detail in later sections). For most tests, the box was comprised of seawater, which, like in EMPro, had relative permittivity of 81, relative permeability of 0.999991, bulk conductivity of 4 S/m, and dielectric loss tangent of 0. The only exception was in the conductivity tests, where it was swept from 0.001 to 10 S/m.

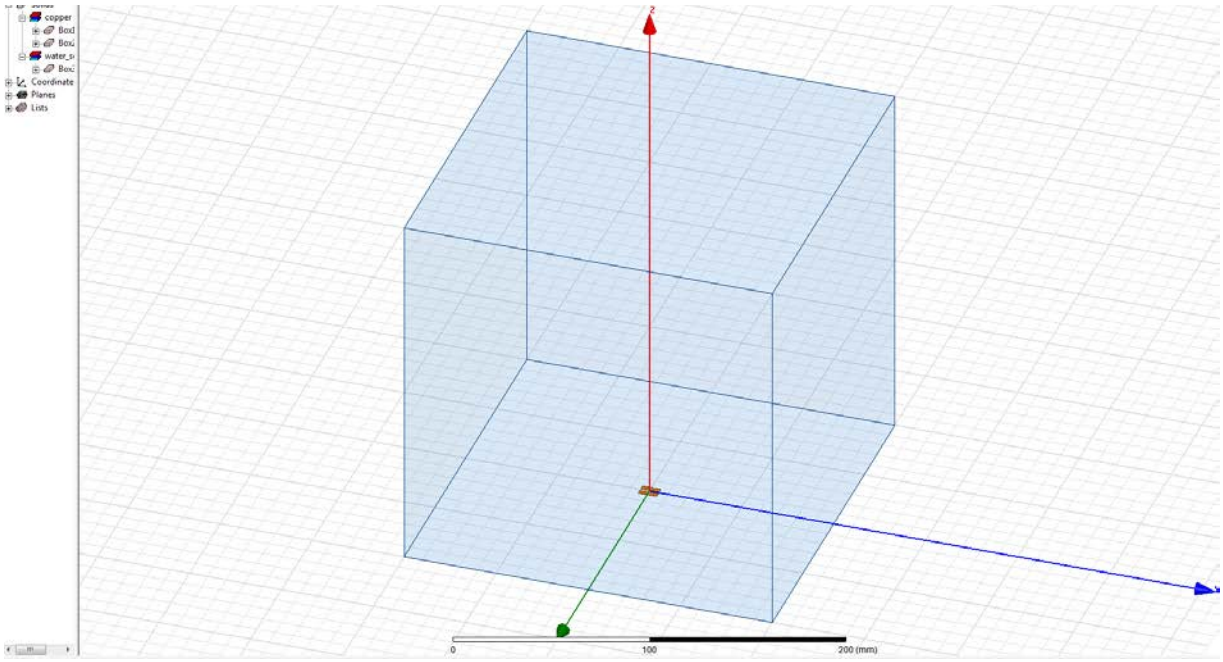

Figure 4.14: Simulation setup in Q3D Extractor

Like in the EMPro simulation, the setting for generating a mesh had to be modified in order to obtain accurate results. To improve the accuracy of the simulations, the size of the electrodes' meshes generated by the simulator was manually defined. Figure 4.15 shows that the maximum length of each element in the electrodes' meshes could not be greater than 5% of the size of $x. In the simulation, $x is the width of the electrode. Without this constraint, the accuracy of the simulations was significantly worse. This lack of accuracy was especially noticeable when running parametric sweeps, where the calculated results tended to incorrectly drift higher or lower over the sweep. Figure 4.16 shows an example of the mesh generated for the electrodes. The mesh elements in Figure 4.16 are so small that it is difficult to disguise the separate elements. Figure 4.17 shows a zoomed in view of the electrodes to give a better picture of the electrodes' meshes.

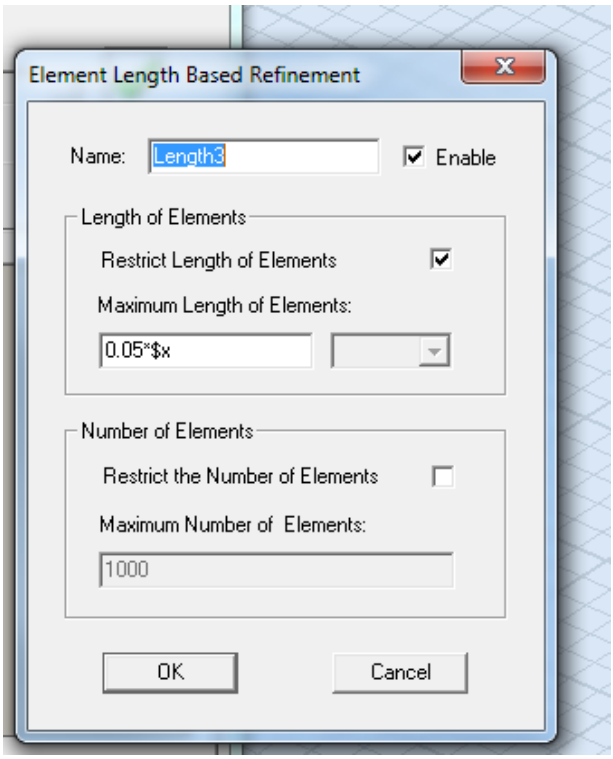

Figure 4.15: Constraint for the electrodes' mesh elements

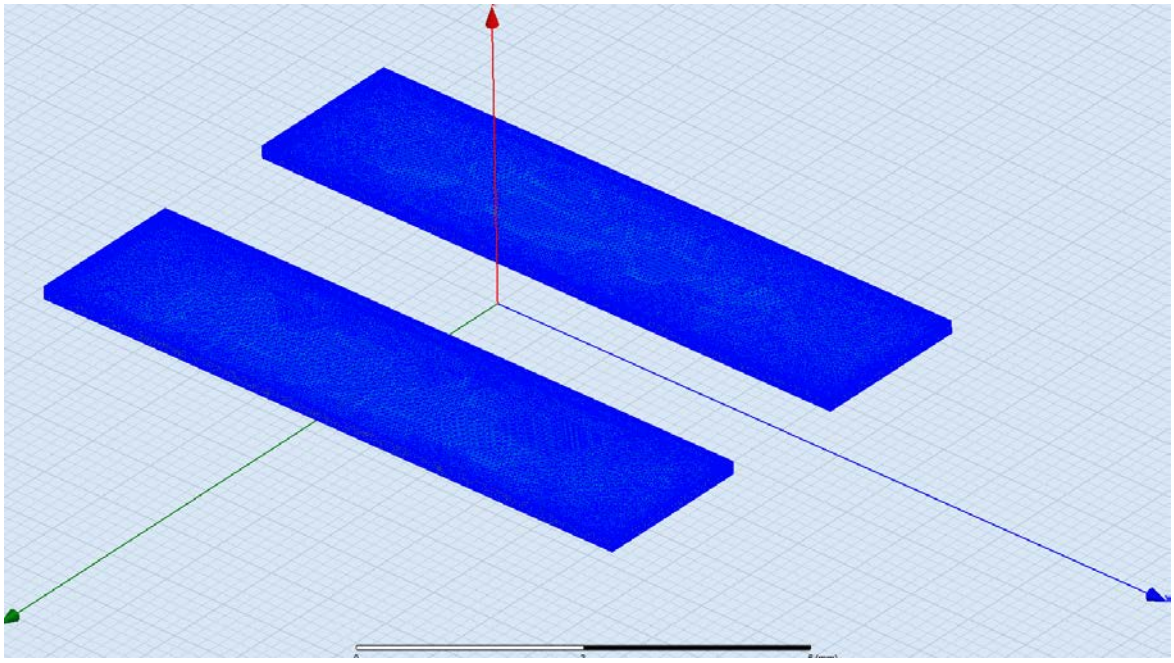

Figure 4.16: Example of the mesh generated for the electrodes

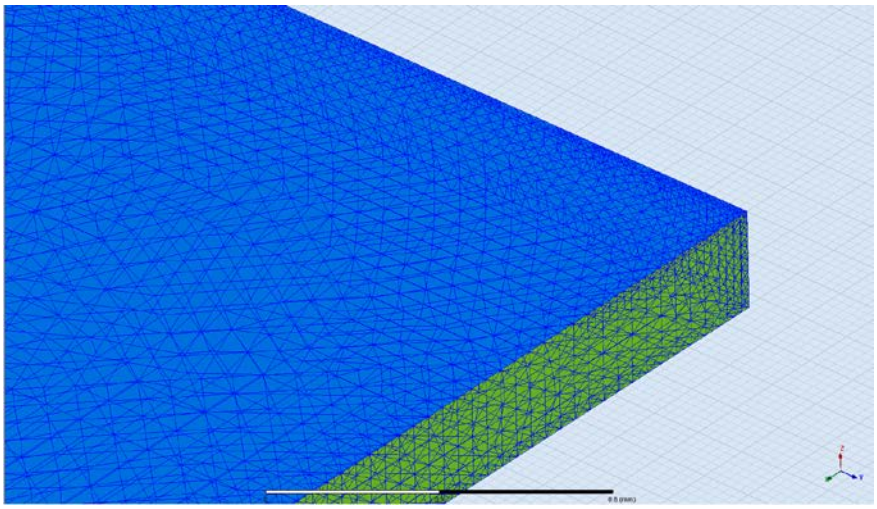

Figure 4.17: Close up view of the electrode's mesh

While this constraint improved the accuracy of the simulation, it also greatly increased the time it took to run the simulation. To save time, no constraints were applied to box's mesh. Figure 4.18a shows the mesh generated for the box. Figure 4.18b shows the mesh at the bottom of the box where the electrodes are. Notice that the mesh where the electrodes are located is much more compact than the rest of the box. Figure 4.19 shows mesh statistics for simulating the sensor with its original dimensions and a box that is 20 cm^3. In this situation, the mesh for each electrode was comprised of 48,752 elements, while the mesh for the box was comprised of 78,536 mesh elements.

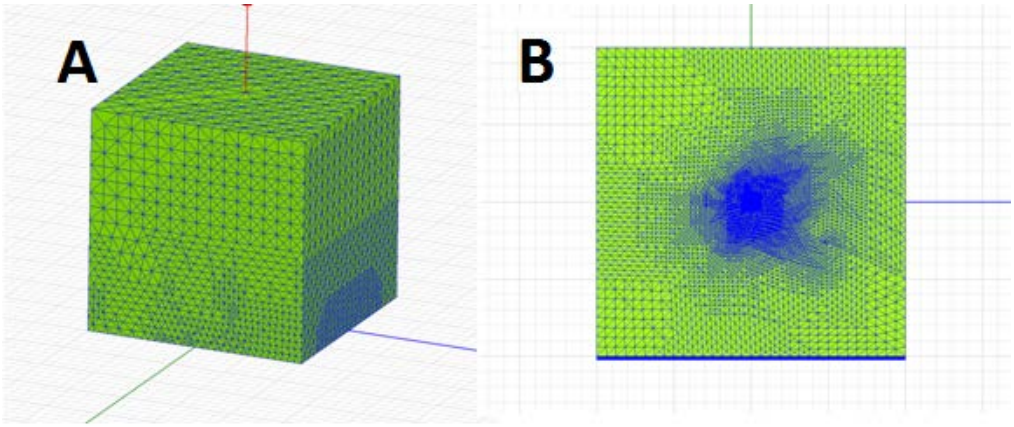

Figure 4.18: Isometric view of the box's mesh (A) and a view of the mesh near the electrodes (B)

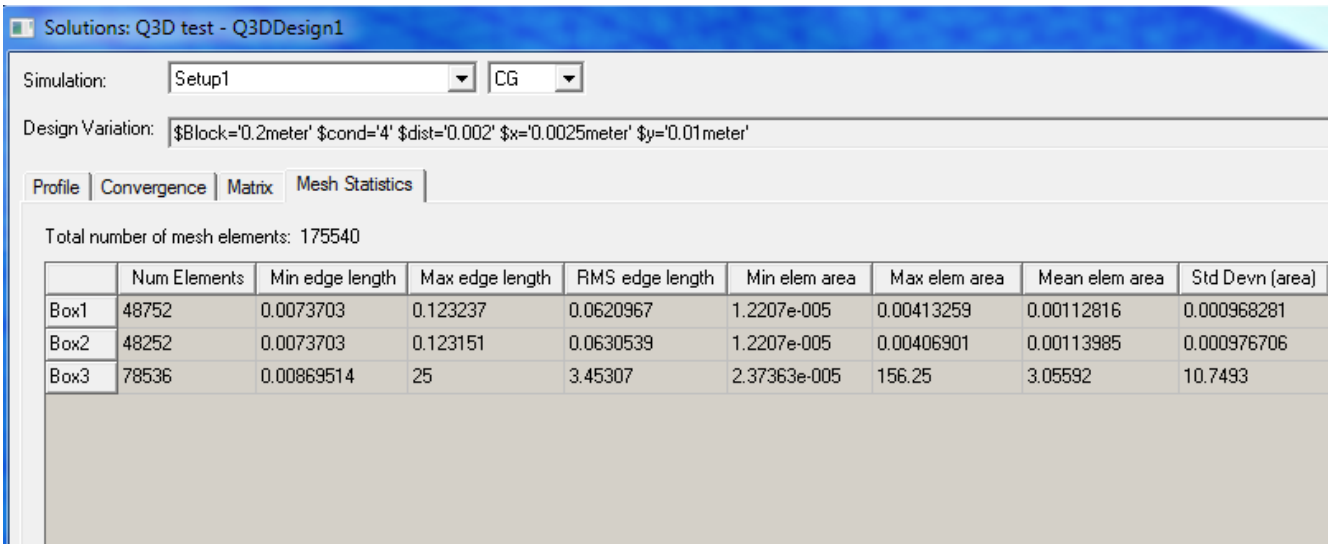

	Num Elements	Min edge length	Max edge length	RMS edge length	Min elem area	Max elem area	Mean elem area	Std Devn (area)
Box1	48752	0.0073703	0.123237	0.0620967	1.2207e-005	0.00413259	0.00112816	0.000968281
Box2	48252	0.0073703	0.123151	0.0630539	1.2207e-005	0.00406901	0.00113985	0.000976706
Box3	78536	0.00869514	25	3.45307	2.37363e-005	156.25	3.05592	10.7493

Figure 4.19: The mesh statistics for simulating the sensor

The simulation setup is shown in Figure 4.20. For most of the simulations done, the solution frequency was 10 Hz, and the simulator was set to calculate the capacitance and conductance. Later testing showed that the solution frequency did not have any effect on the simulation (discussed in greater detail in later sections). To improve accuracy, the solution order was set to be “Very High.” The simulator was allowed to attempt 30 passes before giving up trying to find a solution. In order for the solution to be considered acceptable, the last two solutions need to be within 0.5% of each other. If they are not, the simulator will generate a new mesh comprised of more cells and attempt another pass. On average, it took 15 passes for the simulations to converge. Figure 4.21 shows how long it took for the simulation of the default sensor design to converge. In that case, it took seven passes for the percent difference between the previous two solutions to drop below 0.5%.

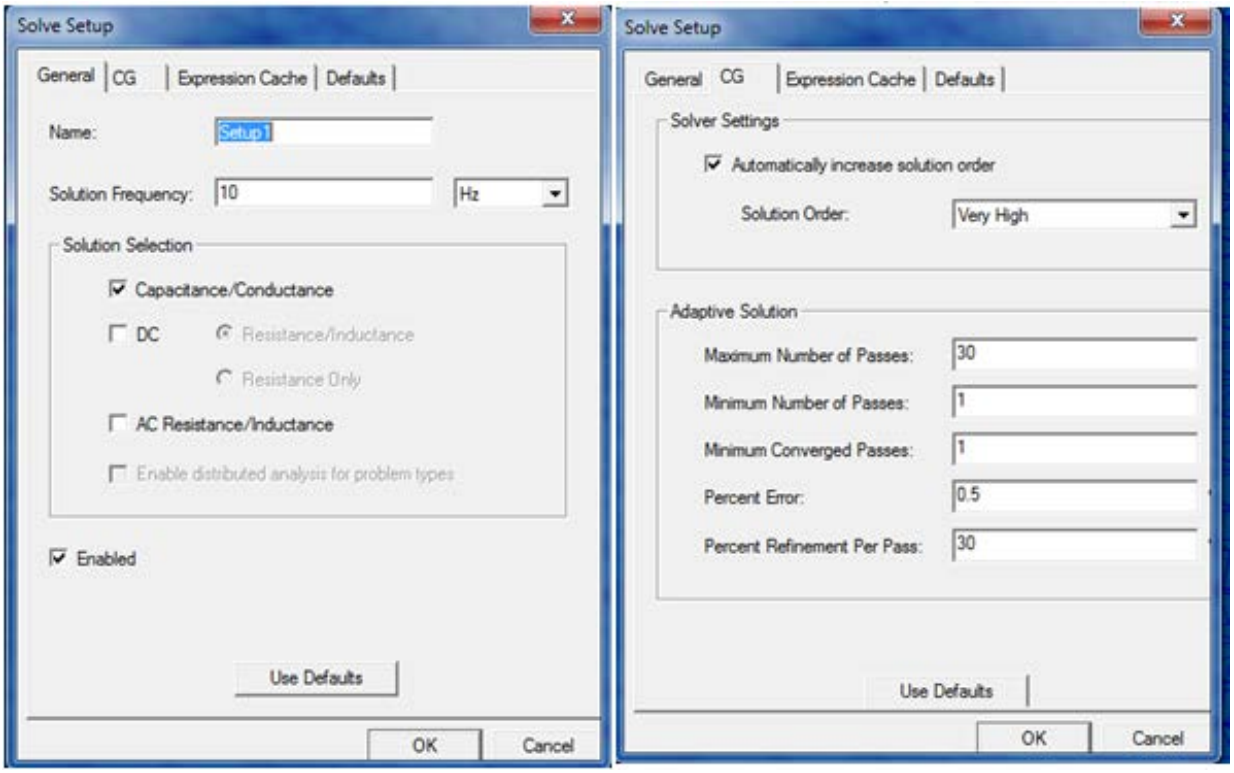

Figure 4.20: Setup for the simulation in Q3D Extractor

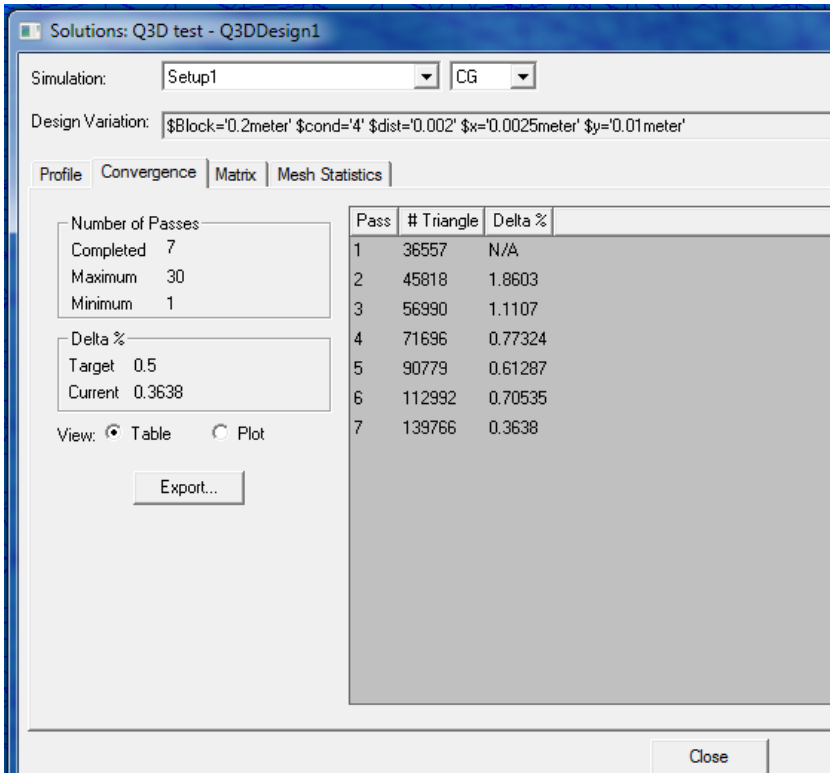

Figure 4.21: Example of simulation convergence

4.4 Properties not accounted for

While both simulators are very powerful, they could not take all properties into account. The properties not taken into account are temperature, pressure, and electrode polarization. In real life measurements these properties influence the conductivity of water.

4.4.1 Temperature

As mentioned previously, temperature can have a major effect on measurement accuracy. A solution of water at a higher temperature will have a higher conductivity since it will contain more dissociated ions [22]. Changing the temperature can have a major impact on the conductivity of water. For example, the conductivity of saltwater with a salinity of 35 ppt (which is common for seawater) will vary between 4.2738 S/m and 5.2848 S/m over a temperature range of 15ºC to 25ºC. As a consequence, conductivity is reported at a certain reference temperature; usually at either at 20ºC or 25ºC [17], [22], [25].

There are number of ways of compensating for temperature. In solutions with moderate to high salinities, conductivity has a roughly linear relationship with temperature. Temperature's effect on the conductivity can be calculated as

$$\sigma_T = \sigma_{ref}\left[1 + \alpha\left(T - T_{ref}\right)\right] \tag{4.7}$$

where σ_T is the conductivity measured at any temperature (in degrees Celsius), σ_{ref} is the conductivity at the reference temperature T_{ref}, T is the measurement temperature, and α is the temperature coefficient of solution at the reference temperature [22], [25]. The value of the temperature coefficient depends on the makeup of the solution. For example, the coefficient is between 2.2 to 3 per ºC for saltwater and 2 per ºC for drinking water [25]. This relationship is accurate only as long as the difference between the reference temperature and the measurement temperature is small. An example comparison between how the equation predicts how the

conductivity of a solution changes with temperature and how it actually does change is shown in Figure 4.22.

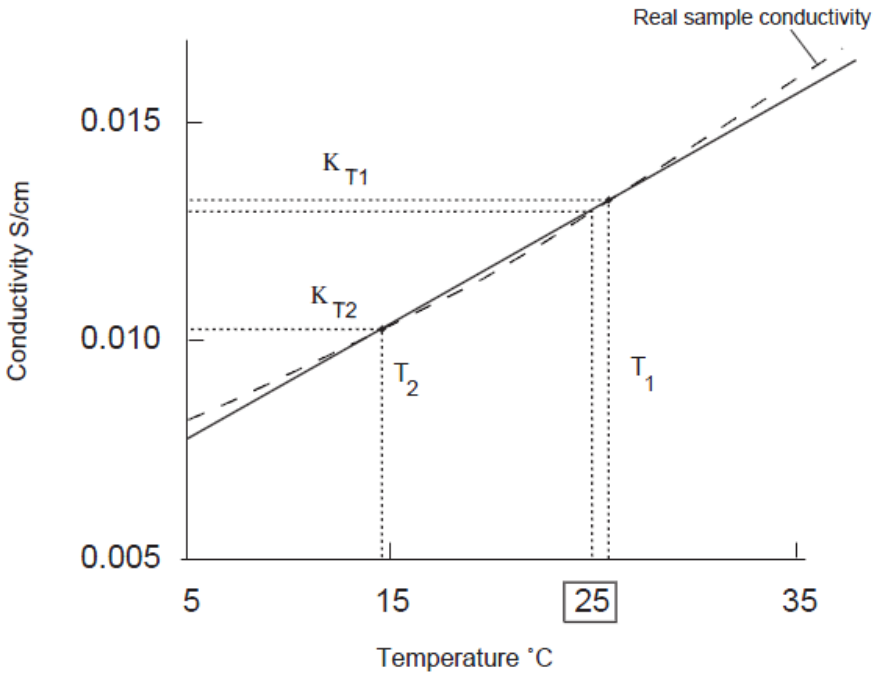

Figure 4.22: Comparison between the effect the predicted and measured temperature has on conductivity [25]

Equation (4.5) is not suitable to compensate for temperature change in solutions with low salinities. For these cases, the effects of temperature can be compensated only for using a nonlinear function. The simplified form of this equation is

$$\sigma_{25} = f_{25}(T) \times \sigma_T \tag{4.8}$$

where $f_{25}(T)$ is a 4-degree polynomial equation [25].

The effect temperature had on the conductivity was not directly accounted for in the simulations since there was not a simple way of doing so. However, temperature was accounted for when taking measurements using the physical sensors. Since most commercial sensors convert the measured conductivity to the conductivity at 20ºC or 25ºC, the temperature was used

to convert back to the conductivity of the water at the actual temperature [17], [22], [25]. Knowing the actually conductivity when a measurement was taken makes it possible to compare to the results of the simulation.

4.4.2 Pressure

Pressure is another important property when determining the characteristics of a sample of seawater. Both PSS-78 and TEOS-10 require compensating for pressure when taking measurements [3], [15]. However, pressure does not have a noticeable impact on the conductivity of seawater until it is much greater than the one atmosphere such as under the ocean [11], [41]. Since the PCB sensors are not intended for use in high pressure environments and all measurements were performed at one atmosphere, the effects of pressure are not considered in this work.

4.4.3 Electrode Polarization

One of the biggest obstacles for accurately measuring the conductivity of water using contact conductivity sensors is electrode polarization. Electrode polarization is the result of ions in the water being attracted to the interface between the water and the metal electrodes [6], [22], [25]. When the electrodes are first placed in the water, both the water and the electrodes are electrically neutral. However, as soon as they make contact, a chemical reaction occurs where the electrons in the water become attracted to the metal electrode. This attraction causes a charge difference between the electrode and the water creating an electric field opposing the chemical reaction by forcing electrons from the electrode and into the water (oxidation). As the original chemical reaction continues, the strength of the electric field (and as a result the oxidation reaction) will increase. The electric field will continue increasing until electrochemical equilibrium is established [6]. At this point the electron flow to and from the metal electrode is

equal. The electric field will also cause the dipoles of nearby water molecules to align with it. This alignment creates a layer of water molecules over the electrodes surface, called a hydration sheath (referred to as “first row water” in Figure 4.23).

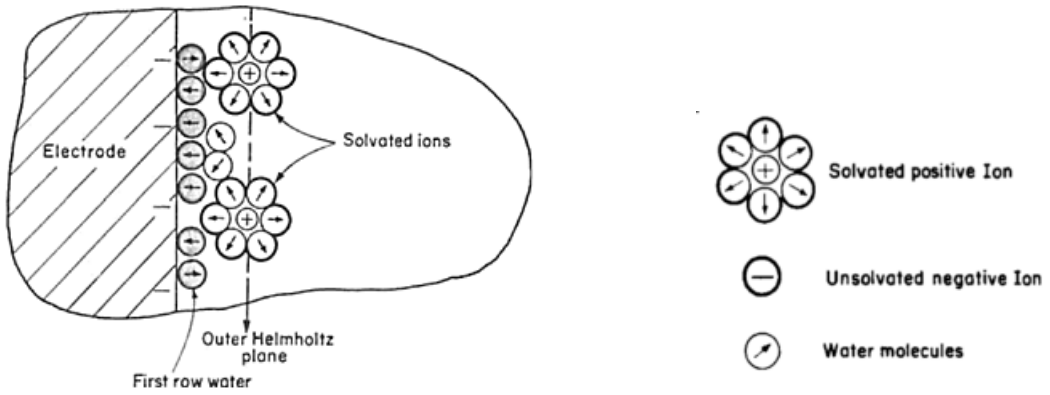

Figure 4.23. Representation of the electrical double layer on the submerged electrode. [42]

Salt ions in the water are then attracted to the water molecules in the hydration sheath, forming the outer Helmholtz plane. Some salt ions will also be chemically bonded to the surface of the electrode. These salt ions form the inner Helmholtz plane. Together, the two Helmholtz planes create what is referred to as the electrical double layer [6].

The electrical double layer can be modeled as two series capacitors in parallel with the impedance. The two capacitors are estimations of the capacitance of the area between the electrode and the outer Helmholtz layer (called the stern capacitance or C_S) and the capacitance between the outer Helmholtz layer and the cloud of ions in the region near the outer Helmholtz layer (called the diffuse capacitance or C_D) [6]. The capacitances can be added together to find the total double layer capacitance (C_{DL}) using (4.9).

$$\frac{1}{C_{DL}} = \frac{1}{C_S} + \frac{1}{C_D} \tag{4.9}$$

The parallel impedance (called the Faradaic impedance) is caused by current flowing across the interface between the electrode and the water when a voltage is applied [6]. The Faradaic impedance is difficult to predict because it changes nonlinearly with applied voltage.

The problem with electrode polarization is that when conductivity measurements are being taken, a voltage drop across the double layer capacitance and the Faradaic impedance will cause an error in the measurement. Randle's equivalent circuit can be used to model the electrical behavior of the water and the sensor for small sinusoidal excitations (shown in Figure 4.24). In the circuit, R_W represents the resistance of the water, C_{DL} represents the double layer capacitance, Z_F represents the Faradaic impedance, and C_P represents the parasitic capacitance between the electrodes. The resistance from the Faradaic impedance can cause the resistance measured by the sensor to increase. Since the simulators have no way of simulating the effects of electrode polarization, it needs to be accounted for in the measurements. Otherwise, the measured resistance will be higher than the simulated resistance.

Since the double layer capacitance and Faradaic impedance depend on the salinity of the water it can be difficult to calculate. Instead, the best option is to increase the excitation frequency so that it will short across the double layer capacitance. However, if the excitation frequency is too high, the parasitic capacitance will affect the measurement by causing the excitation signal to short across it. Usually the parasitic capacitance is so low that there is a frequency range where the measured resistance is just a result of the resistance of the water [6], [43].

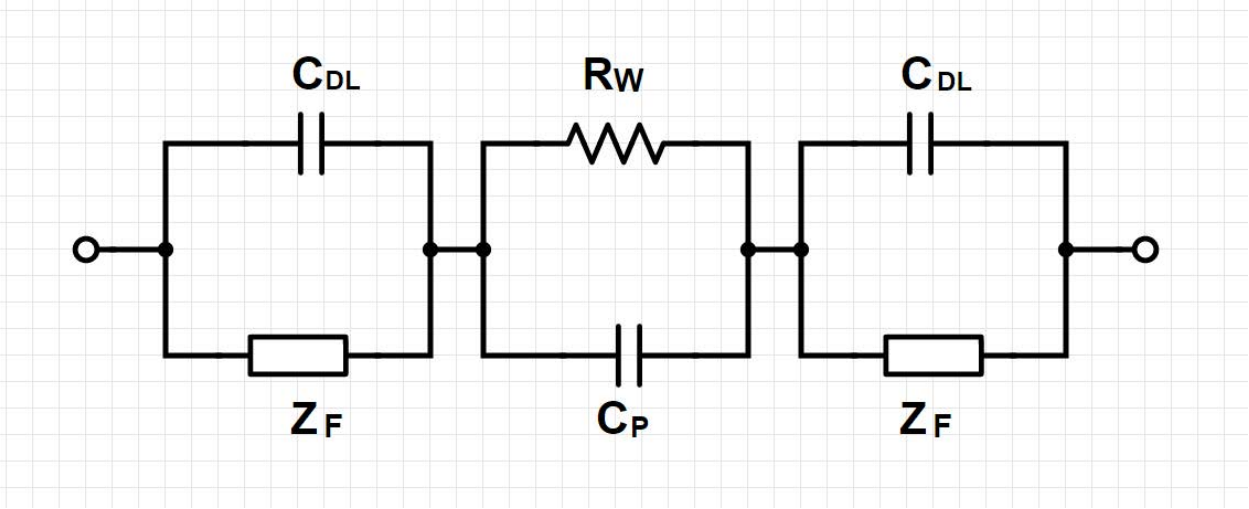

Figure 4.24: Randle's equivalent circuit model [6] [43]

Chapter 5

Testing Process

To characterize the PCB sensor, a series of sensors were manufactured and used to take measurements on different samples of water. Originally, 18 PCB sensors were manufactured for testing. Twelve had the default electrode geometry of 10 mm by 2.5 mm. To observe how the measurements changed with electrode size, the other six sensors had different electrode geometries. Two of the other sensors were 10 mm by 5 mm, two were 20 mm by 2.5 mm, and two were 20 mm by 5 mm. Later, 12 new sensors were constructed and tested alongside the original sensors. The electrodes on the new sensors were 20 mm by 5 mm, giving the sensors an area that was four times as large as the original sensors. This increase in size was undertaken to decrease the impact electrode polarization had on the sensor's measurements. The electrodes on three of the new sensors were gold-plated to protect the electrode from the elements better than the original sensors. The goal was to see if the performance of the gold-plated sensors improved enough to justify the increase in cost

Water samples from the Gulf of Mexico, Turkey Creek in Niceville, Florida, and Lake Jackson in Florala, Alabama were used in testing. Later, rain water gathered in Auburn, Alabama was added. The first set of tests involved using the PCB sensors to measure the resistance of pure samples of each type of water. From the resistances, the conductivity and salinity could be determined. Next, three commercial sensors were used to measure the salinity of the water. Each of the commercial sensors measured the salinity using a different method (described in Section

2.2). The goal was to compare the accuracy and measurement range of the PCB sensors to that of salinity sensors already on the market.

The second set of tests was the concentration tests. Here, the goal was to observe the effect that varying the salinity of the water had on the PCB sensors' measurements. In the concentration test, 100 mL of Turkey Creek, Lake Jackson, or rain water was poured into a beaker. Then, seawater was added incrementally to the beaker, while the PCB sensors were used to measure the resistance each time more seawater was added. After 100 mL of seawater was added, the beaker was emptied. The process was then repeated, except that a freshwater sample was incrementally added to the seawater. The results demonstrate how the measured resistance changed as the water under testing went from being 0% seawater to 100% seawater.

To ensure the repeatability, a rigorous testing method was defined. However, due to unforeseen complications in the testing, the testing process had to be refined twice, and testing had to be repeated. The original method, the methods for using the commercial sensors, and the two modified testing methods are described below.

5.1 Original Testing Method

The equipment used for testing is listed in Table 5.1. Five separate beakers were used for holding the water samples during testing. A 1000 mL beaker was used for the tap water (used for cleaning), a 100 mL beaker was used for seawater, two 20 mL breakers were used for the Turkey Creek and Lake Jackson water samples, and a 250 mL beaker was used for the concentration tests. The sizes of the breakers were based on what was available at the time. The 5 mL pipettes were used to fill the beakers with the water sample. To avoid contamination, each water sample had its own pipette and beaker. Rubber gloves were worn when handling the PCB sensors to avoid contaminating the electrodes.

Table 5.1: Equipment used for testing

Equipment	Quantity
1000 mL KIMAX Beaker	1
250 mL KIMAX Beaker	1
100 mL KIMAX Beaker	1
20 mL KIMAX Breaker	2
5 mL KIMAX Pipette	3
100 mL Graduated Cylinder	1
Crews Safety Glasses	1
Rubber Gloves	2
GW Instek LCR-841 Meter	1
4192A LF Impedance Analyzer	1
4366 Traceable Conductivity/TDS Pen	1
Instant Ocean SeaTest Hydrometer	1
MA887-BOX Digital Refractometer	1

In the first and second testing methods, the GW Instek LCR-841 Meter (shown in Figure 5.1) was used for measuring the resistance between the PCB sensor's electrodes. The LCR meter is a benchtop, high precision LCR meter developed by GW Instek for component and material measurements [44]. It has a measurement frequency between 12 Hz and 200 kHz and has an accuracy of within 0.05% and 0.1% depending on its settings.

Figure 5.1: The GW Instek LCR-841 meter

When the PCB sensor was used to take measurements, the breaker was first filled with the water sample using the corresponding pipette. The amount of water poured into the beaker depended on whether a pure sample of water (water from a single source) was being tested, or a concentration test was being performed. Next, the PCB sensor was submerged in the water. To operate correctly, the electrodes needed to be completely submerged and the remain perpendicular to the bottom of the beaker. The sensor also needed to remain near the center of the beaker with the bottom of the sensor not touching the bottom of the beaker. A demonstration of how the sensor was positioned in the beaker is shown in Figure 5.2.

Figure 5.2: Submerging the PCB sensor in water

Once the electrodes were completely submerged in the water, the resistance between them was measured using either the LCR meter or the impedance analyzer. Figure 5.3 shows the LCR meter's settings during the original testing. The meter was set in R/Q mode so that its primary measurement was resistance and its secondary measurement was the quality factor. The quality factor was not relevant in this situation. This mode was selected because it gave the highest precision for measuring resistance. The LCR meter's measurement signal was set to be 1 V peak-to-peak at a frequency of 5 kHz and no DC offset. Originally, the measurement frequency was chosen at random. As discussed in the following sections, later testing showed that the measurement frequency needed to be higher. The meter was set to the slow measurement speed, taking at least one measurement per second [44]. This setting had the best accuracy, within 0.05%.

Figure 5.3: The GW Instek LCR-841 meter's settings during original testing

After the measurement was completed, the sensor was removed from the sample and disconnected from the meter. The sensor was then cleaned using the tap water in the 1000 mL beaker and placed on a paper towel to dry. The process was then repeated for the other sensors.

5.2 Using the Commercial Sensors

To determine how well the PCB sensors functioned, three commercial sensors were selected for comparison. They were the MA887-BOX Digital Refractometer, Instant Ocean SeaTest Hydrometer, and the 4366 Traceable Conductivity/TDS Pen. A description of how each commercial sensor works is provided in Section 2.2.

The testing procedure used for the commercial meters depended on the specific meter. When the MA887-BOX Digital Refractometer (shown in Figure 2.6) was used, a pipette first dropped a small amount of the water sample onto the surface of the refractometer's sample well. The exact amount was not important, as long the sample well was completely filled. Next, the salinity was measured in PSU, ppt, and specific gravity and the temperature in degrees Celsius. The conductivity of the water sample was calculated from the salinity in PSU and the temperature using the PSS-78 algorithm. Afterwards, the refractometer's sample well was cleaned using tap water and dried with a paper towel.

Using the Instant Ocean SeaTest Hydrometer (shown in Figure 2.4) was straightforward. First, the hydrometer was filled with 150 mL of the water sample. The back of the hydrometer's packaging recommends dislodging air bubbles by tapping gently with a pencil. The hydrometer was then placed on a flat surface, and the salinity was determined in ppt and specific gravity based on where on the hydrometer's scale the pointer was directed. The conductivity of the water was found by first converting the salinity to PSU and then using the PSS-78 algorithm to calculate the conductivity [10]. The water was then poured out, and the hydrometer was cleaned using tap water.

When the 4366 Traceable Conductivity/TDS Pen (shown in Figure 5.4) was used, a quantity of the water sample was first poured into a beaker. The protective cover was removed

from the pen's probe head. The pen was turned on and set to measure conductivity. It was then immersed deep enough in the water to completely submerge both the probe head and the temperature sensor. The pin was used to stir the water to ensure adequate movement of the water around the probe head. The manual recommended that the water needed to be moving at least 0.2 to 0.3 meters per second [45]. Once the pen's measurements leveled off, the conductivity, the salinity in ppt or ppm (parts per million) and temperature were recorded. Once the measurement was complete, the pen was removed from the sample and cleaned using tap water.

Generally, conductivity measurements are reported at a specific reference temperature, typically 20ºC or 25ºC [25]. By default, the pen displays the conductivity at 25ºC. The pen converts its measurements to the conductivity at 25 ºC using a temperature compensation coefficient. This coefficient is 2.1ºC by default [45]. Furthermore, the salinity is not measured directly; instead it is estimated from the conductivity. The pen calculates the salinity by multiplying the measured conductivity (in µS/cm or mS/m) by the Total Dissolved Solids (TDS) factor. TDS is a measurement of the total concentration of ions in a solution. The TDS factor depends on the makeup of the solution and can be used to convert the conductivity to salinity [25]. By default, the pen uses a TDS of 0.5 [45]. Since it is a very simplistic estimation, the salinity measured by the pen was used only as basic reference in this work.

Figure 5.4: The 4366 Traceable Conductivity/TDS Pen

5.3 Improved Testing Process

Several months after the original testing had been completed, new water samples were gathered from both the original locations and rain water from Auburn, Alabama. Twelve new 20 mm by 5 mm PCB sensors were manufactured for further testing. The process outlined in the Section 5.1 had already been used extensively to test the original PCB sensors. However, it was discovered that this setup introduced an unacceptable amount of error to the measurements. This error had two causes: electrode polarization and the settings of the LCR meter. Electrode polarization (discussed in greater detail in Section 4.4.3) results a layer of salt ions forming over the electrodes of the PCB sensor when placed in water. Randle's equivalent circuit model demonstrates that the salt ions can be treated as a parallel impedance (called the Faradaic impedance) and capacitance, which are both in series with the resistance of the water. When attempting to measure the resistance, the extra resistance from electrode polarization causes the measured resistance to increase.

The only way to compensate for this problem is to increase the measurement frequency until it is high enough to short across the capacitive component [25]. Figure 5.5 and Table A.4 demonstrate the effect that varying the measurement frequency has on the PCB sensor's measurements. The data in the table were obtained by sweeping the LCR meter's measurement frequency from 1 kHz to 200 kHz, while a PCB sensor was placed in seawater. The measured resistance started out large when the frequency is small; however, as the frequency was increased, the resistance dropped rapidly before leveling out. Afterwards, the resistance continued to slowly decrease. If the frequency were to continue to increase, eventually the resistance would start to rapidly drop again. This drop would occur when the frequency becomes high enough for the parasitic capacitance in the system to influence the measurements. This

behavior was not shown in Figure 5.5, because the measurement frequency of the LCR meter could not go higher than 200 kHz.

According to simulation, the measured resistance of the original sensor should be around 20 Ω depending of the temperature and exact salinity of the seawater. Since the measured resistance was the closest to the simulation results at 200 kHz, the frequency was set to 200 kHz, the highest frequency allowable for the LCR meter. At 200 kHz, the accuracy of the measurements improved; however, this frequency introduced new errors.

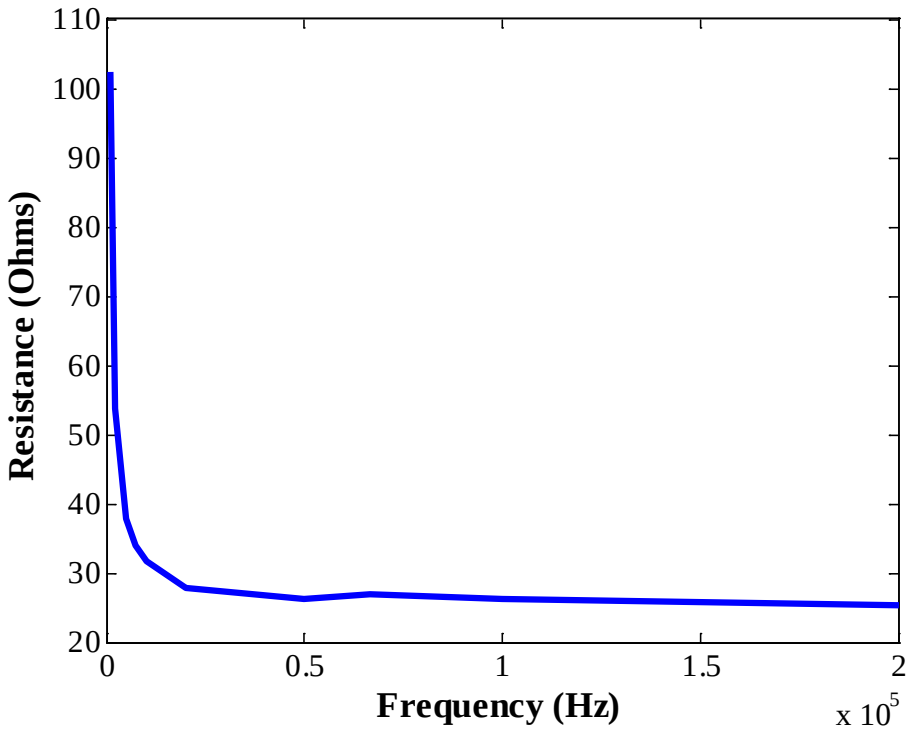

Figure 5.5: Measured resistance as measurement frequency is swept

As mentioned earlier, in the original tests, the LCR meter was set in series mode and to operate at 5 kHz. While increasing the measurement frequency to 200 kHz helped compensate for the effects of the electrode polarization, it resulted in the LCR meter's other settings causing new errors. LCR meter's manual recommends setting the meter to series mode at 1 kHz when the

expected resistance is less than 1 kΩ and setting the meter to parallel mode when the expected resistance is between 1 kΩ and 10 MΩ, as shown in Figure 5.6. Since the measurement frequency needed to be 200 kHz, none of the recommendations were applicable. Furthermore, early testing reported in Section 6.1.1 had shown that, depending on the salt concentration of the water, the measured resistance could be between tens of Ohms to the thousands of Ohms. Since the LCR meter was the only meter available at the time, a series of tests was performed to determine the settings that would provide the most accurate measurements.

General Resistors A series inductance circuit is the best equivalent circuit for low resistance (<1kΩ) and a parallel capacitance circuit for high resistances (>10MΩ).

Test Frequency	Expected Resistance		
	<1kΩ	1kΩ~10MΩ	>10MΩ
0.03kHz	—	—	Parallel
0.25kHz	—	Parallel	—
1kHz	Series	—	—

Figure 5.6: The settings for measuring resistance recommended by the LCR meter's manual [44]

The testing setup is shown below in Figure 5.7. It was based on the Randle's equivalent circuit model; however, the series capacitances resulting from the double layer were not included since the testing frequency was assumed to be high enough to short across them. The setup was comprised of a resistor and capacitor connected in series on a breadboard. The LCR meter was used to measure the resistance across them in both series and parallel mode. The measurement frequencies were 30 Hz, 250 Hz, 1 kHz, 10 kHz, 100 kHz, and 200 kHz. To determine how the value of the resistance and capacitance affected the accuracy, a 4 Ω to 1 MΩ resistor and a 1.66 pF or 22.29 pF capacitor were used. Tables A.2 to A.5 show the results of this testing. The results demonstrate that, for both series and parallel mode, the LCR meter's accuracy decreased

as the frequency became large; however, this decrease in accuracy did not occur until the resistance was large (greater than 10 kΩ). Furthermore, while the accuracy decreased using either mode, the decrease was far less using the parallel mode. Therefore, the LCR meter was set in parallel mode with a test frequency of 200 kHz for the rest of the measurements (as shown in Figure 5.8).

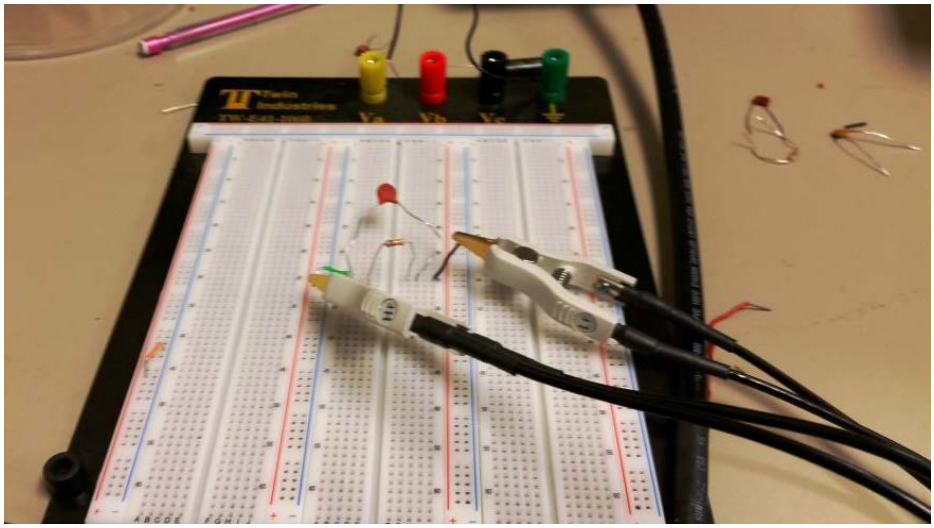

Figure 5.7: Setup for determining the LCR meter's settings

Figure 5.8: The GW Instek LCR-841 meter’s new settings

The setup for the concentration tests was modified along with the LCR meter's setting. Originally, each sensor was used one at a time for the concentration testing. However, this way of testing proved to be time consuming and increased the chance of errors. Furthermore, it was observed that this process resulted in a large amount of water loss. At the end of a concentration test, the amount of water left in the beaker was measured. It was found that approximately 175 mL of water was in the beaker instead of the expected 200 mL. This loss was likely caused by the PCB sensors themselves. Whenever a PCB sensor was used to take a measurement, some of the water adhered to the surface of the sensor when it was removed from the beaker. While only a small amount adhered to each sensor, the concentration tests included nine PCB sensors, and each sensor was used to take 27 measurements during a concentration test. With so many measurements, the water loss became noticeable. This loss made it difficult to accurately determine the amount of seawater in the beaker during testing, which made it difficult to determine how accurate the PCB sensors' measurements were. This problem was not discovered during the original concentration testing because only three of the original PCB sensors were used, and they had a much smaller surface area than the new PCB sensors.

To stop the water loss and speed up testing, the container shown in Figures 5.8 and 5.9 was constructed. The container was designed to hold all nine of the PCB sensors used in the concentration tests in the beaker at once. By holding the sensors in the water for the entire test, the container was able to eliminate the major source of water loss. The sensors were arranged to be far enough away to not interfere with each other. The simulations discussed later in Section 7.3 demonstrate that the electric field from the sensors' electrodes do not penetrate far into the water. Therefore, the sensors did not need to be very far apart. Wires were soldered to the terminals of each sensor and connected to the breadboard. Jumper wires were used to connect the

LCR meter's probes to the breadboard. The breadboard and wires added extra resistance to the measurements. This extra resistance was measured separately and subtracted from the testing results.

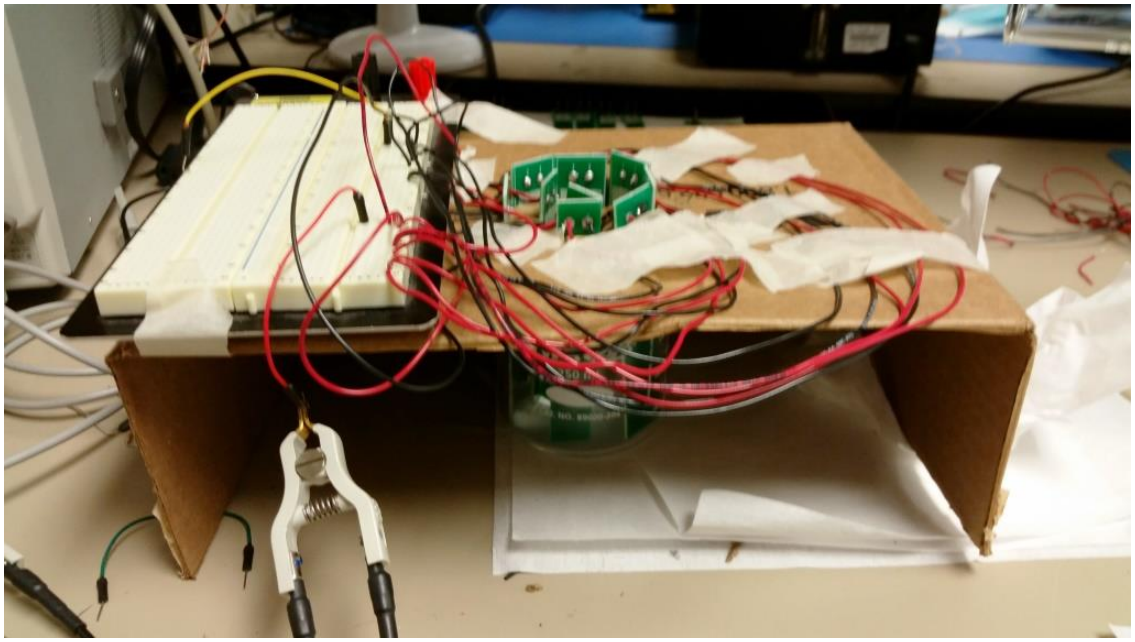

Figure 5.9: Side view of the concentration testing setup

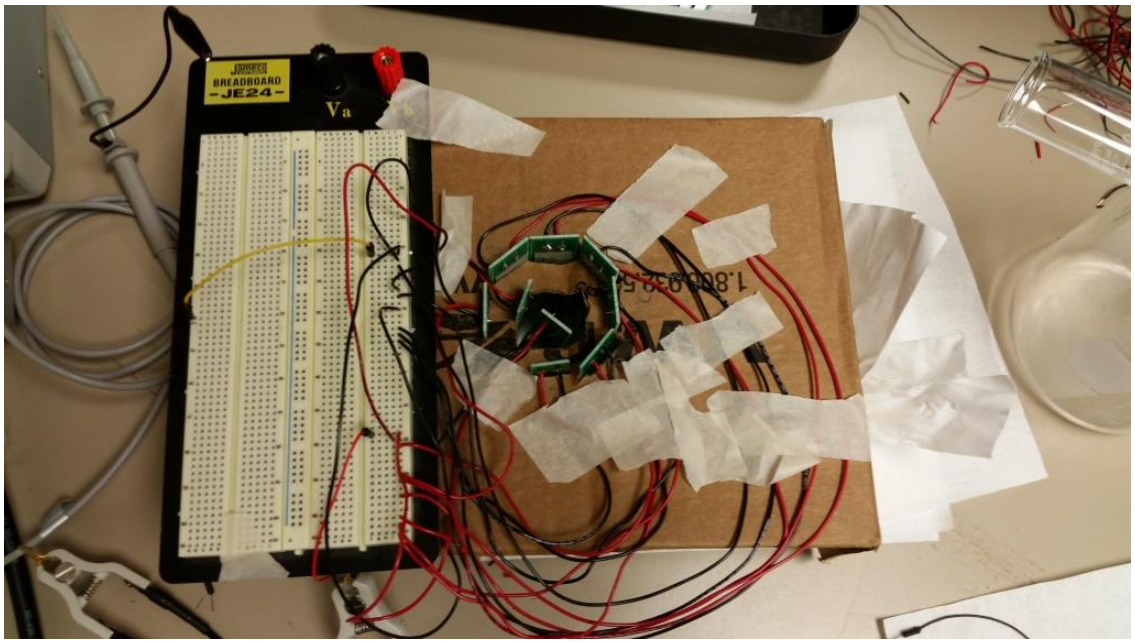

Figure 5.10: Top view of the concentration test setup

The container itself was made of cardboard. While cardboard weakens when exposed to water, it was easy to work with. When adding water to the beaker, care was taken to not spill any on the cardboard. The water sample to be added to the beaker was stored in a 100 mL graduated cylinder. The graduated cylinder made it simple to keep track of exactly how much water had been added.

5.4 Final Testing Method

While the process in Section 5.3 improved the accuracy of the measurement results, it introduced a new problem. Unfortunately, the wires connecting the PCB sensors to the breadboard introduced a noticeable amount of resistance to the measurements. Worse, the resistance varied depending on the orientation of the wires, making it nearly impossible to accurately subtract the resistance out of the measurements. To fix this problem, the stand was abandoned, and the wires were removed. Instead, the boards were again tested one at a time by placing the sensor in the beaker and then removing it. While abandoning the container eliminated the extra resistance, it also meant that water loss was again an problem.

To minimize the amount of water lost, the stand in Figure 5.11 was constructed. During testing, the PCB sensors not in use were hung on the bar at the top of the stand, similar to clothes on a clothes line. A trough was attached to the stand underneath in hopes of redirecting any drops of water coming off of the sensors into the beaker below. However, the trough proved ineffective. Instead of sliding down, any water that fell on the trough tended to adhere to it until evaporating. While the trough proved ineffective, the use of the stand still decreased the average water loss from 25 mL to 8 mL. This decrease was the result of hanging the PCB sensors. By hanging the sensors instead of placing them on a paper towel, most of the water that had adhered

to the sensor was still on it the next time it was placed back in the beaker, allowing some of the water to return to the beaker.

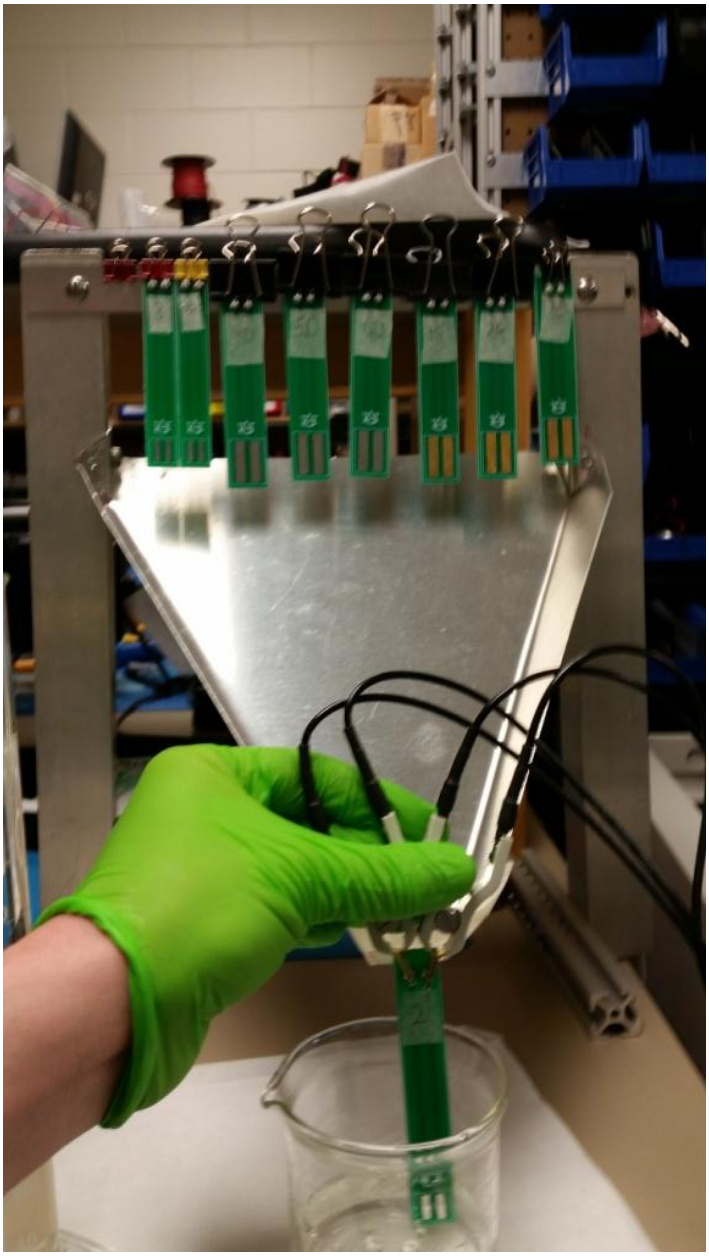

Figure 5.11: Stand for holding the PCB sensors during testing

While the stand helped decrease the amount of water lost during testing, it did not eliminate the loss completely. As mentioned before, this loss added a degree of uncertainty to the ratio of seawater to freshwater in the beaker, making it difficult to determine what salinity a

sensor measurement corresponded to. Worse, it was unknown whether the water loss was constant over the entire test. At what point the water is lost has a large effect on concentration tests because the water in the beaker changes throughout the test. The salinity of the lost water depends on at what point during the test it is lost. The water lost from removing the sensors had been assumed to be fairly constant; however, it was not the only possible cause. Another source of loss was the water dripping from the pipette when adding water to beaker. Furthermore, the accuracy of the pipette was unknown. While the pipette was likely fairly accurate, any error could have had a major effect on the testing given how much water has used. It was discovered early on that the scale on the 250 mL beaker used in the concentration testing was not accurate, giving precedence to the possibility that other glassware used in the testing may not be accurate.

The uncertainties resulting from the undetermined loss of water and the possibly of inaccurate equipment used in testing not only made it difficult to determine what salinity the resistance measured by the PCB sensor corresponded to, but also made it difficult to compare the results of the testing to the simulations. Originally, the plan was to calculate the salinity of the water in the beaker based on the salinity of the seawater and of the freshwater used. Since the salinity the water samples was known, the amount of salts in a specific volume could be determined. From the salinity, the conductivity of the water could be calculated using the PSS-78 algorithm (described in Section 2.2). The resistance measured by the sensor could then be compared to the resistance predicted for that conductivity by the simulations and the equation developed in Chapter 8. However, the water loss made the amounts of freshwater and seawater in the beaker impossible to accurately determine. As a result a new process was developed.

As described in (3.16), the conductivity of the water sample can be calculated by dividing the cell constant of the sensor (κ) by resistance measured by the PCB sensor. As long as the

geometry of the PCB sensor does not change and the volume of the surrounding water is large, the cell constant will be the same for any conductivity. As mentioned in Section 3.2, mathematically determining the cell constant for the PCB sensor is difficult. However, if the resistance measured by the PCB sensor could be determined for a known conductivity, the cell constant can be calculated using (3.16). To accomplish this calculation, two of the commercial salinity sensors (the reflectometer and conductivity pen) were used measure the conductivity alongside the PCB sensor during the concentration tests. Both salinity sensors had drawbacks (the conductivity pen could only measure up to 2 S/m while the reflectometer lacked precision) that stopped them from being used to measure the conductivity at every point during the concentration tests. However, they provided enough information to determine the cell constants of the PCB sensors. From the cell constants, the conductivities of the water samples were determined for every step of the concentration tests. Commercial sensors use the same process to determine conductivity [25]. Using of the cell constants allowed the results of the tests to be compared to the results of the simulations and the equation derived in Chapter 8.

Another change to the testing method was the meter used to measure the resistance. The LCR meter used in previous tests was replaced with the 4192A LF Impedance Analyzer, shown in Figure 5.12. The impedance analyzer was capable of operating at a much higher measurement frequency than the 200 kHz the LCR meter was limited to. In order to determine the new measurement frequency, a sensor was placed in a sample of seawater, and the measurement frequency was swept from 5 kHz to 10 MHz. The resistance measured during this process is shown in Figure 5.13 and later in Table A.17. Like in Section 5.1, the resistance decreased rapidly before leveling out. However, after 1 MHz, the resistance started to increase again. This increase contradicts the conclusion that the parasitic capacitance of the sensor's PCB would

cause the measurement signal to short across the water after the frequency was large enough. The likely cause for this disagreement is the cable used to connect the impedance analyzer to the sensor. Since the measured resistance was lowest at 1 MHz, a measurement frequency of 1 MHz was used for the rest of the tests. The other settings were similar to the settings for the LCR meter. The impedance analyzer was set in parallel measurement and set to average measurement mode to improve the accuracy.

Figure 5.12: The 4192A LF Impedance Analyzer

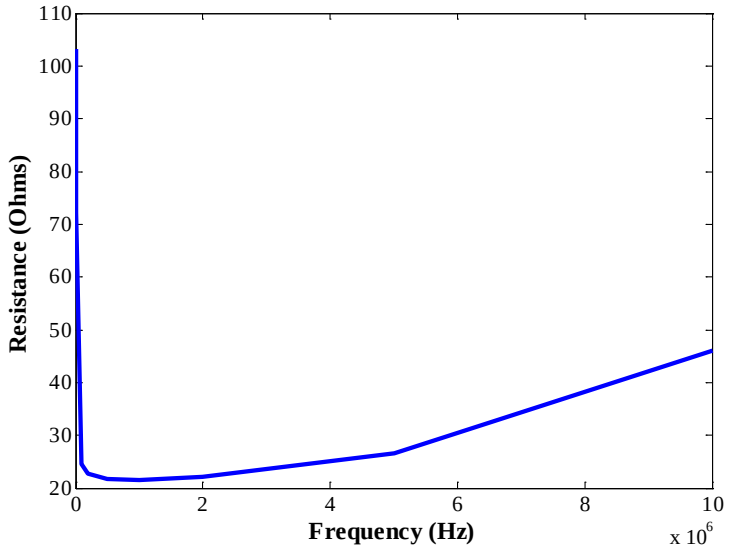

Figure 5.13: Resistance as measurement frequency of the impedance analyzer is swept

Chapter 6

Testing results

To observe the behavior of the PCB sensors, they were used to measure the salinity of different samples of water. Originally 18 sensors were used. Twelve of the sensors had the default electrode dimensions, while the other six had a variety of electrode dimensions. The goal was to determine the effect the dimensions of electrodes had on the measured resistance and what size produced the most accurate measurements. After the first round of testing, 12 more sensors were manufactured and tested alongside the original 18.

The water included samples from the Gulf of Mexico, Turkey Creek, and Lake Jackson. Rain water collected in Auburn, Alabama was included in later tests. Each sample was from a different location and had a different chemical composition. If the PCB sensor is sensitive enough, it should be able to identify the differences in salinity among the samples. Using the methods outlined in Chapter 1, the salinity of the pure samples of water and at varying saltwater concentrations was measured. Unfortunately, errors resulting from the method used to acquire the data required the testing to be repeated twice.

6.1 First Round of Testing

The first round of testing involved measuring the salinity of the seawater, Turkey Creek, and Lake Jackson water samples using the method described in Section 5.1. In this case, only the original 18 PCB sensors were used. The electrodes of 12 of the sensors were 10 mm by 2.5 mm, two were 10 mm by 5mm, two were 20 mm by 2.5 mm, and two were 20 mm by 5 mm. The

electrode separation distance for all of the sensors was 2.54 mm. The sensors were first tested in pure samples of each water source. Their results were then compared to the measurements obtained using the commercial reflectometer, hydrometer, and conductivity pen described in Section 5.2. Afterwards, concentration tests were performed.

6.1.1 Pure Water Measurements

First, the PCB sensors were used with the pure water samples (except rain water). To provide a baseline, the sensors were also tested in deionized water. Deionized water has had its salt ions removed using a special ion exchange resin. Theoretically, all of the ions should be removed using this process, making the conductivity very low. Unlike with distilling, organics will not be removed through deionization [46]. Table 6.1 shows the results obtained using all 18 sensors in all of the water samples. The row for sensor 6 was left blank because it was damaged.

Table 6.1: Results of testing the pure water samples using the original testing process

Sensor #	Seawater (Ω)	Turkey Creek (Ω)	Lake Jackson (Ω)	Deionized (Ω)
1	45.726	48,510	41,998	573,750
2	37.349	61,699	40,805	645,720
3	34.669	53,424	39,697	610,910
4	32.787	52,013	40,773	599,480
5	36.725	54,677	38,667	573,780
6	X	X	X	X
7	35.768	53,543	39,008	568,420
8	37.602	53,816	41,516	585,260
9	34.525	50,286	41,197	512,360
10	38.637	51,892	42,099	577,860
11	35.959	48,797	40,832	547,670
12	36.451	49,294	40,586	548,300
1A (10x5)	24.510	40,171	27,183	439,160
2A	24.152	34,624	25,716	465,540
1B (20x2.5)	18.490	26,967	16,854	297,830
2B	18.930	27,817	16,954	336,950
1C (20x5)	13.890	24,098	12,267	268,780
2C	13.970	24,152	12,178	279,180

Two conclusions can be drawn based on the data in Table 6.1. First, the seawater has a much lower resistance than the samples from the freshwater sources. This lower resistance is unsurprising since the salinity of the seawater is much greater than the salinity of the freshwater sources. It can also be seen that the resistance of the deionized water was much greater than all of the other water samples. The deionized water should have had almost no salts in it; therefore, the resistance measurement should have been very large. Because both the Turkey Creek and the Lake Jackson samples had a lower resistance than the deionized water, it can be concluded that, while neither had a high salinity, they did not a nonzero salinity.

The fact that Turkey Creek had a higher resistance than Lake Jackson implies that it had a lower salinity. This conclusion was supported by later measurements. Another important observation is the measurement differences between the boards with different electrode dimensions. While both the 10 mm by 5 mm (labeled A) and the 20 mm by 2.5 mm (labeled B) boards have the same electrode area, their resistances are not equal. Furthermore, the resistances measured by the B sensors are close to being half the resistances measured by the original sensors, which have half of the electrode area of the B boards. These differences imply that the measured resistance is inversely proportional to the electrode length but not to the electrode width. These relationships are shown and discussed in the Section 7.2.

6.1.2 Commercial Sensor Measurements

Next, the salinities of the water samples were measured using the commercial sensors. Table 6.2 shows the measurements obtained using the MA887-BOX Digital Refractometer. The temperature for all tests was around 22°C; however, the conductivity was calculated at a temperature of 25°C to make it easier to compare to the conductivity pen's measurements. The measurements were repeated five times each, and the averages were calculated. The conductivity

for the measured salinity was calculated using the PSS-78 algorithm. Based on the measurements, it can be concluded that the seawater has a conductivity of around 4.6 S/m at 25ºC. Usually the conductivity of seawater is between 4 and 5 S/m, so this result appears accurate [47]. The results of measuring the conductivity in the Turkey Creek water and Lake Jackson water; however, do not appear to have been accurate. According the reflectometer, both the Turkey Creek and Lake Jackson samples have a salinity of zero. The PCB sensors' measurements indicated that both samples have a low but nonzero salinity. The reason for the disagreement was that the salinity of the two samples was too low for the reflectometer to detect. The reflectometer cannot measure a salinity lower than 1 PSU, which was much greater than the salinity of the Turkey Creek and Lake Jackson samples. The fact that the PCB sensor was able to measure a difference indicates that it was much more sensitive than the reflectometer.

Table 6.2: Salinity measurements obtained using the reflectometer

	Seawater			Turkey Creek			Lake Jackson		
Test #	(PSU)	(ppt)	(S.G.)	(PSU)	(ppt)	(S.G.)	(PSU)	(ppt)	(S.G.)
1	31	32	1.024	0	0	1	0	0	1
2	31	31	1.024	0	0	1	0	0	1
3	31	32	1.024	0	0	1	0	0	1
4	31	31	1.024	0	0	1	0	0	1
5	31	32	1.024	0	0	1	0	0	1
Ave	**31**	**31.6**	**1.024**	**0**	**0**	**1**	**0**	**0**	**1**
Ave Cond at 25°C	**4.5295**	**4.6072**	**4.6469**	**0**	**0**	**0**	**0**	**0**	**0**

Table 6.3 shows the salinity measurements obtained using the Instant Ocean SeaTest Hydrometer. The measurements were repeated three times each, and the averages were calculated. The conductivity was again calculated using the PSS-78 algorithm. Based on the measurements, the seawater has a conductivity of greater than 5 S/m, slightly higher than what is

expected based on the reflectometer results. The reason for this discrepancy is that the hydrometer is not as accurate as the reflectometer. The hydrometer determines the salinity based on the location of a floating pointer, with the higher the pointer indicating a higher salinity. However, the location of the pointer can be strongly influenced by bubbles. Any bubbles adhering to the pointer's surface will cause it to float higher than it should, giving the impression that the salinity is higher than it actually is. This behavior was the likely cause of the difference between the reflectometer and the hydrometer.

Similar to the reflectometer, the hydrometer measured a salinity of zero for the Turkey Creek and the Lake Jackson samples. As mentioned before, these results occurred because the salinity of the samples was too low for the hydrometer to detect. The fact that the PCB sensor was able to detect a difference in the samples indicates that it has a higher measurement range and sensitivity than the hydrometer.

Table 6.3: Salinity measurements obtained using the hydrometer

	Seawater		Turkey Creek		Lake Jackson	
Test #	(ppt)	(S.G.)	(ppt)	(S.G.)	(ppt)	(S.G.)
1	38	1.028	0	1	0	1
2	35	1.025	0	1	0	1
3	38	1.028	0	1	0	1
Ave	**37**	**1.027**	**0**	**1**	**0**	**1**
Ave Cond at 25°C	**5.2491**	**5.0976**	**0**	**0**	**0**	**0**

Table 6.4 shows the salinity measurements obtained using the 4366 Traceable Conductivity/TDS Pen. The measurements were repeated three times each, and the averages were calculated. Since the pen automatically calculated conductivity, the PSS-78 algorithm was not used. Based on the measurements, it can be concluded that the water sample from Turkey

Creek had a conductivity of 1.1 mS/m, and the water sample from Lake Jackson had a conductivity of around 2 mS/m at 25º C. These results align with the measurements obtained using the PCB sensor. Both conductivities were very small, with Turkey Creek's being the smallest. Unlike the reflectometer and the hydrometer, the pen was not able to measure the conductivity of the seawater. According to its manual, the pen cannot measure a conductivity higher than 2 S/m [45]. This limitation means that the PCB sensor has larger measurement range than the pen.

Table 6.4: Salinity measurement obtained using the conductivity pen

	Seawater		Turkey Creek		Lake Jackson	
Test #	Cond (S/m)	TDS (ppm)	Cond (S/m)	TDS (ppm)	Cond (S/m)	TDS (ppm)
1	Too high	Too high	0.0011	6	0.0021	10
2	Too high	Too high	0.0011	6	0.0020	10
3	Too high	Too high	0.0011	6	0.0021	11
Ave Cond at 25°C	**Too high**		**0.0011**		**0.00207**	

6.1.3 Original Concentration Test Results

Next, the PCB sensors were used to measure the change in resistance as the concentration of seawater in a sample was varied. As described in Chapter 5, this variability was achieved by starting with one of the fresh water samples and slowly adding more and more seawater to it until the amount of water from both samples was equal. The process was then repeated in reverse: one of the fresh water samples was added to the seawater until the amount of water from both is equal.

Figure 6.1 and Table A.6 show the results of running a concentration test using the water from Turkey Creek. Sensors 2, 3, and 12 were used because their earlier measurements were closest to the average. To make the shape of the plot easier to view, the y-axis was limited to only 250 Ohms. At 0% seawater the resistance was so large (around 45000 Ohms) that the rest of the plot became difficult to see if it were included. In all of the concentration tests, the resistances measured by the PCB sensors were very large (but not infinite) at 0% seawater. This high resistance was caused by the very low conductivity of the freshwater samples.

The resistance measurements from all three sensors were very close, implying that there was little variation among sensors. The plot are fairly smooth. The small discontinuity at 50% resulted from the testing method. During the test, the 0% to 50% seawater was measured by adding seawater to 100 mL of Turkey Creek water, while the 50% to 100% was measured by adding Turkey Creek water to 100 mL of seawater. The discontinuity indicates a difference in conductivity at the end of the two tests. There are two potential causes for the difference. First, a small difference in that amount of water in the two solutions could cause a difference in the ratio of water samples. Second, a difference in temperature when the measurements were taken would result in a difference in the conductivity. However, the discontinuity was small enough to not be a concern in this case.

The results show that as seawater was added to the solution, the resistance measured by the PCB sensors decreased. Before any seawater had been added, the measured resistance was in the tens of thousands of Ohms because the conductivity of the Turkey Creek water was so small. However, the measured resistance dropped quickly after only a small amount of the seawater was added. Adding seawater had a strong impact on the resistance when the percentage of seawater was small, but its impact decreased as more seawater was added.

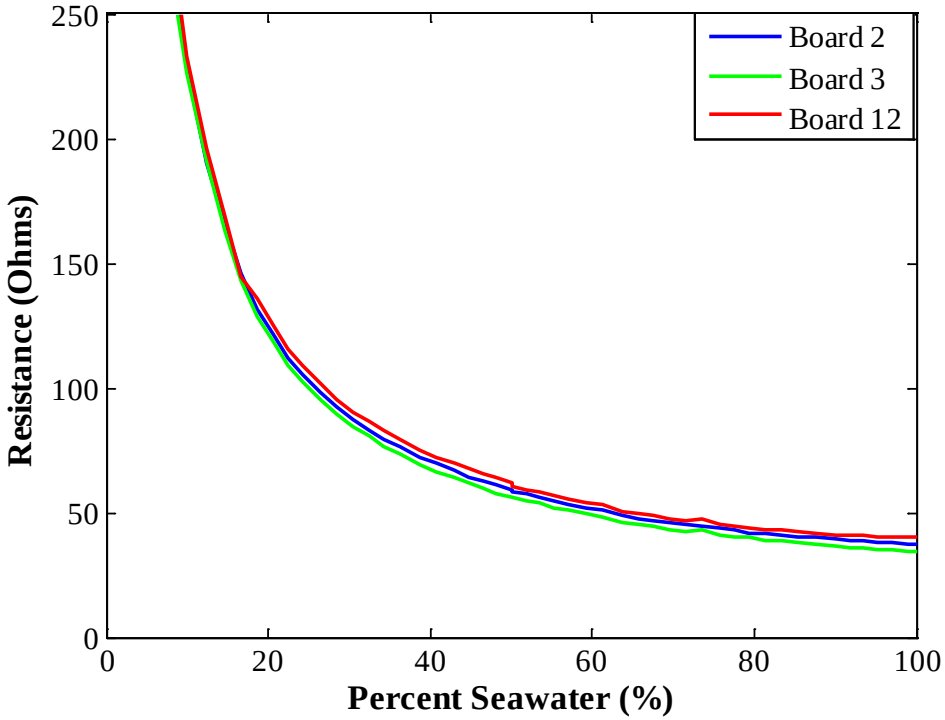

Figure 6.1: Change in measured resistance as seawater was added to water from Turkey Creek

Figure 6.2 and Table A.7 show the results of running a concentration test using the water from Lake Jackson. The plots are very similar to the Turkey Creek plots. The measured resistance started high (in the tens of thousands of Ohms) and then dropped abruptly when seawater was first added, before tapering off as the amount of seawater increased. As mentioned before, the sensors' measurements were within only a few Ohms of each other. Again, a discontinuity at 50% occurred, but it was small enough to not be a concern. Comparing Figure 6.1 and Figure 6.2 revels that the results were nearly identical. Before any seawater was added, Turkey Creek had a higher resistance; however, as seawater was added, the plots quickly approached the same values. This similarity occurred because the salinities of samples from Turkey Creek and Lake Jackson were so small that their impact was outweighed by the seawater.

According to the conductivity pen, the conductivity of the two freshwater samples was thousands of times smaller than the conductivity of the seawater. It required only a small amount of seawater to completely overshadow the influence of the freshwater.

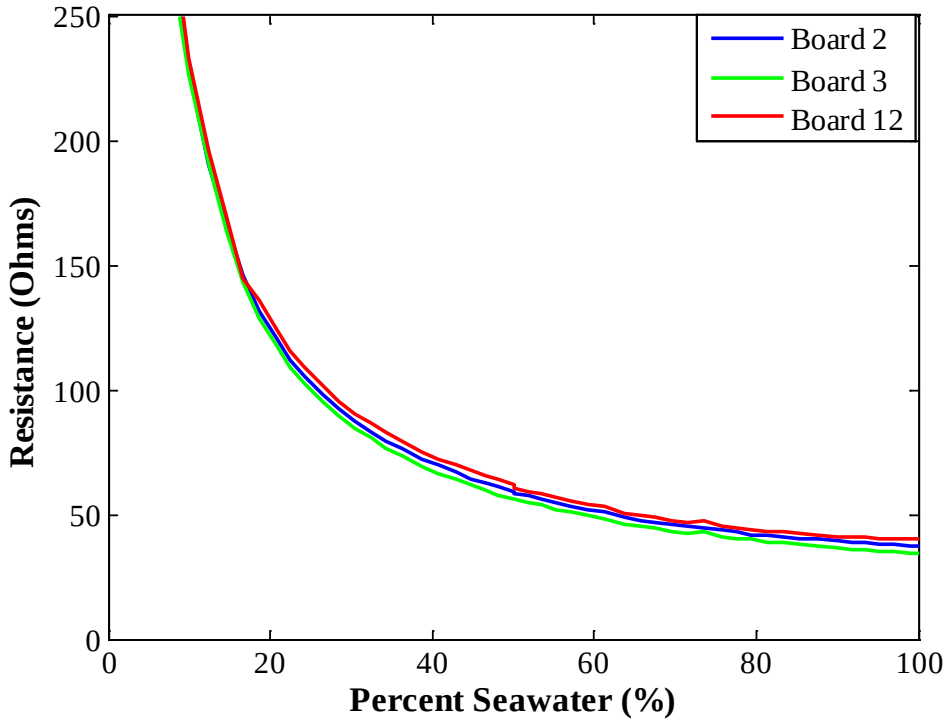

Figure 6.2: Change in measured resistance as seawater was added to water from Lake Jackson

6.2 Second Round of Testing

After determining that the results presented in Section 6.1 were not accurate enough, the testing was repeated. This time the method outlined in Section 5.3 was used. Rain water gathered in Auburn was tested along with new samples of water from the ocean, Turkey Creek, and Lake Jackson. The measurement frequency of the LCR meter was increased from 5 kHz to 200 kHz. Also, the new PCB sensors were tested alongside the original sensors used in the previous section.

6.2.1 Pure Water Measurements

Tables 6.5 and 6.6 show the seawater, Turkey Creek, Lake Jackson, and rain water resistance measurements obtained using the original and new sensors. To further demonstrate the effect measurement frequency had on the resistance measured, the Turkey Creek, Lake Jackson, and rain water were measured at both 200 kHz and 250 Hz. The results were unsurprising. First, the measurements obtained by the same type of sensor in the same water sample were close to one another, indicating little variability in how the individual sensors preformed. The results also show that as the electrode area increases, the measured resistance decreases. As discussed in Section 6.1.1, increasing the length of the electrodes had a larger effect on the resistance than increasing the width. Also, comparing the resistance measurements made by the non-gold plated new sensors (1D through 9D) with the gold-plated sensors indicates little difference in their behavior. The gold-plated sensors' measurements were slightly lower than the non-gold plated sensors, but otherwise their results were nearly identical.

Comparing the results of the 200 kHz and 250 Hz tests supports the concerns raised about electrode polarization. Despite being the same sensors and in the same water sample, the resistances measured at 250 Hz were much higher than the resistances measured at 200 kHz. The percent differences between the averages of the 200 kHz and 250 Hz are calculated at the bottom of the tables. They demonstrate that electrode polarization has a larger impact on the old 10 mm by 2.5 mm sensors than the 20 mm by 5 mm sensors. The percent difference for the old sensors was always greater than 5%, while it was never greater than 2% for the new sensors. This behavior is unsurprising since increasing the size of the electrode should decrease the effect of electrode polarization [6].

Table 6.5: Results of testing the new pure water samples using the modified testing process with the original boards

Sensor #	Seawater at 200 kHz (Ω)	Turkey Creek at 200 kHz (Ω)	Turkey Creek at 250 Hz (Ω)	Lake Jackson at 200 kHz (Ω)	Lake Jackson at 250 Hz (Ω)	Rain Water at 200 kHz (Ω)	Rain water at 250 Hz (Ω)
1	25.89	54,155	67,722	48,347	55,633	95,469	124,620
2	23.85	55,141	66,951	48,650	55,392	95,827	126,090
3	23.46	53,863	67,600	48,735	54,914	96,296	124,060
4	23.07	54,396	64,835	47,280	54,987	92,685	124,540
5	23.54	54,140	66,329	48,195	54,381	96,409	123,970
6	X	X	X	X	X	X	X
7	22.94	54,029	63,653	48,047	54,301	95,551	123,640
8	23.37	52,857	64,434	48,559	54,345	96,327	123,400
9	23.11	52,313	62,310	46,986	54,447	91,811	123,960
10	23.63	51,941	63,932	47,861	54,498	95,753	123,290
11	22.94	50,988	61,313	47,379	54,048	93,465	124,800
12	23.48	51,871	62,355	47,829	53,648	94,218	121,630
1A (10x5)	16.73	40,817	46,274	37,575	41,067	76,514	93,261
2A	16.69	39,780	46,138	37,683	40,850	75,503	92,917
1B(20x2.5)	12.44	31,336	31,784	29,080	30,000	60,520	66,079
2B	12.53	30,614	31,810	29,029	30,466	61,408	64,903
1C(20x5)	9.59	27,822	29,242	24,375	25,413	48,998	52,243
2C	9.59	28,288	30,329	24,505	25,083	49,389	51,900
Average (#1-#12)	**23.57**	**28,207**	**28,949**	**22,582**	**23,199**	**51,518**	**53,323**
Percent Difference			**9.69%**		**6.44%**		**13.30%**

Table 6.6: Results of testing the new pure water samples using the modified testing process with the new boards

Sensor #	Seawater at 200 kHz (Ω)	Turkey Creek at 200 kHz (Ω)	Turkey Creek at 250 Hz (Ω)	Lake Jackson at 200 kHz (Ω)	Lake Jackson at 250 Hz (Ω)	Rain water at 200 kHz (Ω)	Rain water at 250 Hz (Ω)
1D	9.90	29,484	29,799	23,043	23,755	53,476	54,677
2D	10.07	29,201	30,503	23,190	23,971	52,526	55,210
3D	9.80	29,972	28,874	22,867	23,447	52,200	54,206
4D	9.87	28,511	30,288	22,615	23,551	52,076	54,733
5D	9.87	28,946	30,043	22,777	22,681	52,554	53,614
6D	9.94	28,610	29,784	22,421	23,431	51,385	53,841
7D	9.67	28,400	28,643	22,885	22,923	51,626	53,160
8D	9.70	26,776	28,596	22,222	23,509	50,927	53,196
9D	9.99	27,784	28,306	22,809	23,046	51,104	52,252
1G	9.19	27,443	27,985	22,042	22,931	50,431	52,718
2G	9.37	27,304	27,760	22,296	22,394	51,318	51,677
3G	9.18	26,053	26,812	21,815	22,747	48,595	50,588
Average	**9.87**	**28,207**	**28,949**	**22,582**	**23,199**	**51,518**	**53,323**
Percent Difference			**1.30%**		**1.35%**		**1.72%**

6.2.2 Commercial Sensors New Measurements

Since the water samples used in the new testing were taken at a different time than the samples used in Section 6.1.2, the salinity of the seawater, Turkey Creek, and Lake Jackson samples were measured again using the commercial sensors. The measuring process was the same as before. The only difference was that the rain water was measured as well. Table 6.7 shows the results of measuring the salinity using the reflectometer. Like before, the salinities of the water from Turkey Creek and Lake Jackson were too small for the reflectometer to measure. The measurements on the rain water indicated that its salinity was also too low to be measured by the reflectometer. This is unsurprising since the rain water was gathered in Auburn, which is far enough inland to have little salt in the rain water. The salinity of the seawater was higher than

in the previous samples, going from 31.6 ppt to 35.33 ppt. This increase was not concerning since the salinity was still within the expected salinity range of 33 to 37 ppt for seawater [47].

Table 6.7: Salinity measurements of the new water obtained using the reflectometer

	Seawater			Turkey Creek			Lake Jackson			Rain Water		
Test #	PSU	ppt	S.G.	PSU	ppt	S.G.	PSU	ppt	S.G.	PSU	ppt	S.G.
1	34	35	1.027	0	0	1	0	0	1	0	0	1
2	34	35	1.027	0	0	1	0	0	1	0	0	1
3	35	36	1.027	0	0	1	0	0	1	0	0	1
Ave	**34.33**	**35.33**	**1.027**	**0**	**0**	**1**	**0**	**0**	**1**	**0**	**0**	**1**
Ave Cond (S/m) At 25°C	**4.9109**	**5.0380**	**5.0976**	**0**	**0**	**0**	**0**	**0**	**0**	**0**	**0**	**0**

Since earlier testing had already shown that the salinities of the Turkey Creek, Lake Jackson, and rain water were too small for the hydrometer to measure, it was used only on the seawater. The results are shown in Table 6.8. Unlike the reflectometer, the hydrometer did not measure a noticeable increase in the salinity of the seawater, going from 37 ppt to 36.67 ppt. This discrepancy could be the result of natural fluctuations in salinity of the seawater caused by freshwater runoff entering the Gulf at the shoreline. The seawater samples were taken a day after it had rained. The rainwater could have caused the decrease in salinity. However, since the reflectometer measured an increase in salinity in the same samples, it is more likely that the discrepancy was caused by the poor accuracy of the hydrometer. As mentioned before, the hydrometer was very sensitive to bubbles adhering to the pointer. Due to this lack of accuracy, the hydrometer's measurements were considered less important than those from the reflectometer.

Table 6.8: Salinity measurements of the new seawater obtained using the hydrometer

Test #	(ppt)	(S.G.)
1	36	1.026
2	38	1.028
3	38	1.028
Ave	**36.67**	**1.0273**
Ave Cond 25°C	**5.5307**	**5.4707**

Table 6.9 shows the results of measuring the salinities of the water samples using the conductivity pen. The measurements are similar to the results in Table 6.4. Like before, the salinity of the seawater was too large for the conductivity pen to measure. The conductivities of both the Turkey Creek water and the Lake Jackson samples are the same as in Table 6.4. The conductivity of the rain water was less than all of the others. This lower conductivity matches behavior observed in the previous section.

Table 6.9: Salinity measurement obtained using the conductivity pen

	Seawater		Turkey Creek		Lake Jackson		Rain Water	
Test #	Cond (S/m)	TDS (ppm)	Cond (S/m)	TDS (ppm)	Cond (S/m)	TDS (ppm)	Cond (S/m)	TDS (ppm)
1	too high	too high	0.0011	6	0.0021	10	0.0004	2
2	too high	too high	0.0011	6	0.0021	10	0.0004	2
3	too high	too high	0.0010	5	0.0021	11	0.0004	2
Ave Cond at 25°C	**Too high**		**0.00107**		**0.0027**		**0.0004**	

6.2.3 Second Concentration Test Results

Next, the PCB sensors were again used to measure the change in resistance as the concentration of saltwater in a sample was varied. Three of the original PCB sensors (numbers 2, 3, and 12), three of the new non-gold plated PCB sensors (numbers 4D, 5D, and 6D), and the new three gold-plated sensors were used. This time the concentration tests were done using the Turkey Creek, Lake Jackson, and rain water samples.

Figure 6.3 and Table A.8 show the results obtained using the original sensors in the Turkey Creek concentration test. Tables A.9 and A.10 show the data obtained using the non-gold plated and gold-plated sensors, and the data is plotted in Figure 6.4. Next, Figures 6.5 and 6.6 show the measurements made by the original and new sensors during the Lake Jackson concentration test. The data plotted in the two figures are recorded in Table A.11 through A.13. Finally, Figures 6.7 and 6.8 show the measurements made by the original and new sensors during the rain water connection test. The data plotted in the figures are recorded in Tables A.14 through A.16.

Comparing the old sensors' measurements to the previous measurements in Section 6.1.3 show a similar behavior; however, the new measurements were lower than in the previous section. This decrease was due to the increase in the measurement frequency. The increased frequency minimized the effect of electrode polarization and as a result improved the accuracy of the measurements. The shapes of all of the plots in this section are similar. In all, the measured resistance began high, in the tens of thousands of Ohms, before it rapidly decreased as more seawater was added. As the percentage of seawater became large, the decrease in resistance leveled out. The resistances measured by the original sensors were larger than the resistances measured by the new sensors. This behavior matches what was seen in Section 6.2.1 and was

due to the electrodes of the new sensors being larger than the original sensors. Also, the measurements obtained by sensors with the same electrode geometry were very similar in all three sets of concentration tests. Furthermore, the resistances measured in all of the tests by the non-gold plated new sensors and the gold-plated sensors were very close together, indicating that the gold plating did not have a large effect on the behavior of the sensors.

The main problem with the results is obvious. The plots in all six figures have a smooth section and non-smooth section separated by a large discontinuity. The non-smooth regions of the plots indicate that the resistance measurements were fluctuating as the resistance was measured. For the Turkey Creek and Lake Jackson plots, the non-smooth region is located between 0% and 50%. For the rain water plots, the non-smooth region is located between 50% and 100%. Since the non-smooth region was not on the same part of the plot for all of the tests, the non-smooth regions were not the result of some property of the water at a certain salinity. Also, the behavior of the resistance measurements was not consistent for each sensor in the non-smooth regions of the plots. Instead, measurements from each sensor behaved differently. The resistances measured by all of the sensors did not spike together. Instead, one or two of the sensors may have measured a spike in resistance, while the rest of the sensors may have continued to measure a smooth transition or even a sharp decrease. This lack of consistency indicates that the non-smooth regions were not caused by adding the wrong amount of water to the solution during testing.

The most likely cause of the non-smooth regions of the plots was the test setup itself. As discussed in Section 5.3, to make testing easier, long wires had been soldered to the ends of the sensors' headers, and the wires had been plugged into separate rows on a breadboard. Jumper wires connected to the LCR meter could then be plugged into the rows corresponding to a

specific sensor to measure the resistance. This setup decreased the amount of water lost during testing. The resistances of the wires and the breadboard were measured separately in an attempt to remove their influence on the results. As evidenced by the plots, this attempt proved ineffective. Instead, the resistance of the wires varied greatly with the wires' physical orientation. Bending the wires caused the resistance measured by the LCR meter to vary by several Ohms. As a result, the extra wires were removed, and the setup was modified to what was described in Section 5.4.

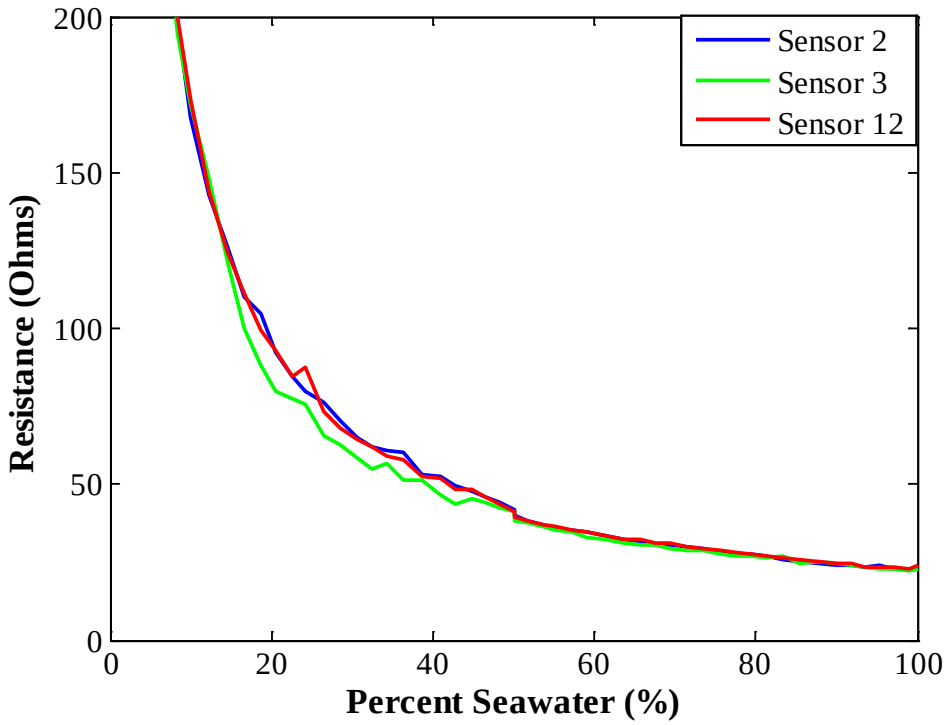

Figure 6.3: Results of the second Turkey Creek concentration tests using the original sensors

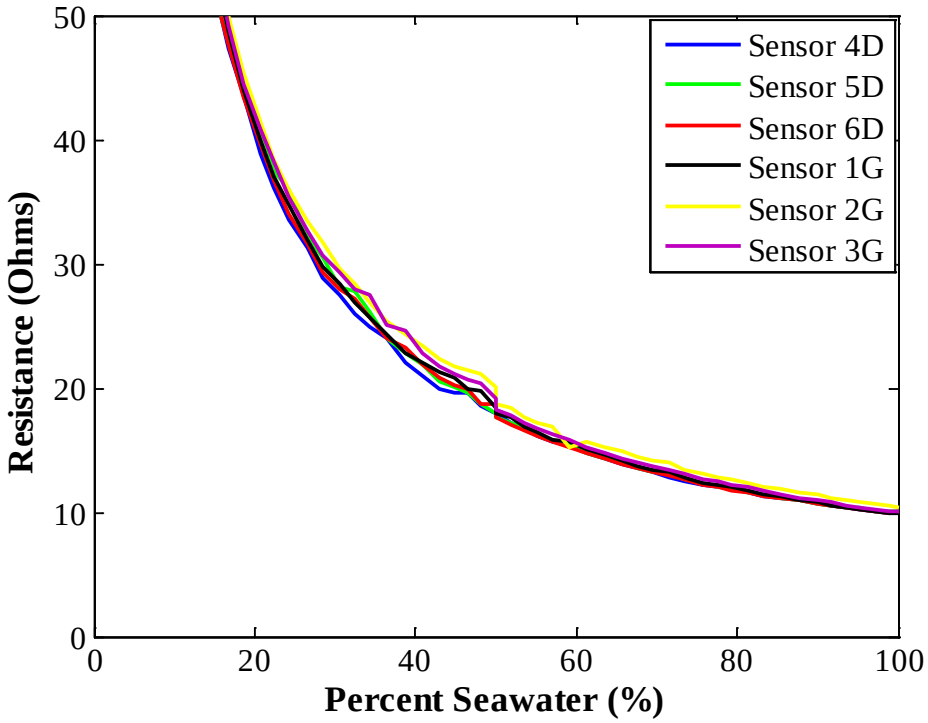

Figure 6.4: Results of the second Turkey Creek concentration tests using the new sensors

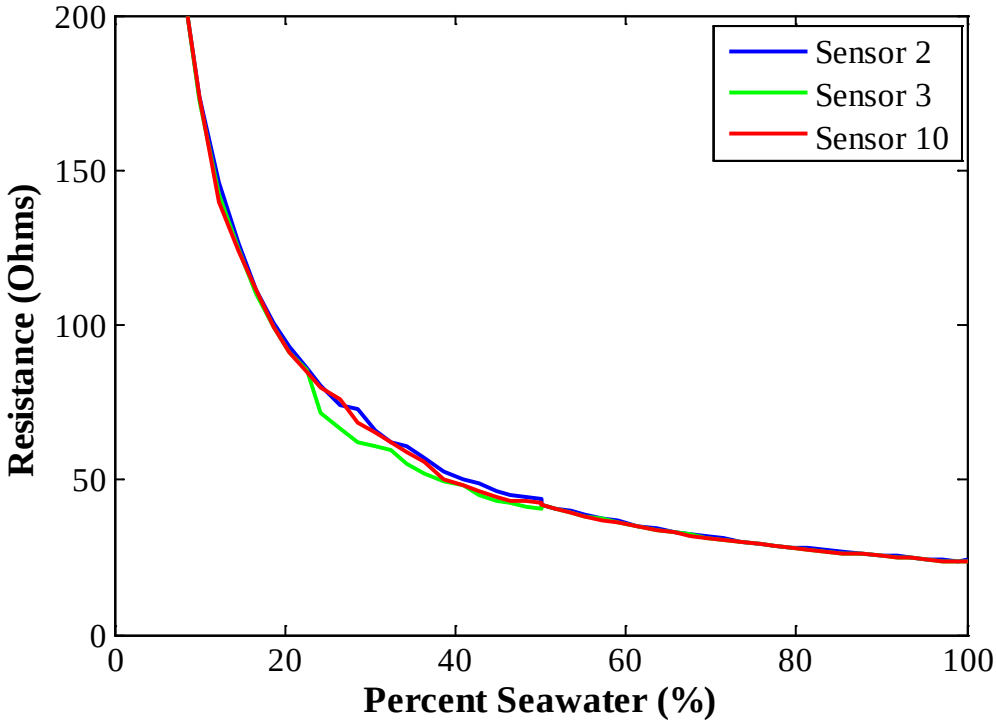

Figure 6.5: Results of the second Lake Jackson concentration tests using the original sensors

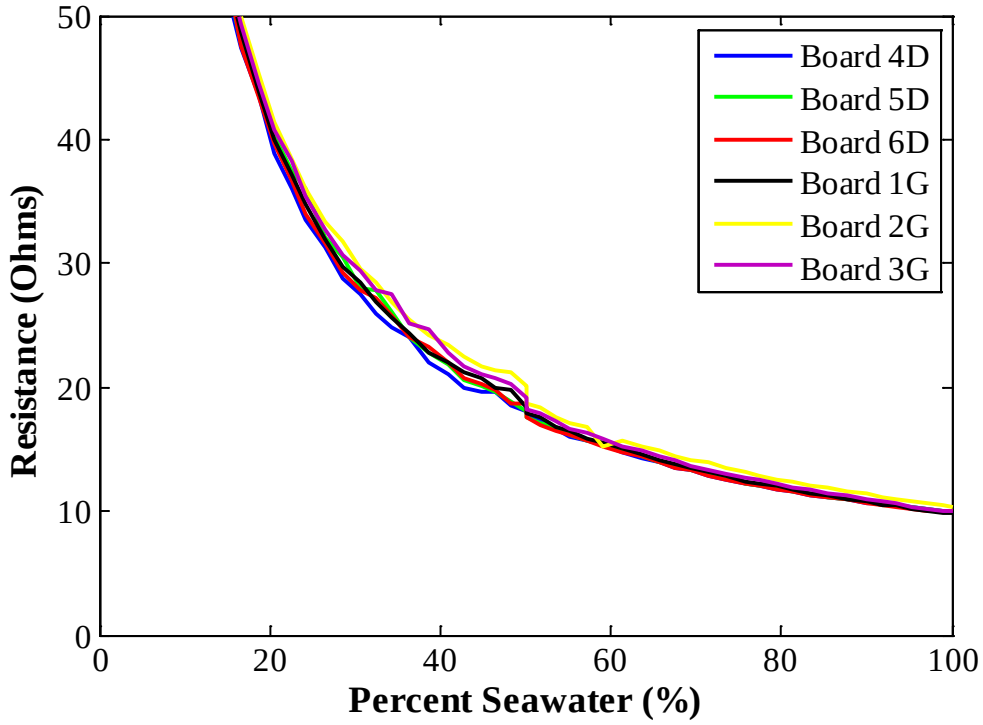

Figure 6.6: Results of the second Lake Jackson concentration tests using the new sensors

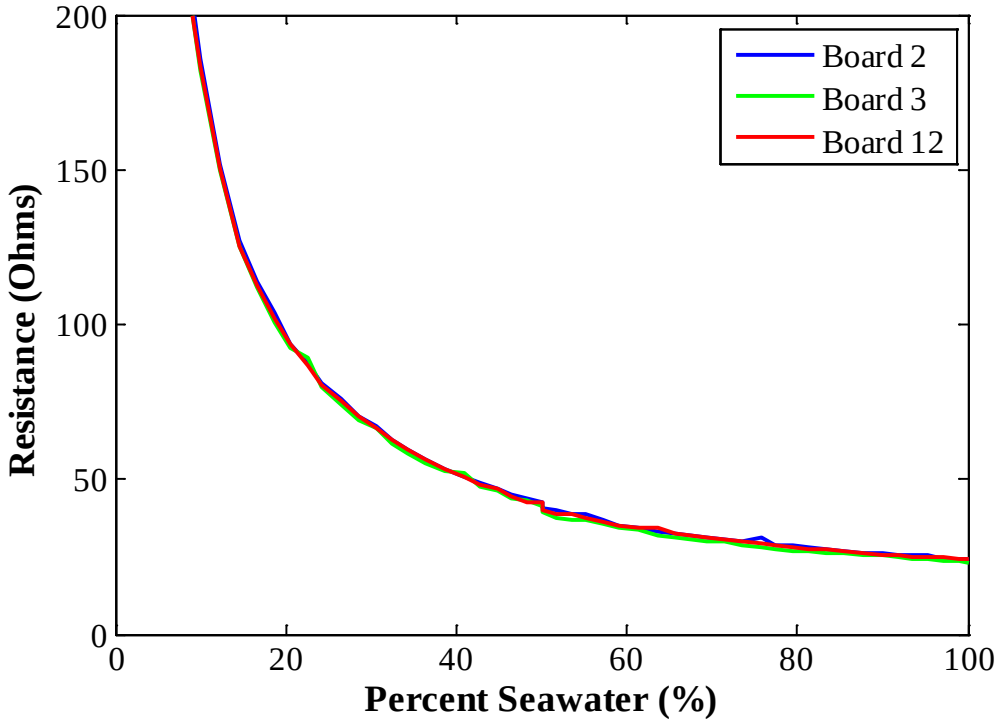

Figure 6.7: Results of the first rain concentration tests using the original sensors

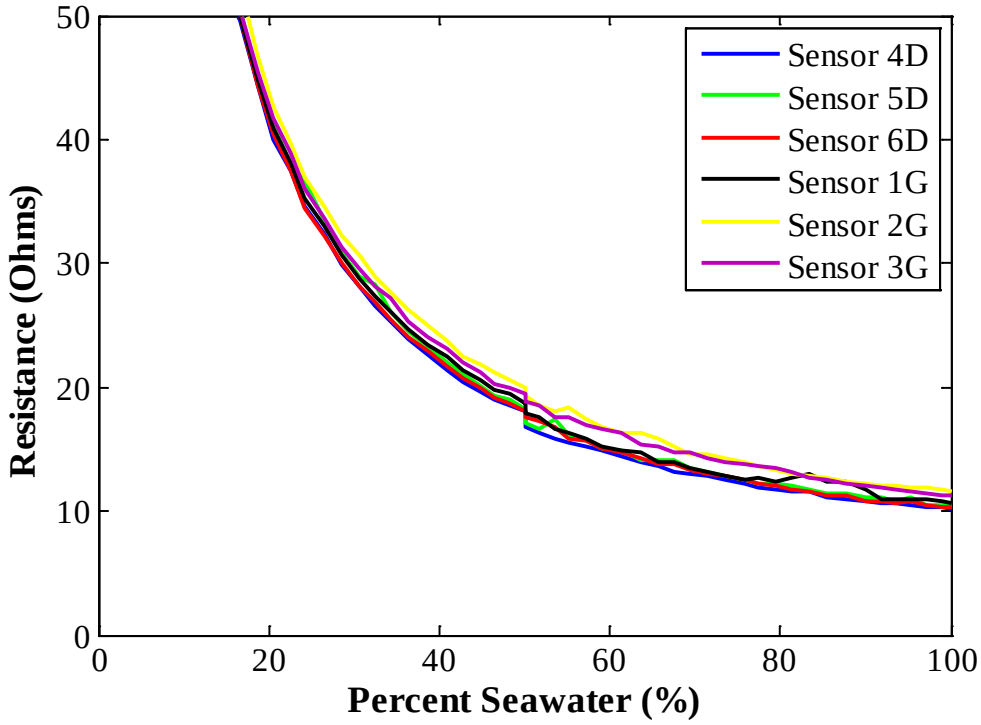

Figure 6.8: Results of the first rain concentration tests using the new sensors

6.3 Final Round of Testing

For the final round of testing, the method outlined in Section 6.1.3 was used. The LCR meter was replaced with the 4192A LF Impedance Analyzer, and the measurement frequency was increased to 1 MHz. Since the same water was being used, the commercial reflectometer, hydrometer, and conductivity pen were not reused.

6.3.1 Calculating the Cell Constant

Using the method outlined in Section 5.4, concentration tests were repeated using the original sensors and the new non-gold plated and the gold-plated sensors. These new tests were performed at a testing frequency of 1 MHz and on the testing stand shown in Figure 5.11. Using the stand helped minimize water loss, but an average of 8 mL of water was still lost during each test. Since it is difficult to know when the water was lost, it is difficult to determine the actual

salinity at every measurement during the test. This uncertainty made it challenging to compare the results of the test to what would be predicted using the simulations and the equation developed in Chapter 8.

To compensate for the loss of water, the commercial conductivity pen and the reflectometer were used to measure the conductivity of the water during the concentration tests. Both sensors have limitations that meant they could not be used at every point during testing. The conductivity pen could only measure conductivities less than 2 S/m. Since the seawater had a conductivity of greater than 5 S/m, the pen was useful for only about a quarter of the testing. The reflectometer could cover the entire range of the concentration test; however, it did not have the resolution the conductivity pen did. The reflectometer calculated the salinity to the nearest PSU or ppt, limiting its accuracy. Furthermore, the reflectometer required a significant amount of water to be removed from the breaker to take a measure, exacerbating the water-loss problem. Instead, the conductivity pen was used to measure the conductivity at low salinities, and the reflectometer was used to measure the salinity at the end of the tests. The conductivity pen's measurements were used to calculate the cell constant of the PCB sensors, and then the cell constant was used to calculate the conductivity at each step of the tests. The reflectometer's measurements were converted to conductivity and compared to the conductivities calculated from the cell constants to ensure that the calculated conductivities were at least close. The temperature of the water was recorded for every step so that the salinity and conductivity measurements could be converted back and forth using the PSS-78 algorithm.

As explained earlier in Sections 3.2 and 5.3, the conductivity of the water can be calculated by dividing the cell constant of the PCB sensor by the resistance the sensor measured while in the water. Since the conductivity pen was able to measure the conductivity of the low

concentrations, the cell constants of the PCB sensors could be determined at those concentrations.

During the concentration tests, the pen was able to measure the conductivity of the first 16 concentrations for all three tests. For these tests, between 0 mL and 40 mL of seawater had been added. The conductivities measured by the pen and the average resistances measured by the PCB sensors over this range are shown in Tables 6.10 through 6.12. The measured conductivities and resistances are similar for the three tests. The conductivities shown in the tables are for the water at the measured temperature instead of 25ºC. They were calculated by using the PSS-78 algorithm. Also, despite being given in the tables, the conductivities on the first row (when no seawater was added) were not determined using the PSS-78 algorithm. The salinities of the pure freshwater samples were too low for the algorithm to calculate the conductivities. To use the algorithm, the salinity must be between 2 PSU and 42 PSU [3].

Table 6.10: Measured conductivities and average resistances for the Turkey Creek concentration tests

Seawater (mL)	Conductivity(S/m)	Original (Ω)	Non-plated (Ω)	Plated (Ω)
0	X	66,459.73	31,514.56	30,992.99
1	0.0659	1,609.36	696.06	699.31
3	0.1908	575.60	246.93	246.81
5	0.3115	354.86	151.00	151.50
7	0.4237	261.19	111.96	112.71
9	0.5403	204.52	87.77	87.96
11	0.6460	171.94	73.71	74.04
14	0.7889	140.74	59.82	60.17
17	0.9351	119.83	50.94	51.20
20	1.0688	105.06	44.72	45.17
23	1.1920	93.90	40.04	40.67
26	1.3095	86.19	36.53	36.82
29	1.4189	79.60	33.76	34.34
32	1.5328	74.61	31.51	32.11
36	1.6660	68.40	28.96	29.45
40	1.7922	64.01	26.94	27.43

Table 6.11: Measured conductivities and average resistance for the Lake Jackson concentration tests

Seawater (mL)	Conductivity(S/m)	Original (Ω)	Non-plated (Ω)	Plated (Ω)
0	X	41,720.80	20,492.21	19,880.93
1	0.0805	1,326.69	573.84	577.82
3	0.2137	512.10	220.67	220.85
5	0.3326	329.47	141.58	142.10
7	0.4548	243.07	104.25	104.43
9	0.5707	194.36	83.52	83.80
11	0.6761	164.50	70.32	70.67
14	0.8364	133.26	57.04	57.19
17	0.9777	114.08	48.73	49.09
20	1.1167	100.18	42.70	43.12
23	1.2504	89.43	37.97	38.37
26	1.3843	81.22	34.55	34.89
29	1.5005	75.08	31.93	32.31
32	1.6091	70.10	29.78	30.12
36	1.7463	64.67	27.57	27.79
40	1.8759	60.12	25.83	26.09

Table 6.12: Measured conductivities and average resistance for the rain concentration tests

Seawater (mL)	Conductivity(S/m)	Original (Ω)	Non-plated (Ω)	Plated (Ω)
0	X	130,821.14	60,715.39	55,122.83
1	0.0663	1,610.75	693.32	693.48
3	0.1962	564.44	242.23	243.11
5	0.3165	348.64	150.11	150.76
7	0.4285	260.85	111.70	112.18
9	0.5355	207.87	89.07	89.33
11	0.6396	178.26	75.61	76.01
14	0.7835	143.56	61.14	61.77
17	0.9220	122.25	52.19	52.79
20	1.0493	107.74	45.70	46.16
23	1.1679	97.99	41.50	42.06
26	1.2815	89.20	37.75	38.26
29	1.3941	82.60	34.88	35.51
32	1.4955	76.20	32.38	32.87
36	1.6608	69.67	29.36	29.85
40	1.7744	65.10	27.46	27.93

Next, using the data in the tables above, the cell constant was calculated for each case using

$$\kappa = \sigma_{measured} R_{ave.} \tag{6.1}$$

To calculate the cell constant for the new sensors, the resistances measured by the non-gold plated and gold-plated sensors were averaged together. Since the new sensors had the same electrode geometry, their cell constant should be nearly the same. Table 6.13 shows the cell constants calculated for the original and the new PCB sensors for all the concentration tests with the bottom row showing the averages. It should be noted that the cell constants tended to increase as more seawater was added. This increase was not expected; the cell constant should remain nearly constant as seawater is added. It was expected that if a change occurred, it would be a slight decrease in the cell constant since the additional water would increase the volume the current could travel through.

A number of factors likely contribute to this increase. The first is electrode polarization, which has been a concern throughout this work. While the measurement frequency has been increased to 1 MHz in order to minimize the impact, it might still be affecting the measurements. According to Randle's equivalent circuit (shown in Figure 4.24), the effect of electrode polarization is represented by a resistance in series with the resistance of the water. When no seawater has been added, the conductivity would be low and, as a result, the resistance of the water would be very high. The resistance of the water would be so much larger than the Faradic impedance that this resistance overshadows influence of electrode polarization on the calculated cell constant. When the conductivity is higher, the resistance of the water is much lower, giving electrode polarization a bigger influence on the calculated cell constant. Any extra resistance in

the testing setup would have a similar impact on the cell constant. This resistance could come from the cables used to connect the PCB sensor to the impedance analyzer and the traces on the sensors. As mentioned before, as the conductivity of the water increases, the influence this extra resistance has on the calculated cell constant increases. Another factor that could have influenced the calculation of the cell constant is the accuracy of the conductivity pen. Throughout this work the conductivity pen has been treated as being 100% accurate. Obviously this assumption is not true. While the pen's manual does not list its accuracy, the pen is not a scientific instrument. Its measurements appear to be fairly accurate, but some error is likely; due to both the limitations of the instrument and the mistakes made by the user.

Table 6.13: Cell constants calculated for the original and new PCB sensors

Seawater added (mL)	TC original cell constant (m^{-1})	TC new cell constant (m^{-1})	LJ original cell constant (m^{-1})	LJ new cell constant (m^{-1})	Rain original cell constant (m^{-1})	Rain new cell constant (m^{-1})
1	106.06	45.98	106.80	46.35	106.79	45.97
3	109.82	47.10	109.43	47.18	110.74	47.61
5	110.54	47.11	109.58	47.18	110.34	47.61
7	110.67	47.60	110.55	47.45	111.77	47.97
9	110.50	47.47	110.92	47.75	111.31	47.77
11	111.08	47.72	111.22	47.66	114.02	48.49
14	111.03	47.33	111.46	47.77	112.48	48.15
17	112.05	47.76	111.54	47.82	112.71	48.40
20	112.29	48.04	111.87	47.92	113.05	48.20
23	111.93	48.10	111.83	47.73	114.45	48.79
26	112.86	48.03	112.44	48.07	114.30	48.71
29	112.94	48.31	112.65	48.20	115.15	49.06
32	114.36	48.76	112.80	48.19	113.96	48.79
36	113.95	48.66	112.94	48.34	115.71	49.16
40	114.71	48.72	112.77	48.70	115.52	49.14
Average	**111.65**	**47.78**	**111.25**	**47.75**	**112.82**	**48.25**

While the increase in the cell constant was unexpected, it was small enough to not have a large impact on the calculating the conductivities. Using the data in Table 6.13, an average cell constant was calculated for the original and the new PCB sensors. The cell constant for the original sensors was calculated to be 111.91 m^{-1}. The cell constant for the new sensors was calculated to be 47.93 m^{-1}. The conductivities for all parts of the three concentration tests were then calculated by solving (6.1) for the conductivity. Tables A.18 through A.20 list the conductivities calculated for all of the tests and show a comparison between the conductivities calculated using the cell constants of the original and new sensors and a comparison between the measured and calculated conductivities. The percent differences were calculated using

$$Percent\ Difference = \frac{\left|\sigma_{original} - \sigma_{new}\right|}{0.5\left(\sigma_{original} + \sigma_{new}\right)} \times 100\% \qquad (6.2)$$

The tables show that the conductivities calculated using the old and new sensors' cell constants are very close. The difference between the calculated conductivities was usually less than 1%. The only exceptions are the first rows where they 10% to 15% apart. This larger difference was likely due to errors with the measurements.

The tables also demonstrate that the calculated conductivities are very close to the conductivities measured by the pen. The first 16 conductivities were measured using the conductivity pen and are assumed to be fairly accurate. While the first value was too low to convert using the PSS-78 algorithm, the other 15 can be compared to the calculated conductivities. The measured and calculated conductivity were usually within 2% of each other. The only exceptions were on the second rows of the tables, when the conductivities were less than 0.08 S/m. There, the percent differences were around 4%, which is still fairly low. The likely cause was errors in the measurements resulting from the conductivities being very low.

6.3.2 Final Concentration Test Results

With the conductivities from all three concentration tests calculated, the results could be plotted. The results of the Turkey Creek tests using both the original and new sensors are plotted versus the percentage of seawater in the water sample in Figures 6.9 and 6.10. The results of the Lake Jackson tests are plotted in Figures 6.11 and 6.12. The results of the rain water tests are plotted in Figures 6.13 and 6.14. A secondary x-axis was added to the top of all six figures to demonstrate how the measured resistance changed with the conductivity of the water. For a closer examination, the results of all of the concentration tests are recorded in Tables A.21 through A.29. The results of the concentration tests were consistent with one another. All of the plots for the electrode geometry have the same shape and cover nearly the same range. Any differences in the ranges were likely due to differences in temperature. Also, the resistances measured by each sensor with the same geometry were consistent with one another. The measurements were so close to each other that it is difficult to distinguish the plots of each sensor separately. Figures 6.15 and 6.16 show a comparison of the measurements obtained by sensor 2 and 4D during all three concentration tests. For both sensors, the results from the tests are nearly indistinguishable from one another, demonstrating that the measurements are repeatable. Furthermore, these results provide support to the conductivity values calculated in Section 6.3.1 by demonstrating that the calculated conductivities correspond to similar resistances across all three tests.

The results shown below are much more useful than the results in the previous sections. Unlike in the earlier results in Section 6.2.3, the plots are smooth, indicating that the sensors and the measurement setup were functioning correctly. This data was later used to evaluate the equation derived in Chapter 8.

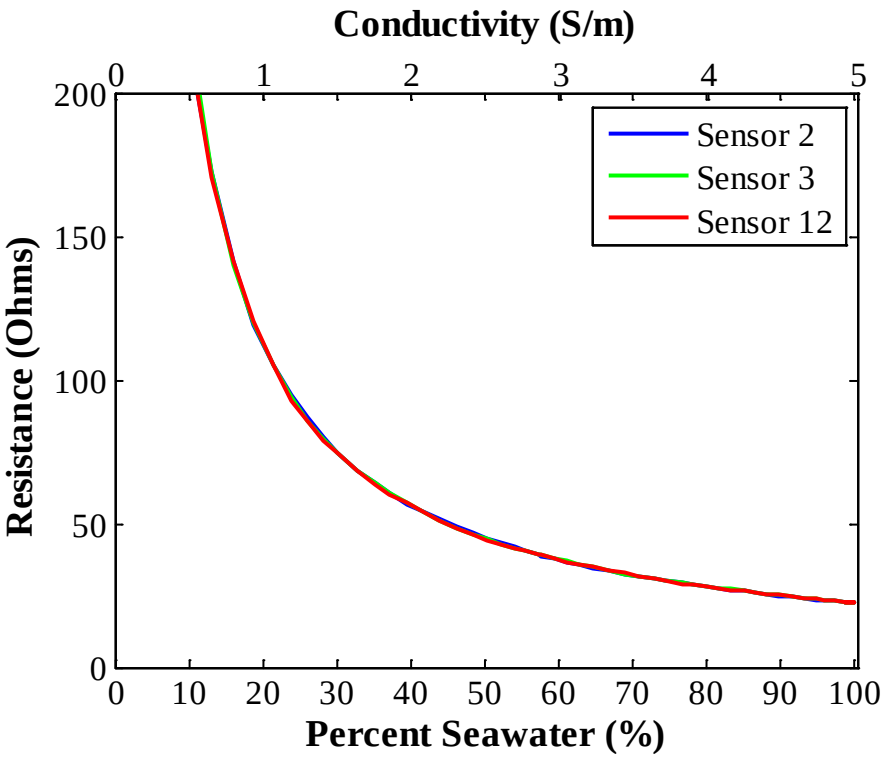

Figure 6.9: Final Turkey Creek concentration test results using the original sensors

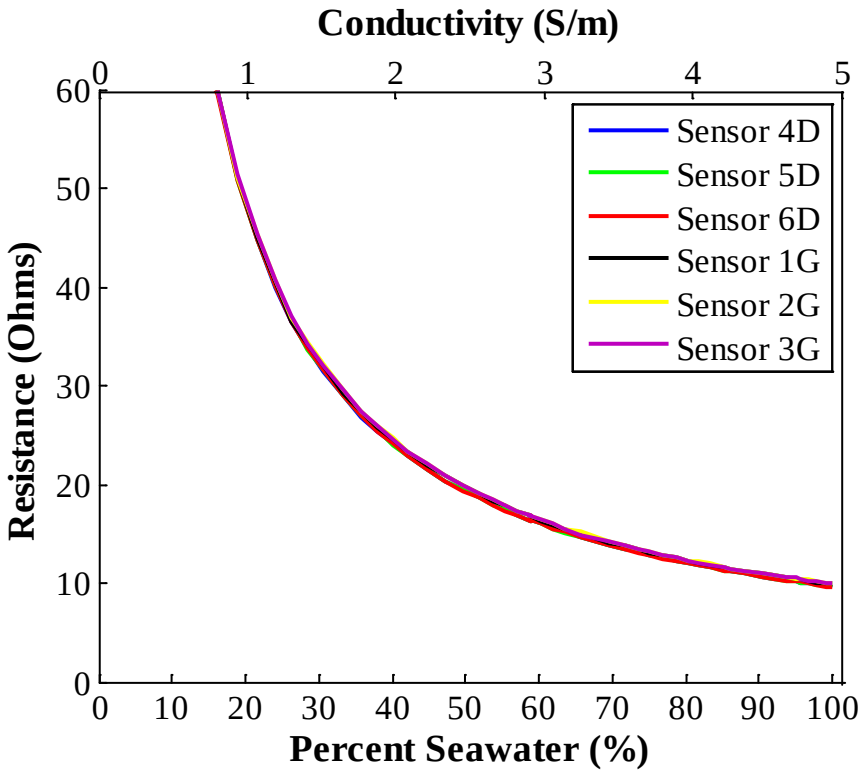

Figure 6.10: Final Turkey Creek concentration test results using the new sensors

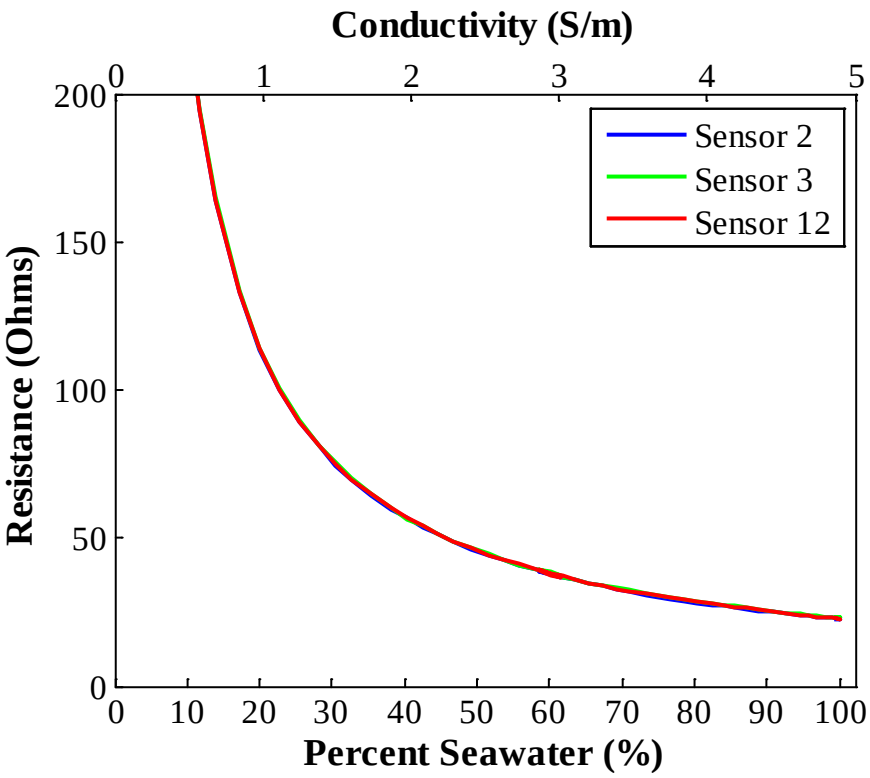

Figure 6.11: Final Lake Jackson concentration test results using the original sensors

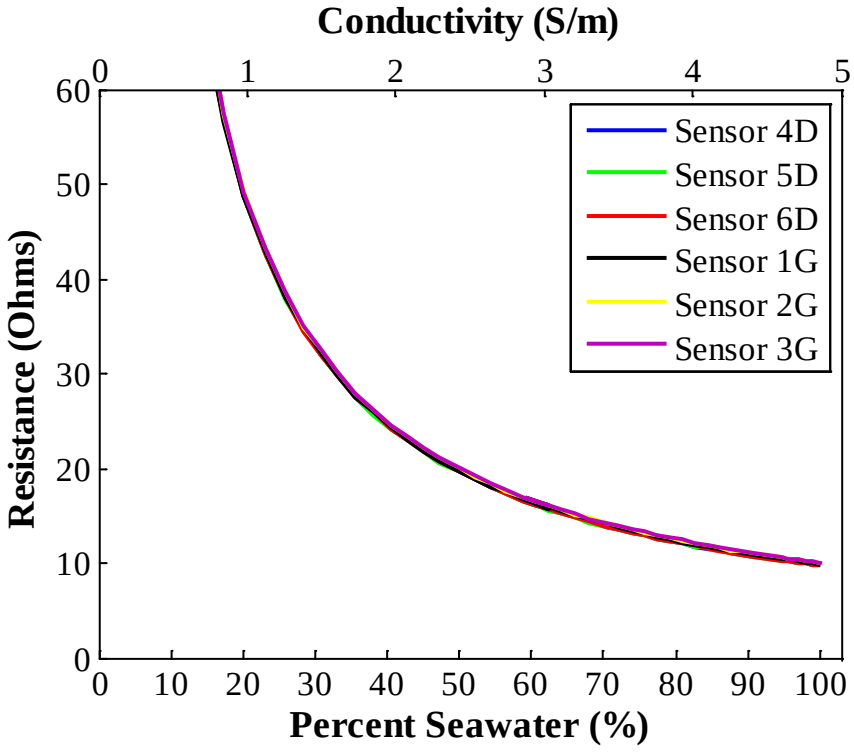

Figure 6.12: Final Lake Jackson concentration test results using the new sensors

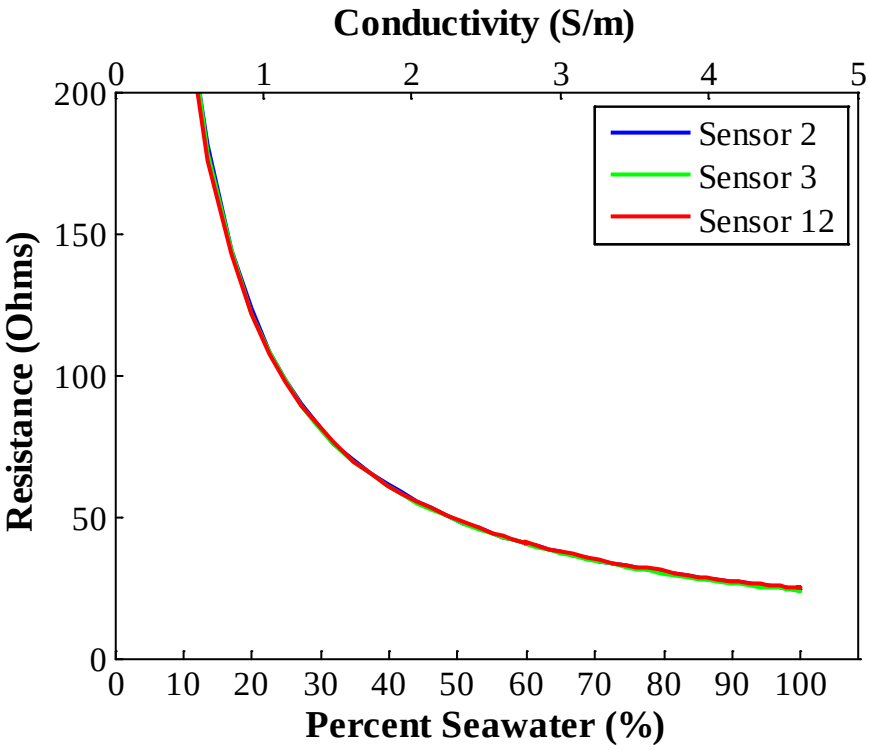

Figure 6.13: Final rain water concentration test results using the original sensors

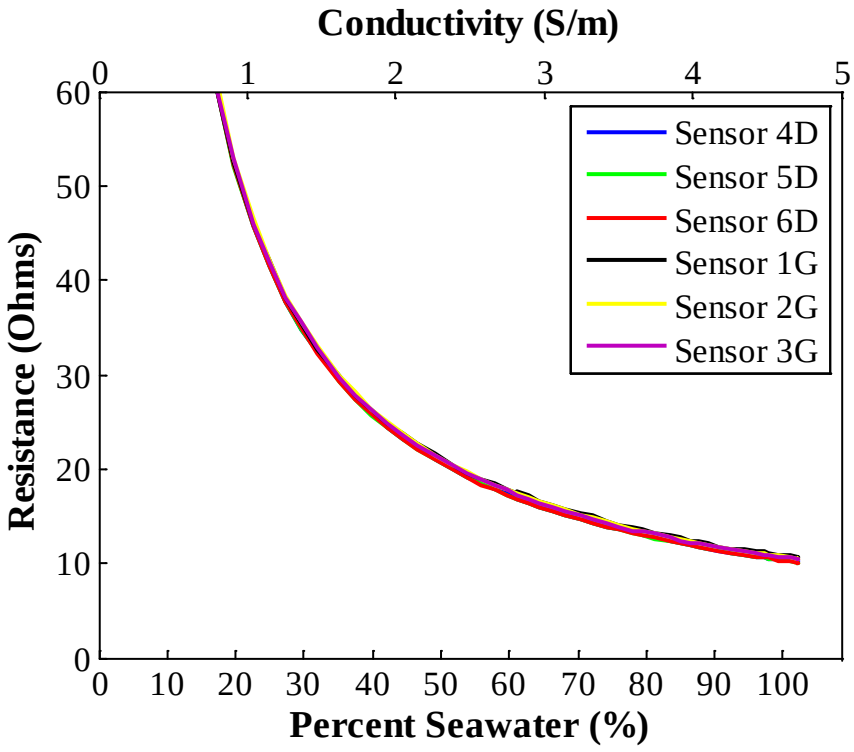

Figure 6.14: Final rain water concentration test results using the new sensors

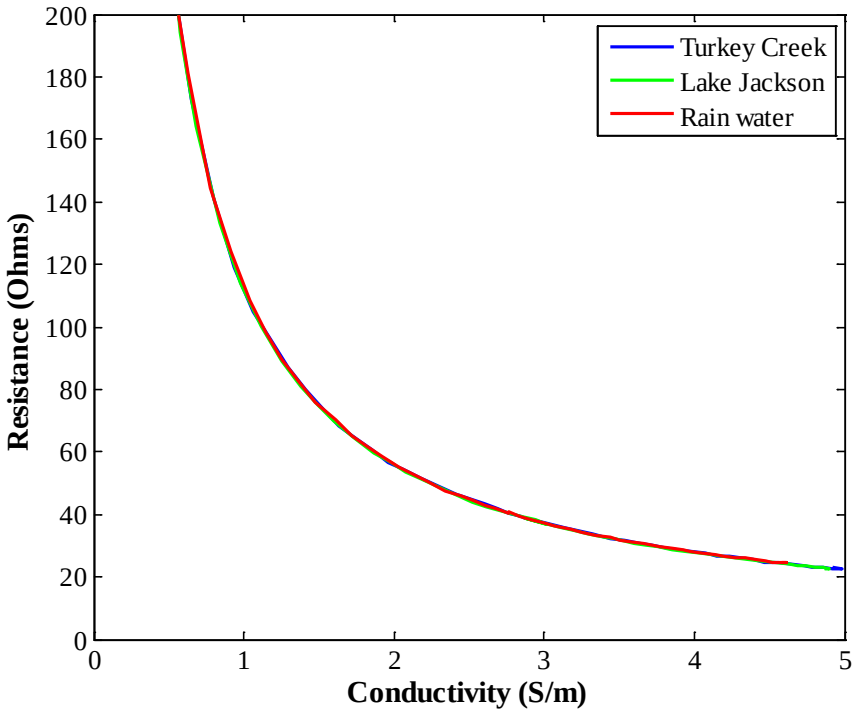

Figure 6.15: Comparison between sensor 2's measurements for all three concentration tests

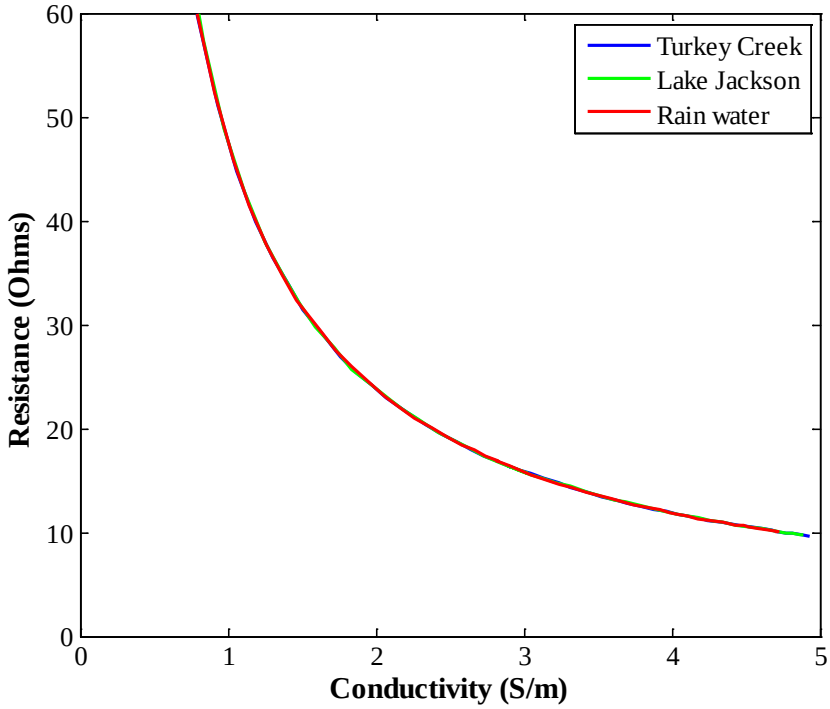

Figure 6.16: Comparison between sensor 4D's measurements for all three concentration tests

Chapter 7

Simulations

To determine the behavior of the PCB sensor, it was simulated using EMPro and Q3D Extractor. Both were used to simulate the influence of the electrical conductivity of the water and the dimensions of the electrodes. However, due to the limitations of both simulators, some simplifications had to be made to the simulation setup. For example, since both simulators had difficulty enclosing the sensor in a cylinder of water (similar to testing the water samples in a beaker), a block of test material with the electrical properties of water was instead placed over the sensor's electrodes.

In the following sections, the simulations of the conductivity and electrode dimensions and their results are discussed. Next, the simplifications done to the simulation setup are described as well as a justification for why their impact on the results can be ignored. The final section is a comparison of the results generated by EMPro and Q3D. The fact that the results generated by both simulators are similar helps legitimize the accuracy of the simulations.

7.1 Electrical Conductivity

The first parameter tested was the effect the electrical conductivity of the water had on the resistance measured by the sensor. It is obvious from the equation for the basic resistance measurement setup, (3.13), that the measured resistance is inversely proportional to the conductivity for any electrode geometry. However, this assumption still needed to be proven.

Simulating the conductivity also proved a good way to test the validity of the two EM simulators.

To observe the influence of the water's conductivity, it was first swept from 0.0001 S/m to 10 S/m, in both EMPro and Q3D. Depending on salinity, the conductivity of water is from $5.5x10^{-6}$ S/m (ultra-pure water) to around 4 or 5 S/m (seawater) [48]. The physical setup for the simulations was the default setup. In the setup, the water was represented by a 20 cm^3 box and the electrodes were 10 mm long, 2.5 mm wide and separated by 2 mm. The simulation results are shown in Figure 7.1 and Table A.30. Figure 7.1 is a plot of the conductance between the sensor's electrodes vs. the water's conductivity. Conductance is the inverse of resistance. Conductance was plotted instead of resistance because it was easier to observe the influence of the water's conductivity. In the figure, the conductance was proportional to the conductivity, making the measured resistance inversely proportional to conductivity or

$$R \propto \frac{1}{\sigma} \tag{7.1}$$

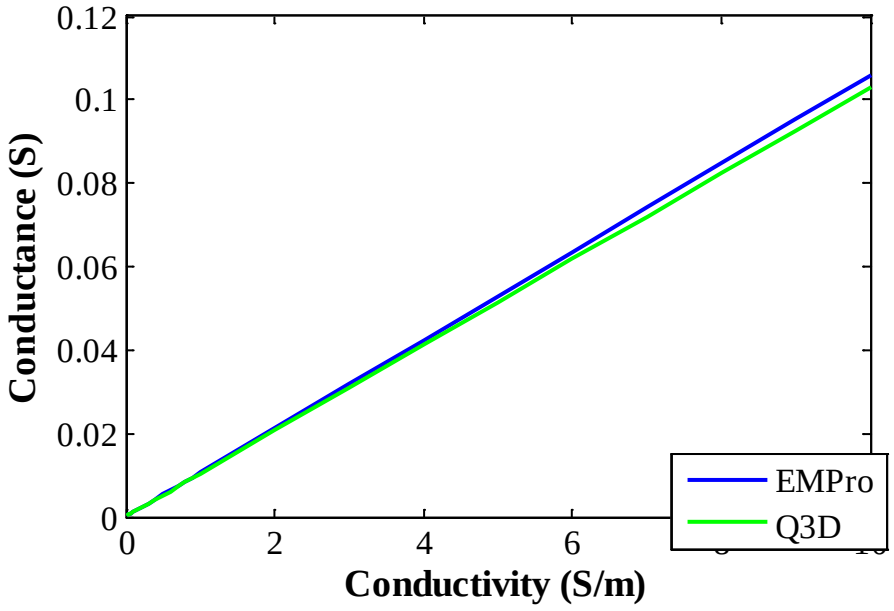

Figure 7.1: Measured conductance vs. the water's conductivity simulated in EMPro and Q3D

Next, to prove that the relationship in (7.1) held for all electrode geometries, the electrode separation distance was swept from 1 mm to 10 mm for conductivities of 0.01 S/m, 0.1 S/m, and 1 S/m. For all three cases, the simulations were done in Q3D. The electrode width was 2.5 mm, and the electrode length was 10 mm. The results are shown in Table 7.1. For all separation distances, the resistance measurements for a conductivity of 0.001 S/m were all 10 times greater than for a conductivity of 0.1 S/m and 100 times greater than for a conductivity of 1 S/m. These results confirm that the relationship between the resistance and the conductivity is not dependent on the electrode separation distance. Further testing could be done to demonstrate the same is true for electrode width and length, but this relationship has been well established. For the rest of the simulations, conductivity was treated as an independent variable equal to 4 S/m.

Table 7.1: Resistance for different conductivities as electrode separation distance is swept

Separation Distance (m)	Conductivity = 0.01 S/m Width = 2.5 mm Length = 10 mm (Ω)	Conductivity = 0.1 S/m Width = 2.5 mm Length = 10 mm (Ω)	Conductivity = 1 S/m Width = 2.5 mm Length = 10 mm (Ω)
0.001	8,452.29944	845.229944	84.5229
0.002	9,845.95995	984.595995	98.4596
0.003	10,716.32067	1,071.632067	107.1632
0.004	11,347.91177	1,134.791177	113.4791
0.005	11,837.04275	1,183.704275	118.3704
0.006	12,218.57864	1,221.857864	122.1858
0.007	12,495.72178	1,249.572178	124.9572
0.008	12,702.14995	1,270.214995	127.0215
0.009	13,011.91136	1,301.191136	130.1191
0.01	13,203.61224	1,320.361224	132.0361

7.2 Electrode Dimensions

Most of the simulation work involved varying the separation distance, length, and width of the sensor's electrodes. The goal was to use the results of these simulations to derive an

equation for the resistance measured by the sensor as a function of not only the water's conductivity but also the electrode's geometry. Originally, each property was swept separately for several different electrode geometries using EMPro.

7.2.1 Electrode Separation Distance

First, the electrode separation distance was swept from 0.1 mm to 0.5 m for the case when the electrodes had a length of 10 mm and a width of 2.5 mm, a length of 10 mm and a width of 5 mm, a length of 20 mm and a width of 2.5 mm, and both a length and a width of 10 mm. These simulations were done several times with different mesh settings until the results were considered reasonably accurate. To be considered reasonably accurate, the plots of the results needed to be fairly smooth with no sharp spikes or discontinuities.

Figure 7.2 and Table A.31 show the results of the final set of simulations done using EMPro. The X's in Table A.31 indicates where EMPro failed to generate a mesh. While the data plotted in Figure 7.2 show only a few electrode geometries, the figure gives a useful description of the behavior of the measured resistance as the electrode separation distance is increased. It demonstrates that the resistance is very small when the electrodes are very close. This behavior is similar to what was seen in equation (3.13) and should be expected since decreasing the distance decreases the amount of material between the electrodes. However, as the separation distance increases, the measured resistance first increases rapidly before appearing to leveling out. In reality the resistance still increases with separation distance; however, the increase is so small that the resistance appears constant. The difference between the plots of the different electrode geometries in Figure 7.2 is how high the resistance is when the plot levels out. Based on the plots, it appears that the smaller the electrode area, the larger the increase in the resistance. However, the effect changing the area depends on whether the electrode length or the width is

changed. The 10 mm by 5 mm sensors have the same electrode area as the 20 mm by 2.5 mm sensors, but their plots do not match. Instead, doubling the electrode length causes a greater decrease in the resistance than doubling the width. This behavior matches what was seen in Chapter 5 when comparing the measurements made using different size sensors.

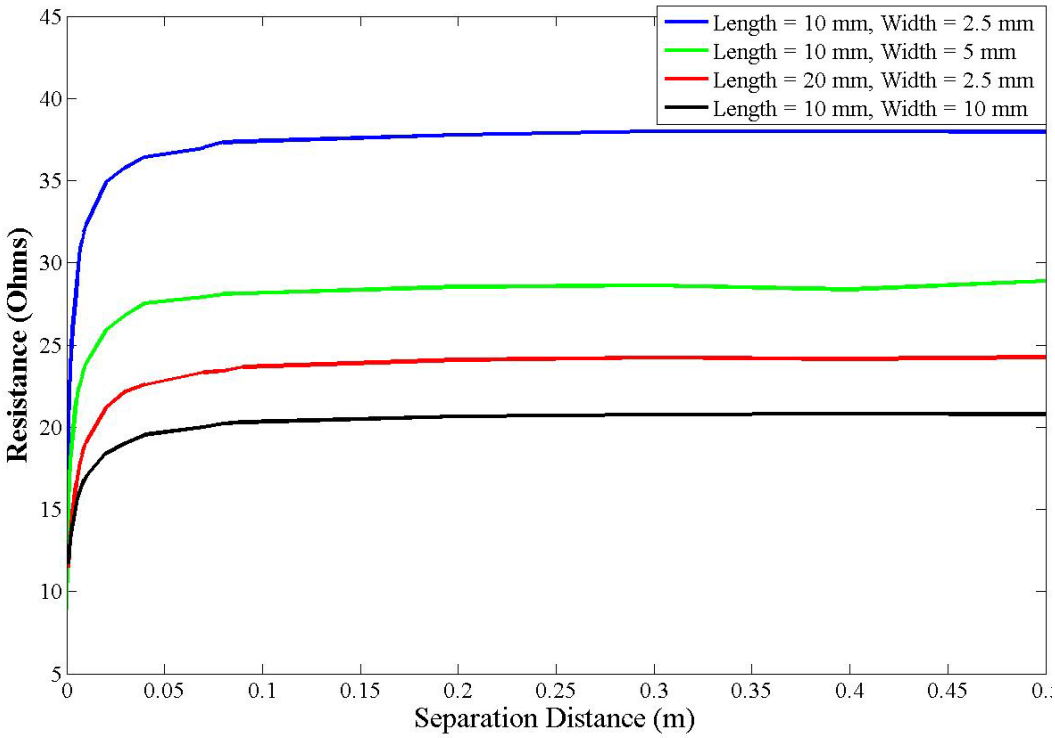

Figure 7.2: Simulated resistance vs. electrode separation distances for four electrode geometries

Unlike in the basic resistance measurement setup described in Section 3.1, once the separation distance reaches a certain size, the resistance remains nearly constant. The reason for this difference is, that unlike in the basic setup, the electric field is not uniform. As shown in the Figure 3.9, the electric field decreases the further it is from the electrodes. Most of the voltage drop occurs within a small volume around each electrode where the electric field is high. Past that volume, the voltage drop becomes inconsequential. A similar phenomena occurs when measuring the resistance of an Earth ground [49].

It is difficult to demonstrate this behavior analytically because the shape of the sensor's electrodes causes the electrode field distribution to be very complicated. However, this behavior can be demonstrated in a simplified situation. To simplify the calculations, the two flat electrodes can be replaced with two charged spheres, and the two spheres are then submerged a very large volume of water. A constant voltage is applied between the spheres and the resistance is measured as the spheres are moved further apart. Using Ohm's Law, the general expression for the resistance between any two points is

$$R = \frac{V}{I} = \frac{-\int_d^a \boldsymbol{E} \cdot d\boldsymbol{L}}{\int \sigma \boldsymbol{E} \cdot d\boldsymbol{S}} \tag{7.2}$$

where R is the resistance, V is the voltage applied to the spheres, I is the current flowing between the spheres, σ is the conductivity of the water, E is the electric field, a is the radius of the spheres, and d is the separation distance [21]. To solve (7.2), the electric field needs to first be calculated. The electric field can be calculated using Gauss's Law; however, to save space this step is not shown. The electric field is

$$E = \frac{Vad}{(d-a)r^2} \tag{7.3}$$

where r is the radius of a sphere between spheres of radius a and d. Using (7.2) and (7.3), the resistance can be calculated to be

$$R = \frac{1}{4\pi\sigma}\left(\frac{1}{a} - \frac{1}{d}\right). \tag{7.4}$$

When the distance between the two spheres is small, the resistance increases rapidly. However, as the distance becomes large the 1 divided by d will become almost zero, causing the resistance to level out. This matches the behavior seen in Figure 7.2. As long as the volume of the water is sufficiently large, this behavior will continue as the separation distance increases.

7.2.2 Electrode Length

A similar process was used for determining the influence of the electrode length and width. Figure 7.3 and Table A.32 show the results of sweeping the electrode length from 1 mm to 10 mm for different electrode separation distances and widths. The electrode length was limited to that range because EMPro crashed when the length became too large. The figure shows that the conductance measured by the sensor increases linearly with electrode length, and therefore the resistance is inversely proportional to the electrode length. The one outlier on the 100 mm trace was likely the result of a simulation error. Conductance was plotted instead of resistance because it is easier to observe the relation between the measured output and the electrode length. Unlike with the traditional sensor, the slope of the lines again approaches some value as the separation distance is increased. This behavior matches what was seen in the separation distance simulations.

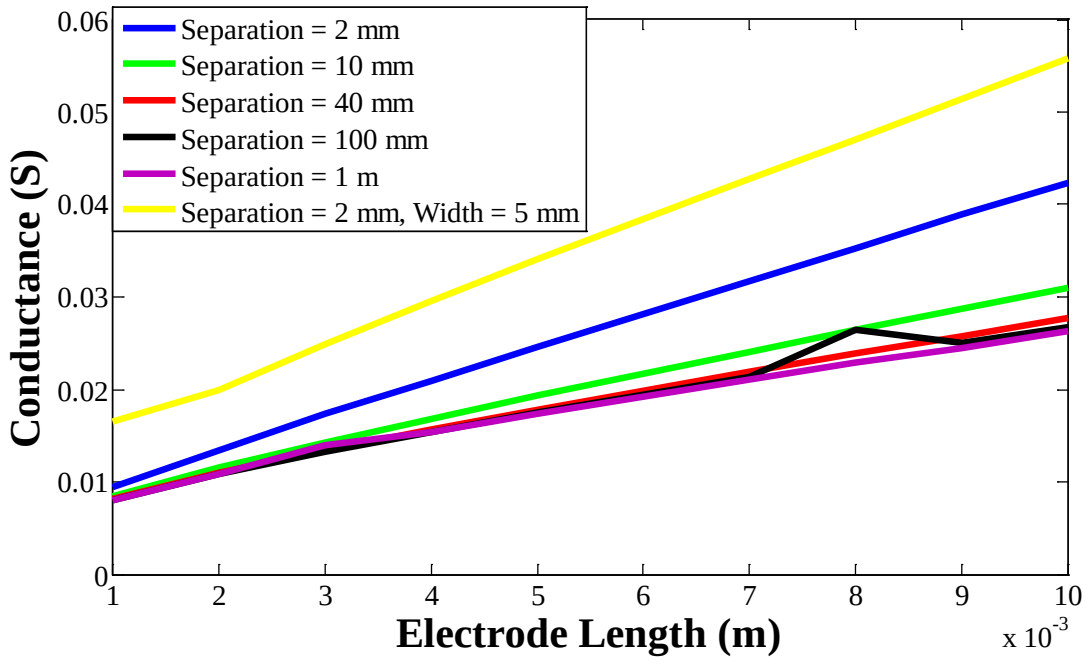

Figure 7.3: Simulated conductance vs. electrode length for six electrode geometries

7.2.3 Electrode Width

Figure 7.4 and Table A.33 show the results of sweeping the electrode width from 10 mm to 1 m with the electrodes separated by 0.05 mm, 0.1 mm, 2 mm, 10 mm, 100 mm, and 1 m. As Figure 7.4 demonstrates, when the width is large, the resistance measured by the sensor is inversely proportional to the width of the electrodes. Unlike with the length, the conductance increases rapidly at small widths. Also unlike the length, changing the separation distance does not have as large of an effect on the slope of the lines. Based on these results, it can be concluded that electrode width and separation distance are closely related. This finding is not surprising since both the width and the separation are in the same direction. The effect of changing the width affects the electric field leaving the electrode edges that are not facing the other electrode.

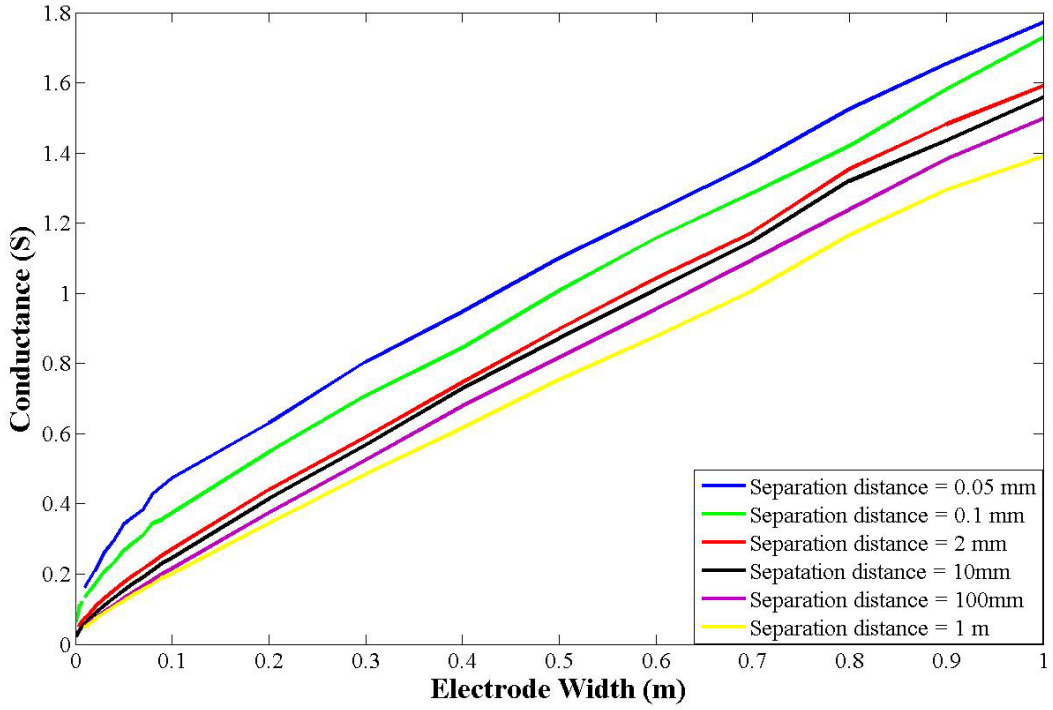

Figure 7.4: Simulated measured conductance vs. electrode width for six electrode geometries

7.2.4 Later Simulations

As mentioned before, using EMPro to simulate the sensor's behavior over a large variety of electrode dimensions proved to be difficult. To obtain an understanding of the sensor's behavior over a much larger range of electrode geometries, Q3D Extractor was used. In Q3D, all three electrode dimensions were varied at once. The electrode separation distance was swept over a range of 10 μm to 50 mm. A minimum separation distance was selected to be 10 μm because it was below the 152.4 μm minimum trace spacing that Advance Circuits is capable of manufacturing on a PCB [49]. The length of the electrodes was swept from 1 mm to 20 mm, and the width of the electrode was swept from 1 mm to 10 mm. More separation distances were simulated than width and length because the relationship between the resistance and separation distance appeared more complicated based on the previous simulations. The simulations resulted in 2750 resistance values.

The simulation results were used by the genetic algorithm discussed in Chapter 8 to generate the equation describing the behavior of the PCB sensors. To make it easy for the genetic algorithm to process, the results were formatted into a table with 25 rows and 440 columns. Every four columns are comprised of resistances for a specified electrode length and width as the separation distance was swept.

Plotting all of the data generated using Q3D would take up too much space. Instead a few examples are shown below. First, the result of sweeping the separation distance when the length is 10 mm was plotted for all simulated width in Figure 7.5. The plots behave as expected based on the earlier simulation results in EMPro. For all widths, the resistance started small and increased rapidly. After the separation distance was greater than a few millimeters, the resistance increase tapered out, remaining nearly constant. The figure also shows that increasing the width

causes the resistance to decrease. This finding was expected since increasing the width increases the electrode size. The plots themselves are fairly smooth. Close examination reveals some small resistance spikes and fluctuations. These are the result of errors by the simulations; however, the errors were not a major concern. Most were only a few tenths of an Ohm off, and any simulation results that were off by more were removed.

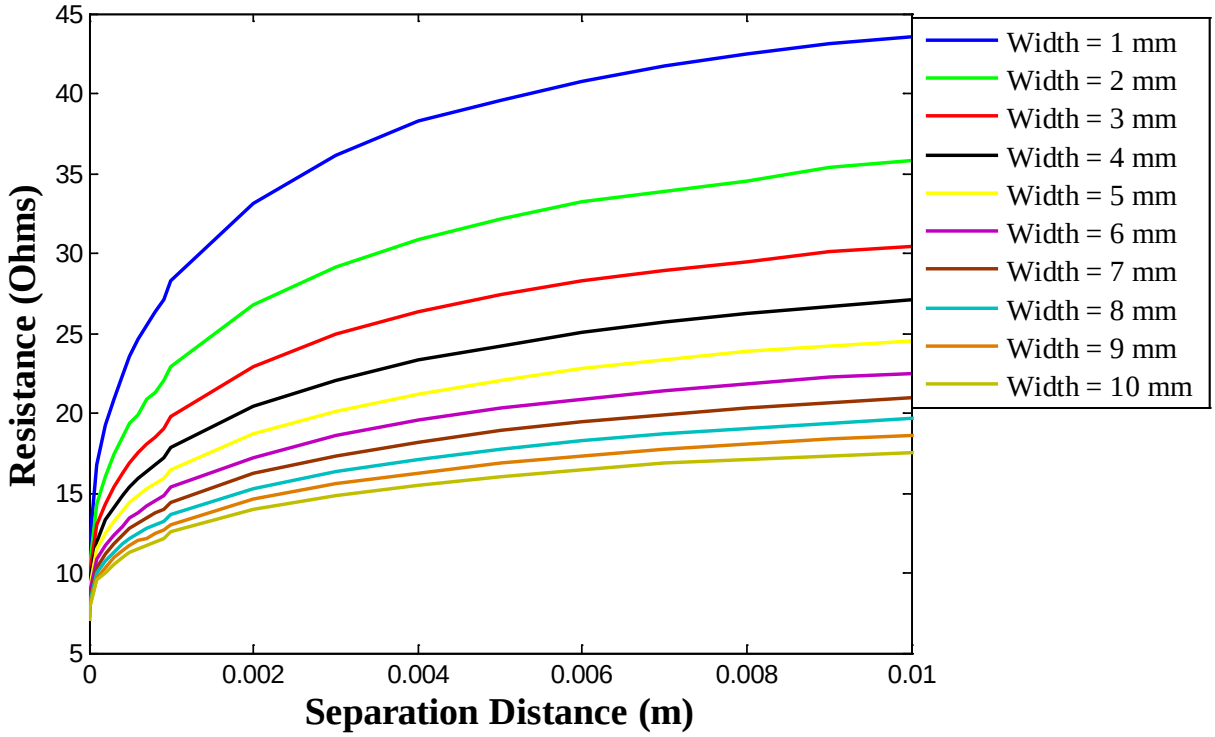

Figure 7.5: Q3D results for all widths when the distance was swept and the length was 1 mm

Next, the results of sweeping the electrode length while the width was 2 mm and the separation distance was 1 to 10 mm are shown in Figure 7.6. Again, the results were similar to what was observed using EMPro in Figure 7.3. As the separation distance was increased, the conductance decreased. However, the decrease was not proportional to the increase in the separation distance. This proportionality was expected since Figure 7.5 demonstrates that the resistance does not change linearly with the separation distance.

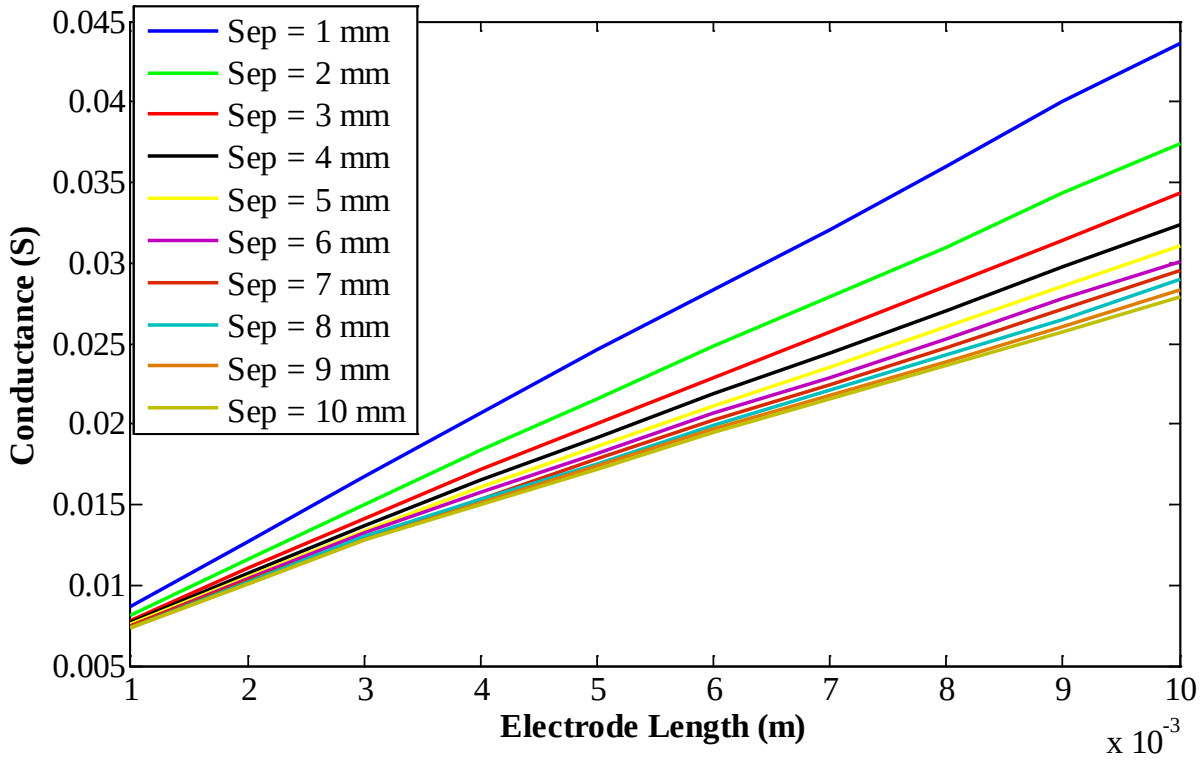

Figure 7.6: Q3D results for 10 distances when the length was swept and the width was 2 mm

Finally, the results of sweeping the electrode width while the length is 10 mm and the separation distance is 1 mm to 10 mm are shown in Figure 7.7. As the width increased, the conductance increased as well. However, instead of being proportional to the width, the conductance curved. This behavior is similar to what was seen in the results from EMPro in Figure 7.4 when the width is less than 10 mm. Also like in EMPro, the conductance decreased with separation distance. However, the decrease was not linear.

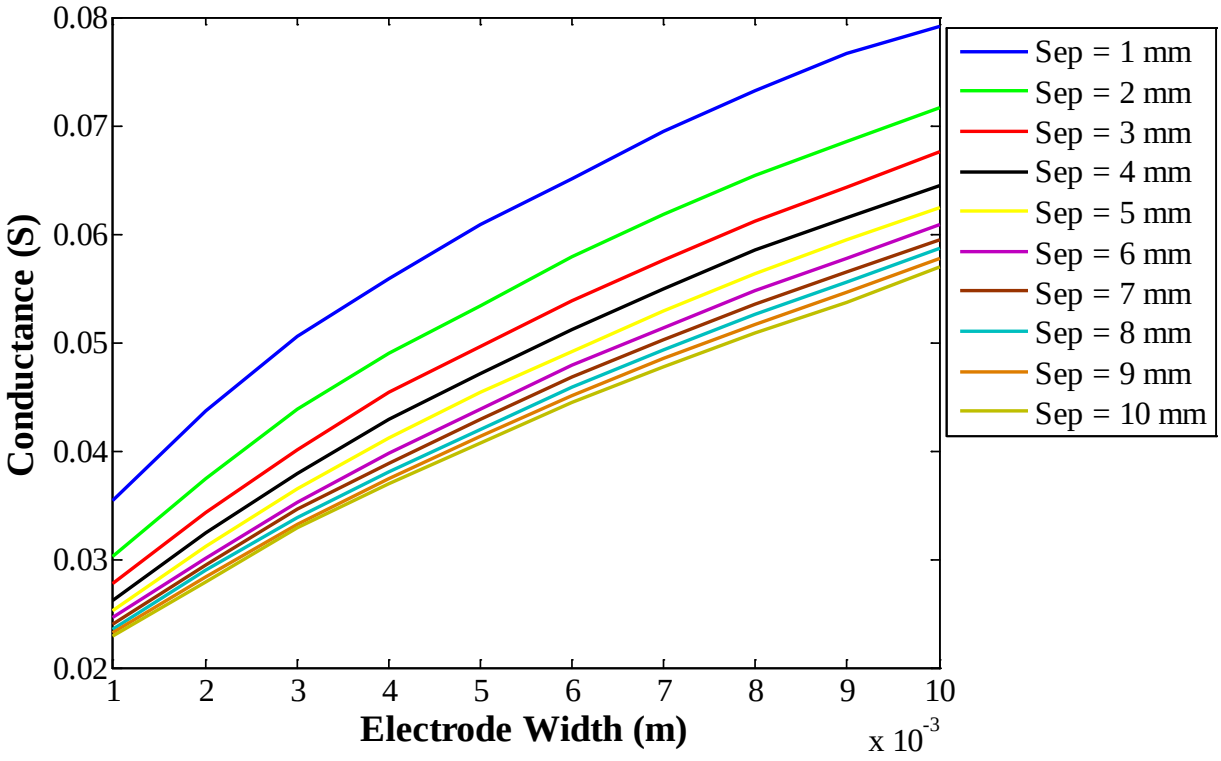

Figure 7.7: Q3D results for 10 distances when the width was swept and the length was 10 mm

7.3 Size of the Water Sample

To ensure the accuracy of the previous simulations, the influence of the volume and shape of the water was investigated. The concern was that the electric field from the sensor's electrodes extended far enough that the edges of the block representing the water in the simulation to effect the measured resistance. To test the influence of the water's volume, the three different electrode geometries were simulated in Q3D as the dimensions of the box of water were swept. The three electrode geometries all had a separation distance of 2 mm. The first geometry had a width of 2.5 mm and a length of 10 mm. The second had a width of 5 mm and a length 20 mm. The third had both a width and length of 50 mm, the maximum dimensions simulated in Q3D. The length, width, and height of the block were equal for all of the

simulations. They were swept from the minimal value required to completely cover the electrodes to 20 cm.

Table 7.2 shows the results of the simulations. The results show that the volume of the water did affect the measured resistance. However, after the sides of the block were more than three to four times the area of the sensor, the resistance change became small. The resistance was much larger when the block was small because the sides of the electrodes not facing the other electrode were close to the edge of the block. The electric field, and as a result the current, emanating from the edges of the electrodes was constrained to a small area, increasing the resistance. Increasing the size of the block increased the area the electric field flowed through. The resistance did not continue to decrease as the size of the block increased because the magnitude of the electric field decreased as it traveled in a conductor [21]. This behavior was similar to what was observed when sweeping the electrode separation distance. Most of the electric field was contained within a small volume around the electrodes. Once the block was much larger than that volume, only a small part of the electric field interacted with the block's edges. This interaction had only a small effect on the measured resistance. This result also indicates that in the real life testing, as long as the volume of water is large enough, it will not have a large impact on the resistance measured by the sensor.

Table 7.2: Measured resistance for different electrode geometries as the block dimensions are swept

	Measured Resistance (Ω) when:		
Block Dimensions (m)	Separation distance = 2 mm Length = 10 mm Width = 2.5 mm	Separation distance = 2 mm Width = 5 mm Length = 20 mm	Separation distance = 2 mm Width = 50 mm Length = 50 mm
0.01	32.60691	Block too small	Block too small
0.02	25.28515	13.03118	Block too small
0.03	24.82558	11.02294	Block too small
0.04	24.64080	10.74918	Block too small
0.05	24.53796	10.66122	3.846290
0.06	24.46802	10.62275	3.336106
0.07	24.41460	10.59717	3.065783
0.08	24.24716	10.56662	2.873338
0.09	24.19649	10.55452	2.723957
0.10	24.08778	10.52911	2.604409
0.11	24.15769	10.52733	2.511204
0.12	24.11521	10.51390	2.449814
0.13	24.02815	10.49914	2.403493
0.14	24.37142	10.47960	2.366873
0.15	24.14830	10.46960	2.343326
0.16	24.31978	10.45024	2.322344
0.17	24.31032	10.44139	2.305568
0.18	24.06946	10.43594	2.291633
0.19	24.29982	10.42072	2.284803
0.20	24.30598	10.39508	2.278619

7.4 Shape of the Water

While the setup used in the simulations was simple to implement, the water would not behave the same way in real life. In practice, a large cube of water obviously cannot be placed on top of the sensor's electrodes as in the simulation; instead, the sensor is placed in the water. In this case, the water surrounds the sensor on all sides, possibly impacting the electric field distribution. If the electric field distribution during the testing was significantly different from

the field distribution in the simulations, the measured and simulated resistances could not be compared, invalidating the simulations.

To address this concern, the simulation setup was modified as shown in Figure 7.8. The new setup was based on how the sensor would be used in real life. The electrodes were mounted on a box representing the sensor's PCB. The box had the size and shape of the PCB and the electrical properties of FR-4. On the top of the PCB and the sides of the electrodes was a layer representing the nonconductive solder mask. It was given the properties of free space to ensure it was nonconductive. The solder mask was given the same height as the electrodes. This treatment ensured that there would not be any water directly between the sides of the electrodes because the water would greatly decrease the measured resistance. A cube of water was placed around the sensor. A cube was used instead of a cylinder because it was easier to model in Q3D.

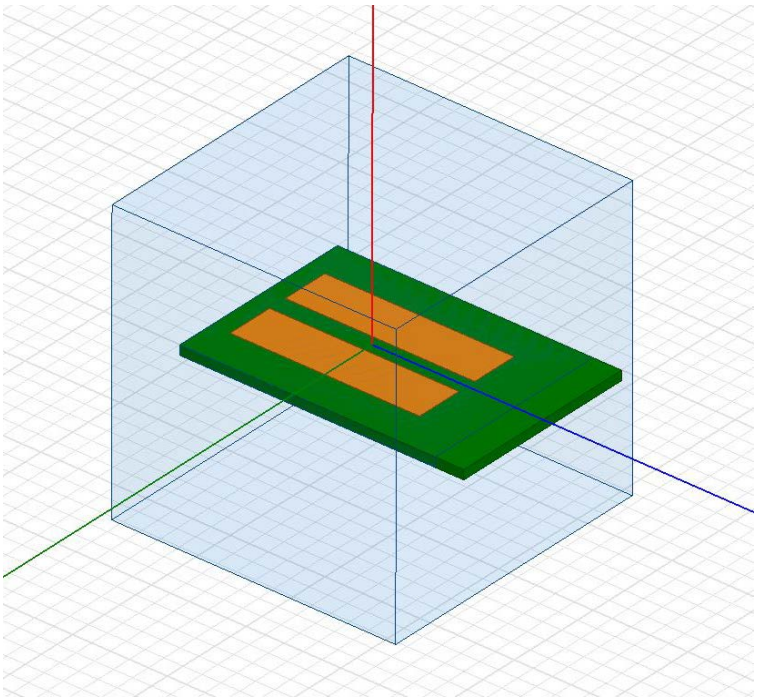

Figure 7.8: Simulation setup with water surrounding the sensor

This setup was simulated three times with the dimensions of the electrodes and the cube varied in order to determine their impact on the results. Table 7.3 shows the results of the new configuration compared to the simulation results using the normal configuration. The difference between the results of the two simulations was fairly small, less than 2 Ohms, while the percent difference was below 5%. Some of this difference came from variations in the simulation results due to variations in how the mesh is generated. While the percent difference was larger than desired, it was still small enough to imply that the normal simulation setup was adequate for determining the behavior of the sensor.

Table 7.3: Simulation results of surrounding the sensor in water verses the original setup

Setup	Resistance (Ω) in new setup	Resistance (Ω) in original setup	Difference (Ω)	Percent Difference
Separation distance = 2 mm, Length = 10 mm, Width = 2.5 mm, and Block dimensions = 400 mm	22.627	23.645	1.018	4.40%
Separation distance = 2 mm, Length = 20 mm, Width = 5 mm, and Block dimensions = 400 mm	9.908	10.395	0.487	4.80%
Separation Distance = 2 mm, Length = 20 mm, Width = 5mm, and Block dimensions = 60 mm	10.361	10.395	0.034	0.33%

7.5 Simulation Frequency

A common property simulated in both EMPro and Q3D is the effect of the simulation frequency. In EMPro, the behavior can be simulated over multiple frequencies. In Q3D, the behavior is simulated at only one frequency at a time. As stated in Section 4.3, the simulation frequency used in both simulators was 10 Hz. Since the testing was done at much higher

frequencies, the frequency difference could have an effect on the results of the simulation. To determine the impact the frequency had on the simulation results, the frequency was swept from 10 Hz to 100 kHz with the original electrode configuration of the sensor. Table 7.4 shows that the simulation frequency had no effect on the measured resistance.

Table 7.4: Effect of increasing the simulation frequency on resistance in Q3D

Simulation Frequency (Hz)	Resistance (Ω)
10	24.30598
100	24.30598
1,000	24.30598
5,000	24.30598
10,000	24.30598
100,000	24.30598

It should be noted that the measurements are independent of frequency only in the simulations. As stated earlier, the measurement frequency will have an effect on the measured resistance in real life. Electrode polarization will cause an increase in the measured resistance. The results of the simulations should match the results of the real life testing when the measurement frequency is high enough for the measurement signal to short across the double layer capacitance. As discussed in Section 4.4.3, the effects of the electrode polarization were not included in the simulation because they were difficult to accurately model.

7.6 Simulator Comparisons

As explained in Chapter 4, early simulations were done using EMPro, while later work was done using Q3D. Because the two simulators were made by different companies and use different computational methods, their simulation results might differ, putting their results into

question. To determine whether the simulators provide similar results, they were both used to simulate a number of properties and their results were compared.

For all of the simulations in this subsection, the simulation frequency was set to 10 Hz, the conductor mesh elements were set to be no larger than 10% of the size of the electrode width, and the material had a conductivity of 4 S/m. For all of the tests, the geometry of the electrode was the same as the original except for any properties that were being swept.

7.6.1 Conductivity Comparison

The first property that was compared was the conductivity. Figure 7.1 and Table A.30 (discussed earlier in Section 7.1) show the resistance values obtained by both simulators as well as the percent difference. The percent difference was calculated as

$$Percent\ Difference = \frac{\left|R_{EMPro} - R_{Q3D}\right|}{0.5\left(R_{EMPro} + R_{Q3D}\right)} \times 100\%. \tag{7.2}$$

For all conductivity values, the percent difference between the EMPro's and Q3D's results was around 2.94%. Although the results do not match exactly, the percent error was small. Furthermore, the plots from both simulators have the same behavior; in both simulators the resistance was inversely proportion to the conductivity. Because the percent error was fairly small and the behavior matches, it can be concluded that the simulators agree with each other on the influence the conductivity had on the measured resistance.

7.6.2 Electrode Separation Distance Comparison

The next property compared was the separation distance. First, the separation distance was swept from 1 mm to 100 mm, while the electrode length was 10 mm and the width was 2.5 mm. A comparison between the results generated by both simulators is shown in Figure 7.9 and Table A.34. In the plots, the results started out very close before diverging as the separation

distance became large. However, the comparison in Table A.34 demonstrates that the difference was not a large as it appears. The table shows that the difference between the results was at most 1.03 Ohms, and the percent difference was never greater than 4%. This small difference indicates that the results from both simulators were in close agreement, adding validity to the results and conclusions presented about the behavior of the sensor.

The fact that the results do not match exactly was not surprising. Earlier simulation work had also demonstrated that the results from both simulators tended to vary even when the same geometry was being simulated using the same settings. Usually, this variation was only a few Ohms. This small variation was due to how the meshes were generated. If a slightly different mesh was generated, this mesh would produce slightly different results. Given that EMPro and Q3D generate their own meshes separately and use a different process to generate the meshes, it was not surprising that their results do not match completely.

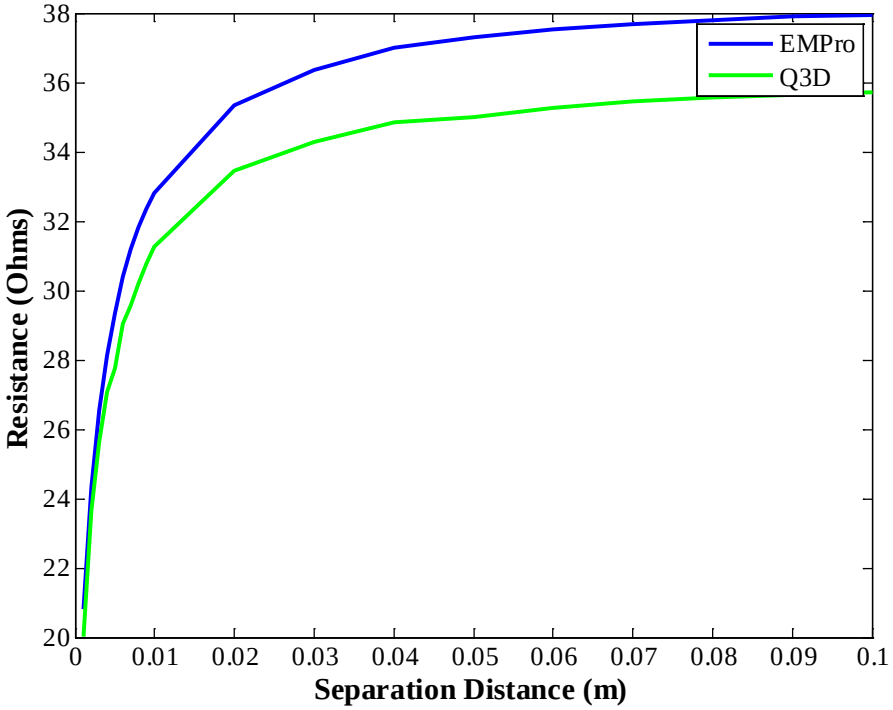

Figure 7.9: Comparison between EMPro and Q3D results as separation distance was swept

7.6.3 Electrode Length Comparison

Figure 7.10 and Table A.35 show the comparison between the results of sweeping the electrode length using both simulators. For the simulations, the separation distance and the electrode width were kept constant (at 2 mm and 2.5 mm respectively), and the electrode length was swept from 1 mm to 100 mm. During the simulations, EMPro failed to generate a mesh when the electrode length was 20 mm and 10 mm. In Table A.35, an X was used to represent cases where EMPro failed to generate a mesh. To match the previous plots, conductance was plotted in Figure 7.10 instead of resistance. The plots in Figure 7.10 are nearly identical. In fact, the plots are almost on top of one another. Table A.35 shows that the results were always less than 3 Ω. The percent difference was also very small, under 4%. Based on the results, it appears that the simulations become closer the larger the length; however, even when the length was small, the results are very close.

The cause of these differences is the same as for the separation distances. The results of the simulations tended to vary slightly each time, even when the same geometry was being simulated. This variation can be attributed to differences in how the mesh was formed. Also, both simulations have been known to produce errors, including EMPro's failure to generate a mesh for two of the cases.

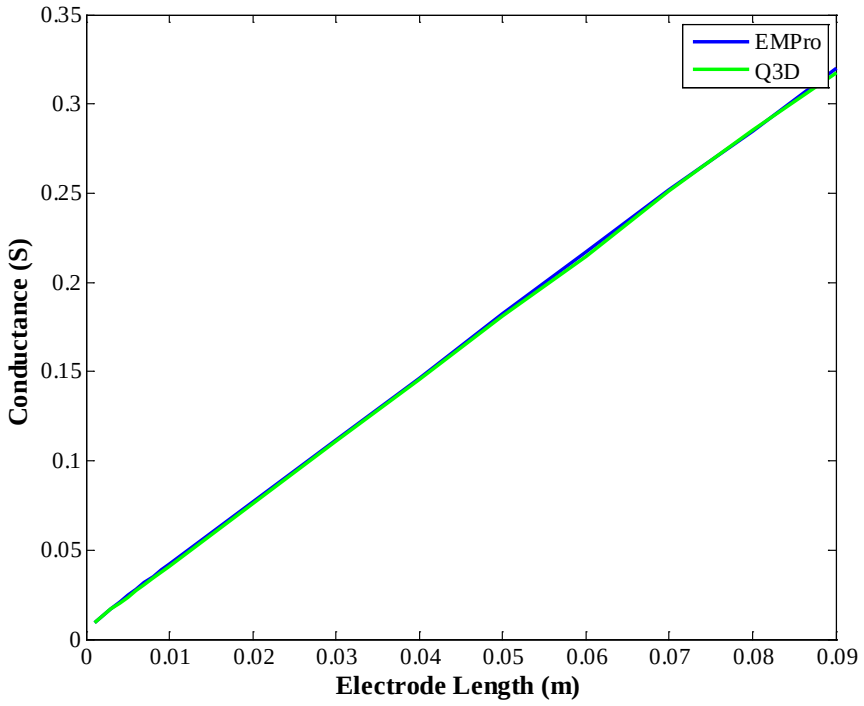

Figure 7.10: Comparison between EMPro and Q3D results as electrode width was swept

7.6.4 Electrode Width Comparison

Table A.36 and Figure 7.11 show the results of sweeping the electrode width using both simulators. For the simulations, the electrode's length and separation distance were kept at 10 mm and 2 mm respectively. The electrode width was swept from 1 mm to 100 mm. As the figure below illustrates, the two simulators were in agreement when the width was small. However, as the width increases, so did the difference between the simulators. For the entire range, the difference between the results was always less than 1 Ω; however, since the resistance decreased as the width increased, the percent difference increased with it. In order to keep the results of the two simulators in agreement, the width was limited to 10 mm or less. Figure 7.12 shows that over that range, the results from both simulators remained in agreement.

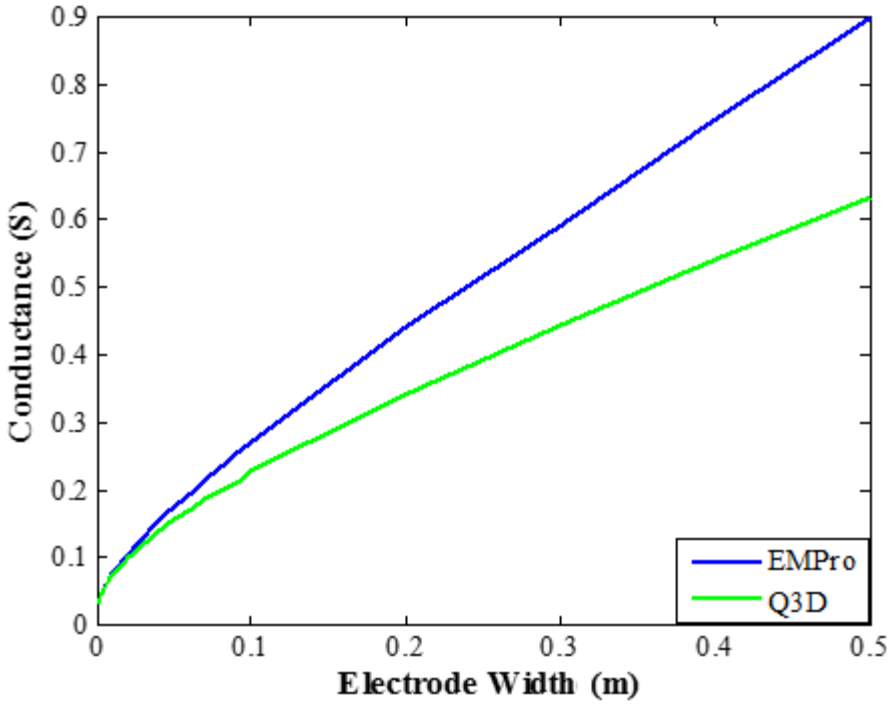

Figure 7.11: Comparison between EMPro and Q3D results as electrode width was swept

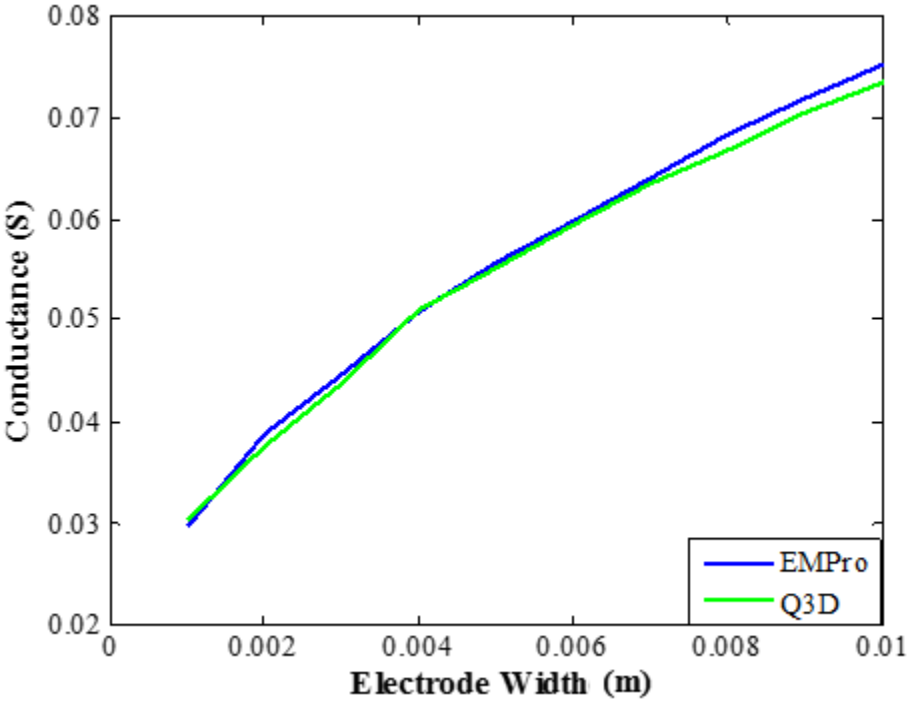

Figure 7.12: Comparison between EMPro and Q3D results as electrode width was swept over a small range

Chapter 8

Deriving an Equation

A genetic algorithm was used to derive an equation that can predict the resistance measured by the PCB sensor. In this work, hundreds of potential solutions were generated as the genetic algorithm was refined. Many of these solutions proved to be unacceptable due to multiple reasons, including complexity, a limited range, or simply being inaccurate. In the following sections, an brief overview of genetic algorithms is first provided. Then one of the earliest potential solutions is discussed along with its flaws. Lastly, the final equation is discussed, and its performance is evaluated.

8.1 Overview of Genetic Algorithms

A genetic algorithm is an optimization process based on the concepts of natural selection and evolution. GAs force the individuals in a population to evolve to a solution for a design problem [50]. They are used in engineering and scientific fields as such as drug design, financial prediction, data mining, and even the composition of poetry and music [51]. They are effective at finding an approximate global maximum in situations with large domains and multiple variables in a nearly optimal manner.

In a GA, a population of potential solutions is first randomly generated and each individual in the population is comprised of a string of numbers. These numbers are a coded representation of the parameters of the potential solution. The values representing each

parameter of an individual are referred to as “genes,” and all together the genes are referred to as a “chromosome” [50], [51]. By encoding the parameters as genes, the GA is able to operate independently of the solution space of the problem and its constraints. In general, GAs tend to have a population of anywhere between 30 and 10,000 individuals. The size of the population depends on the problem being solved [51]. The population size determines the size of the gene pool and the how much of the search space is investigated. While a large population will increase the number of potential solutions investigated, it also makes the algorithm slow to respond to good solutions. Solutions generated using large populations also tend to be less than the optimum since the large population tends to overpower above-average individuals located in a small portion of the solution space. Usually, running a GA with a small population several times will produce better solutions than running it once with a large population [51].

After the population is generated, each individual is subjected to some evaluation method that determines their fitness (or how good they are as a solution). The procedure used to evaluate an individual’s fitness is referred to as the “fitness function.” The fitness function is the only part of the GA that connects back to the original problem [51]. Once each individual is evaluated, the individual is assigned a fitness score based on how good of a solution they are.

After the fitness of all individuals in the population has been determined, the next generation of individuals is produced. Two accomplish this task, the GA will select individuals from the previous population to “breed” and generate new individuals. The chance of being selected as a parent is related to the fitness score of the individual. The better the fitness score, the better the chance of being selected. However, some less fit individuals need to be selected. Otherwise, the algorithm risks eliminating potential useful genes too early. Although GAs allow multiple selection strategies, some of the more popular are population decimation, proportionate

selection, and tournament selection. The selection strategies differ based on how they ensure some less fit individuals are used as parents without selecting so many that the algorithm cannot converge to an optimal solution.

In the algorithm used in this work, tournament selection is used. Tournament selection is one of the most commonly used and straightforward selection methods [51]. In tournament selection, parents are chosen from a small pool of randomly selected individuals from the larger population. The individual with the best fitness is selected to be a parent. A new tournament is held to select each parent. The number of parents needed to generate a new individual depends on the algorithm; however, it is common to use only two [51]. Tournament selection ensures that less fit individuals have a chance to reproduce, while favoring more fit individuals.

Once parents are selected, the algorithm determines whether crossover is used to generate the children. In crossover, the chromosomes of the children are generated from a combination of the parents' genes. To determine whether crossover occurs, a GA uses a random number generator to obtain a crossover value and then compares it with the crossover chance. The crossover chance is defined at the beginning of the algorithm and is between 0 and 1. If the crossover value is less than the crossover chance, crossover does not occur, and the children are exact copies of the parents. If the crossover value is greater than the crossover chance, than crossover will occur [51]. A crossover chance of 0.6 to 0.8 has been found to work well in most situations [51].

In crossover, how the genes for the children's chromosomes are selected depends on the GA. One of the simplest ways is to have two parents generate two children, where each child has a certain percentage of genes from each parent (for example 60% and 40%). In this situation, one parent gives the first 60% of its chromosome to one child and supplies the latter 40% to the other

child, while the other parent does the reverse (demonstrated in Figure 8.1). After the crossover is completed, the children's chromosomes are potentially mutated. Mutation causes part of the child's genes to change values. Mutation helps the GA explore previously unrepresented solutions by adding variety to the population. The probability of mutation is usually very small to ensure that desirable solutions are not lost.

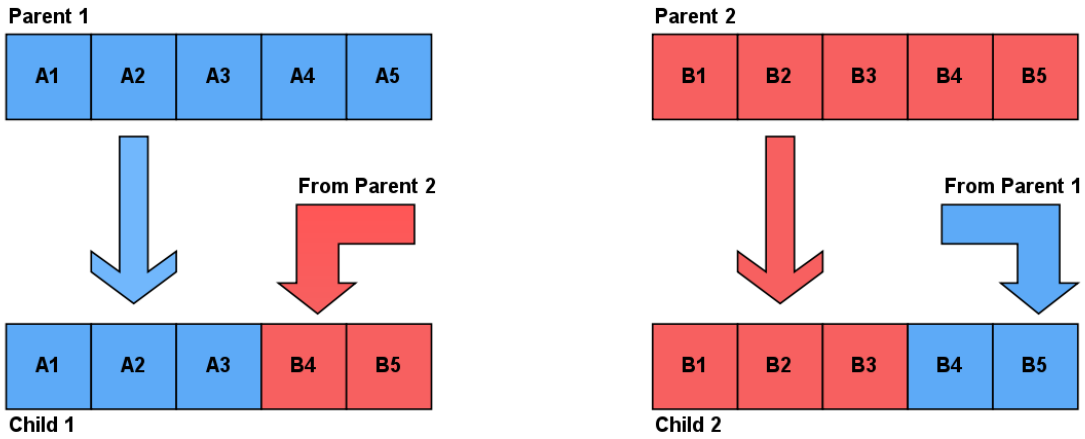

Figure 8.1: Example of crossover between Parent 1 and Parent 2

Once the new population is generated, the process repeats itself. The fitness of the individuals in the new population is evaluated, and a newer population is generated. This process will continue, in theory, until the optimal solution is generated. In practice, GA stops once it meets some condition defined by its creator. This stop condition could be after a certain fitness value is reached or after a certain percentage of the population has the same maximum fitness value.

8.2 The Genetic Algorithm Developed

A genetic algorithm was written in MATLAB to derive an equation that could accurately determine the cell constant of the PCB sensor for any electrode geometry in water of any conductivity. The algorithm was based off a verbal description of a simple GA found in

Electromagnetic Optimization by Genetic Algorithms. The book described a GA designed to find the maximum of the two dimensional function,

$$f(x,y) = \left|\frac{\sin(\pi(x-3))}{\pi(x-3)}\right| \times \left|\frac{\sin(\pi(y-3))}{\pi(y-3)}\right| \tag{8.1}$$

While it is simple to find the maximum of f(x,y) with basic knowledge of the properties of the sinc function, the book's description of the GA proved to be a useful proof of concept. First, a GA was written to find the maximum of f(x,y) based on the book's description. Once the algorithm proved successful, it was modified into the MATLAB Script in Appendix B. This algorithm was then used to derive the equation describing the behavior of the sensor. In the new algorithm the original sinc function was replaced with the sensor's equation. The form of this equation is defined before the algorithm is run. Instead the algorithm focuses on determining the coefficients needed for the equation to fit the provided data. The equation is a function of the electrode separation distance, length, and width and is comprised of a number of mathematical operators and coefficients. It was originally based on observing how the simulation results appeared to behave. It later changed significantly as the algorithm was run multiple times.

The algorithm starts by cleaning the workspace and defining its constants. These constants include the population size, the minimum and maximum allowable coefficient values, the maximum number of allowable generations, the crossover percentage, and the mutation chance. In the algorithm, the coefficients serve as the individual solution's genes. The population is comprised of a preset number of individuals. The number of individuals varied throughout the work. Usually a population comprised of between 30 and 100 individuals was used. In the first generation, the individual's genes are generated using one of MATLAB's random number generators.

Next, the simulation results discussed in Section 7.2 are read into MATLAB. Originally a small set of data generated from EMPro was used. Later, the EMPro data were replaced with a much larger set of data generated using Q3D. In both cases, the data were generated by simulating the effect that sweeping the electrode separation distance, length, and width had on the measured resistance. The conductivity was left constant since it does not affect the cell constant, and its influence on the resistance is simple to account for.

After reading in the simulation results, the algorithm enters a large while loop. It remains in this loop until either the maximum allowable generations have passed or the conditions for an early exit are met. In the loop, the algorithm first evaluates the fitness of the individuals in the most recent population. To evaluate the fitness of an individual, the algorithm sets the equation's coefficients equal to the values defined by the individual's genes. The algorithm then uses the equation to calculate the measured resistance for all electrode geometries represented in the simulation's result. Next, to determine the accuracy of the equation's predictions, the coefficient of determination is calculated between the equation and the simulation results. The coefficient of determination is also referred to as the R squared value, R^2 value, or the r^2 value. To avoid confusion with resistance, it is referred to as the r^2 value here. The r^2 value measures the total variation of the predicted data about the mean of the actual data [52]. It is regularly used to evaluate how well an equation matches a data set. The closer the r^2 value is to 1, the less variation there is between the predicted and actual values. The basic equation for calculating the r^2 value is

$$r^2 = 1 - \frac{RSS}{TSS} \tag{8.2}$$

where RSS referred to as the residual sum of squares and TSS is the total sum of squares [53]. RSS represents how much the predicted data vary from the actual data, and TSS represents how much the actual data vary from its mean.

Instead of calculating the r^2 value for the entire range at once, the algorithm first breaks the data into groups and then calculates the r^2 of each group separately. Each group represents the result of sweeping the separation distance while keeping the length and width constant. By breaking the calculation up in this manner, the impact of poorly correlated data points is increased. Because of the large range of the measured resistance, the impact of geometries with lower measured resistance is under represented. After the r^2 values are calculated for all lengths and widths, the mean is calculated in order to generate a single value.

When determining the r^2 value of an individual, the algorithm calculates the means of the groups. The means of each group of results are calculated using

$$\overline{R}_{sim,lw} = \frac{1}{D}\sum_{d=1}^{D}\left(R_{sim,dlw}\right)^2 \tag{8.3}$$

where $\overline{R}_{sim,lw}$ is the mean of the simulated resistances when the length and width are constant and the distance is swept. In the equation *l* is the length of the electrodes, *w* is the width of the electrodes, *d* is the separation distance, *D* is the total number of separation distances in the set, and $R_{sim,dlw}$ is the simulated resistance at the specific separation distance, length, and width. After the means are calculated, RSS can be calculated using

$$RSS_{lw} = \sum_{d=1}^{D}\left(R_{sim,dlw} - R_{Eq,dlw}\right)^2 \tag{8.4}$$

where RSS_{lw} is the residual sum of squares for the specified length and width and $R_{Eq,dlw}$is the resistance calculated using the individual's genes at the specified distance, length, and width [52], [53]. TSS is then calculated using

$$TSS_{lw} = \sum_{d=1}^{D} \left(R_{sim,dlw} - \bar{R}_{sim,lw}\right)^2 \tag{8.5}$$

where TSS_{lw} is the total sum of squares for a certain length and width [52], [53]. Next, the r^2 value of each group is calculated using

$$r_{lw}^2 = 1 - \frac{RSS_{lw}}{TSS_{lw}} \tag{8.6}$$

where r_{lw}^2 is the total sum of squares for a certain length and width [52], [53]. The algorithm then averages the r^2 values of all groups using

$$r_{total}^2 = \frac{1}{LW} \sum_{l=1}^{L} \sum_{w=1}^{W} r_{lw}^2 \tag{8.7}$$

where r_{total}^2 is the average r^2 for all electrode configurations. This average is used as the individual's fitness score by the algorithm. Averaging the r^2 values into a single number makes it easier for the algorithm to compare the fitness of different individuals.

After the fitness scores are calculated for all individuals, the algorithm moves on to producing the next generation of individuals. It first selects parents for the next generation of individuals using tournament selection. When generating every two children, the algorithm randomly selects five individuals from the previous population. The individual in the tournament with the highest fitness score is selected to be a parent. The algorithm then selects the second parent with another tournament. Once both parents are selected, their offspring are generated using crossover. First, the algorithm uses MATLAB's random number generator to determine whether the parents' genes are crossed. If the number generated by the random number generator

is less than or equal to the crossover chance, crossover does not occur. Instead, the two children are exact duplicates of the parents. If the number from the random number generator is greater than the crossover chance, crossover occurs. A crossover chance of 0.7 is used in the algorithm. During crossover, the chromosomes of both parents are split in two at a random point, and each half is given to one child. Where the chromosome is split is determined by using the random number generator to select a number between 1 and the number of genes in the chromosome.

After crossover, the new children are potentially mutated. First, a number is found using the random number generator and compared to the mutation chance. If the generated number is greater than the mutation chance, the children are not mutated. If it is less than the mutation chance, one of the child's genes is selected at random and a random value is either added or subtracted. After mutation, if the gene is no longer within the allowable range of values, it is rounded to the closest allowable value. A mutation chance of 0.09 is used in the algorithm.

All but three of the children are generated using the above process. Two more children are copies of the individuals with the highest fitness from the previous generation (elitism). Elitism ensures the most fit individuals are not lost in between generations. The genes of the last child are generated using the random number generator, similar to how the individuals from the original generation were produced. This last individual is added to improve the diversity of the population and help prevent the algorithm from prematurely converging to a less optimal solution [50].

Once all of the children are generated, the algorithm determines whether it should restart the loop and evaluate the fitness scores of the new population or exit the loop. If there has already been greater than a preset number of generations and the average fitness scores of the last four generations are within a certain amount of each other, the algorithm exits the loop. If the

number of generations has reached the maximum number allowed, the algorithm will also exit the loop. Otherwise, the algorithm returns to the start of the loop.

Once the algorithm exits the loop, it determines which individual from the last generation had the highest fitness. It then calculates the r^2 values for every group of constant length and width. To make it easier for the user to evaluate the solution, the algorithm also plots a comparison between the simulated and predicted resistance/conductance for every electrode geometry as a function of all three variables (one plot at a time).

8.3 The Original Equation

Using the GA described above, several potential solutions were derived. Early solutions were based on a small data set generated using EMPro. This data covered a much smaller range of electrode geometries than the data later generated using Q3D. The EMPro data covered four cases where the electrode length and width were constant while the separation distance was swept from 1 mm to 500 mm. The electrode dimensions were 10 mm by 2.5 mm, 20 mm by 2.5 mm, 10 mm by 5 mm, and 10 mm by 10 mm. The data also covered six cases where the electrode length and separation distance were fixed and the width was swept from 1 mm to 2 m. In all six cases, the length was 10 mm while the separation distance was 50 µm, 100 µm, 2 mm, 10 mm, 100 mm, and 1m. Furthermore, the data covered five cases were the separation distance and width were kept constant while the electrode length was swept from 1 mm to 100 mm. In all five cases the width was 2.5 mm while the separation distance was 2 µm, 10 mm, 40mm, 100 mm, and 1m. The algorithm groups the simulation results based on what electrode dimensions are kept constant. When using the Q3D data, discussed later, the data was grouped by constant length and width.

After a potential equation was generated, its performance was tested using a second set of data that was not covered in the original data. This second set of data demonstrated whether the solution could accurately describe the behavior of electrode geometries outside the ones used to generate it. This data came from varying the dimensions of five different sensor geometries. By default, these geometries were 12 mm by 3 mm separated by 3 mm, 8 mm by 2 mm separated by 1 mm, 15 mm by 4 mm separated by 8 mm, and 24 mm by 12 mm separated by 4 mm. Each dimension was swept separately while the other dimensions were constant. The separation distance was swept from 1 mm to 500 mm, the electrode length was swept from 1 mm to 90 mm, and the electrode width was swept from 1 mm to 1 m.

One of the earliest equations generated by the algorithm using this data was

$$R_{Equ} = \frac{2.63 - 1.17e^{-146.14d}}{\sigma(l + 0.00272)(171.32w + 1)} \tag{8.8}$$

where d was the separation distance, l was the length, w was the width, and σ was the conductivity. In this equation, the predicted resistance is inversely proportional to both electrode length and width, while the exponential term causes the resistance to level out when the distance becomes large. To obtain a better view of the performance of the potential solution, the algorithm calculates the r^2 value for each geometry separately and then averages them. As shown in Figure 8.2, the r^2 value over all of the data was 0.98812, while the r^2 values for most of the individual geometries were above 0.9. However, when the electrode width was swept and the separation distance was 50 µm and 100 µm, the r^2 values were 0.35686 and 0.69606. While these values are lower than desired, the accuracy of EMPro's results tended to worsen at very small or very large dimensions. Furthermore, the two configurations were at the edge of the data range, where the accuracy of the equation was likely to decrease. If the rest of the r^2 values were around 0.9, this error would be acceptable; however, the r^2 value from sweeping the separation distance

of the 10 mm by 5 mm sensors was only 0.60466. This configuration was in the middle of the data range, so if the equation could accurately predict the performance of the sensor, it should have had a higher r^2 value.

```
R Squared for "All data" is 0.98812
R Squared for "Swept distances for 2.5x10mm" is 0.93245
R Squared for "Swept distances for 5x10mm" is 0.60466
R Squared for "Swept distances for 2.5x20mm" is 0.91625
R Squared for "Swept distances for 10x10mm" is 0.97473
R Squared for "Swept widths when distance is 0.05mm" is 0.35686
R Squared for "Swept widths when distance is 0.1mm" is 0.69606
R Squared for "Swept widths when distance is 2mm" is 0.97053
R Squared for "Swept widths when distance is 10mm" is 0.98439
R Squared for "Swept widths when distance is 100mm" is 0.90823
R Squared for "Swept widths when distance is 1m" is 0.87276
R Squared for "Swept lengths when distance is 2mm" is 0.95038
R Squared for "Swept lengths when distance is 10mm" is 0.98711
R Squared for "Swept lengths when distance is 40mm" is 0.99115
R Squared for "Swept lengths when distance is 100mm" is 0.98674
R Squared for "Swept lengths when distance is 1m" is 0.98128
```

Figure 8.2: The r^2 values for the original solution

To further evaluate the performance of the equation, it was tested with the second set of data. Figure 8.3 shows the r^2 values for the second set of data. In this set, the results of sweeping the length and width have high r^2 values; however, the results of sweeping the separation distances did not. While the results for the first three configurations are acceptable, the results for the 24 mm by 12 mm configuration had an r^2 value of -0.92, indicating a very poor agreement between the simulation and equation.

```
R Squared for "all of the new data" is 0.97898
R Squared for "Setup 1 (sd = 3, l = 12 and w = 3) as distance is swept" is 0.8504
R Squared for "Setup 2 (sd = 1, l = 8, w = 2) as distance is swept" is 0.87946
R Squared for "Setup 3 (sd = 8, l = 15, w = 4) as distance is swept" is 0.79189
R Squared for "Setup 4 (sd= 4, l = 24, w = 12) as distance is swept" is -0.92012
R Squared for "Setup 1 as width is swept" is 0.99872
R Squared for "Setup 2 as width is swept" is 0.9383
R Squared for "Setup 3 as width is swept" is 0.97769
R Squared for "Setup 4 as width is swept" is 0.95343
R Squared for "sd and l =8mm as width is swept" is 0.98581
R Squared for "Setup 1 as length is swept" is 0.98969
R Squared for "Setup 2 as length is swept" is 0.94766
R Squared for "Setup 3 as length is swept" is 0.97512
R Squared for "Setup 4 as length is swept" is 0.90636
```

Figure 8.3: The r^2 values for the original equation using the second set of data

To help obtain a better idea of how well the equation predicts the behavior of the sensor, the predicted and simulation values were plotted. Figure 8.4 shows the comparison between the original simulation data (represented by asterisks) and the prediction made by the equation (represented by a line) as the distance was swept. The behavior of the plots match what is expected based on the r^2 values in Figure 8.2. In the figure, the plots of the data and the equation have the same general behavior; however, comparing plot for the 10 mm by 5 mm (in green) shows that when the distance is large, the values predicted by the equation are too low.

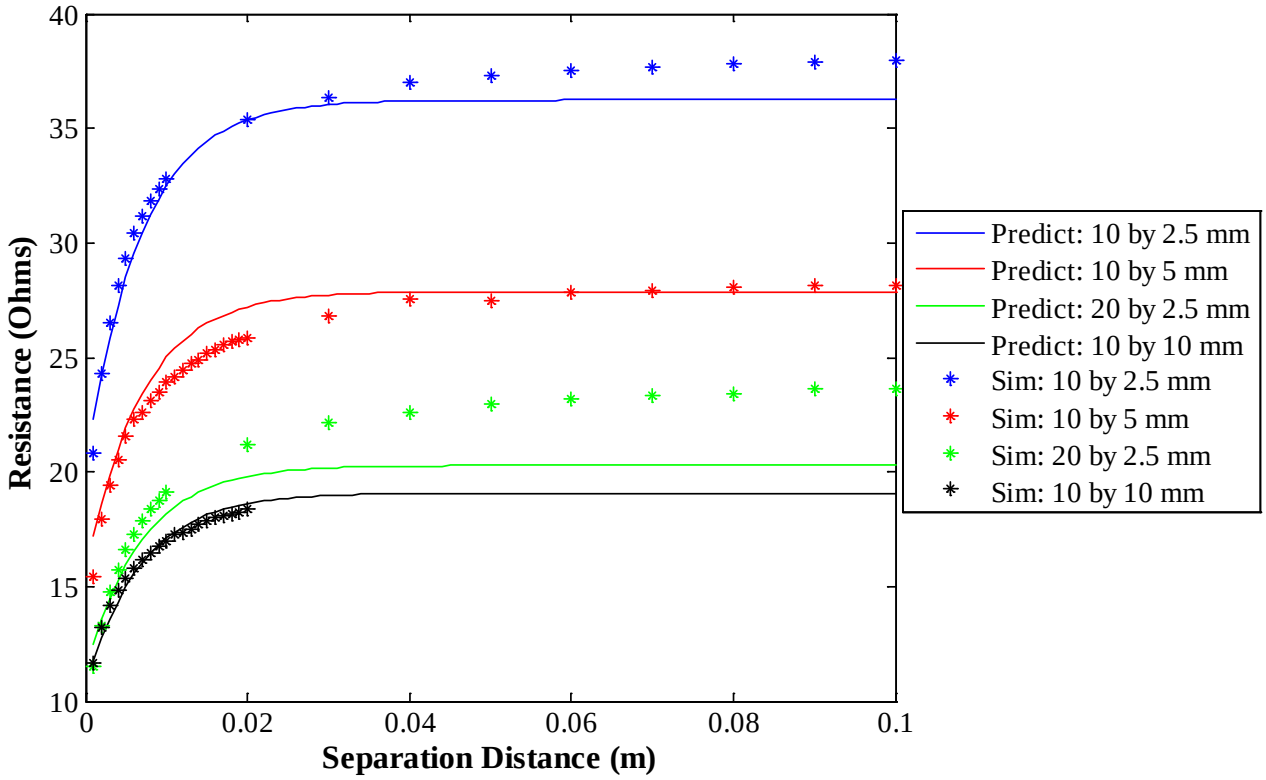

Figure 8.4: Comparing the simulated and resistances predicted by the original equation as the separation distance was swept

Next, Figure 8.5 shows a comparison between the simulated and predicted results as the electrode length was swept. In this case the results match nearly perfectly. This agreement was not surprising given that the r^2 values were all greater than 0.95.

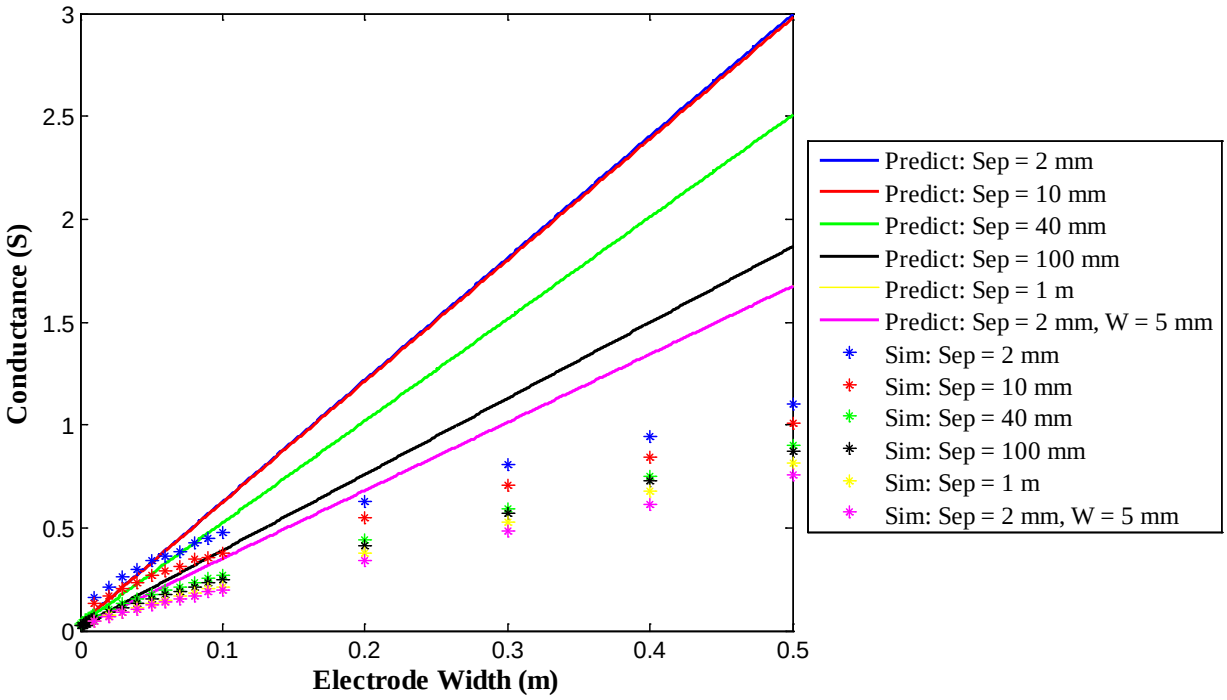

Figure 8.5: Comparing the simulated conductance and the conductance predicted by the original equation as the electrode length was swept

Finally, Figure 8.6 shows a comparison between the simulated and predicted values as the width was swept. In this case, none of the results match very well. The cause of this mismatch w that in the equation the resistance is inversely proportional to the electrode width. However, earlier simulation work in Section 7.2 has demonstrated that this relationship is not true. Instead, when the width is small, the conductance will increase rapidly. As the width increases, the slope of the conductance tappers out to a smaller value. To obtain the best r^2 value possible, the GA ensured that when the width was small, the predicted results and the simulation results were close. However, as the width became large, the difference became large. Since more data points were taken when the width was small, this resulted a fairly high r^2 value.

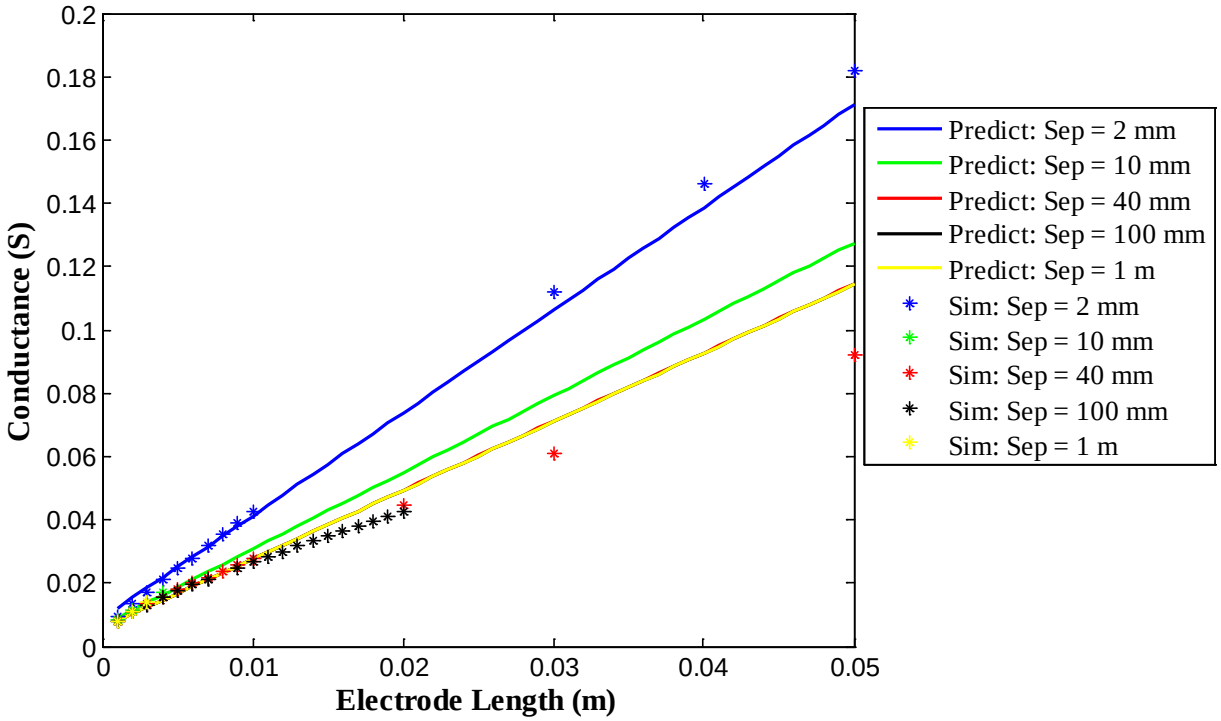

Figure 8.6: Comparing the simulated conductance and the conductance predicted by the original equation as the electrode width was swept

The fact the r^2 values from sweeping the widths were so large despite the non-matching plots in Figure 8.6 indicates that how the algorithm evaluated the potential solutions is not adequate. To fix this problem, Q3D was used to simulate the performance of the PCB sensor over a much larger range of electrode dimensions. Increasing the number of simulated geometries ensures that the potential solution cannot achieve a high r^2 by focusing on a few geometries and ignoring the rest. At the same time, the range of potential values was confined to much more reasonable values. In the original data, many of the dimensions were swept to 1 meter, which is too large to be implemented on a PCB. In the Q3D simulations, the dimensions were limited to 50 mm.

Table 8.1 shows the r^2 values calculated when comparing the original equation to the new data. As the table shows, the r^2 values varied greatly over the data range. When the width and length were small, the r^2 was also very small. However, as the length and width increased, the r^2 improved, reaching 0.9 in some cases. The average r^2 for the entire data range was 0.6547. Based on the table, the equation does not predict the performance of the PCB sensor very well.

Table 8.1: The r^2 values resulting from comparing the original equation to the new data.

		Electrode Width (mm)									
		1	2	3	4	5	6	7	8	9	10
Electrode Length (mm)	1	-2.719	-0.523	0.306	0.476	0.298	0.236	0.229	-0.039	-0.267	-0.315
	2	-0.128	0.675	0.782	0.724	0.587	0.465	0.349	0.316	0.250	0.278
	3	0.431	0.808	0.791	0.723	0.616	0.557	0.527	0.546	0.495	0.552
	4	0.596	0.827	0.782	0.739	0.694	0.635	0.659	0.711	0.705	0.723
	5	0.680	0.826	0.790	0.750	0.722	0.710	0.759	0.781	0.803	0.835
	6	0.713	0.813	0.789	0.762	0.748	0.754	0.806	0.838	0.845	0.872
	7	0.725	0.811	0.788	0.781	0.791	0.810	0.846	0.875	0.893	0.904
	8	0.732	0.803	0.792	0.790	0.813	0.830	0.872	0.891	0.912	0.923
	9	0.750	0.798	0.787	0.796	0.815	0.841	0.872	0.897	0.907	0.914
	10	0.776	0.793	0.790	0.802	0.827	0.849	0.871	0.893	0.902	0.901
	20	0.754	0.768	0.778	0.797	0.822	0.835	0.833	0.827	0.793	0.753

8.4 Final Equation

After the new data was generated using Q3D, the genetic algorithm was run several times with different forms of the equations. After several revisions, the algorithm derived (8.9) for predicting the resistance measured by the PCB sensor with electrode dimensions *d*, *l*, and *w* in a sample of water with an electrical conductivity of σ.

$$R_{Equ} = \frac{2.14 + 2.017ln(1.31 + \frac{33d}{w})}{\sigma\left[7.87l + 0.0108 + w(1 + 37.3l)ln(1.31 + \frac{33d}{w})\right]} + \frac{1}{3866\sigma lw} \qquad (8.9)$$

The units of the electrode separation distance, length, and width are meters and the unit for the conductivity is S/m. The equation for the sensor's cell constant can then be determined from (3.17) and (8.9) to be

$$\kappa_{Equ} = \frac{2.14 + 2.017ln(1.31 + \frac{33d}{w})}{\left[7.87l + 0.0108 + w(1 + 37.3l)ln(1.31 + \frac{33d}{w})\right]} + \frac{1}{3866lw} \qquad (8.10)$$

The only difference between (8.9) and (8.10) is that (8.9) takes the conductivity into account. The new equation is comprised of two parts. The first part is the large fraction made up of several terms, including two natural logarithms. The natural logarithm controls the shape of the resulting plots. It causes the resistance to rise quickly when the separation distance is small and to flatten out as the distance becomes large (such as in the plots in Figure 7.5). The second part of the equation is 1 divided by the length and width and a constant. This provides an offset based on the size of the electrodes. In the equation, the cell constant (and by extension the resistance) is almost inversely proportional to the electrode length, as mentioned previously in Section 7.2. The influence of electrode width is much more complicated, which was also observed in Section 7.2. As seen with the length, the cell constant, decreases as the width increases; however, this decrease is not linear.

The fitness score the genetic algorithm calculated for the equation was 0.9779. Table 8.2 shows the r^2 values calculated for all of the different groups of constant lengths and widths. The r^2 value for all but one group was over 0.9. The only instance the r^2 was below 0.9 occurs when the electrodes were 1 mm by 10 mm. Close examination of the table shows that the lowest r^2 values occurred when either the electrode length or width was low. This relationship is not surprising since these dimensions were on the edge of the data range; therefore, there was less pressure for the results of the equation to match than in the middle of the data range.

Furthermore, it has been observed that the accuracy of Q3D's simulations also tended to decrease when the dimensions of the electrodes were small. As mentioned in Section 7.2, at times small fluctuations or spikes occurred in the simulation results. These errors were noticeable when the results were plotted.

Table 8.2: The r^2 values resulting from comparing the final equation to the new data

		Electrode Width (mm)									
		1	2	3	4	5	6	7	8	9	10
Electrode Length (mm)	1	0.934	0.952	0.956	0.951	0.958	0.971	0.909	0.935	0.922	0.869
	2	0.963	0.977	0.969	0.976	0.979	0.981	0.989	0.990	0.979	0.966
	3	0.955	0.986	0.981	0.983	0.979	0.979	0.980	0.987	0.977	0.976
	4	0.957	0.988	0.987	0.988	0.989	0.980	0.985	0.990	0.985	0.977
	5	0.949	0.988	0.992	0.991	0.990	0.985	0.989	0.989	0.988	0.987
	6	0.947	0.986	0.993	0.994	0.990	0.989	0.992	0.992	0.987	0.987
	7	0.943	0.983	0.993	0.995	0.996	0.996	0.994	0.995	0.993	0.992
	8	0.940	0.978	0.990	0.995	0.996	0.996	0.997	0.996	0.996	0.995
	9	0.933	0.975	0.988	0.993	0.996	0.996	0.996	0.995	0.995	0.994
	10	0.943	0.973	0.985	0.991	0.994	0.995	0.996	0.996	0.995	0.993
	20	0.923	0.954	0.969	0.973	0.976	0.976	0.972	0.974	0.969	0.965

To provide a visual representation of how well the equation agrees with the simulation results, Figure 8.7 shows a scatter plot of the resistances predicted by the equation vs. the resistances from the simulation. The data points are represented by the red circles, while the blue line represents where the data points should be if the resistances from the equation and simulation are equal (the r^2 equals 1). As the figure demonstrates, nearly all of the data points are either on blue line or very close, indicating a close agreement. While there are a few outliers, for the most part, the equation and the simulation appear to agree.

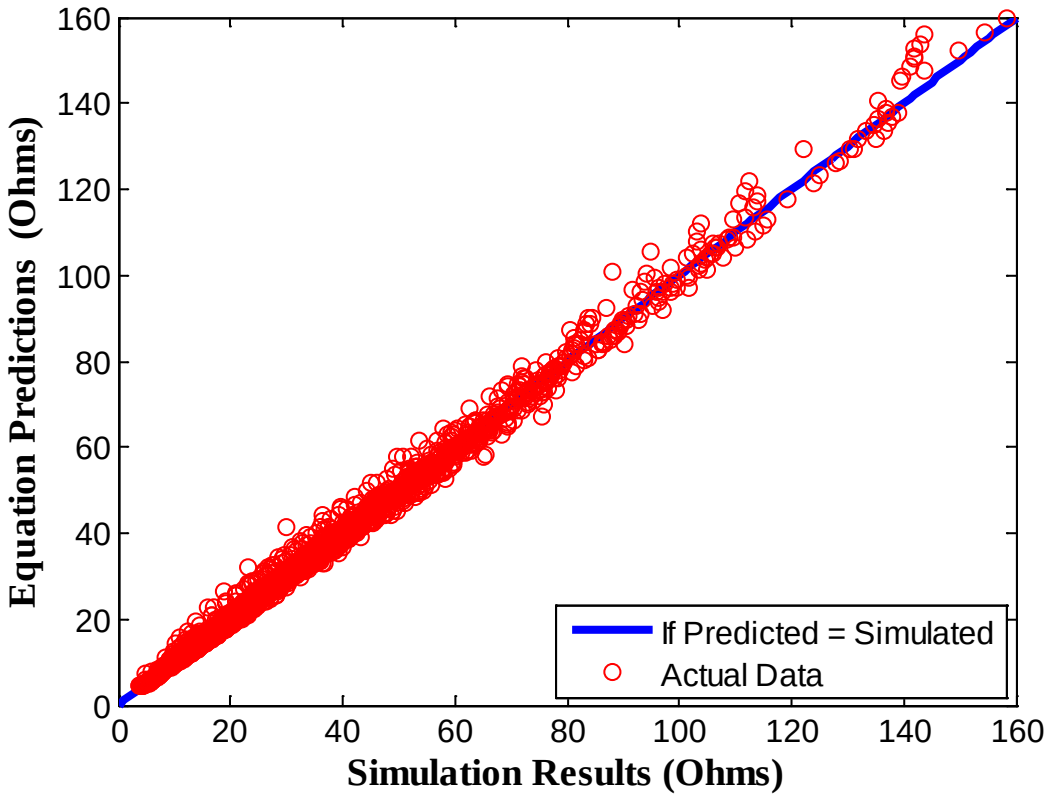

Figure 8.7: Scatter plot of the simulated verses predicted resistances

For further comparison, the simulated and predicted resistances are plotted vs. the electrode separation distance, electrode length, and electrode width in the figures shown below. First, Figure 8.8 shows the comparison between the predicted and simulated resistances as the distance was swept. In the figure, the electrode length was 10 mm, the width was 1 mm to 10 mm, the asterisks represent the simulated resistances, and the traces represent the predicated resistances. The top plot, in blue, shows the results from when the electrode width was 1 mm, while each successive plot represents the result of increasing the width by 1 mm. A comparison of the simulated and predicted resistance demonstrates a significant amount of agreement (which is unsurprising given that their r^2 values were between 0.943 and 0.996). However, the results do not match exactly. When the width was 1 mm, the simulated and predicted resistances disagree

the most. From a separation distance of 0 mm to 3 mm, the predicted resistance was noticeably higher than the simulated. After 3 mm, the predicted resistances for all of the widths were lower than the simulated. These disagreements are not very concerning since the r^2 values were still at least 0.943.

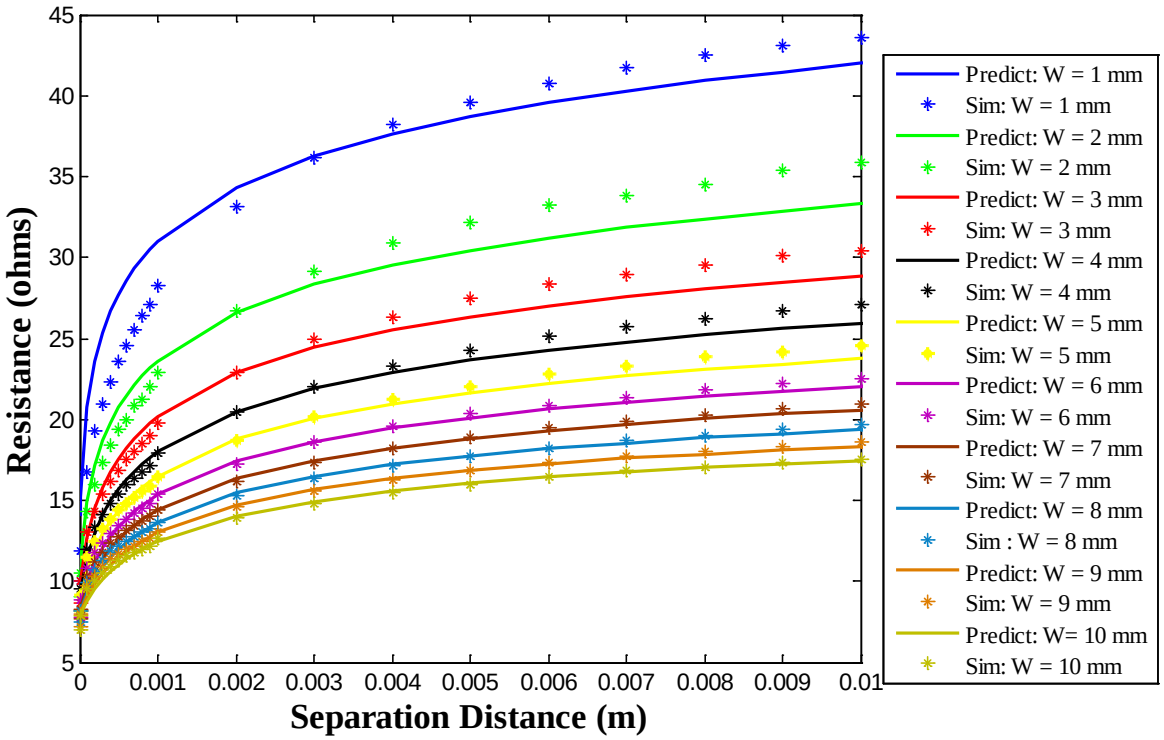

Figure 8.8: Comparison between the simulated and predicted resistance as separation distance was swept, length was 10 mm, and width was 1 mm to 10 mm

For further evaluation. Figure 8.9 shows a comparison between the simulated and predicted resistances with the lowest r^2 value. This low r^2 occurred when the electrode length was 1 mm and the width was 10 mm. In this situation, the predicted and simulated resistances were close until the separation distance reaches 5 mm. Afterwards the predicted resistance flattened out, while the simulated resistance continued to increase slowly. A similar situation can be observed for other electrode dimensions; however, this example presents the worst scenario.

While disagreement is very noticeable in this situation, the resistances were still within 5 Ω of one another, and the r^2 value was still 0.869. Given that the lowest r^2 was above 0.8 and the r^2 values for the rest of the electrode geometries were all above 0.9, the equation still serves as an acceptable solution. To contrast the results in Figure 8.9, Figure 8.10 shows a comparison between the simulated and predicted resistances for the electrode geometry with the highest r^2 (length was 8 mm and width was 7). It can be seen that the two matched almost perfectly, giving an r^2 value of 0.996.

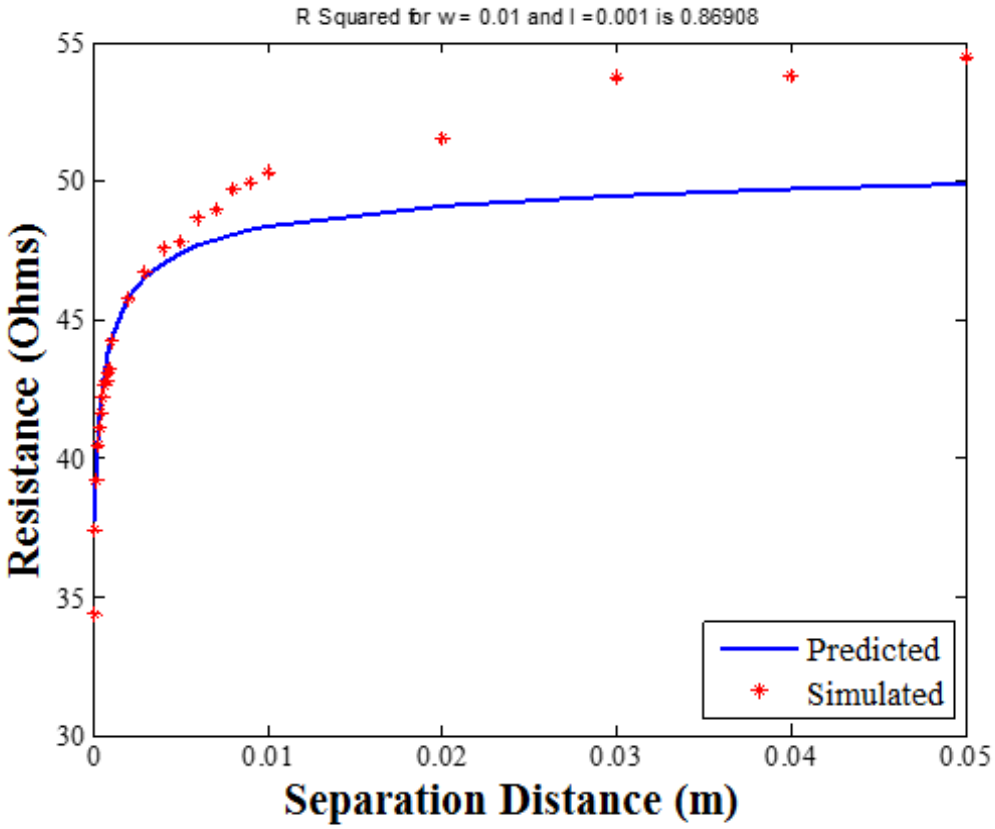

Figure 8.9: Comparison between the simulated and predicted plot with the worst r^2 (distance was swept, length was 1 mm, and width was 10 mm)

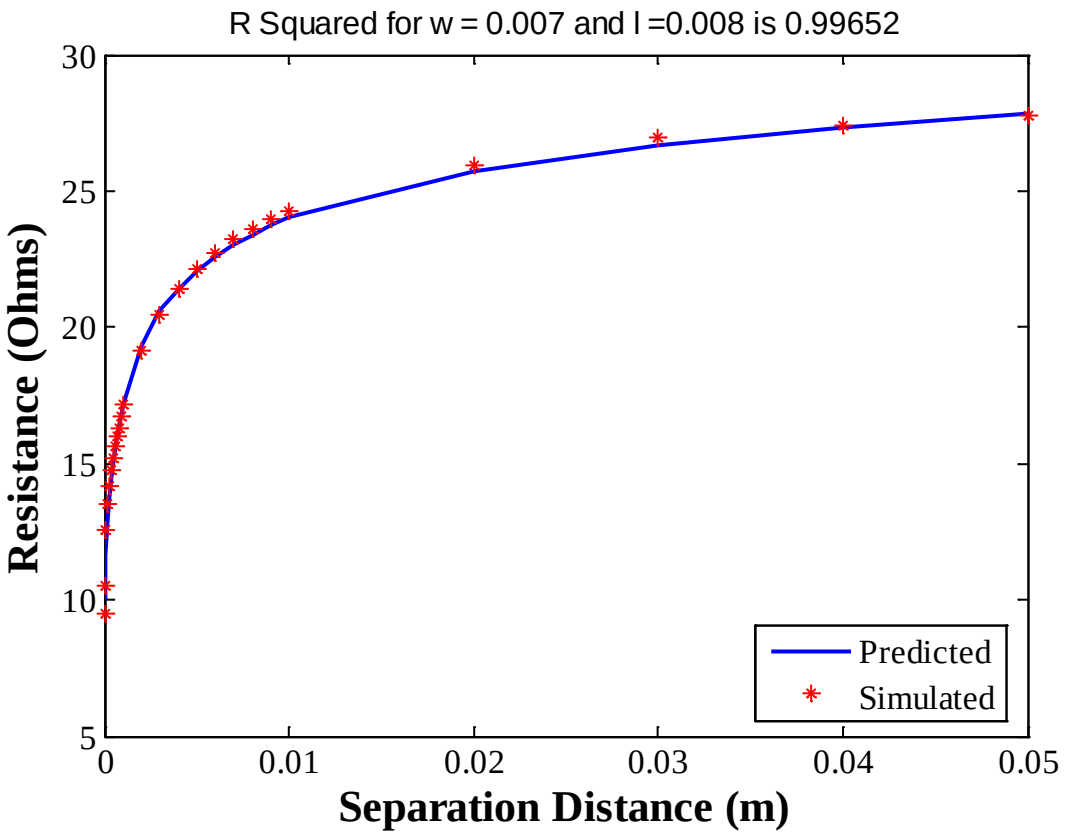

Figure 8.10: Comparison between the simulated and predicted plot with the best r^2 (distance was swept, length was 8 mm, and width was 7 mm)

Next, Figure 8.11 shows the comparison between the predicted and simulated conductance as the electrode length was swept. In the figure, the separation distance was 1 mm to 10 mm, the electrode width was 2 mm, the asterisks represent the simulated conductance, and the traces represent the predicated conductance. The top plot, in blue, was when the separation distance was 1 mm, while each successive plot represents the result of increasing the separation distance by 1 mm. Comparing the simulated and predicted conductance shows a significant amount of agreement. When the length was small, the simulated and predicted plots nearly matched; however, as the electrode length increased, they drifted further apart. When the separation distance was 1 mm, the simulated conductance became larger; however, when the distance was large, the predicted conductance became larger. This behavior can also be observed

with other electrode geometries not shown. The disagreement indicates that the equation does not agree with the simulation exactly and that the disagreement worsens as the electrode separation distance and length become large. This behavior is not surprising since the higher lengths are at the edge of the data range the algorithm used. The further away the electrodes' dimensions are from the center of the data range, the less accurate the equation will be at predicting the resistance. However, this disagreement is not a concern since the values predicted by the equation are still close to the simulated values (as indicated by the high r^2 values).

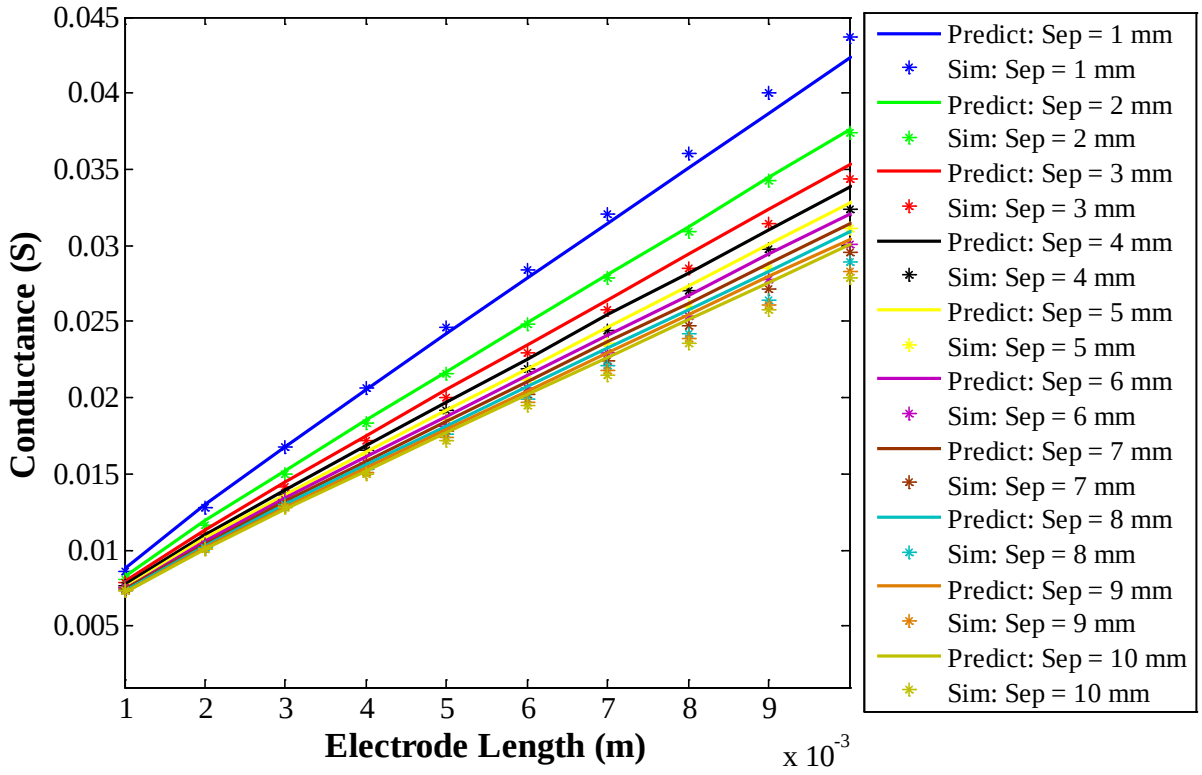

Figure 8.11: Comparison between the simulated and predicted resistance as the length was swept, the separation distance was 1 mm to 10 mm, and the width was 2 mm

Finally, Figure 8.12 shows the comparison between the predicted and simulated conductance as the electrode width is swept. In the figure, the separation distance was 1 mm to 10 mm, the electrode length was 10 mm, the asterisks represent the simulated conductance, and

the traces represent the predicated conductance. The top plot, in blue, shows when the separation distance was 1 mm, while each successive plot represents the result of increasing the separation distance by 1 mm. Comparing the simulated and predicted conductance again shows a significant amount of agreement. When the width was low, there was noticeable disagreement between the plots; however, as the electrode width increased, the plots nearly matched. For most of the geometry not shown, predicted and simulated conductance match about as well as in Figure 8.12. However, some exceptions should be noted.

Figure 8.13 shows a comparison between the simulated and predicted conductance when the electrode separation distance was 10 μm and the length was 8 mm. In this case, the predicted conductance was always lower than the simulated conductance. Furthermore, the shape of the simulated conductance was nearly linear, while the predicted conductance was curved. The biggest disagreement occurred when the width was small. The predicted conductance dropped to nearly zero while the simulated one did not. A similar disagreement can be observed for other lengths as long as the separation distance was small (at 10 μm to 100 μm). Furthermore, the difference between the conductance increased as the length was increased. Once the separation distance reached 200 μm, the agreement between the plots improved significantly. There were several causes for this disagreement. First, Q3D's accuracy tended to decrease as the electrode dimensions decreased. A number of simulations had to be rerun due to noticeable errors when the separation distance was 10 μm. Another cause of this disagreement was discussed previously. The very low separation distances are on the edge of the data range the algorithm used to fit the equation. The equation predicts the behavior of electrode geometries in the middle of the data range better than geometries near the edges.

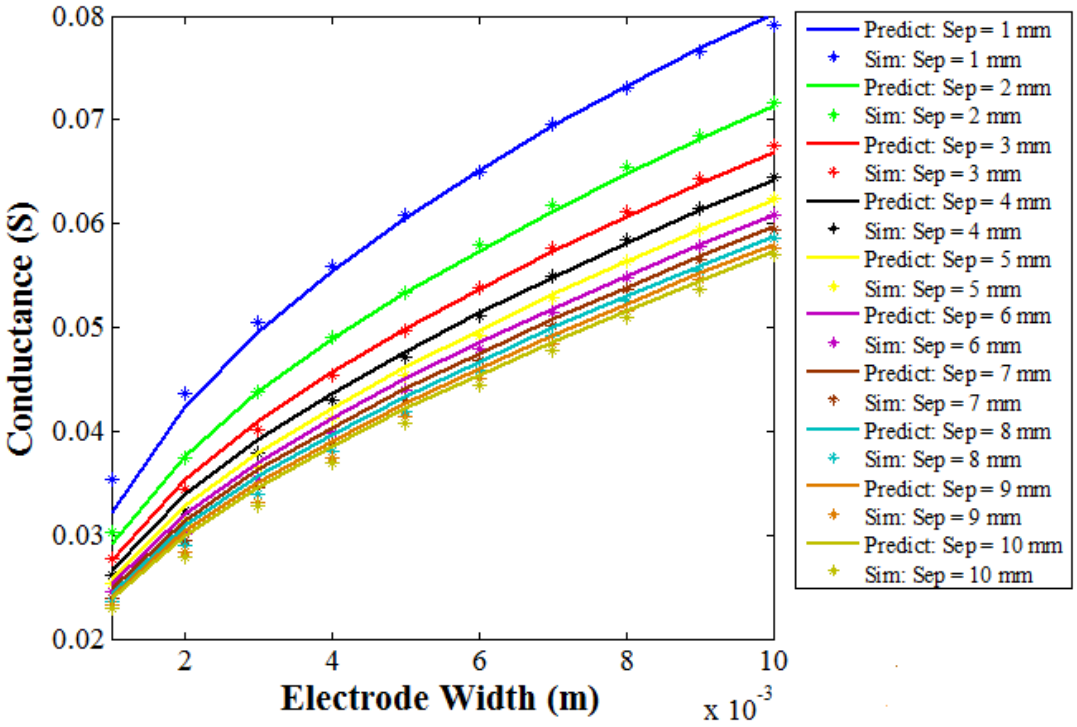

Figure 8.12: Comparison between the simulated and predicted conductances as width was swept, the separation distance was 1 mm to 10 mm, and the length was 10 mm

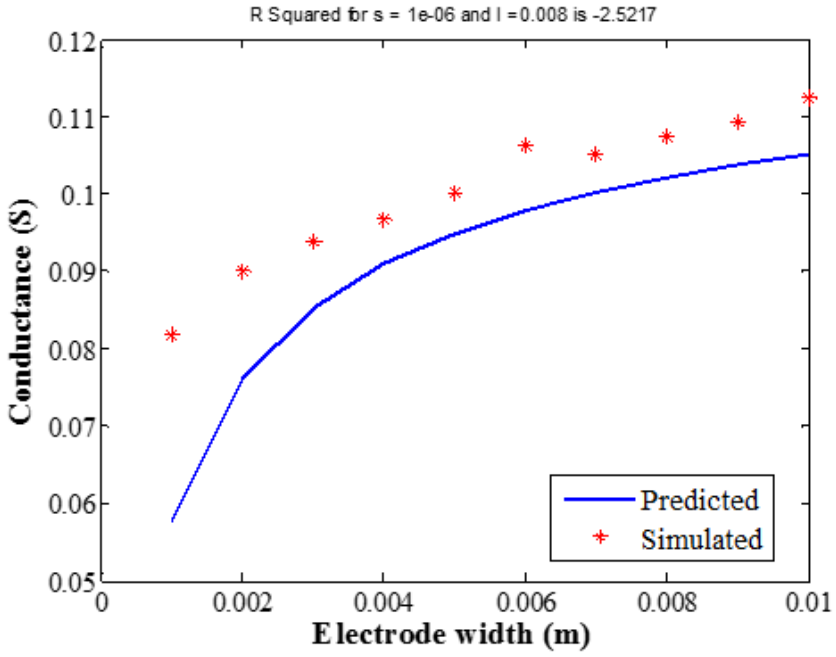

Figure 8.13: Example of poor agreement between the simulated and predicted conductances when the electrode width was swept, the separation distance was 10 µm, and the length was 8 mm

As the above tables and plots demonstrate, while the equation was able to predict the behavior of most electrode geometries very well, its performance tended to decrease when the dimensions became very small. In Table 8.2, the worst r^2 values were located at the edges of the data range, especially when the electrode length was small. Close examination shows that while the r^2 values were still large when the length was 20 mm, they start to decrease as well. This behavior illustrates an important property of the equation: its accuracy decreases the further away the electrode dimensions are from the center of the data range used to generate it. While this behavior is not desired, it likely has minimal effects of the viability of the equation. The data range used to generated to equation was based on several factors. The minimum trace size for Advanced Circuit is 152.4 μm, which is smaller than the smallest electrode lengths and widths. However, an electrode with dimensions that small is not practical. In real life, the dimensions of the electrodes need to be much larger in order to measure a usable resistance and to minimize the impact of the electrode polarization. On the other end of the range, the electrode lengths and widths were not simulated larger than 20 mm. After this point, increasing the electrode sizes also greatly increases the size and cost of the sensor, making the sensor impractical. It was also observed that the simulation and the equation tended to disagree when the separation distance became 10 μm. This disagreement is not a concern since a sensor would likely not be manufactured with such a small separation distance.

8.5 Comparison between Predicted and Measured Resistance

With (8.10), the cell constants for the original and new PCB sensors tested in Chapter 6 can be predicted. Using the equation, the cell constants for the original and new sensors were 99.908 m^{-1} and 42.969 m^{-1}, respectively. In Section 6.3.2, the cell constants of the two sensor

configurations were determined to be 111.91 m^{-1} and 47.93 m^{-1}. A comparison between the cell constants determined from the measurements and from (8.10) is shown in Table 8.3. The measured cell constants for the 10 mm by 5 mm and 20 mm by 2.5 mm were determined in the same manner as the cell constants for the original and new sensors in Section 6.3.1. However, the measured cell constants for the 10 mm by 5 mm and the 20 mm by 2.5 mm are likely not as accurate as the other two because they were determined from only a single measurement.

As Table 8.3 demonstrates, while the cell constants from the simulation and those predicted by (8.10) are close to the measured cell constants, they do not match exactly. Both the original and the new sensors have percent differences greater than 10%. For a better view of the impact of this difference, Figure 8.14 and Figure 8.15 show a comparison between the average resistances measured during the Turkey Creek concentration test and the resistances predicted by the simulation and the equation. In both figures, the plots from the simulation and the equation are nearly identical; however, they are both a few Ohms below the plots of the measured resistance. This disagreement is due to the difference in the cell constants.

Table 8.3: Comparison between measured and predicted cell constants

	Measured Cell Constants (m^{-1})	Simulated Cell Constants (m^{-1})	Predicted Cell Constants (m^{-1})	Difference between Measured and Predicted (m^{-1})	Percent Difference between Measured and Predicted (m^{-1})
10 mm by 2.5 mm (Original)	111.91	99.14	99.91	12.00	11.33%
10 mm by 5 mm	80.04	76.088	76.66	3.38	4.32%
20 mm by 2.5 mm	59.25	52.75	54.72	4.53	7.95%
20 mm by 5 mm (New)	47.93	43.05	42.97	4.96	10.92%

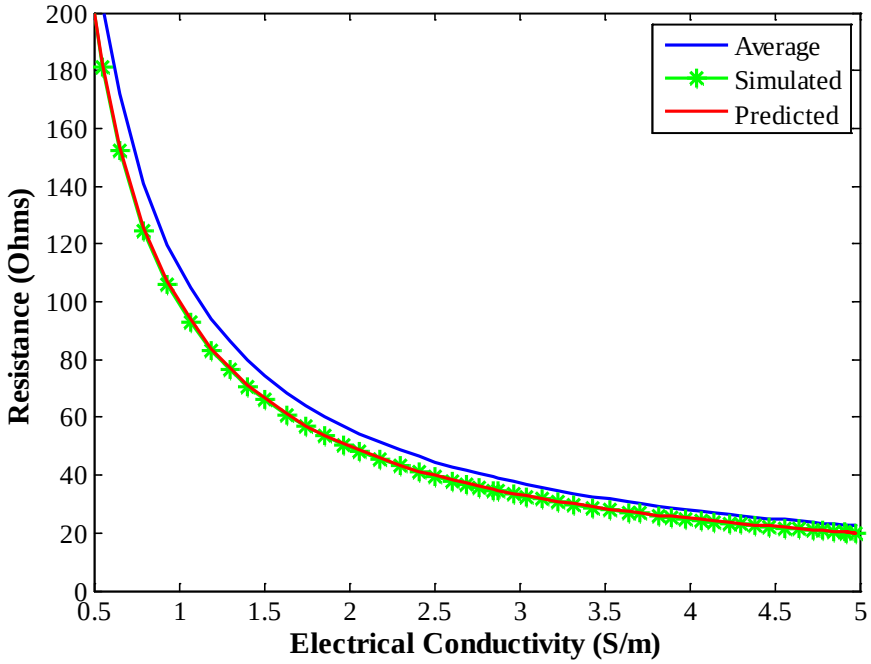

Figure 8.14: Comparison between the average measured, simulated, and predicted resistances for the Turkey Creek concentration tests using the original sensors

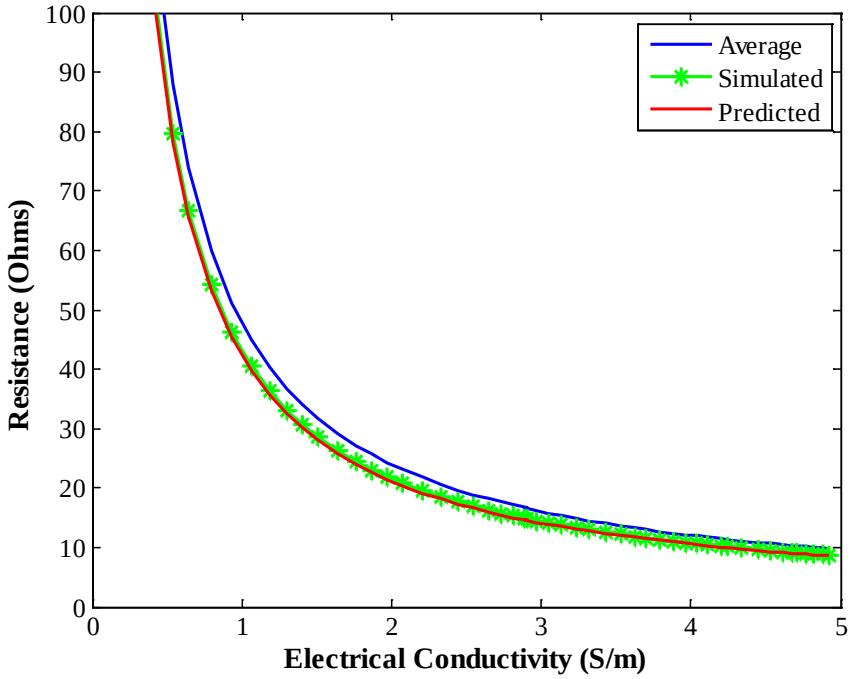

Figure 8.15: Comparison between the average measured, simulated, and predicted resistances for the Turkey Creek concentration tests using the new sensors

While the disagreement between the cell constants is noticeable, it does not result from a problem with the genetic algorithm. The equation and the simulation results are in strong agreement, indicating that the algorithm was able to derive an equation that matches the data it was provided. Instead, the problem is that the measurements and the simulations do not match exactly. While the simulation is able to predict the general behavior of the measured resistance, the cell constants for the simulation are about 10% off from the measurements. Along with the possibility of user error, this disagreement can be attributed to several potential causes.

The first possibility is that the disagreement could be a result of the differences between the measurement and simulation setups. As discussed in Chapter 7, a number of simplifications were made to the simulation setup to make it easier for the simulators to work with. Unlike in the real life testing, where a cylinder of water surrounded the sensor on all sides, in the simulation, a large block of water was placed on the top of the water. While the water wrapping around the sensors affected the resistance, the effect was very small. Furthermore, having water surround the sensor causes the resistance to decrease since the volume the current is confided to increases [21]. Since the measured resistance is higher than the simulated effect is likely outweighed by other factors.

A related difference between the two setups is that the water used in the measurements is confined to a beaker, while in the simulations, the volume of the water is much larger. A large volume was used in the simulations in order to minimize the influence of the edges of the water's container. As discussed in Section 7.3, the volume of the water has a small but noticeable impact on the measured resistance. This behavior is the result of the current flowing between the electrodes being confided to a smaller volume. A larger volume of water means that the current is confided to a larger volume, decreasing the resistance. Since the volume of the beaker used

when taking measurements can vary significantly, its influence on the simulation was minimized by using a very large volume of water. As a result, the beaker likely caused an increase in measured resistance. However, Section 7.3 also demonstrated that the influence of the volume decreased as the volume became large (due to the decrease in the magnitude of the electric field as it penetrated deeper into the water). Since the cell constants were calculated using the concentration testing measurements and the breaker used for those tests was fairly large (a diameter of 68 mm), it is likely that the cell constant calculated from the measurements was only increased by a small amount.

Another difference between the simulation and measurement setups comes from the PCB sensor's solder mask. As mentioned in Chapter 3, the edges of the electrodes are covered by the solder mask. While the impact the solder mask has on the area of the electrodes was taken into account in the simulations, the height of the solder mask was not. For the simulations, the electrodes were assumed to be flush with one side of the block of water. However, in reality, a small ring of solder mask with a nonzero height was around the edges of the electrodes. When the PCB sensor is placed in the water, the ring encloses a small box of water between the electrode and the larger volume of water. This volume has the length and width of the part of the electrodes not covered by the solder mask and a height equal to the thickness of the solder mask. A cross section of the PCB sensor with the solder mask ring is shown in Figure 8.16. The current entering or leaving the electrodes is confined to this small volume for a short period of time, causing an increase in resistance. This extra volume can be treated as being in series with the large volume of water. Therefore, the cell constant from the smaller volume can be added to the cell constant calculated using the equation. If the electric field is assumed to be uniform in this volume the cell constant of this volume can be estimated using

$$\kappa = \frac{h}{lw} \tag{8.11}$$

where h is the thickness of the solder mask. While the electric field is likely not uniform, (8.11) serves as a simple way to estimate the influence of the solder ring. The cell constant then needs to be doubled to account for the fact that both electrodes have this small box above them. It is difficult to measure the thickness of the solder mask; however, according to the company used to manufacture the PCB sensors (Advanced Circuits), the thickness of the solder mask is between 5.08 µm to 76.2 µm and is typically around 17.78 µm [49]. If it is assumed that the solder mask is the maximum thickness, the cell constants calculated using (8.10) and (8.11) become 105.81 m^{-1} and 44.44 m^{-1} for the original and new PCB sensors, respectively. When the solder mask ring is taken into account in the simulation, the cell constants become 108.27 m^{-1} and 45.64 m^{-1}. While taking the solder mask ring into account does make the cell constants predicted by the simulation and equation closer to the measured cell constants, they still do not match exactly, implying there may be other factors at play.

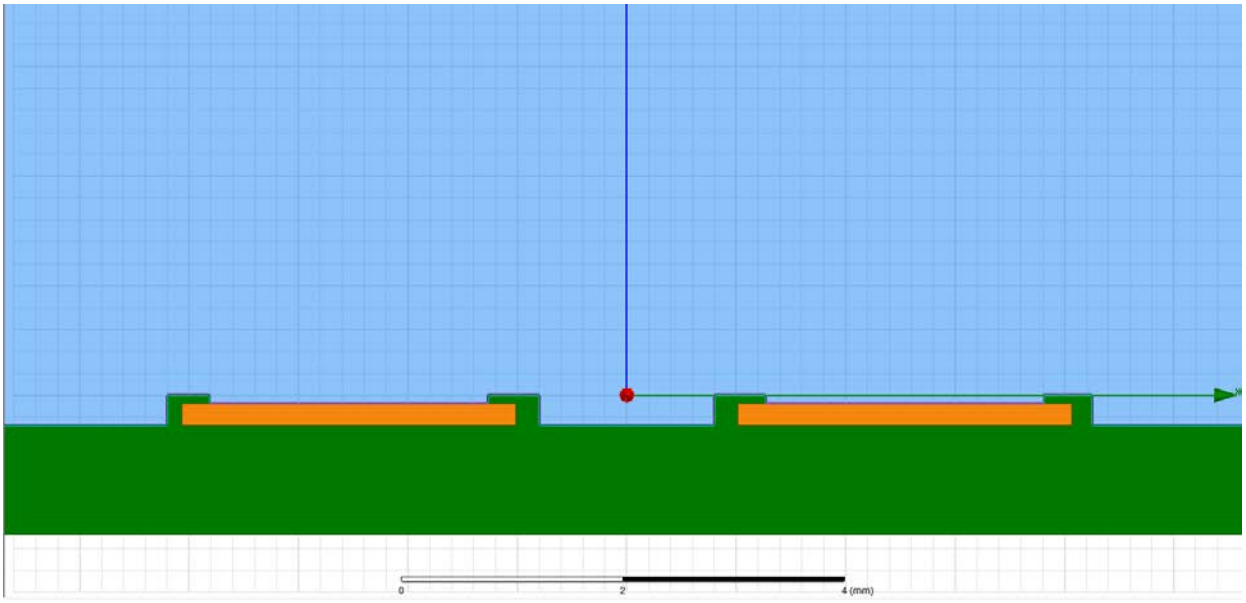

Figure 8.16: Cross-section of the PCB sensor with the solder mask ring

Other differences between the electrodes in the simulations and in real-life potentially contributed to the differences in cell constants too. Unlike in the simulations, the electrodes in real-life are not going to be flat and smooth. Instead, the electrodes' surfaces will have uneven areas resulting from the manufacturing process and scratches resulting from prolonged usage. Furthermore, the electrodes' plated Tin surface will likely have some oxidation on it. Both of these properties would result in increasing the sensors' contact resistance that was not taken into account in the simulations.

Another potential cause for the difference in the cell constants is that the cell constants calculated in Section 6.3.1 may not be completely accurate. A number of potential reasons for this inaccuracy are possible. First, the resistance measurements used to calculate the cell constant may be incorrect. Since the resistance measured by each sensor tend to agree with one another, an error due to differences between the individual sensors is unlikely. Instead, it is more likely that extra resistance came from the cables connecting the sensor to the analyzer and the traces on the PCB.

It is also possible that the electrode polarization still had an effect on the measurements. While the measurement frequency was set to 1 MHz to minimize the influence of the electrode polarization, its influence may not have been completely gone. If the electrode polarization was still influencing the measurements, an increase in the resistance would result.

Another potential cause is from the commercial conductivity pen. In Section 6.3.1, the conductivity measurements made using the pen were used to calculate the cell constants of the PCB sensors; therefore, any error from the pen would have an effect on the calculated cell constants. As can be observed in Table 6.13, the cell constants increase slightly as the measured conductivity increases. Since the cell constants should not change, this increase was likely the

result of an error with the pen's measurements. Given that the predicted and measured results are so close, any error from the pen was probably not very large.

The final potential cause is from the simulator. It is possible that Q3D's simulation results do not match the measurement results because of an error with the simulator and not because of an issue with the setup or measurements. It has been noticed throughout this work that the simulator occasionally produced errors. These errors appeared as unexpected spikes or drops in resistance in an otherwise smooth plot. If enough of these errors occurred in the data used to derive the equation, differences between the predicted and measured results can occur. It is also difficult to determine the accuracy of Q3D. However, given that the behavior of the simulation and measurements are the same and the simulated and measured resistances are within several Ohms of one another, Q3D is likely fairly accurate.

While it is likely that none of the potential cases individually had a large impact on the results, when taken together, it is unsurprising that the cell constants predicted by the equation do not match the measurements exactly. Even through a large majority of this section focuses on the differences between the predicted and measured cell constants, it is important to emphasize that the predicted behavior is still close to the measurements. As shown in Figures 8.14 and 8.15, the equation was able to predict how the measured resistance changes as the conductivity changes. Furthermore, Table 8.3 shows that while the cell constants predicted by the equation are a little too small, changing the dimensions of the electrodes has the same effects on both the measured and predicted cell constants. If the measurements are accurate, the accuracy of the equation can be increased by improving the accuracy of the simulation data used to derive it. Since the behavior predicted by the equation appears to be correct, only the equation's coefficients, most likely the 2.14, need to be changed and not its form. For example, increasing the 2.14 to 3.14

caused the predicted cell constants for the original and new PCB sensors to increase to 109.6 m^{-1} and 48.063 m^{-1}, making both closer to the measured cell constants.

Chapter 9

Conclusions

In the previous chapters, a PCB-based electrical conductivity sensor developed for measuring salinity was presented. It has been shown through significant testing and simulation work that this sensor is capable of measuring the salinity of water. The PCB sensor is comprised of two metal electrodes integrated onto a PCB. It measures the resistance between the two electrodes when placed in the water, and the salinity can then be determined from the resistance.

9.1 Overview of Results

Two electrode geometries for the PCB sensor were extensively tested. The sensors had an electrode length and width of 10 mm by 2.5 mm and of 20 mm by 5 mm. Furthermore, the impact of gold-plating the 20 mm by 5 mm sensors was investigated. Early testing showed that increasing the measurement frequency improved the accuracy of the measurement significantly. Comparing the performance of both electrode sizes did not indicate much difference in the accuracy of the measurements. The measurements made using different individual sensors with the same electrode dimensions had nearly identical results, indicating little variation in performance between them. Furthermore, comparing the measurements from both sensor geometries to the simulation results shows similar agreement. Based on the testing outlined in Chapter 6, it is difficult to determine whether the performance of either geometry is better.

However, it should be noted that the impact of electrode polarization decreases with electrode size, favoring the 20 mm by 5 mm configuration. Comparing the performance of the non-plated and gold-plated sensors also does not show much difference in performance. Since the gold-plating increases the cost of the sensor, it is recommended that the sensors not be gold-plated.

After the testing and simulations were completed, the results of the simulations were used by a genetic algorithm to derive an equation to predict the behavior of the PCB sensor over a variety of electrode geometries. This equation has been shown to predict the behavior of the simulations with a high accuracy. However, comparing the equation's predictions to the measurements indicated a small but noticeable disagreement. While the equation can predict the general behavior of the PCB sensors, the values it predicts are off by a small amount. Potential causes of this disagreement include errors with the simulations, electrode polarization, or differences between the sensors' setup in real life testing. Despite this disagreement, the equation is able to predict the behavior of the sensor as its electrode dimensions are varied and is accurate enough for the intended purpose of the PCB sensor. Since the sensor is not a scientific instrument but instead is designed to measure saltwater intrusion, the equation does not need to be 100% accurate.

9.2 Future Work

Future work includes developing the sensor into a commercial product, addressing unanswered questions, and improving the accuracy of the equation. In order for the sensor to be used outside of a lab setting, sensing electronics need to be designed. If the sensor is going to be used as a handheld device, the electronics need to be integrated onto the PCB. A water-tight housing also needs to be developed to protect the electronics from exposure to water.

Furthermore, a temperature sensor may need to be designed and integrated into the PCB to compensate for the effect temperature has on the conductivity of the water.

More testing may also need to be done to address several concerns not mentioned above. One test is observing the effect of leaving the PCB sensor in the water for a prolonged period of time. In this work, a sensor was left in a water sample for two to three hours at one point. This amount of time did not have any noticeable effect on the sensor or its readings. It was not left in the water longer because of the possibility that the PCB would absorb water. While the PCB sensor is intended to be a handheld device, determining the effect a prolonged constant exposure to water has on its electrodes is useful for assessing its reliability.

Along the same line, the impact prolonged use has on the sensor (using the sensor hundreds of separate times) also needs investigation. In this work, several of the sensors were likely used more than 400 times. By the end of the testing, some small spots and blemishes appeared on the electrodes; however, their cause is unknown. Although no noticeable change in the performance of the sensors occurred, long-term performance was also not the focus of the work. Changes in the performance of the sensors over time are difficult to determine because changing the testing frequency had an impact on later measurements. It is possible that prolonged use could have caused an increase in the measured resistance. This undocumented increase would help explain the differences between the simulated and measured resistances. On the other hand, gold-plating was intended to protect the sensors' electrodes from the elements. The lack of notable difference observed between the non-plated and plated sensors implies that the prolonged usage did not impact the performance (or that the gold-plating did not help).

Another concern that needs to be investigated relates to something that was observed during testing. Early on, when determining the effects of increasing the measurement frequency

had on the resistance (Figure 5.5), bubbles were observed after the frequency reached 100 kHz. After the test was complete, one of the sensor's electrodes had become black. This result likely occurred because of the ions in the water being electroplated to the electrode. Since this phenomena had not been observed before, it was originally assumed that the hydrolysis was caused by increasing the frequency. However, later testing, where the frequency was set even higher, was not able to repeat the results. It is currently believed that the LCR meter was unknowingly set to apply a DC offset with its measurement signal when the hydrolysis occurred. This theory has not been tested yet since the sensors were needed for further experiments.

Other potential future work relates to the simulation and equation. As discussed in Section 8.5, while the behavior predicted by the equation matches the simulation very well, a small but noticeable difference between it and the measurements has been observed. One way to improve the accuracy of the equation includes re-simulating the sensor at a higher accuracy. This re-simulation was not done in this work because it would take too much time (it took a month to complete the original simulations) and would likely require too much memory. Another way to improve the accuracy is to use a high accuracy commercial salinity sensor to determine the conductivity of the water samples during testing. In Section 6.3.1, the PCB sensors' cell constants were calculated using the resistance measured by the PCB sensors and the conductivity measured by the commercial sensors. Any errors in the commercial sensor's measurements would have resulted in an error with the cell constants. Because the cell constant appears to slightly increase as the conductivity increases, an error is possible. A more accurate commercial sensor would eliminate this concern.

Another way to improve the accuracy is to compare the behavior predicted by the equation to PCB sensors with a larger variety of electrode dimensions. In this work, only four

electrode geometries were used to take measurements. Testing PCB sensors with more electrode geometries would further test the equation's accuracy.

Bibliography

[1] "Pump/Recharge Rate Affects Saltwater Intrusion," Solinst, [Online]. Available: http://www.solinst.com/resources/papers/101c4salt.php. [Accessed 17 May 2016].

[2] P. M. Barlow, "Ground Water in Freshwater-Saltwater Environments of the Atlantic Coast," USGS Publications Warehouse, 2013.

[3] N. P. Fofonoff and R. C. Millard Jr., "Algorithms for Computation of Fundamental Properties of Seawater," *Unesco Techical Papers in Marine Science,* vol. 44, pp. 1-54, 1983.

[4] T. J. McDougall and P. M. Barker, *2011: Getting started with TEOS-10 and the Gibbs Seawater (GSW) Oceanographic Toolbox,* SCOR/IAPSO WG127, 2011.

[5] R. N. Dean, F. T. Werner and M. L. Adams, "A PCB Technology Electrical Conductivity Sensor Probe for the Measurement of Saltwater Contamination," in *11th International Microelectronics Assembly and Packaging Society Conference and Exhibition on Device Packaging*, Fountain Hills, AZ, 2015.

[6] W. Gong, "Ocean Sensors -- for marine environmental monitoring," *University of Southampton Research Repository.*

[7] B. D. Newport, "Salt Water Intrusion in the United States," EPA, Ada, Oklahoma, 1977.

[8] D. Murgulet and G. Tick, "The extent of saltwater intrusion in southern Baldwin County, Alabama," *Environmental Geology,* vol. 55, no. 6, pp. 1235-1245, 2008.

[9] P. Barlow, "Saltwater Intrusion," EPA, [Online]. Available: http://water.usgs.gov/ogw/gwrp/saltwater/salt.html. [Accessed 22 May 2016].

[10] F. J. Millero, R. Feistel, D. G. Wright and T. J. McDougall, "The composition of Standard Seawater and the definition of the Reference-Composition Salinity Scale," *Deep Sea Research Part I: Oceanographic Research Papers,* vol. 55, no. 1, pp. 50-72, January 2008.

[11] I. Shkvorets, "Practical Salinity Scale – 1978," 2016. [Online]. Available: http://salinometry.com/pss-78/. [Accessed 19 May 2016].

[12] "Liquids - Specific Gravities," [Online]. Available: http://www.engineeringtoolbox.com/specific-gravity-liquids-d_336.html. [Accessed 19 May 2016].

[13] P. Barker and A. Sarraf, "The Thermodynamic Equation Of Seawater - 2010," IOC, SCOR, and IAPSO, [Online]. Available: http://www.teos-10.org/. [Accessed 19 May 2016].

[14] R. Pawlowicz, "The electrical conductivity of seawater at high temperatures and salinities," *Desalination*, vol. 300, pp. 32-39, 15 August 2012.

[15] R. Pawlowiz, "What every oceanographer needs to know about TEOS-10," 2013.

[16] R. Holmes-Farley, "Chemistry and the Aquarium: Specific Gravity: Oh How Complicated!," Advanced Aquarist, January 2002. [Online]. Available: http://www.advancedaquarist.com/2002/1/chemistry. [Accessed 20 May 2016].

[17] D. F. Reid, "Conversion of Specific Gravity to Salinity for Ballast Water Regulatory Management," Great Lakes Environmental Research Laboratory, Ann Arbor, Michigan, 2006.

[18] "http://www.theaquariumsolution.us/measuring-salinity-and-specific-gravity-your-aquarium," The Aquarium Solution USA, 2010. [Online]. Available: http://www.theaquariumsolution.us/measuring-salinity-and-specific-gravity-your-aquarium. [Accessed 20 May 2016].

[19] "Refractormeter Overview," 2011. [Online]. Available: http://www.refractometer.pl/. [Accessed 19 May 2016].

[20] A. DePalma, "Refractometer Uses in Industry and Selection," Rudolph Research Analytical, [Online]. Available: http://rudolphresearch.com/refractometers-use-selection/#.Vz4uUfkrLmF. [Accessed 19 May 2016].

[21] S. M. Wentworth, Applied Electromagnetics, Hoboken, New Jersey: Wiley & Sons, 2007.

[22] P. M. Ramos, J. M. D. Pereira, H. M. G. Ramos and A. L. Ribeiro, "A Four-Terminal Water-Quality-Monitoring Conductivity Sensor,," *IEEE Transactions on Instrumentation and Measurement*, vol. 57, no. 3, pp. 577-583, March 2008.

[23] K. Striggow and R. Dankert, "The exact theory of inductive conductivity sensors for

oceanographic application," *IEEE Journal of Oceanic Engineering,* vol. 10, no. 2, pp. 175-179, April 1985.

[24] "Automatic Analyzers for Water Pollution Monitoring Station," [Online]. Available: http://nett21.gec.jp/CTT_DATA/WMON/CHAP_4/html/Wmon-097.html. [Accessed 17 May 2016].

[25] "Conductivity Theory and Practice," Radiometer Analytical, Villeurbanne Cedex, France, 2004.

[26] R. N. Dean, A. K. Rane, M. E. Baginski, J. Richard, Z. Hartzog and D. J. Elton, "A capacitive fringing field sensor design for moisture measurement based on printed circuit board technology," *IEEE Trans. on Instrumentation and Measurement,* vol. 61, no. 4, pp. 1105-1112, 2012.

[27] R. N. Dean, M. C. Hamilton and M. E. Baginski, "Capacitive fringing field moisture sensors implemented in flexible printed circuit board technology," *IMAPS Journal of Microelectronics and Electronic Packaging,* vol. 11, no. 3, pp. 122-127, 2014.

[28] R. N. Dean and A. K. Rane, "A digital frequency-locked loop system for capacitance measurement," *IEEE Trans. on Instrumentation and Measurement,* vol. 62, no. 4, pp. 777-784, 2013.

[29] Y. Meng and R. N. Dean, "A technique for improving the linear operating range for a relative phase delay capacitive sensor interface circuit," *IEEE Trans. on Instrumentation and Measurement,* vol. 65, no. 3, pp. 624-630, 2016.

[30] D. J. Griffiths, Introduction to Electrodynamics, Upper Saddle River: Prentice-Hall, 1999.

[31] J. D. Jackson, Classical Electrodynamics, Hoboken, New Jersey: Wiley & Sons, 1999.

[32] W. Olthuis, W. Streekstra and P. Bergveld, "Theoretical and experimental determination of cell constants of planar-interdigitated electrolyte conductivity sensors," *Sensors and Actuators B: Chemical,* vol. 24, no. 1-3, pp. 252-256, 1995.

[33] M. N. O. Sadiku and A. F. Peterson, "A Comparison Of Numerical Methods For Computing Electromagnetic Fields," in *IEEE Southeastcon '90. Proceedings,* New Orleans, LA, 1990.

[34] C. Yavuzturk and K. Ksaibati, "Assessment of Temperature Fluctuations in Asphalt Pavements Due to Thermal Environmental Conditions using a Two-Dimensional Transient Finite Difference Aproach," October 2002.

[35] D. Morris, "Which Electromagnetic Simulator Should I Use?," Agilent Technologies, Stockport, 2012.

[36] S. M. Rao and N. Balakrishnan, "Computational Electromagnetics - A Review," [Online]. Available: http://www.iisc.ernet.in/~currsci/nov25/articles24.htm. [Accessed 19 5 2016].

[37] "EMPro 3D EM Simulation Software," Keysight Technologies, 2016. [Online]. Available: http://www.keysight.com/en/pc-1297143/empro-3d-em-simulation-software?cc=US&lc=eng. [Accessed 19 May 2016].

[38] "ANSYS Q3D Extractor," ANSYS, 2016. [Online]. Available: http://ansys.com/en/Products/Electronics/ANSYS-Q3D-Extractor. [Accessed 19 May 2016].

[39] M. C. Zaretsky, L. Mouayad and J. R. Melcher, "Continuum Properties from Interdigital Electrode Dielectrometry," *IEEE Transactions on Electrical Insulation,* vol. 23, no. 6, pp. 897-917, 1988.

[40] J. Acero, C. Carretero, O. Lucia, J. M. Burdio and R. Alonso, "An application example to gain an insight into the electromagnetic quasistatic approach concept for graduate students," in *Promotion and Innovation with New Technologies in Engineering Education (FINTDI)*, Teruel, 2011.

[41] R. A. Horne and G. R. Frysinger, "The Effect of Pressure on the Electrical Conductivity of Sea Water," *Journal of Geophysical Research,* vol. 68, no. 7, pp. 1967-1973, 1963.

[42] J. O. M. Bockris and A. K. N. Reddy, Modern Electrochemistry: an Introduction to an Interdisciplinary Area, New York: Plenum Press, 1970.

[43] X. Wang, Y. Wang, H. Leung, S. C. Mukhopadhyay, M. Tian and J. Zhou, "Mechanism and Experiment of Planar Electrode Sensors in Water Pollutant Measurement," *IEEE Transactions on Instrumentation and Measurement* , vol. 64, no. 2, pp. 516-523, 2014.

[44] "LCR-800 Series," GW Instek, 2015. [Online]. Available: http://www.gwinstek.com/en-global/products/LCR_Meters/Benchtop_LCR_Meters/LCR-800. [Accessed 19 May 2016].

[45] "4366 Traceable Conductivity/TDS Pen," Traceable Products, 2015. [Online]. Available: https://traceable.com/products/conductivity-ph/4366.html. [Accessed 19 May 2016].

[46] "Deionized/Demineralized Water," Lenntech, 2016. [Online]. Available: http://www.lenntech.com/applications/process/demineralised/deionised-demineralised-water.htm. [Accessed 19 5 2016].

[47] "Sea Water," National Weather Service and National Oceanic and Atmospheric Administration, [Online]. Available: http://www.srh.noaa.gov/jetstream/ocean/seawater.html. [Accessed 19 May 2016].

[48] "Water Conductivity," Lenntech, 2016. [Online]. Available: http://www.lenntech.com/applications/ultrapure/conductivity/water-conductivity.htm. [Accessed 30 May 2016].

[49] "Capabilities," Advanced Circuits, June 2011. [Online]. Available: http://www.4pcb.com/media/detailed-capabilities.pdf. [Accessed 26 May 2016].

[50] X. Meng and B. Song, "Fast Genetic Algorithms Used for PID Parameter Optimization," in *International Conference on Automation and Logistics*, Jinan, China, 2007.

[51] Y. Rahmat-Samii and E. Michielssen, Electromagnetic Optimization by Genetic Algorithms, Hoboken, New Jersey: Wiley & Sons, 1999.

[52] A. G. Asuero, A. Sayago and A. G. Gonzalez, "The Correlation Coefficient: An Overview," *Critical Reviews in Analytical Chemistry*, vol. 36, pp. 41-59, 2006.

[53] O. Renaud and M. Victoria-Feser, "A robust coefficient of determination for regression," *Journal of Statistical Planning and Inference*, vol. 140, no. 7, pp. 1852-1862, 2010.

[54] Y. Orito, J. Takano, M. Takeda and H. Yamamoto, "Index Fund Optimization Using GA Based on Coefficients of Determination," in *5th IEEE/ACIS International Conference on Computer and Information Science*, 2006.

[55] AEMC Instruments, "Understanding Ground Resistance Testing," [Online]. Available: http://www.rainbirdservices.com/Training/Documents/Understanding%20Earth%20Ground%20Resistance%20by%20AEMC.pdf. [Accessed 6 June 2016].

Appendix A

Referenced Tables

Table A.1: Resistance as the measurement frequency of the LCR meter is swept while in seawater

Frequency (Hz)	Resistance (Ω)
1,000	102.330
2,000	53.804
5,000	37.801
7,500	33.964
10,000	31.816
20,000	27.924
50,000	26.187
66,670	26.978
100,000	26.225
200,000	25.231

Table A.2: Testing the accuracy of the LCR meter when in parallel mode with a 1.66 pF capacitor

	f = 30 Hz (Ω)	f = 250 Hz (Ω)	f =1 kHz (Ω)	f= 10 kHz (Ω)	f = 100 kHz (Ω)	f = 200kHz (Ω)
R = 3.994 Ω	4	4.013	4.013	4.014	4.014	4.004
R = 99.81 Ω	99.53	99.53	99.54	99.53	99.5	99.4
R = 995.6 Ω	995.6	995.7	995.7	995.6	995.8	995.4
R = 9849 Ω	9849	9850	9850	9850	9848	9788
R = 110.6 kΩ	110.6k	110.6k	110.6k	110.3k	110.3k	109.1k
R = 1022 kΩ	1102k	1021k	1022k	1022k	1000k	948.7k

Table A.3: Testing the accuracy of the LCR meter when in series mode with a 1.66 pF capacitor

	f = 30 Hz (Ω)	f = 250 Hz (Ω)	f =1 kHz (Ω)	f= 10 kHz (Ω)	f = 100 kHz (Ω)	f = 200kHz (Ω)
R = 3.994 Ω	4.018	4.018	4.018	4.021	4.017	3.999
R = 99.81 Ω	99.53	99.54	99.54	99.54	99.5	99.4
R = 995.6 Ω	995.6	995.7	995.7	995.6	995.8	995.4
R = 9849 Ω	9845	9850	9850	9850	9845	9776
R = 110.6 kΩ	110.6k	110.6k	110.6k	110.6k	106.3k	93.85k
R = 1022 kΩ	1022k	1022k	1021k	1002k	363.2k	127.4k

Table A.4: Testing the accuracy of the LCR meter when in parallel mode with a 22.29 pF capacitor

	f = 30 Hz (Ω)	f = 250 Hz (Ω)	f =1 kHz (Ω)	f= 10 kHz (Ω)	f = 100 kHz (Ω)	f = 200kHz (Ω)
R = 3.994 Ω	4.016	4.024	4.024	4.018	4.026	4.02
R = 99.81 Ω	99.7	99.7	99.7	99.7	99.7	99.5
R = 995.6 Ω	995.7	995.7	995.7	995.7	995.8	995.4
R = 9849 Ω	9849	9849	9849	9849	9846	9780
R = 110.6 kΩ	110.6k	110.6k	110.6k	110.6k	110.2k	108.7k
R = 1022 kΩ	1022k	1022k	1022k	1024k	997.8k	919.3k

Table A.5: Testing the accuracy of the LCR meter when in series mode with a 22.29 pF capacitor

	f = 30 Hz (Ω)	f = 250 Hz (Ω)	f =1 kHz (Ω)	f= 10 kHz (Ω)	f = 100 kHz (Ω)	f = 200kHz (Ω)
R = 3.994 Ω	4.016	4.024	4.024	4.018	4.024	4.01
R = 99.81 Ω	99.7	99.7	99.7	99.73	99.7	99.6
R = 995.6 Ω	995.7	995.7	995.7	995.7	995.7	995.7
R = 9849 Ω	9849	9849	9849	9847	9663	9090
R = 110.6 kΩ	110.6k	110.6k	110.6k	108.6k	32.25k	10.31k
R = 1022 kΩ	1022k	1020k	1001k	330.3k	5.005k	1.0347k

Table A.6: Turkey Creek concentration test results using the original testing setup

			Turkey Creek+Seawater			Seawater+Turkey Creek		
total added	% added	Delta (mL)	Board 2 (Ω)	Board 3 (Ω)	Board 12 (Ω)	Board 2 (Ω)	Board 3 (Ω)	Board 12 (Ω)
0	0	0	45,846.0	45,750.0	42,617.0	37.583	34.75	40.269
1	0.99	1	2,109.7	2,130.6	2,145.9	37.585	34.667	39.889
3	2.91	2	689.58	708.56	785.3	37.744	34.986	40.199
5	4.76	2	460.1	457.77	469.96	38.26	35.193	40.437
7	6.54	2	333.13	329.62	335.51	38.593	35.844	40.785
9	8.26	2	268.85	264.97	275.38	38.968	36.228	40.997
11	9.91	2	228.56	226.24	233.32	39.136	36.402	41.222
14	12.28	3	190.13	190.84	195.93	39.856	37.202	41.715
17	14.53	3	166.42	163.12	169.22	40.267	37.767	42.379
20	16.67	3	146.36	143.02	144.61	40.879	38.435	42.905
23	18.7	3	131.61	128.67	135.67	41.787	38.812	43.413
26	20.63	3	121.31	118.27	124.68	41.984	39.945	44.199
29	22.48	3	111.62	109.02	115.47	42.822	40.252	44.767
32	24.24	3	105.16	102.33	108.83	43.6	40.806	45.162
36	26.47	4	98.422	95.617	101.48	44.484	42.887	47.275
40	28.57	4	92.239	89.295	95.631	45.242	42.578	46.896
44	30.56	4	87.534	84.738	90.25	46.005	43.286	47.775
48	32.43	4	83.104	80.602	86.495	46.786	44.231	48.798
52	34.21	4	79.45	76.796	82.986	47.781	45.023	49.487
57	36.31	5	76.349	73.189	79.223	48.834	45.965	50.613
63	38.65	6	71.782	69.403	75.274	50.726	48.171	52.974
69	40.83	6	69.673	66.276	72.281	52.094	49.4	54.054
75	42.86	6	66.758	63.806	69.789	53.54	50.772	55.366
81	44.75	6	64.485	61.811	67.57	54.759	51.946	56.76
87	46.52	6	62.644	59.532	65.469	56.326	53.654	58.172
93	48.19	6	60.929	57.944	63.779	57.312	54.584	59.205
100	50	7	59.35	56.434	62.198	58.662	56.071	60.548

Table A.7: Lake Jackson concentration test results using the original testing setup

			Lake Jackson+Seawater			Seawater+Lake Jackson		
total added	% added	Delta (mL)	Board 2 (Ω)	Board 3 (Ω)	Board 12 (Ω)	Board 2 (Ω)	Board 3 (Ω)	Board 12 (Ω)
0	0	0	35,712	36,487	38,396	38.902	34.27	42.661
1	0.99	1	1,804.3	1,806.6	1,825.4	38.962	34.212	42.098
3	2.91	2	627.49	624.38	640.49	38.796	34.466	42.421
5	4.76	2	422.46	418.56	432.71	39.212	34.820	42.572
7	6.54	2	310.88	314.01	324.84	39.408	35.170	42.952
9	8.26	2	259.46	255.57	266.41	39.685	35.645	43.279
11	9.91	2	220.83	218.9	229.67	40.151	36.031	43.675
14	12.28	3	183.71	181.19	191.08	40.645	36.660	44.329
17	14.53	3	158.49	156.71	165.22	41.328	37.310	44.858
20	16.67	3	142.99	138.63	147.91	42.001	37.862	45.421
23	18.7	3	127.83	123.66	132.27	42.611	38.574	45.951
26	20.63	3	119.57	113.41	122.37	43.307	39.167	46.714
29	22.48	3	111.68	108.24	115.98	44.065	39.927	47.446
32	24.24	3	103.69	100.12	108.43	44.458	40.513	47.774
36	26.47	4	96.750	93.246	101.59	45.659	41.365	48.657
40	28.57	4	91.799	88.832	95.884	46.463	42.306	49.589
44	30.56	4	86.678	83.489	91.671	47.328	42.999	50.345
48	32.43	4	83.59	79.528	86.584	47.978	43.922	51.182
52	34.21	4	79.208	75.258	83.247	48.837	44.825	52.046
57	36.31	5	74.817	71.104	79.211	49.540	45.769	52.921
63	38.65	6	71.978	68.357	76.372	51.103	46.923	54.325
69	40.83	6	69.100	65.322	73.389	52.408	48.445	55.685
75	42.86	6	67.300	63.068	71.241	53.732	49.844	57.326
81	44.75	6	64.256	61.169	69.353	55.163	51.131	58.817
87	46.52	6	63.043	59.455	67.540	56.359	52.528	60.056
93	48.19	6	61.468	57.583	66.038	57.828	53.708	61.151
100	50	7	60.306	56.085	64.514	59.508	55.496	63.004

Table A.8: Turkey Creek concentration test results using the modified testing setup and the original sensors

			Turkey Creek+Seawater			Seawater+Turkey Creek		
total added	% added	Delta (mL)	Board 2 (Ω)	Board 3 (Ω)	Board 12 (Ω)	Board 2 (Ω)	Board 3 (Ω)	Board 12 (Ω)
0	0	0	57,140.18	52,012.18	56,113.18	22.60	23.07	23.89
1	0.99	1	1,545.68	1,401.48	1,512.48	22.95	22.29	22.80
3	2.91	2	452.28	426.85	449.70	23.05	22.71	23.15
5	4.76	2	321.18	299.63	315.02	23.86	22.92	23.52
7	6.54	2	239.63	241.23	246.23	23.47	23.23	23.69
9	8.26	2	198.63	194.64	202.19	23.91	23.82	24.34
11	9.91	2	167.43	171.86	173.80	24.13	24.85	24.45
14	12.28	3	142.92	147.85	143.87	24.77	25.36	25.00
17	14.53	3	126.13	121.31	124.58	25.43	24.89	25.63
20	16.67	3	110.05	100.29	111.03	25.89	26.78	26.40
23	18.7	3	104.92	88.00	99.31	26.84	26.17	27.06
26	20.63	3	92.10	79.85	93.12	27.54	26.81	27.50
29	22.48	3	84.45	77.64	84.74	27.76	27.07	27.90
32	24.24	3	79.90	75.73	87.62	28.35	27.64	28.76
36	26.47	4	76.00	65.82	73.07	29.12	28.65	29.23
40	28.57	4	70.17	62.36	68.11	29.75	29.03	29.80
44	30.56	4	65.00	58.47	64.51	30.53	29.62	30.87
48	32.43	4	62.25	55.17	61.99	30.80	30.28	31.35
52	34.21	4	60.75	56.89	58.98	31.89	30.79	32.50
57	36.31	5	60.34	51.30	58.14	32.52	31.38	32.58
63	38.65	6	53.40	51.19	52.52	33.82	32.07	33.26
69	40.83	6	52.57	46.56	51.79	34.52	33.09	34.66
75	42.86	6	49.77	43.48	48.40	35.52	34.73	35.39
81	44.75	6	47.99	45.53	48.13	36.16	35.54	36.24
87	46.52	6	45.82	43.92	46.06	37.34	36.57	37.24
93	48.19	6	44.15	42.24	43.81	38.56	37.51	38.29
100	50	7	41.96	41.05	41.08	39.85	38.29	39.69

Table A.9: Turkey Creek concentration test results using the modified testing setup and the new sensors

			Turkey Creek+Seawater			Seawater+Turkey Creek		
total added	% added	Delta (mL)	Board 4D (Ω)	Board 5D (Ω)	Board 6D (Ω)	Board 4D (Ω)	Board 5D (Ω)	Board 6D (Ω)
0	0	0	30,925	29,414	30,047	9.65	10.31	9.66
1	0.99	1	781.19	837.10	796.44	10.13	9.65	9.48
3	2.91	2	238.48	215.70	218.09	9.55	9.77	9.57
5	4.76	2	151.86	146.37	145.04	9.55	9.97	9.62
7	6.54	2	112.13	111.08	112.98	9.65	10.20	9.78
9	8.26	2	92.40	94.02	91.61	9.79	10.43	9.96
11	9.91	2	79.35	76.54	76.89	9.81	10.41	10.05
14	12.28	3	65.14	62.11	64.25	10.13	10.58	10.33
17	14.53	3	53.93	55.04	53.01	10.48	11.32	10.61
20	16.67	3	47.51	47.42	48.37	10.95	11.01	10.83
23	18.7	3	42.41	43.32	42.57	11.13	11.34	11.13
26	20.63	3	39.95	41.11	40.56	11.42	11.53	11.28
29	22.48	3	37.05	36.99	36.40	11.62	11.68	11.45
32	24.24	3	34.94	33.68	35.06	11.82	11.90	11.68
36	26.47	4	31.30	33.38	32.88	12.05	12.33	12.03
40	28.57	4	29.50	29.06	31.04	12.37	12.64	12.41
44	30.56	4	29.00	28.40	29.99	30.53	29.62	30.87
48	32.43	4	26.78	26.75	28.64	30.80	30.28	31.35
52	34.21	4	24.52	25.44	27.74	31.89	30.79	32.50
57	36.31	5	24.56	24.06	25.89	32.52	31.38	32.58
63	38.65	6	24.00	23.55	24.35	33.82	32.07	33.26
69	40.83	6	22.72	23.20	22.14	34.52	33.09	34.66
75	42.86	6	20.52	22.35	22.13	35.52	34.73	35.39
81	44.75	6	20.48	21.92	21.57	36.16	35.54	36.24
87	46.52	6	19.37	21.91	20.82	37.34	36.57	37.24
93	48.19	6	18.94	20.55	19.95	38.56	37.51	38.29
100	50	7	17.98	18.86	17.65	39.85	38.29	39.69

Table A.10: Turkey Creek concentration test results using the modified testing setup and the new gold plated sensors

			Turkey Creek+Seawater			Seawater+Turkey Creek		
total added	% added	Delta (mL)	Board 1G (Ω)	Board 2G (Ω)	Board 3G (Ω)	Board 1G (Ω)	Board 2G (Ω)	Board 3G (Ω)
0	0	0	28,661	30,231	30804	9.39	10.11	10.18
1	0.99	1	728.14	756.61	714.49	9.63	10.63	10.20
3	2.91	2	206.58	216.12	203.89	9.92	10.71	10.19
5	4.76	2	139.95	148.10	142.61	9.98	10.79	10.35
7	6.54	2	108.84	114.48	107.95	10.21	10.95	10.52
9	8.26	2	89.52	94.24	95.63	10.21	11.15	10.66
11	9.91	2	75.46	82.18	87.00	10.34	11.24	10.82
14	12.28	3	62.91	68.35	74.87	10.69	11.77	11.09
17	14.53	3	58.59	57.13	58.68	11.05	12.27	11.28
20	16.67	3	47.74	50.74	48.68	11.19	12.25	11.56
23	18.7	3	42.85	45.60	48.02	11.60	12.45	12.21
26	20.63	3	41.04	44.41	41.68	11.82	12.71	12.52
29	22.48	3	37.64	40.33	40.39	11.98	12.93	12.60
32	24.24	3	34.78	37.70	37.56	12.22	13.19	12.88
36	26.47	4	31.60	36.08	37.95	12.48	13.52	13.13
40	28.57	4	30.17	34.48	37.08	12.79	13.70	13.45
44	30.56	4	27.65	33.77	28.55	13.38	14.17	13.76
48	32.43	4	27.43	28.47	28.26	13.62	14.36	14.03
52	34.21	4	26.59	28.11	28.05	13.99	14.85	14.35
57	36.31	5	25.32	26.02	27.36	14.15	15.11	14.67
63	38.65	6	22.75	23.84	27.15	15.03	15.44	15.25
69	40.83	6	21.89	22.37	23.16	14.83	15.91	15.67
75	42.86	6	21.25	21.93	21.61	15.35	16.39	16.17
81	44.75	6	21.29	21.63	22.48	15.67	16.96	16.31
87	46.52	6	19.89	20.02	20.26	16.12	17.20	17.39
93	48.19	6	18.50	19.64	18.99	16.74	17.93	17.84
100	50	7	17.99	18.24	18.22	17.13	18.45	18.32

Table A.11: Lake Jackson concentration test results using the modified testing setup and the original sensors

			Lake Jackson+Seawater			Seawater+Lake Jackson		
total added	% added	Delta (mL)	Board 2 (Ω)	Board 3 (Ω)	Board 12 (Ω)	Board 2 (Ω)	Board 3 (Ω)	Board 12 (Ω)
0	0	0	41,163.50	40,913.50	40,887.50	24.28	23.49	23.78
1	0.99	1	1496.10	1430.10	1466.00	23.89	23.55	23.62
3	2.91	2	546.24	516.75	534.40	24.20	23.92	23.95
5	4.76	2	351.13	346.95	340.72	24.57	24.24	24.25
7	6.54	2	256.79	249.63	253.26	24.92	24.66	24.62
9	8.26	2	209.13	204.32	206.02	25.33	24.96	24.96
11	9.91	2	174.01	172.85	173.67	25.72	25.33	25.41
14	12.28	3	146.11	142.20	139.84	26.10	25.87	25.98
17	14.53	3	126.73	124.83	124.19	26.74	26.39	26.48
20	16.67	3	111.50	109.97	111.14	27.23	26.89	26.97
23	18.7	3	100.91	99.51	99.65	27.77	27.56	27.50
26	20.63	3	93.21	91.06	90.96	28.33	27.98	28.04
29	22.48	3	85.96	85.45	84.89	28.95	28.68	28.59
32	24.24	3	80.45	71.78	79.66	29.48	29.09	29.20
36	26.47	4	74.10	66.55	76.03	30.26	29.91	29.90
40	28.57	4	72.96	62.36	68.65	30.93	30.66	30.66
44	30.56	4	65.66	60.74	65.49	31.68	31.38	31.35
48	32.43	4	62.01	59.77	62.37	32.41	32.22	32.12
52	34.21	4	61.11	55.23	58.95	33.26	33.03	32.96
57	36.31	5	57.20	51.89	55.77	34.22	34.00	33.98
63	38.65	6	52.76	49.29	50.09	35.30	35.07	35.19
69	40.83	6	50.44	47.96	48.01	36.65	36.20	36.31
75	42.86	6	48.63	45.08	46.21	37.73	37.31	37.12
81	44.75	6	46.57	43.01	44.70	38.65	38.34	38.23
87	46.52	6	45.12	42.75	43.26	39.99	39.71	39.61
93	48.19	6	44.45	41.56	43.26	40.95	40.53	40.45
100	50	7	43.83	40.68	42.34	42.23	42.24	42.02

Table A.12: Lake Jackson concentration test results using the modified testing setup and the new sensors

			Lake Jackson+Seawater			Seawater+Lake Jackson		
total added	% added	Delta (mL)	Board 4D (Ω)	Board 5D (Ω)	Board 6D (Ω)	Board 4D (Ω)	Board 5D (Ω)	Board 6D (Ω)
0	0	0	21,619	21,810	21,145	10.03	10.03	10.01
1	0.99	1	733.56	704.27	722.09	10.00	10.01	9.99
3	2.91	2	254.59	247.08	245.26	10.11	10.14	10.07
5	4.76	2	150.85	156.80	154.29	10.27	10.31	10.22
7	6.54	2	115.05	112.03	110.81	10.43	10.45	10.39
9	8.26	2	91.92	90.28	89.32	10.58	10.55	10.52
11	9.91	2	75.99	76.52	75.54	10.68	10.73	10.65
14	12.28	3	62.46	63.40	62.09	10.96	10.96	10.93
17	14.53	3	53.99	53.89	53.78	11.14	11.12	11.10
20	16.67	3	47.34	47.79	47.59	11.32	11.38	11.31
23	18.7	3	43.56	43.59	43.47	11.57	11.59	11.55
26	20.63	3	38.93	40.33	39.66	11.83	11.99	11.82
29	22.48	3	36.08	37.53	36.74	12.10	12.06	12.07
32	24.24	3	33.57	36.01	34.03	12.27	12.27	12.23
36	26.47	4	31.34	32.17	31.58	12.54	12.67	12.58
40	28.57	4	28.86	30.47	29.28	12.87	13.04	12.90
44	30.56	4	27.55	28.04	27.91	13.29	13.32	13.26
48	32.43	4	25.95	27.87	27.19	13.56	13.61	13.53
52	34.21	4	24.86	26.17	25.72	13.93	13.99	13.91
57	36.31	5	24.03	24.07	24.04	14.33	14.39	14.38
63	38.65	6	22.07	22.87	23.20	14.77	14.83	14.75
69	40.83	6	21.01	21.86	21.93	15.32	15.38	15.25
75	42.86	6	19.95	20.54	20.78	15.65	15.76	15.76
81	44.75	6	19.69	20.13	20.22	16.06	16.22	16.17
87	46.52	6	19.61	19.67	19.87	16.72	16.75	16.54
93	48.19	6	18.57	18.79	18.72	17.26	17.18	17.00
100	50	7	17.99	17.99	18.69	17.90	17.66	17.63

Table A.13: Lake Jackson concentration test results using the modified testing setup and the gold plated sensors

			Lake Jackson+Seawater			Seawater+Lake Jackson		
total added	% added	Delta (mL)	Board 1G (Ω)	Board 2G (Ω)	Board 3G (Ω)	Board 1G (Ω)	Board 2G (Ω)	Board 3G (Ω)
0	0	0	20,817	21,165	20,130	9.86	10.35	10.02
1	0.99	1	700.96	720.18	767.06	9.87	10.49	10.06
3	2.91	2	240.53	244.01	253.91	10.04	10.62	10.19
5	4.76	2	153.00	155.19	154.69	10.24	10.83	10.38
7	6.54	2	111.50	113.77	143.92	10.42	11.02	10.59
9	8.26	2	91.03	92.60	92.05	10.56	11.20	10.81
11	9.91	2	76.51	78.79	77.51	10.80	11.40	10.98
14	12.28	3	62.92	64.59	63.92	11.00	11.60	11.20
17	14.53	3	54.50	56.25	55.26	11.26	11.89	11.46
20	16.67	3	48.69	49.91	49.22	11.47	12.07	11.69
23	18.7	3	43.97	45.38	44.52	11.77	12.32	11.98
26	20.63	3	39.94	41.44	40.79	12.05	12.61	12.27
29	22.48	3	37.07	38.41	38.19	12.22	12.86	12.48
32	24.24	3	34.73	36.00	35.35	12.38	13.11	12.71
36	26.47	4	31.95	33.34	32.69	12.79	13.45	13.06
40	28.57	4	29.78	31.76	30.61	13.21	13.95	13.38
44	30.56	4	28.39	29.58	29.39	13.44	14.09	13.69
48	32.43	4	26.93	28.40	27.89	13.75	14.44	14.06
52	34.21	4	25.70	26.90	27.50	14.14	14.93	14.37
57	36.31	5	24.36	25.43	25.12	14.56	15.30	14.83
63	38.65	6	22.77	24.27	24.63	15.03	15.70	15.29
69	40.83	6	22.02	23.36	22.73	15.61	16.24	15.86
75	42.86	6	21.28	22.40	21.71	15.87	16.83	16.35
81	44.75	6	20.81	21.68	21.08	16.51	17.19	16.71
87	46.52	6	19.88	21.44	20.69	16.86	17.63	17.22
93	48.19	6	19.72	21.15	20.31	17.58	18.34	17.83
100	50	7	18.36	20.12	19.12	17.98	18.76	18.25

Table A.14: Rain water concentration test results using the modified testing setup and the original sensors

			Rain Water+Seawater			Seawater+Rain Water		
total added	% added	Delta (mL)	Board 2 (Ω)	Board 3 (Ω)	Board 12 (Ω)	Board 2 (Ω)	Board 3 (Ω)	Board 12 (Ω)
0	0	0	57,313.00	62,589.00	56,130.00	24.60	23.33	24.23
1	0.99	1	2,907.90	3,016.30	2,855.50	24.51	23.55	24.27
3	2.91	2	626.21	627.79	559.46	24.53	23.72	24.63
5	4.76	2	380.32	393.30	354.69	25.36	24.04	24.91
7	6.54	2	269.21	278.07	283.22	25.28	24.28	25.13
9	8.26	2	223.21	218.61	214.81	25.45	24.62	25.44
11	9.91	2	185.56	182.07	183.13	26.30	25.27	25.85
14	12.28	3	151.57	149.98	150.70	26.37	25.57	26.49
17	14.53	3	126.97	125.00	125.20	26.83	25.97	26.75
20	16.67	3	113.62	111.93	112.38	27.26	26.47	27.18
23	18.7	3	103.50	100.76	101.76	27.87	27.00	27.71
26	20.63	3	93.88	92.35	93.50	28.47	27.13	28.24
29	22.48	3	87.50	89.36	86.97	28.93	27.57	28.59
32	24.24	3	81.03	79.79	80.58	31.25	28.29	29.09
36	26.47	4	76.28	74.30	75.49	29.92	28.97	29.76
40	28.57	4	70.33	68.91	70.27	30.46	29.86	30.39
44	30.56	4	67.07	66.45	66.52	31.00	30.17	31.09
48	32.43	4	62.70	61.58	62.75	31.93	30.65	31.74
52	34.21	4	59.71	58.56	59.58	32.28	31.26	32.41
57	36.31	5	56.58	55.34	56.62	33.34	32.04	34.40
63	38.65	6	53.19	52.38	53.27	34.50	33.63	34.14
69	40.83	6	50.93	51.91	50.77	35.22	34.48	35.30
75	42.86	6	48.63	47.41	48.51	36.96	35.75	36.05
81	44.75	6	46.98	46.17	46.71	38.71	36.89	37.26
87	46.52	6	45.06	43.83	44.74	38.99	36.94	38.82
93	48.19	6	44.13	43.46	42.28	40.05	37.80	38.92
100	50	7	42.50	41.62	42.40	40.77	39.21	40.15

Table A.15: Rain water concentration test results using the modified testing setup and the new sensors

			Rain Water+Seawater			Seawater+Rain Water		
total added	% added	Delta (mL)	Board 4D (Ω)	Board 5D (Ω)	Board 6D (Ω)	Board 4D (Ω)	Board 5D (Ω)	Board 6D (Ω)
0	0	0	36,950.00	36,643.00	38,181.00	10.25	10.57	10.26
1	0.99	1	1,384.60	1,486.70	1,344.90	10.37	10.53	10.26
3	2.91	2	328.84	318.77	330.19	10.34	10.55	10.42
5	4.76	2	193.19	185.08	187.03	10.54	11.15	10.83
7	6.54	2	129.08	125.18	126.68	10.63	10.84	10.61
9	8.26	2	100.46	100.37	99.93	10.67	11.13	10.80
11	9.91	2	78.94	81.25	80.40	10.78	11.17	10.88
14	12.28	3	66.04	67.13	65.91	11.01	11.42	11.23
17	14.53	3	55.60	56.44	56.11	11.17	11.51	11.32
20	16.67	3	49.54	50.58	49.93	11.53	11.77	11.53
23	18.7	3	44.38	45.09	44.41	11.59	12.05	11.79
26	20.63	3	39.91	41.21	40.50	11.82	12.19	12.05
29	22.48	3	37.40	37.98	37.41	11.97	12.27	12.25
32	24.24	3	34.64	36.65	34.53	12.20	12.52	12.54
36	26.47	4	32.44	33.50	32.24	12.49	12.90	12.81
40	28.57	4	29.94	30.76	30.02	12.83	13.17	13.09
44	30.56	4	28.09	29.00	28.20	13.00	13.47	13.39
48	32.43	4	26.55	28.36	26.83	13.24	14.05	13.74
52	34.21	4	25.37	26.03	25.47	13.61	14.08	13.82
57	36.31	5	23.97	24.55	24.02	13.96	14.19	14.29
63	38.65	6	22.60	23.20	22.87	14.47	14.95	14.80
69	40.83	6	21.30	22.02	21.66	14.90	15.11	15.01
75	42.86	6	20.42	21.09	20.73	15.21	15.77	15.76
81	44.75	6	19.70	20.14	19.90	15.46	16.20	15.91
87	46.52	6	18.96	19.31	19.16	15.89	17.46	16.81
93	48.19	6	18.58	19.02	18.73	16.27	16.68	17.25
100	50	7	18.07	18.29	18.04	16.85	17.14	17.58

Table A.16: Rain water concentration test results using the modified testing setup and the gold plated sensors

			Rain Water+Seawater			Seawater+Rain Water		
total added	% added	Delta (mL)	Board 1G (Ω)	Board 2G (Ω)	Board 3G (Ω)	Board 1G (Ω)	Board 2G (Ω)	Board 3G (Ω)
0	0	0	34,642.00	30,089.00	31,079.00	10.72	11.59	11.27
1	0.99	1	1,445.70	1,470.50	1,335.90	10.78	11.72	11.27
3	2.91	2	281.69	288.19	264.89	10.97	11.87	11.49
5	4.76	2	166.17	173.52	158.61	10.99	11.98	11.64
7	6.54	2	117.47	123.34	115.53	11.01	12.00	11.79
9	8.26	2	97.20	100.62	96.79	11.04	12.05	11.91
11	9.91	2	80.78	83.22	81.09	11.76	12.22	12.00
14	12.28	3	66.34	68.47	66.52	12.32	12.38	12.29
17	14.53	3	55.81	57.95	56.04	12.38	12.68	12.48
20	16.67	3	50.09	52.04	50.24	13.00	12.80	12.68
23	18.7	3	44.87	46.72	45.44	12.77	13.03	13.17
26	20.63	3	40.93	42.66	41.77	12.45	13.33	13.53
29	22.48	3	38.10	39.72	38.89	12.76	13.62	13.57
32	24.24	3	35.20	36.97	35.97	12.56	13.98	13.72
36	26.47	4	32.98	34.65	33.67	12.91	14.28	13.89
40	28.57	4	30.68	32.29	31.34	13.14	14.61	14.21
44	30.56	4	28.79	30.63	29.62	13.49	14.66	14.77
48	32.43	4	27.44	28.92	28.10	13.96	15.21	14.81
52	34.21	4	26.10	27.70	27.14	13.98	15.82	15.21
57	36.31	5	24.74	26.28	25.35	14.68	16.32	15.37
63	38.65	6	23.40	24.96	24.05	14.92	16.37	16.27
69	40.83	6	22.48	23.66	23.04	15.20	16.75	16.60
75	42.86	6	21.45	22.54	21.95	15.80	17.37	17.01
81	44.75	6	20.61	21.80	21.19	16.40	18.40	17.51
87	46.52	6	19.78	21.17	20.33	16.72	18.08	17.52
93	48.19	6	19.46	20.52	19.92	17.65	18.50	18.55
100	50	7	18.68	19.98	19.44	17.85	19.25	18.92

Table A.17: Results as the measurement frequency of the impedance analyzer is swept while in seawater

Frequency (Hz)	Resistance (Ω)
1,000	102.330
2,000	53.804
5,000	37.801
7,500	33.964
10,000	31.816
20,000	27.924
50,000	26.187
66,670	26.978
100,000	26.225
200,000	25.231

Table A.18: Conductivities calculated for the final Turkey Creek concentration test

Measured Conductivity (S/m)	Calculated conductivity using original sensors (S/m)	Calculated conductivity using new sensors (S/m)	Original and new sensors percent difference	Calculated and measured percent difference
X	0.0017	0.0015	11.09%	X
0.0659	0.0695	0.0682	1.90%	4.44%
0.1908	0.1945	0.1924	1.09%	1.36%
0.3115	0.3154	0.3146	0.27%	1.12%
0.4237	0.4285	0.4243	1.00%	0.64%
0.5403	0.5473	0.5412	1.12%	0.73%
0.6460	0.6510	0.6444	1.01%	0.26%
0.7889	0.7953	0.7940	0.16%	0.73%
0.9351	0.9341	0.9324	0.18%	0.20%
1.0688	1.0653	1.0621	0.31%	0.48%
1.1920	1.1920	1.1864	0.47%	0.24%
1.3095	1.2987	1.3002	0.12%	0.77%
1.4189	1.4062	1.4068	0.04%	0.88%
1.5328	1.5002	1.5073	0.47%	1.91%
1.6660	1.6364	1.6400	0.22%	1.68%
1.7922	1.7487	1.7632	0.82%	2.04%
X	1.8524	1.8680	0.84%	X
X	1.9640	1.9736	0.49%	X
X	2.0584	2.0712	0.62%	X
X	2.1819	2.2086	1.22%	X
X	2.3027	2.3307	1.21%	X
X	2.4139	2.4431	1.20%	X

X	2.5076	2.5493	1.65%	X
X	2.6049	2.6451	1.53%	X
X	2.6885	2.7317	1.59%	X
X	2.7617	2.8144	1.89%	X
2.766	2.8512	2.9083	1.98%	4.04%
2.731	2.8713	2.8880	0.58%	5.28%
X	2.9654	2.9724	0.24%	X
X	3.0449	3.0531	0.27%	X
X	3.1314	3.1306	0.03%	X
X	3.2232	3.2358	0.39%	X
X	3.3236	3.3179	0.17%	X
X	3.4336	3.4268	0.20%	X
X	3.5336	3.5292	0.12%	X
X	3.6399	3.6225	0.48%	X
X	3.7086	3.6996	0.24%	X
X	3.8203	3.7894	0.81%	X
X	3.8925	3.8787	0.36%	X
X	3.9791	3.9640	0.38%	X
X	4.0694	4.0343	0.86%	X
X	4.1421	4.1059	0.88%	X
X	4.2358	4.2041	0.75%	X
X	4.3022	4.2436	1.37%	X
X	4.3861	4.3320	1.24%	X
X	4.4651	4.4547	0.23%	X
X	4.5603	4.5354	0.55%	X
X	4.6401	4.6167	0.51%	X
X	4.7277	4.6784	1.05%	X
X	4.7849	4.7104	1.57%	X
X	4.8506	4.7698	1.68%	X
X	4.9223	4.8190	2.12%	X
X	4.9797	4.8817	1.99%	X
5.057	4.9155	4.9270	0.23%	2.73%

Table A.19: Conductivities calculated for the final Lake Jackson concentration test

Measured Conductivity (S/m)	Calculated conductivity using original sensors (S/m)	Calculated conductivity using new sensors (S/m)	Original and new sensors percent difference	Calculated and measured percent difference
X	0.0027	0.0023	13.68%	X
0.0805	0.0844	0.0835	0.99%	4.18%
0.2137	0.2185	0.2172	0.61%	1.93%

0.3326	0.3397	0.3385	0.33%	1.94%
0.4548	0.4604	0.4598	0.14%	1.16%
0.5707	0.5758	0.5738	0.34%	0.72%
0.6761	0.6803	0.6816	0.18%	0.71%
0.8364	0.8398	0.8404	0.07%	0.44%
0.9777	0.9810	0.9835	0.26%	0.46%
1.1167	1.1171	1.1224	0.47%	0.27%
1.2504	1.2513	1.2623	0.87%	0.51%
1.3843	1.3778	1.3871	0.67%	0.13%
1.5005	1.4906	1.5010	0.69%	0.31%
1.6091	1.5964	1.6096	0.83%	0.38%
1.7463	1.7303	1.7385	0.47%	0.68%
1.8759	1.8616	1.8557	0.31%	0.92%
X	1.9774	1.9886	0.57%	X
X	2.0759	2.0998	1.14%	X
X	2.1741	2.1979	1.09%	X
X	2.2862	2.3143	1.22%	X
X	2.4053	2.4427	1.54%	X
X	2.5240	2.5545	1.20%	X
X	2.6169	2.6585	1.58%	X
X	2.7299	2.7579	1.02%	X
X	2.8514	2.8871	1.24%	X
X	2.9395	2.9683	0.97%	X
3.0438	3.0143	3.0530	1.28%	0.34%
3.1193	2.8649	2.9138	1.69%	7.65%
X	2.9443	2.9916	1.59%	X
X	3.0227	3.0733	1.66%	X
X	3.1059	3.1522	1.48%	X
X	3.2017	3.2434	1.29%	X
X	3.2901	3.3420	1.56%	X
X	3.3961	3.4663	2.05%	X
X	3.4651	3.5372	2.06%	X
X	3.5922	3.6409	1.35%	X
X	3.6675	3.7226	1.49%	X
X	3.7582	3.8018	1.15%	X
X	3.8507	3.8862	0.92%	X
X	3.9343	3.9777	1.10%	X
X	4.0338	4.0719	0.94%	X
X	4.1137	4.1432	0.71%	X
X	4.1800	4.2185	0.92%	X
X	4.2640	4.3043	0.94%	X

X	4.3483	4.3873	0.89%	X
X	4.4348	4.4750	0.90%	X
X	4.5341	4.5608	0.59%	X
X	4.6295	4.6519	0.48%	X
X	4.6876	4.7102	0.48%	X
X	4.7421	4.7652	0.49%	X
X	4.7988	4.8197	0.43%	X
X	4.8508	4.8574	0.13%	X
X	4.8961	4.9147	0.38%	X
5.1604	4.8621	4.9283	1.35%	5.27%

Table A.20: Conductivities calculated for the final rain water concentration test

Measured Conductivity (S/m)	Calculated conductivity using original sensors (S/m)	Calculated conductivity using new sensors (S/m)	Original and new sensors percent difference	Calculated and measured percent difference
X	0.0009	0.0008	8.95%	X
0.0663	0.0695	0.0685	1.42%	3.99%
0.1962	0.1983	0.1961	1.12%	0.51%
0.3165	0.3210	0.3164	1.45%	0.70%
0.4285	0.4291	0.4252	0.91%	0.31%
0.5355	0.5385	0.5333	0.96%	0.07%
0.6396	0.6279	0.6282	0.05%	1.82%
0.7835	0.7797	0.7769	0.35%	0.67%
0.922	0.9156	0.9101	0.60%	1.00%
1.0493	1.0389	1.0393	0.04%	0.98%
1.1679	1.1422	1.1446	0.21%	2.12%
1.2815	1.2549	1.2581	0.26%	1.97%
1.3941	1.3551	1.3618	0.50%	2.59%
1.4955	1.4689	1.4671	0.12%	1.86%
1.6608	1.6065	1.6180	0.71%	2.97%
1.7744	1.7192	1.7299	0.62%	2.85%
X	1.8244	1.8379	0.74%	X
X	1.9222	1.9480	1.33%	X
X	2.0363	2.0547	0.90%	X
X	2.1180	2.1456	1.29%	X
X	2.2281	2.2632	1.56%	X
X	2.3419	2.3793	1.58%	X
X	2.4467	2.4865	1.61%	X
X	2.5352	2.5789	1.71%	X
X	2.6030	2.6619	2.24%	X

X	2.6807	2.7423	2.27%	X
2.737	2.7631	2.8223	2.12%	2.01%
2.731	2.7575	2.8139	2.03%	1.97%
X	2.8355	2.8961	2.12%	X
X	2.9131	2.9697	1.93%	X
X	2.9985	3.0512	1.74%	X
X	3.0715	3.1421	2.27%	X
X	3.1727	3.2427	2.18%	X
X	3.2461	3.3226	2.33%	X
X	3.3447	3.4230	2.32%	X
X	3.4338	3.5077	2.13%	X
X	3.5049	3.5919	2.45%	X
X	3.5710	3.6640	2.57%	X
X	3.6644	3.7441	2.15%	X
X	3.7657	3.8527	2.28%	X
X	3.8503	3.9246	1.91%	X
X	3.9216	3.9825	1.54%	X
X	3.9709	4.0411	1.75%	X
X	4.0399	4.1053	1.61%	X
X	4.1384	4.1774	0.94%	X
X	4.1876	4.2604	1.72%	X
X	4.2744	4.3443	1.62%	X
X	4.3352	4.4300	2.16%	X
X	4.3956	4.4846	2.01%	X
X	4.4717	4.5110	0.88%	X
X	4.5167	4.5802	1.40%	X
X	4.5568	4.6525	2.08%	X
X	4.6105	4.7130	2.20%	X
4.894	4.5781	4.6971	2.57%	5.37%

Table A.21: Final Turkey Creek concentration test results using the original sensors

Percent Salt water	Measured conductivity (S/m)	Calculated conductivity (S/m)	Board 2 (Ω)	Board 3 (Ω)	Board 12 (Ω)
0.00%	0	0.002	64,850.84	63,856.96	70,671.38
0.99%	0.066	0.070	1,605.91	1,612.12	1,610.05
2.91%	0.191	0.195	576.70	575.71	574.38
4.76%	0.312	0.316	354.86	354.36	355.37
6.54%	0.424	0.429	260.96	261.64	260.96
8.26%	0.540	0.548	204.92	205.55	203.09

9.91%	0.646	0.651	172.71	172.30	170.82
12.28%	0.789	0.796	141.26	139.63	141.34
14.53%	0.935	0.935	118.92	120.02	120.55
16.67%	1.069	1.066	104.91	105.16	105.12
18.70%	1.192	1.193	95.06	93.81	92.83
20.63%	1.310	1.299	87.18	85.47	85.91
22.48%	1.419	1.407	80.00	79.74	79.05
24.24%	1.533	1.501	74.96	74.40	74.46
26.47%	1.666	1.637	68.17	68.54	68.49
28.57%	1.792	1.750	64.06	64.10	63.86
30.56%	X	1.854	60.57	60.46	60.24
32.43%	X	1.965	56.72	57.08	57.18
34.21%	X	2.060	54.32	54.59	54.23
36.31%	X	2.183	51.41	51.39	51.10
38.65%	X	2.304	48.85	48.57	48.40
40.83%	X	2.415	46.60	46.36	46.15
42.86%	X	2.509	44.76	44.76	44.39
44.75%	X	2.607	43.20	42.92	42.79
46.52%	X	2.690	41.77	41.56	41.56
48.19%	X	2.763	40.58	40.44	40.57
50.00%	2.766	2.853	39.32	39.20	39.25
50.00%	2.731	2.873	38.76	38.91	39.28
51.81%	X	2.967	37.61	37.78	37.85
53.48%	X	3.047	36.64	36.86	36.78
55.25%	X	3.133	35.61	35.84	35.78
57.14%	X	3.225	34.67	34.75	34.76
59.17%	X	3.326	33.59	33.73	33.72
61.35%	X	3.436	32.47	32.63	32.70
63.69%	X	3.536	31.48	31.72	31.84
65.79%	X	3.642	30.58	30.84	30.84
67.57%	X	3.711	30.04	30.23	30.28
69.44%	X	3.823	29.33	29.56	29.00
71.43%	X	3.895	28.61	28.85	28.80
73.53%	X	3.982	28.06	28.15	28.18
75.76%	X	4.072	27.41	27.46	27.64
77.52%	X	4.145	26.87	27.11	27.08
79.37%	X	4.238	26.41	26.40	26.46
81.30%	X	4.305	25.93	26.06	26.06
83.33%	X	4.389	25.41	25.61	25.54
85.47%	X	4.468	24.84	25.15	25.21
87.72%	X	4.563	24.41	24.59	24.62

90.09%	X	4.643	23.94	24.23	24.20
91.74%	X	4.731	23.43	23.75	23.85
93.46%	X	4.788	23.27	23.43	23.48
95.24%	X	4.854	22.96	23.07	23.20
97.09%	X	4.925	22.67	22.79	22.76
99.01%	X	4.983	22.35	22.54	22.54
100.00%	5.057	4.919	22.86	22.78	22.67

Table A.22: Final Turkey Creek concentration test results using the new non-plated sensors

Percent saltwater	Measured conductivity (S/m)	Calculated conductivity (S/m)	Board 4D (Ω)	Board 5D (Ω)	Board 6D (Ω)
0.00%	X	0.002	31,446.54	31,250.00	31,847.13
0.99%	0.066	0.068	696.38	696.86	694.93
2.91%	0.191	0.192	247.10	246.79	246.91
4.76%	0.312	0.315	150.85	151.38	150.76
6.54%	0.424	0.424	112.07	111.84	111.96
8.26%	0.540	0.541	88.00	87.46	87.86
9.91%	0.646	0.644	73.64	73.75	73.75
12.28%	0.789	0.794	59.81	60.10	59.56
14.53%	0.935	0.932	51.07	50.89	50.86
16.67%	1.069	1.062	44.76	44.66	44.74
18.70%	1.192	1.186	39.87	40.18	40.06
20.63%	1.310	1.300	36.42	36.68	36.50
22.48%	1.419	1.407	33.83	33.72	33.75
24.24%	1.533	1.507	31.48	31.55	31.52
26.47%	1.666	1.640	28.94	29.01	28.94
28.57%	1.792	1.763	26.85	27.02	26.95
30.56%	X	1.868	25.41	25.54	25.33
32.43%	X	1.974	24.11	24.03	24.06
34.21%	X	2.071	22.97	22.91	22.92
36.31%	X	2.209	21.56	21.51	21.45
38.65%	X	2.331	20.40	20.36	20.37
40.83%	X	2.443	19.42	19.52	19.39
42.86%	X	2.549	18.65	18.61	18.64
44.75%	X	2.645	17.99	17.98	17.91
46.52%	X	2.732	17.42	17.38	17.37
48.19%	X	2.814	16.90	16.89	16.84
50.00%	2.766	2.908	16.36	16.35	16.29
50.00%	2.731	2.888	16.49	16.41	16.45

51.81%	X	2.972	16.01	15.96	15.96
53.48%	X	3.053	15.62	15.52	15.54
55.25%	X	3.131	15.21	15.13	15.18
57.14%	X	3.236	14.74	14.70	14.60
59.17%	X	3.318	14.32	14.31	X
61.35%	X	3.427	13.84	13.88	13.86
63.69%	X	3.529	13.47	13.49	13.42
65.79%	X	3.622	13.14	13.14	13.07
67.57%	X	3.700	12.84	12.82	12.85
69.44%	X	3.789	12.56	12.57	12.48
71.43%	X	3.879	12.25	12.22	12.27
73.53%	X	3.964	11.98	12.01	11.96
75.76%	X	4.034	11.81	11.76	11.75
77.52%	X	4.106	11.56	11.57	11.57
79.37%	X	4.204	11.31	11.28	11.30
81.30%	X	4.244	11.17	11.17	11.24
83.33%	X	4.332	10.96	10.96	10.97
85.47%	X	4.455	10.62	10.69	10.68
87.72%	X	4.535	10.49	10.48	10.45
90.09%	X	4.617	10.31	10.27	10.29
91.74%	X	4.678	10.19	10.15	10.12
93.46%	X	4.710	10.09	10.06	10.11
95.24%	X	4.770	9.95	9.99	9.93
97.09%	X	4.819	9.90	9.84	9.83
99.01%	X	4.882	9.75	9.75	9.69
100.00%	5.057	4.927	9.65	9.61	9.66

Table A.23: Final Turkey Creek concentration tests using the new gold-plated sensors

Percent saltwater	Measured conductivity (S/m)	Calculated conductivity (S/m)	Board 1G (Ω)	Board 2G (Ω)	Board 3G (Ω)
0.00%	X	0.002	30,769.23	31,250.00	30,959.75
0.99%	0.066	0.068	697.84	701.75	698.32
2.91%	0.191	0.192	246.49	246.73	247.22
4.76%	0.312	0.315	151.72	151.33	151.45
6.54%	0.424	0.424	112.56	112.97	112.60
8.26%	0.540	0.541	87.83	88.11	87.95
9.91%	0.646	0.644	73.96	74.07	74.07
12.28%	0.789	0.794	60.20	60.13	60.17
14.53%	0.935	0.932	51.10	51.10	51.41

16.67%	1.069	1.062	44.90	45.31	45.31
18.70%	1.192	1.186	40.58	40.67	40.75
20.63%	1.310	1.300	36.55	36.90	37.02
22.48%	1.419	1.407	34.23	34.44	34.34
24.24%	1.533	1.507	31.96	32.26	32.10
26.47%	1.666	1.640	29.21	29.56	29.59
28.57%	1.792	1.763	27.46	27.40	27.43
30.56%	X	1.868	25.85	25.91	25.96
32.43%	X	1.974	24.55	24.70	24.59
34.21%	X	2.071	23.41	23.38	23.41
36.31%	X	2.209	21.93	22.14	22.03
38.65%	X	2.331	20.87	20.86	20.90
40.83%	X	2.443	19.84	19.89	19.93
42.86%	X	2.549	19.14	19.14	19.14
44.75%	X	2.645	18.36	18.46	18.46
46.52%	X	2.732	17.88	17.89	17.93
48.19%	X	2.814	17.30	17.35	17.35
50.00%	2.766	2.908	16.84	16.84	16.82
50.00%	2.731	2.888	16.78	16.82	16.83
51.81%	X	2.972	16.26	16.39	16.41
53.48%	X	3.053	15.87	15.97	15.98
55.25%	X	3.131	15.44	15.53	15.54
57.14%	X	3.236	15.08	15.24	14.95
59.17%	X	3.318	X	X	X
61.35%	X	3.427	14.13	14.22	14.21
63.69%	X	3.529	13.77	13.80	13.82
65.79%	X	3.622	13.40	13.44	13.50
67.57%	X	3.700	13.11	13.21	13.20
69.44%	X	3.789	12.77	12.82	12.84
71.43%	X	3.879	12.57	12.61	12.58
73.53%	X	3.964	12.19	12.29	12.24
75.76%	X	4.034	12.05	12.13	12.06
77.52%	X	4.106	11.80	11.93	11.86
79.37%	X	4.204	11.60	11.64	11.63
81.30%	X	4.244	11.38	11.42	11.44
83.33%	X	4.332	11.23	11.23	11.26
85.47%	X	4.455	10.96	11.05	11.04
87.72%	X	4.535	10.77	10.88	10.84
90.09%	X	4.617	10.58	10.61	10.65
91.74%	X	4.678	10.37	10.50	10.51
93.46%	X	4.710	10.33	10.33	10.37

95.24%	X	4.770	10.22	10.32	10.24
97.09%	X	4.819	10.08	10.17	10.12
99.01%	X	4.882	9.97	10.04	10.03
100.00%	5.057	4.927	9.94	10.00	9.99

Table A.24: Final Lake Jackson concentration test results using the original sensors

Percent saltwater	Measured conductivity (S/m)	Calculated conductivity (S/m)	Board 2 (Ω)	Board 3 (Ω)	Board 12 (Ω)
0.00%	X	0.003	41,050.90	42,444.82	41,666.67
0.99%	0.081	0.084	1,323.28	1,326.79	1,330.00
2.91%	0.214	0.219	510.20	513.08	513.00
4.76%	0.333	0.340	329.49	329.92	329.00
6.54%	0.455	0.461	242.37	243.84	243.00
8.26%	0.571	0.576	194.17	194.89	194.00
9.91%	0.676	0.681	164.20	165.29	164.00
12.28%	0.836	0.840	133.10	133.69	133.00
14.53%	0.978	0.982	113.78	114.47	114.00
16.67%	1.117	1.118	100.02	100.52	100.00
18.70%	1.250	1.252	89.05	89.85	89.40
20.63%	1.384	1.379	80.97	81.30	81.40
22.48%	1.501	1.492	74.68	75.64	74.90
24.24%	1.609	1.598	69.88	70.42	70.00
26.47%	1.746	1.732	64.52	64.81	64.70
28.57%	1.876	1.863	59.45	60.50	60.40
30.56%	X	1.979	56.63	56.56	56.60
32.43%	X	2.078	53.80	54.02	53.90
34.21%	X	2.176	51.31	51.81	51.30
36.31%	X	2.288	48.80	49.04	49.00
38.65%	X	2.407	46.30	46.69	46.60
40.83%	X	2.526	44.13	44.58	44.30
42.86%	X	2.619	42.44	43.05	42.80
44.75%	X	2.732	40.92	40.87	41.20
46.52%	X	2.854	39.09	39.45	39.20
48.19%	X	2.942	38.10	38.42	37.70
50.00%	3.044	3.017	36.94	37.44	37.00
50.00%	3.119	2.867	38.88	39.15	39.15
51.81%	X	2.947	37.86	38.05	38.11
53.48%	X	3.025	36.95	37.02	37.09
55.25%	X	3.108	35.97	36.06	36.06

57.14%	X	3.204	34.88	35.00	34.98
59.17%	X	3.293	33.89	34.08	34.07
61.35%	X	3.399	32.82	33.10	32.94
63.69%	X	3.468	32.23	32.37	32.29
65.79%	X	3.595	30.96	31.39	31.11
67.57%	X	3.670	30.28	30.74	30.52
69.44%	X	3.761	29.57	29.94	29.82
71.43%	X	3.854	28.87	29.27	29.05
73.53%	X	3.937	28.23	28.63	28.47
75.76%	X	4.037	27.49	27.93	27.82
77.52%	X	4.117	27.03	27.36	27.23
79.37%	X	4.183	26.52	26.95	26.85
81.30%	X	4.267	26.00	26.37	26.36
83.33%	X	4.352	25.50	25.88	25.83
85.47%	X	4.438	25.02	25.40	25.28
87.72%	X	4.538	24.54	24.81	24.69
90.09%	X	4.633	23.98	24.36	24.18
91.74%	X	4.691	23.68	24.13	23.82
93.46%	X	4.746	23.41	23.84	23.55
95.24%	X	4.803	23.17	23.56	23.23
97.09%	X	4.855	22.90	23.39	22.92
99.01%	X	4.900	22.68	23.13	22.77
100.00%	5.160	4.866	22.74	23.20	23.11

Table A.25: Final Lake Jackson concentration test results using the new non-plated sensors

Percent saltwater	Measured conductivity (S/m)	Calculated conductivity (S/m)	Board 4D (Ω)	Board 5D (Ω)	Board 6D (Ω)
0.00%	X	0.003	20,408.16	20,449.90	20,618.56
0.99%	0.081	0.084	574.38	572.08	575.04
2.91%	0.214	0.219	221.04	220.60	220.36
4.76%	0.333	0.340	141.50	141.70	141.52
6.54%	0.455	0.461	104.34	104.30	104.10
8.26%	0.571	0.576	83.58	83.12	83.87
9.91%	0.676	0.681	70.52	70.27	70.18
12.28%	0.836	0.840	57.41	56.85	56.85
14.53%	0.978	0.982	48.80	48.69	48.71
16.67%	1.117	1.118	42.74	42.68	42.70
18.70%	1.250	1.252	38.02	37.86	38.02
20.63%	1.384	1.379	34.63	34.53	34.51

22.48%	1.501	1.492	32.00	31.92	31.88
24.24%	1.609	1.598	29.84	29.73	29.76
26.47%	1.746	1.732	27.80	27.45	27.46
28.57%	1.876	1.863	25.75	25.63	26.10
30.56%	X	1.979	24.22	24.03	24.06
32.43%	X	2.078	22.88	22.81	22.78
34.21%	X	2.176	21.94	21.73	21.75
36.31%	X	2.288	20.77	20.60	20.76
38.65%	X	2.407	19.65	19.60	19.62
40.83%	X	2.526	18.80	18.75	18.74
42.86%	X	2.619	18.06	18.03	18.00
44.75%	X	2.732	17.42	17.36	17.37
46.52%	X	2.854	16.63	16.60	16.57
48.19%	X	2.942	16.17	16.13	16.14
50.00%	3.044	3.017	15.74	15.68	15.68
50.00%	3.119	2.867	16.45	16.43	16.47
51.81%	X	2.947	16.04	16.01	16.02
53.48%	X	3.025	15.60	15.58	15.61
55.25%	X	3.108	15.25	15.17	15.20
57.14%	X	3.204	14.81	14.75	14.77
59.17%	X	3.293	14.40	14.28	14.34
61.35%	X	3.399	13.87	13.81	13.80
63.69%	X	3.468	13.59	13.55	13.52
65.79%	X	3.595	13.17	13.16	13.16
67.57%	X	3.670	12.89	12.87	12.87
69.44%	X	3.761	12.63	12.59	12.61
71.43%	X	3.854	12.35	12.33	12.32
73.53%	X	3.937	12.07	12.05	12.03
75.76%	X	4.037	11.79	11.73	11.80
77.52%	X	4.117	11.57	11.58	11.55
79.37%	X	4.183	11.37	11.37	11.34
81.30%	X	4.267	11.15	11.13	11.13
83.33%	X	4.352	10.95	10.92	10.91
85.47%	X	4.438	10.73	10.73	10.68
87.72%	X	4.538	10.53	10.48	10.51
90.09%	X	4.633	10.33	10.31	10.27
91.74%	X	4.691	10.19	10.17	10.17
93.46%	X	4.746	10.08	10.05	10.05
95.24%	X	4.803	9.96	9.93	9.94
97.09%	X	4.855	9.86	9.86	9.88
99.01%	X	4.900	9.79	9.74	9.73

100.00%	5.160	4.866	9.77	9.71	9.69

Table A.26: Final Lake Jackson concentration test results using the new gold-plated sensors

Percent saltwater	Measured conductivity (S/m)	Calculated conductivity (S/m)	Board 1G (Ω)	Board 2G (Ω)	Board 3G (Ω)
0.00%	X	0.003	19,801.98	19,960.08	19,880.72
0.99%	0.081	0.084	581.06	577.37	575.04
2.91%	0.214	0.219	220.90	220.60	221.04
4.76%	0.333	0.340	142.43	142.11	141.76
6.54%	0.455	0.461	103.73	104.78	104.79
8.26%	0.571	0.576	83.34	84.15	83.93
9.91%	0.676	0.681	70.62	70.57	70.82
12.28%	0.836	0.840	56.54	57.44	57.60
14.53%	0.978	0.982	48.66	49.46	49.14
16.67%	1.117	1.118	42.84	43.29	43.22
18.70%	1.250	1.252	37.95	38.61	38.55
20.63%	1.384	1.379	34.75	34.87	35.06
22.48%	1.501	1.492	32.01	32.44	32.49
24.24%	1.609	1.598	29.83	30.27	30.28
26.47%	1.746	1.732	27.57	27.80	28.00
28.57%	1.876	1.863	25.90	26.21	26.18
30.56%	X	1.979	24.22	24.47	24.61
32.43%	X	2.078	22.93	23.20	23.33
34.21%	X	2.176	21.85	22.25	22.27
36.31%	X	2.288	20.75	21.16	21.17
38.65%	X	2.407	19.68	20.11	20.16
40.83%	X	2.526	18.85	19.06	19.21
42.86%	X	2.619	18.05	18.36	18.45
44.75%	X	2.732	17.50	17.67	17.80
46.52%	X	2.854	16.72	17.00	17.02
48.19%	X	2.942	16.25	16.53	16.55
50.00%	3.044	3.017	15.77	16.06	16.10
50.00%	3.119	2.867	16.81	16.93	16.98
51.81%	X	2.947	16.28	16.47	16.46
53.48%	X	3.025	15.88	16.10	16.06
55.25%	X	3.108	15.40	15.65	15.67
57.14%	X	3.204	14.97	15.15	15.16
59.17%	X	3.293	14.58	14.76	14.72
61.35%	X	3.399	14.13	14.30	14.26

63.69%	X	3.468	13.82	13.98	13.94
65.79%	X	3.595	13.36	13.50	13.59
67.57%	X	3.670	13.06	13.20	13.28
69.44%	X	3.761	12.79	12.94	12.99
71.43%	X	3.854	12.44	12.66	12.72
73.53%	X	3.937	12.19	12.37	12.42
75.76%	X	4.037	11.99	12.12	12.13
77.52%	X	4.117	11.63	11.83	11.92
79.37%	X	4.183	11.48	11.68	11.69
81.30%	X	4.267	11.28	11.36	11.47
83.33%	X	4.352	11.06	11.22	11.28
85.47%	X	4.438	10.87	11.01	11.06
87.72%	X	4.538	10.66	10.76	10.84
90.09%	X	4.633	10.43	10.56	10.64
91.74%	X	4.691	10.33	10.49	10.51
93.46%	X	4.746	10.20	10.34	10.38
95.24%	X	4.803	10.06	10.24	10.28
97.09%	X	4.855	9.95	10.15	10.18
99.01%	X	4.900	9.89	9.98	10.09
100.00%	5.160	4.866	9.87	10.04	10.11

Table A.27: Final rain water concentration tests using the original sensors

Percent Salt water	Measured conductivity (S/m)	Calculated conductivity (S/m)	Board 2 (Ω)	Board 3 (Ω)	Board 12 (Ω)
0.00%	X	0.001	148,148.15	135,501.36	108,813.93
0.99%	0.066	0.070	1,644.47	1,597.19	1,590.58
2.91%	0.196	0.198	564.65	564.33	564.33
4.76%	0.317	0.321	347.71	350.14	348.07
6.54%	0.429	0.429	261.03	260.89	260.62
8.26%	0.536	0.539	208.25	208.28	207.08
9.91%	0.640	0.628	181.00	178.28	175.50
12.28%	0.784	0.780	144.24	143.68	142.78
14.53%	0.922	0.916	123.87	121.55	121.33
16.67%	1.049	1.040	108.21	107.91	107.09
18.70%	1.168	1.143	98.27	97.98	97.73
20.63%	1.282	1.256	89.85	88.88	88.86
22.48%	1.394	1.356	82.92	82.03	82.85
24.24%	1.496	1.470	75.87	76.05	76.69
26.47%	1.661	1.608	70.18	69.40	69.44

28.57%	1.774	1.720	65.10	65.15	65.06
30.56%	X	1.826	61.73	61.16	61.16
32.43%	X	1.923	58.51	58.07	58.11
34.21%	X	2.038	55.25	54.59	55.07
36.31%	X	2.119	53.08	52.41	53.05
38.65%	X	2.230	50.35	50.13	50.23
40.83%	X	2.343	47.64	47.57	48.17
42.86%	X	2.448	45.93	45.50	45.81
44.75%	X	2.537	44.17	43.92	44.37
46.52%	X	2.605	42.96	42.64	43.40
48.19%	X	2.682	41.72	41.58	41.96
50.00%	2.737	2.765	40.57	40.29	40.67
50.00%	2.731	2.759	40.67	40.26	40.85
51.81%	X	2.837	39.53	39.15	39.75
53.48%	X	2.915	38.43	38.12	38.71
55.25%	X	3.000	37.37	37.04	37.58
57.14%	X	3.073	36.43	36.10	36.79
59.17%	X	3.175	35.39	34.92	35.54
61.35%	X	3.248	34.51	34.11	34.83
63.69%	X	3.347	33.49	33.15	33.76
65.79%	X	3.436	32.68	32.06	33.05
67.57%	X	3.507	31.96	31.50	32.35
69.44%	X	3.573	31.23	31.05	31.76
71.43%	X	3.667	30.54	30.08	31.02
73.53%	X	3.768	29.71	29.38	30.08
75.76%	X	3.853	29.33	28.64	29.24
77.52%	X	3.924	28.73	28.14	28.76
79.37%	X	3.973	28.17	27.85	28.55
81.30%	X	4.042	27.72	27.34	28.05
83.33%	X	4.141	27.28	26.66	27.20
85.47%	X	4.190	26.78	26.37	27.03
87.72%	X	4.277	26.18	25.81	26.57
90.09%	X	4.338	25.89	25.32	26.25
91.74%	X	4.398	25.39	25.03	25.97
93.46%	X	4.475	25.06	24.65	25.38
95.24%	X	4.520	24.83	24.37	25.14
97.09%	X	4.560	24.64	24.08	24.98
99.01%	X	4.613	24.38	23.79	24.66
100.00%	4.894	4.581	24.59	23.98	24.78

Table A.28: Final rain water concentration tests using the new non-plated sensors

Percent saltwater	Measured conductivity (S/m)	Calculated conductivity (S/m)	Board 4D (Ω)	Board 5D (Ω)	Board 6D (Ω)
0.00%	X	0.001	59,488.40	60,313.63	62,344.14
0.99%	0.066	0.069	692.04	694.44	693.48
2.91%	0.196	0.196	242.25	242.01	242.42
4.76%	0.317	0.316	150.33	149.86	150.15
6.54%	0.429	0.425	111.56	111.53	112.02
8.26%	0.536	0.533	89.25	89.06	88.88
9.91%	0.640	0.628	74.68	75.93	76.22
12.28%	0.784	0.777	61.16	61.12	61.12
14.53%	0.922	0.910	52.33	52.00	52.25
16.67%	1.049	1.039	45.77	45.66	45.68
18.70%	1.168	1.145	41.49	41.43	41.58
20.63%	1.282	1.258	37.71	37.78	37.78
22.48%	1.394	1.362	34.84	34.86	34.94
24.24%	1.496	1.467	32.40	32.43	32.30
26.47%	1.661	1.618	29.39	29.33	29.34
28.57%	1.774	1.730	27.55	27.37	27.45
30.56%	X	1.838	26.01	25.71	25.82
32.43%	X	1.948	24.46	24.34	24.36
34.21%	X	2.055	23.15	23.15	23.06
36.31%	X	2.146	22.22	22.07	22.13
38.65%	X	2.263	21.01	20.97	20.98
40.83%	X	2.379	20.02	19.94	19.93
42.86%	X	2.486	19.16	19.09	19.07
44.75%	X	2.579	18.47	18.43	18.35
46.52%	X	2.662	17.90	17.82	17.82
48.19%	X	2.742	17.39	17.30	17.27
50.00%	2.737	2.822	16.89	16.81	16.79
50.00%	2.731	2.814	16.89	16.87	16.89
51.81%	X	2.896	16.43	16.38	16.39
53.48%	X	2.970	16.01	16.00	15.97
55.25%	X	3.051	15.59	15.55	15.56
57.14%	X	3.142	15.11	15.10	15.14
59.17%	X	3.243	14.67	14.63	14.65
61.35%	X	3.323	14.30	14.31	14.28
63.69%	X	3.423	13.88	13.88	13.87
65.79%	X	3.508	13.56	13.53	13.54
67.57%	X	3.592	13.32	13.19	13.17

69.44%	X	3.664	13.02	12.94	12.93
71.43%	X	3.744	12.71	12.67	12.68
73.53%	X	3.853	12.34	12.32	12.33
75.76%	X	3.925	12.13	12.10	12.08
77.52%	X	3.983	11.90	11.95	11.93
79.37%	X	4.041	11.77	11.74	11.76
81.30%	X	4.105	11.56	11.59	11.56
83.33%	X	4.177	11.34	11.42	11.35
85.47%	X	4.260	11.14	11.13	11.17
87.72%	X	4.344	10.96	10.93	10.90
90.09%	X	4.430	10.74	10.71	10.72
91.74%	X	4.485	10.61	10.57	10.60
93.46%	X	4.511	10.51	10.50	10.58
95.24%	X	4.580	10.36	10.41	10.34
97.09%	X	4.652	10.22	10.22	10.19
99.01%	X	4.713	10.14	10.05	10.05
100.00%	4.894	4.697	10.12	10.10	10.11

Table A.29: Final rain water concentration results using the new gold-plated sensors

Percent saltwater	Measured conductivity (S/m)	Calculated conductivity (S/m)	Board 1G (Ω)	Board 2G (Ω)	Board 3G (Ω)
0.00%	X	0.001	53,850.30	54,764.51	56,753.69
0.99%	0.066	0.069	693.00	694.44	693.00
2.91%	0.196	0.196	243.13	243.66	242.54
4.76%	0.317	0.316	151.10	150.60	150.58
6.54%	0.429	0.425	111.88	112.41	112.25
8.26%	0.536	0.533	89.18	89.47	89.34
9.91%	0.640	0.628	76.16	76.57	75.30
12.28%	0.784	0.777	61.50	62.11	61.69
14.53%	0.922	0.910	52.52	52.94	52.91
16.67%	1.049	1.039	46.00	46.49	46.00
18.70%	1.168	1.145	42.11	42.23	41.84
20.63%	1.282	1.258	38.21	38.43	38.14
22.48%	1.394	1.362	35.36	35.54	35.63
24.24%	1.496	1.467	32.72	33.11	32.77
26.47%	1.661	1.618	29.86	29.96	29.72
28.57%	1.774	1.730	27.80	28.14	27.85
30.56%	X	1.838	26.32	26.39	26.25

32.43%	X	1.948	24.89	25.01	24.84
34.21%	X	2.055	23.71	23.71	23.53
36.31%	X	2.146	22.72	22.76	22.60
38.65%	X	2.263	21.59	21.53	21.43
40.83%	X	2.379	20.44	20.48	20.42
42.86%	X	2.486	19.64	19.65	19.51
44.75%	X	2.579	18.98	18.97	18.85
46.52%	X	2.662	18.44	18.37	18.25
48.19%	X	2.742	17.84	17.91	17.76
50.00%	2.737	2.822	17.37	17.39	17.23
50.00%	2.731	2.814	17.59	17.50	17.28
51.81%	X	2.896	17.12	16.99	16.81
53.48%	X	2.970	16.63	16.58	16.38
55.25%	X	3.051	16.22	16.13	15.99
57.14%	X	3.142	15.76	15.69	15.52
59.17%	X	3.243	15.29	15.20	15.03
61.35%	X	3.323	15.00	14.86	14.67
63.69%	X	3.423	14.55	14.42	14.27
65.79%	X	3.508	14.13	14.05	13.91
67.57%	X	3.592	13.83	13.65	13.52
69.44%	X	3.664	13.60	13.50	13.37
71.43%	X	3.744	13.28	13.21	13.18
73.53%	X	3.853	12.95	12.84	12.72
75.76%	X	3.925	12.73	12.53	12.41
77.52%	X	3.983	12.46	12.37	12.24
79.37%	X	4.041	12.29	12.22	12.10
81.30%	X	4.105	12.07	12.00	11.90
83.33%	X	4.177	11.83	11.74	11.65
85.47%	X	4.260	11.60	11.50	11.53
87.72%	X	4.344	11.44	11.35	11.24
90.09%	X	4.430	11.29	11.13	11.04
91.74%	X	4.485	11.20	11.04	10.94
93.46%	X	4.511	11.02	10.90	10.82
95.24%	X	4.580	10.89	10.79	10.69
97.09%	X	4.652	10.82	10.69	10.63
99.01%	X	4.713	10.71	10.54	10.50
100.00%	4.894	4.697	10.71	10.62	10.51

Table A.30: Comparison of the results of sweeping the conductivity of the test material in EMPro and Q3D

Conductivity (S/m)	EMPro Results (Ω)	Q3D Results (Ω)	Percent Difference
0.0001	944,081.30	972,238.70	2.94%
0.0005	188,818.80	194,447.90	2.94%
0.001	94,410.99	97,223.96	2.94%
0.002	47,205.77	48,611.96	2.94%
0.003	31,470.72	32,407.98	2.93%
0.004	23,602.87	24,305.98	2.94%
0.005	18,882.28	19,444.79	2.94%
0.006	15,735.27	16,203.99	2.94%
0.007	13,487.33	13,889.13	2.94%
0.008	11,801.41	12,152.99	2.94%
0.009	10,490.17	10,802.66	2.94%
0.01	9,447.15	9,722.40	2.87%
0.02	4,720.58	4,861.20	2.94%
0.03	3,147.05	3,240.80	2.94%
0.04	2,360.29	2,430.60	2.94%
0.05	1,888.23	1,944.48	2.94%
0.06	1,573.53	1,620.40	2.94%
0.07	1,348.74	1,388.91	2.94%
0.08	1,180.14	1,215.30	2.94%
0.09	1,049.02	1,080.27	2.94%
0.1	944.12	972.24	2.94%
0.2	472.06	486.12	2.94%
0.3	314.71	324.08	2.94%
0.4	236.03	243.06	2.94%
0.5	188.82	194.45	2.94%
0.6	157.35	162.04	2.93%
0.7	134.87	138.89	2.93%
0.8	118.01	121.53	2.94%
0.9	104.90	108.03	2.93%
1	94.41	97.22	2.94%
2	47.21	48.61	2.93%
3	31.47	32.41	2.94%
4	23.60	24.31	2.93%
5	18.88	19.44	2.94%
6	15.74	16.20	2.94%
7	13.49	13.89	2.94%
8	11.80	12.15	2.94%

9	10.49	10.80	2.94%
10	9.44	9.72	2.94%

Table A.31: EMPro results of sweeping electrode separation distance for multiple geometries

Separation Distance (m)	Width = 2.5mm, Length = 10mm (Ω)	Width = 5mm, Length = 10mm (Ω)	Width = 2.5mm, Length = 20mm (Ω)	Width = 10mm, Length = 10mm (Ω)
0.0001	12.131	8.947	X	X
0.001	20.219	15.447	11.498	11.692
0.002	23.595	17.928	13.324	13.197
0.003	25.970	19.453	14.748	14.142
0.004	X	20.540	15.759	14.830
0.005	28.191	21.589	16.581	15.357
0.006	29.874	22.332	17.278	15.826
0.007	30.926	22.617	17.873	16.187
0.008	31.320	23.112	18.351	16.470
0.009	31.895	23.474	18.729	16.793
0.01	32.335	23.902	19.099	17.001
0.011	32.653	24.184	X	17.247
0.012	33.037	24.46	X	17.375
0.013	X	24.706	X	17.488
0.014	33.683	24.926	X	17.745
0.015	33.991	25.195	X	17.862
0.016	34.189	25.345	X	17.989
0.017	X	25.556	X	18.072
0.018	34.509	25.707	X	18.185
0.019	34.818	25.77	X	18.261
0.02	34.875	25.892	21.164	18.403
0.03	35.789	26.799	22.170	19.017
0.04	36.459	27.54	22.578	19.531
0.05	X	27.479	22.951	19.709
0.06	X	27.824	23.221	19.931
0.07	36.994	27.926	23.342	20.013
0.08	37.328	28.103	23.406	20.219
0.09	37.362	28.128	23.647	20.287
0.1	X	28.141	23.642	20.289
0.2	37.787	28.543	24.091	20.637
0.3	38.005	28.631	24.226	20.769
0.4	37.990	28.366	24.153	20.818
0.5	37.962	28.898	24.247	20.793

Table A.32: EMPro results of sweeping electrode length for multiple separation distances

Electrode Length (m)	2 mm Separation (Ω)	10 mm Separation (Ω)	40 mm Separation (Ω)	100 mm Separation (Ω)	1 m Separation (Ω)	2 mm Separation and 5 mm width (Ω)
0.001	106.61	119.20	122.87	124.06	124.58	60.43
0.002	74.27	86.64	91.16	92.23	92.50	50.07
0.003	57.77	70.19	74.33	75.46	71.55	40.15
0.004	47.74	59.37	63.53	64.70	65.02	33.83
0.005	40.58	51.73	56.00	57.09	57.49	29.36
0.006	35.71	46.05	50.17	51.38	X	26.02
0.007	31.52	41.55	45.70	46.89	47.39	23.37
0.008	28.32	37.89	41.88	37.90	43.69	21.25
0.009	25.73	34.86	38.86	40.05	40.81	19.46
0.01	23.60	32.34	36.09	37.44	38.09	17.93
0.011	X	30.17	X	35.23	35.90	X
0.012	X	28.21	X	33.36	33.81	15.56
0.013	X	26.56	X	31.59	X	14.60
0.014	X	25.07	X	30.02	30.56	13.70
0.015	X	23.74	X	28.66	29.34	12.95
0.016	X	22.63	X	27.39	27.95	12.32
0.017	X	21.49	X	26.28	26.87	11.71
0.018	X	20.55	X	25.30	25.84	11.14
0.019	X	19.66	X	24.31	24.88	10.65
0.02	X	18.85	22.35	23.44	24.09	10.20
0.03	8.94	X	16.39	X	X	X
0.04	6.83	X	X	X	X	X
0.05	5.49	X	10.85	X	X	X
0.06	4.61	X	9.26	X	X	X
0.07	3.97	X	8.11	X	X	X
0.08	3.51	X	7.22	X	X	X
0.09	3.12	X	6.49	X	X	X

Table A.33: EMPro results of sweeping electrode width for multiple separation distances

Electrode width (m)	0.05 mm Separation (Ω)	0.1 mm Separation (Ω)	2 mm Separation (Ω)	10 mm Separation (Ω)	100mm Separation (Ω)	1 m Separation (Ω)
0.001	X	15.35	33.73	45.28	X	X
0.002	X	12.41	25.87	35.37	X	X
0.003	X	11.60	X	30.05	X	X
0.004	X	9.87	19.71	26.57	X	X
0.005	X	8.91	17.93	23.84	X	X
0.006	X	9.03	16.73	22.21	X	X
0.007	X	8.28	15.65	20.47	X	X
0.008	X	X	14.65	19.01	X	X
0.009	X	X	13.92	17.94	X	X
0.01	6.15	7.41	13.30	17.11	20.28	20.97
0.02	4.80	5.95	9.55	11.57	13.87	14.49
0.03	3.83	4.86	7.68	9.10	10.81	11.32
0.04	3.39	4.31	6.55	7.60	8.99	9.45
0.05	2.93	3.76	5.71	6.53	7.64	8.14
0.06	2.76	3.47	5.14	5.78	6.72	7.16
0.07	2.61	3.23	4.67	5.23	6.05	6.46
0.08	2.34	2.90	4.29	4.76	5.47	5.83
0.09	2.22	2.81	3.94	4.34	4.96	5.28
0.1	2.11	2.68	3.71	4.08	4.65	4.98
0.2	1.59	1.83	2.27	2.42	2.67	2.91
0.3	1.24	1.41	1.69	1.76	1.90	2.07
0.4	1.06	1.18	1.34	1.37	1.47	1.62
0.5	0.91	0.99	1.11	1.15	1.23	1.33
0.6	0.81	0.86	0.96	0.99	1.05	1.14
0.7	0.73	0.78	0.85	0.87	0.91	0.99
0.8	0.66	0.70	0.74	0.76	0.81	0.86
0.9	0.60	0.63	0.67	0.70	0.72	0.77
1	0.56	0.58	0.63	0.64	0.67	0.72

Table A.34: Comparison between sweeping the electrode separation distance in EMPro and Q3D

Length (m)	EMPro Results (Ω)	Q3D Results (Ω)	Difference (Ω)	Percent Difference
0.001	20.81	20.93	0.12	0.57%
0.002	24.33	24.45	0.12	0.50%
0.003	26.53	26.49	0.04	0.16%
0.004	28.13	27.99	0.14	0.48%
0.005	29.35	28.76	0.59	2.00%
0.006	30.41	29.66	0.75	2.48%
0.007	31.19	30.37	0.81	2.61%
0.008	31.84	30.97	0.86	2.71%
0.009	32.36	31.59	0.77	2.39%
0.01	32.80	32.01	0.79	2.41%
0.02	35.35	34.67	0.68	1.94%
0.03	36.34	35.46	0.89	2.44%
0.04	36.98	35.95	1.03	2.80%
0.05	37.31	36.32	0.99	2.65%
0.06	37.52	36.65	0.87	2.31%
0.07	37.68	36.96	0.72	1.91%
0.08	37.79	37.04	0.75	2.00%
0.09	37.90	37.23	0.66	1.75%
0.1	37.94	37.48	0.47	1.23%

Table A.35: Comparison between sweeping the electrode length in EMPro and Q3D

Length (m)	EMPro Results (Ω)	Q3D Results (Ω)	Difference (Ω)	Percent Difference
0.001	106.61	109.58	2.97	2.79%
0.002	74.27	75.96	1.69	2.28%
0.003	57.77	59.44	1.67	2.89%
0.004	47.74	49.42	1.68	3.52%
0.005	40.58	42.08	1.50	3.69%
0.006	35.71	36.45	0.74	2.06%
0.007	31.52	32.50	0.98	3.10%
0.008	28.32	29.11	0.79	2.80%
0.009	25.73	26.48	0.75	2.93%
0.01	23.60	24.31	0.70	2.98%
0.02	X	13.11	X	X
0.03	8.94	9.02	0.08	0.89%
0.04	6.83	6.86	0.03	0.48%
0.05	5.49	5.52	0.02	0.44%

0.06	4.61	4.66	0.05	1.14%
0.07	3.97	3.99	0.01	0.28%
0.08	3.51	3.50	0.01	0.23%
0.09	3.12	3.15	0.02	0.74%
0.1	FaileXd	2.80	X	X

Table A.36: Comparison between sweeping the electrode width in EMPro and Q3D

Width (m)	EMPro Results (Ω)	Q3D Results (Ω)	Difference (Ω)	Percent Difference
0.001	33.73	33.11	0.62	1.82%
0.002	25.87	26.75	0.87	3.38%
0.003	22.38	22.85	0.47	2.12%
0.004	19.71	19.61	0.09	0.48%
0.005	17.93	18.15	0.22	1.24%
0.006	16.73	16.82	0.09	0.51%
0.007	15.65	15.78	0.13	0.85%
0.008	14.65	14.96	0.31	2.15%
0.009	13.92	14.20	0.27	1.97%
0.01	13.30	13.61	0.31	2.33%
0.02	9.55	10.02	0.47	4.90%
0.03	7.68	8.30	0.62	8.02%
0.04	6.55	7.18	0.64	9.75%
0.05	5.71	6.41	0.70	12.22%
0.06	5.14	5.88	0.75	14.51%
0.07	4.67	5.40	0.73	15.53%
0.08	4.29	5.02	0.73	16.96%
0.09	3.94	4.75	0.81	20.61%
0.1	3.71	4.41	0.70	18.93%

Appendix B

The Genetic Algorithm MATLAB Script

```
%GA
%%%%%%%%%%%%%%%%%%%%%%%%%%%%%%%%%%%%%%%%%%%%%%%%%%%%%%%%%%%%%%%%%%%%%%%%%%%%
%%%%%%%%%%%%%%%%%%%%%%%%%%%%%%%%%%%%%%%%%%%%%%%%%%%%%%%%%%%%%%%%%%%%%%%%%%%%
%% Setup
%%%%%%%%%%%%%%%%%%%%%%%%%%%%%%%%%%%%%%%%%%%%%%%%%%%%%%%%%%%%%%%%%%%%%%%%%%%%
%%%%%%%%%%%%%%%%%%%%%%%%%%%%%%%%%%%%%%%%%%%%%%%%%%%%%%%%%%%%%%%%%%%%%%%%%%%%
clc
clear all
close all
pause on
popsize =  100; %sets the size of the population
rangemin =0.000001;% minimum value the equation's coefficient value can be
rangemax =2500; % maximum value the equation's coefficient value can be
MAXGEN =2; % Sets maximum allowable number of generations
cross = 0.7; %the percent of a chromosome that is exchanged when the new
population is generated
mut= 0.09;% the chance that a mutation will occur
number_pops = 8; %sets the number of coefficient used in the equation
gen=1; % sets the initial generation count
disp('New fitness with updated data')
setups = {'All data' }

%Generating the original population using random number generator
newpop = unifrnd(rangemin,rangemax, popsize, number_pops); % generates the
original population of variables used in the equation
[row, col] = size(newpop);
newpop(1, 1:10)= [1490.37581825277,152.257678416239,1.00000000000000e-
06,5.94148991857480,2091.70365720822,28.5723106581932,0.582109906079604,3.935
89065815631,597.125373111360,0.899822321933179;];
%Determining the fitness function (based on the simulation's results)
redata = xlsread('Ordata5.xlsx'); %Reading the simulation data into MATLAB to
compare to the equation's results
[row_count, col_count] = size(redata);

%%%%%%%%%%%%%%%%%%%%%%%%%%%%%%%%%%%%%%%%%%%%%%%%%%%%%%%%%%%%%%%%%%%%%%%%%%%%
%%%%%%%%%%%%%%%%%%%%%%%%%%%%%%%%%%%%%%%%%%%%%%%%%%%%%%%%%%%%%%%%%%%%%%%%%%%%
%% The Genetic Algorithm
%%%%%%%%%%%%%%%%%%%%%%%%%%%%%%%%%%%%%%%%%%%%%%%%%%%%%%%%%%%%%%%%%%%%%%%%%%%%
%%%%%%%%%%%%%%%%%%%%%%%%%%%%%%%%%%%%%%%%%%%%%%%%%%%%%%%%%%%%%%%%%%%%%%%%%%%%
while gen <= MAXGEN %as long as the generation count is lower than the
maximum is will stay in the loop
    pop = newpop;

    %Inserting coefficient (individuals in the population) into the
```

```
    %equation and comparing how well they agree with the simulation
    %results
    for r = 1:row
        red = 1;
        green = 1;
        while red <col_count
           Efs =(log((0.01.*pop(r,4)+pop(r,2).*(redata(:,red)./(redata(1,
red+2))))));%
           E =
1/4.*1.*(100*pop(r,3)+100.*pop(r,1).*Efs)./((1000.*pop(r,5).*redata(1,red+1))
+pop(r,8)+1.*Efs.*redata(1, red+2).*(100.*pop(r,6)+pop(r,7).*10000.*redata(1,
red+1)));


            E = (E(~isnan(E)));

            redcompare = redata(:, red+3);
            redcompare = redcompare(~isnan(redcompare));
            fitred(green) = 1-sum((redcompare-E).^2)/sum((redcompare-
mean(redcompare)).^2);

            red = red+4;
            green = green+1;
        end
        fit(r,1) = mean(fitred);

    end



%Storing all previous values and fitness scores so that they can be reused if
%needed to speed up simulation

    m = (gen-1)*row+1;
    oldpop(m:(m+row-1),1:col) = pop;
    oldpop(m:(m+row-1),col+1) = fit;

    max(fit)


%finish if the average fitness score is above a certain value, if it has
%not changed in a number of generations, or after a certain number of
%generations


%Crossover: uses Tournament selection for crossover selection
%then mutation with low chance of mutation

    %Tournament of 5
    for tourn = 1:2:row-3;
        %if fit(tourn)== max(fit)    %elitism
            %newpop(tourn,1) = pop(tourn,1);
            %newpop(tourn,2) = pop(tourn,2);
       % else
```

```
            for par = 1:2 %parent selection
                for select =1:4
                    participant = round(unifrnd(1,row));
                    comp(select,[1:col]) = pop(participant, [1:col]);
                    fitcomp(select,1) = fit(participant);


                end


                [useless, Rmax] = max(fitcomp);
                parent(par,[1:col]) = comp(Rmax, [1:col]);

            end

            crosschance = unifrnd(1,row);
            if crosschance <= cross
                newpop(tourn, [1:col]) = parent(1, [1:col]);
                newpop(tourn+1, [1:col]) = parent(2, [1:col]);
            else


                  %CROSSOVER SCHEME
                  newpop([tourn, tourn+1], [1:col]) = parent([1,2],[1:col]);
                  crossed_allele = round(unifrnd(1,col));
                  percentcrossed = unifrnd(0,1);
                  newpop(tourn, crossed_allele)=
percentcrossed*parent(1,crossed_allele)+ (1-
percentcrossed)*parent(2,crossed_allele);
                  newpop(tourn+1, crossed_allele)= (1-
percentcrossed)*parent(1,crossed_allele)+
percentcrossed*parent(2,crossed_allele);

            end

            %Mutation
            for j = 1:row-2
                mutchance = unifrnd(0,1);
                if mutchance <= mut
                    mut_allele = round(unifrnd(1,col)); %selecting which
allele is mutated
                    newpop(j, mut_allele) = newpop(j, mut_allele)+
0.01*rangemax*unifrnd(-1,1);
                    if newpop(j, mut_allele)>rangemax     %keeping it with in
the defined range
                        newpop(j, mut_allele) = rangemax;
                    elseif newpop(j, mut_allele)<rangemin
                        newpop(j, mut_allele)=rangemin;
                    end
                else %no mutation
                end
            end
    end
```

```
    %elitism
    for y = 2:3
        [useless, RowTmax] = max(fit);
        newpop(tourn+y, [1:col]) = pop(RowTmax, [1:col]);
        fit(RowTmax,1) = 0;
    end

    newpop(1, [1:col]) = unifrnd(rangemin,rangemax, 1, number_pops); %adds
some randomness into the population to ensure a single solution does not
dominate too soon

      [most_fit, fit_count] = mode(fit);
      %Leaving the loop early if the maximum fitness score has not improved
      %in a few generations
      if gen > 50000 && fit_count >= 0.8*popsize
          abs(avefit(gen)-avefit(gen-1))<= 0.0001 && abs(avefit(gen)-
avefit(gen-2))<= 0.0001 && abs(avefit(gen)-avefit(gen-1))<= 0.0001 ;
          realgen = gen;
          gen = MAXGEN+1;  %finish since the fitness is not changing
      else
%          %return to start of the loop to start TNG
          gen = gen+1;
      end

end

%%%%%%%%%%%%%%%%%%%%%%%%%%%%%%%%%%%%%%%%%%%%%%%%%%%%%%%%%%%%%%%%%%%%%%%%%%%%%%%
%%%%%%%%%%%%%%%%%%%%%%%%%%%%%%%%%%%%%%%%%%%%%%%%%%%%%%%%%%%%%%%%%%%%%%%%%%%%%%%
%% Evaluating the Generated Solutions
%%%%%%%%%%%%%%%%%%%%%%%%%%%%%%%%%%%%%%%%%%%%%%%%%%%%%%%%%%%%%%%%%%%%%%%%%%%%%%%
%%%%%%%%%%%%%%%%%%%%%%%%%%%%%%%%%%%%%%%%%%%%%%%%%%%%%%%%%%%%%%%%%%%%%%%%%%%%%%%

%Determining the individual with the highest fitness score
[max_fit, max_fit_loc] = max(fit);
if max_fit > fit(r)
    r = max_fit_loc;
else
end

% Performing the R squared tests
%%%%%%%%%%%%%%%%%%%%%%%%%%%%%%%%%%%%%%%%%%%%%%%%%%%%%%%%%%%%%%%%%%%%%%%%%%%%%%%
red = 1;
green = 1;
blue= 1;
while red <col_count
    Efs =(log((0.01.*pop(r,4)+pop(r,2).*(redata(:,red)./(redata(1,
red+2))))));%
    Fr(:,green)=
1/4.*1.*(100*pop(r,3)+100.*pop(r,1).*Efs)./((1000.*pop(r,5).*redata(1,red+1))
+pop(r,8)+1.*Efs.*redata(1, red+2).*(100.*pop(r,6)+pop(r,7).*10000.*redata(1,
red+1)));

    Er = Fr(:,green);
    Er = Er(~isnan(Er));
```

```
    rdat = redata(:, red+3);
    redcompare = rdat(~isnan(rdat));


    R_sq(green) = 1-sum((redcompare-Er).^2)/sum((redcompare-
mean(redcompare)).^2);
    red = red+4;
    green = green+1;
    R_equ(blue:(blue+row_count-1))= Er;
    R_equ_norm(blue:(blue+row_count-1))= Er./mean(rdat);
    R_sim(blue:(blue+row_count-1))= rdat;
    R_sim_norm(blue:(blue+row_count-1))= rdat./mean(rdat);


   blue=blue+row_count;

end
pop(r,:)
show = ['R Squared for "', char(setups(1)), '" is ' num2str(fit(r)), '\n'];
fprintf(show)


R_sq

%%Scatter Plot
%%%%%%%%%%%%%%%%%%%%%%%%%%%%%%%%%%%%%%%%%%%%%%%%%%%%%%%%%%%%%%%%%%%%%%%
figure
plot([0:1:160], [0:1:160], R_sim, R_equ, 'o')
xlim([0,160])
ylim([0,160])
pause
plot([0:0.01:1.60], [0:0.01:1.60],R_sim_norm, R_equ_norm, 'o')
pause
R_sq_total = 1-sum((R_sim-R_equ).^2)/sum((R_sim-mean(R_sim)).^2)

%% Plotting vs the distances
%%%%%%%%%%%%%%%%%%%%%%%%%%%%%%%%%%%%%%%%%%%%%%%%%%%%%%%%%%%%%%%%%%%%%%%

figure
for z = 1:110
    plot(redata(:, 1+4*(z-1)), Fr(:, z), redata(:, 1+4*(z-1)), redata(:,
4*(z)), '*')
    show = ['R Squared for w = ',num2str(redata(1, 3+4*(z-1)))  ' and l =',
num2str(redata(1, 2+4*(z-1))),' is ' num2str(R_sq(z))];
    title(show)
    %xlim([0, 0.05]);

    pause

end
y=1;
```

```
%% Plotting vs the widths
%%%%%%%%%%%%%%%%%%%%%%%%%%%%%%%%%%%%%%%%%%%%%%%%%%%%%%%%%%%%%%%%%%%%%%%

wid =[0.001:0.001:0.01];

u=0;
while u<col_count/4
    for q = 1:row_count
        Erw = Fr(q, (u+1):1:(u+10));
        Resw = redata(q, (4*(u+1)):4:(4*(u+10)));
        R_sqw(q+u) = 1-sum((Resw-Erw).^2)/sum((Resw-mean(Resw)).^2);
        plot(wid, 1./Erw, wid, 1./Resw, '*')
        show = ['R Squared for s = ',num2str(redata(q, 1+4*u)) ' and l =',
num2str(redata(1, 2+4*(u))),' is ' num2str(R_sqw(q+u))];
        title(show)

        pause
    end
    u= u+10;
end

R_sqw(1) =mean(R_sqw(2:106));

%% Plotting vs the lengths
%%%%%%%%%%%%%%%%%%%%%%%%%%%%%%%%%%%%%%%%%%%%%%%%%%%%%%%%%%%%%%%%%%%%%%%
wid =[0.001:0.001:0.01];

u=0;
e=2;
while u<10
    for q = 1:row_count
        Erl = [Fr(q, (u+1):10:(u+col_count/4-9))];
        Resl = [redata(q, 4.*(u+1):40:(4.*u+col_count-4.*9))]
        R_sql(e) = 1-sum((Resl-Erl).^2)/sum((Resl-mean(Resl)).^2);
        plot(wid, 1./Erl, wid, 1./Resl, '*')
        show = ['R Squared for s = ',num2str(redata(q, 1+4*u)) ' and w =',
num2str(redata(1, 3+4*(u))),' is ' num2str(R_sql(e))];
        title(show)
        pause
        e=e+1;
    end
    u= u+1;
end

R_sql(1) =mean(R_sql(2:151));
```

Appendix C

MATLAB Script for Calculating the Cell Constant of a PCB Sensor

```
%Calculating Cell Constant

clc
clear all
close all
r =1;

dist = 0.00254; % Defining the electrode separation distance
wid = 0.00254; % Defining the electrode width
len= 0.02032; % Defining the electrode length
cond = 4; %Set conductivity if you want to calculate Resistance, otherwise
cond = 0
Resistance = 42; %Set Resitance if you want to calculate conductivity


%Calculating the Cell Constant

pop(r,1:8)=[ 2.017  33  2.14    1.31    7.87    1   3.73    0.0108  ];
%equation coefficients
Efs =log(pop(r,4)+pop(r,2).*dist./wid);%
E=
1.*(pop(r,3).*1+pop(r,1).*Efs)./((pop(r,5).*len)+pop(r,8)+Efs.*wid.*(pop(r,6)
+pop(r,7).*10.*len))+1./(3866.*len.*wid);

show = ['When the distance is ', num2str(dist),' m the length is ',
num2str(len),' m and the width is ', num2str(wid),' m: \n \nThe cell constant
is ', num2str(E), ' per meter\n\n'];
fprintf(show)

%Calculating the conductivity or Resistance
if cond ==0
   conduct = E./Resistance;
   show = ['And when the resistance is ', num2str(Resistance),' Ohms, the
electrical conductivity is ' num2str(conduct),' S/m\n'];
   fprintf(show)
else
     Res = transpose(E./cond);
     show = ['And when the electrical conductivity is ', num2str(cond),' S/m,
the resistance is ' num2str(Res),' Ohms\n'];
   fprintf(show)
end
```